NMR-based Structure Elucidation of Lipopeptides and their Molecular Interaction with Targets

Dissertation

der Mathematisch-Naturwissenschaftlichen Fakultät

der Eberhard Karls Universität Tübingen

zur Erlangung des Grades eines

Doktors der Naturwissenschaften

(Dr. rer. nat.)

vorgelegt von

Irina Carolin Helmle

aus Freiburg

Tübingen

2023

Gedruckt mit Genehmigung der Mathematisch-Naturwissenschaftlichen Fakultät
der Eberhard Karls Universität Tübingen.

Tag der mündlichen Qualifikation:	05.02.2024
Dekan:	Prof. Dr. Thilo Stehle
1. Berichterstatter:	Prof. Dr. Harald Groß
2. Berichterstatter:	PD Dr. Bertolt Gust

Eigenständigkeitserklärung

Ich erkläre hiermit, dass ich die zur Promotion eingereichte Arbeit mit dem Titel: „NMR-based Structure Elucidation of Lipopeptides and their Molecular Interaction with Targets“ selbständig verfasst, nur die angegebenen Quellen und Hilfsmittel benutzt und wörtlich oder inhaltlich übernommene Stellen (alternativ: Zitate) als solche gekennzeichnet habe. Ich erkläre, dass die Richtlinien zur Sicherung guter wissenschaftlicher Praxis der Universität Tübingen (Beschluss des Senats vom 25.5.2000) beachtet wurden. Ich versichere an Eides statt, dass diese Angaben wahr sind und dass ich nichts verschwiegen habe. Mir ist bekannt, dass die falsche Abgabe einer Versicherung an Eides statt mit Freiheitsstrafe bis zu drei Jahren oder mit Geldstrafe bestraft wird.

Tübingen, Datum:

Unterschrift: _____

Irina Helmle

Table of Content

Abbreviations and Units

°C	degree Celsius
µ	micro (10^{-6})
µ	specific growth rate (in connection with growth determination of bacteria)
1D	one dimensional
2D	two dimensional
A (domain)	adenylation (domain)
AA/aa	amino acid
ACP	acyl carrier protein
AMP	adenosine monophosphate
ADP	adenosine diphosphate
ATP	adenosine triphosphate
BGC	biosynthetic gene cluster
C (domain)	condensation (domain)
calc	calculated
CID	collision induced dissociation
CLP	cyclic lipopeptide
conc	concentrated
COSY	correlated spectroscopy
d	doublet (in connection with NMR data)
Da	Dalton
DAD	diode array detector
dd	doublet of doublets (in connection with NMR data)
ddH_2O	double distilled water
DEPT	distortionless enhancement by polarization transfer
DMB/DMBGly	Davis minimal broth without dextrose / Davis minimal broth without dextrose supplemented with glycerol
DMSO	dimethyl sulfoxide
DNA	deoxyribonucleic acid
dt	doublet of triplets (in connection with NMR data)
E (domain)	epimerisation domain
EIC	extracted-ion chromatogram
Emp	empedopeptin
ESI	electrospray ionisation

EtOAc	ethyl acetate
FA	fatty acid
GlcNAc	N-acetyl glucosamine
h	hours
HCl	hydrochloric acid
HCOOH, FA	formic acid
3-HDA	3-hydroxydecanoic acid
3-HMA	3-hydroxy myristic acid; 3-hydroxytetradecanoic acid
HMBC	heteronuclear multiple-bond correlation spectroscopy
HPLC	high performance liquid chromatography
HR	high resolution
HSQC	heteronuclear single quantum correlation
Hz	hertz
i.e.	Latin 'id est'; that is
IC_{50}	half maximal inhibitory concentration
J	spin – spin coupling constant [Hz]
L	litre
LC	liquid chromatography
LP	lipopeptide
M	molar [mol/L]
m	milli (10^{-3})
m	multiplet (in connection with NMR data)
m/z	mass-to-charge ratio
MHz	megahertz
MIC	minimal inhibitory concentration
min	minute
MoA	mode of action
MR	methicillin-resistant
MRSA	methicillin-resistant *Staphylococcus aureus*
MS	mass spectrometry
MS/MS	tandem mass spectrometry
MurNAc	N-acetylmuramic acid
MW	molecular weight
NaOH	sodium hydroxide
n.d.	not detected
nm	nanometre (10^{-9})
NMR	nuclear magnetic resonance
no.	number

NOE	nuclear Overhauser effect
NOESY	nuclear Overhauser effect spectroscopy
NRPS	nonribosomal peptide synthetase
OD_{600}	optical density at 600 nm
OH-Pyrr	3-hydroxy pyrrolinium
PCP (domain)	peptidyl carrier protein (domain)
pH	potential hydrogenii
PKS	polyketide synthase
Plb	plusbacin
PP_i	pyrophosphate
PPTase	phosphopantetheinyl transferase
Pyrr	1-pyrrolinium
R	residue (in combination with chemical structures)
rdb	ring double bond
RNA	ribonucleic acid
RP	reverse phase
rpm	rounds per minute
RT	room temperature
s	singlet (in connection with NMR data)
SAM	S-adenosyl-methionine
SAR	structure-activity relationship
sec	seconds
spp.	species (plural)
t	triplet (in connection with NMR data)
T (domain)	thiolation (domain)
t_d	doubling time
TE-/TE-II (domain)	thioesterase-/ thioesterase-II (domain)
TFA	trifluoroacetic acid
TIC	total-ion chromatogram
TOCSY	total correlation spectroscopy
t_R	time of retention
UV	ultraviolet
v/v	volume per volume
VIS	visible
VLC	vacuum liquid chromatography
δ	NMR chemical shift [ppm]
Δ	difference

Abbreviations for Amino Acids

amino acid	one letter code	three letter code
alanine	A	Ala
arginine	R	Arg
asparagine	N	Asn
aspartic acid	D	Asp
cysteine	C	Cys
glutamic acid	E	Glu
glutamine	Q	Gln
glycine	G	Gly
histidine	H	His
isoleucine	I	Ile
leucine	L	Leu
lysine	K	Lys
methionine	M	Met
phenylalanine	F	Phe
proline	P	Pro
serine	S	Ser
threonine	T	Thr
tryptophan	W	Trp
tyrosine	Y	Tyr
valine	V	Val

Abbreviations for Unusual Amino Acids

amino acid	three letter code
3-OH aspartic acid	OH-Asp
2,4-diaminobutyric acid	Dab
dehydrobutyrine	Dhb
3-OH proline	3OH-Pro
homoserine	Hse

Summary

Lipopeptides form a structurally diverse group of metabolites produced by a variety of bacteria. The wide structural diversity of lipopeptides suggests that these metabolites have different natural functions, and the present work focuses on two compound families thereof.

Guanidine-containing lipopeptide antibiotics form a group of naturally occurring cyclic lipopeptides including empedopeptin (Emp), plusbacins (Plbs) and tripropeptins (Tpp), which exhibit potent antibacterial activity against a variety of gram-positive pathogens. Despite their considerable structural similarity, these lipopeptides show significant differences in their potency. Previous work identified the molecular targets for empedopeptin and provided a concise picture of the mechanism of action. It was shown that empedopeptin bind lipid II as its primary target in a 2:1 complex in presence of calcium.[1]

The first part of this study aimed to investigate the mechanisms of action of all members of this group in more detail and to gain insights in the molecular targets. Therefore, plusbacins and empedopeptin were obtained by cultivating their producer strains PB-6250 and ATCC 31962, respectively, and isolated chromatographically. Tripropeptin was made available to us by the Institute of Microbial Chemistry (BIKAKEN), Japan.

Plusbacin A_3, the plusbacin derivative of interest, was obtained in a mixture with other plusbacin derivatives, since the isolation of a single component was not achievable. However, it was possible to obtain Plus A_2 as single component employing a phosphate buffer.

In order to increase plusbacin A_3 production, the production medium was supplemented with biosynthetic precursors, generating the branched fatty acids. Thereby, cultivations in linseed medium supplemented with precursors did not reveal a positive effect on the production of plusbacin A_3 while cultivations in R2A medium, supplemented with precursors, instead showed that the production of plusbacins A_2/B_2 was significantly improved in a dose-dependent manner by addition of L-leucine and a slight positive effect on the production of plusbacins $A_3/A_4/B_3/B_4$ was observed by the addition of L-valine.

Empedopeptin was obtained in sufficient amounts to confirm the structure including the ring closure by HR-MS and NMR experiments. The obtained material was provided for serial passaging experiments. Other Emp derivatives obtained could be analysed and illustrated by molecular MS networking.

Summary

For determination of the solution structure of the CLPs with 3-lipid II by NMR, uniformly ^{15}N-labelled lipopeptide was required. ^{15}N-labelled plusbacin A_3 could only be obtained in a mixture of plusbacin derivatives, whereas ^{15}N-labelled empedopeptin was isolated in a sufficient amount to confirm the structure. Additionally, two Emp derivatives were isolated and their structures analysed by NMR.

The initial analysis of the interaction study of ^{15}N-labelled Emp with 3-lipid II revealed that the western hemisphere of Emp and the pyrophosphate moiety of the 3-lipid II are involved in the interaction.

The second part of this study was aimed to find new lipopeptides in *Pseudomonas* bacteria of the strain collection of Tübingen by using genome mining techniques. Seven strains belonging to the species *P. viridiflava* were prioritized and selected for in-depth analysis due to the presence of an octapeptide gene cluster in all of them.

In a first step, a suitable cultivation medium was determined and the best producer for the targeted octalipopeptides was evaluated and identified as *P. viridiflava* P1.A2. It was demonstrated that all seven strains produce the known compounds cichofactins A and B, as well as two minor congeners. The chemical structures of cichofactin A and B were confirmed by NMR and HR-MS analysis. The obtained cichofactins A and B were then subjected to a screening against a variety of human pathogenic bacteria, but the observed activity was moderate, as was the cytotoxicity.

Different strategies were applied to increase the production of the minor derivatives (named as cichofactin C and cichofactin D). In the first strategy, the media was enriched with plant extracts of *Arabidopsis thaliana* known to interact with *P. viridiflava* strains resulting in a doubling of their production rate. In the second approach, L-isoleucine was added to the cultivation medium, which increased the production rate of cichofactin C and D by fourfold. The structures were identified by HR-MS analysis in comparison with the known cichofactins A and B, as the amounts obtained were not sufficient for a complete structural analysis by NMR. Third, the cultivation medium was supplemented with L-leucine which resulted in the production of two additional congeners, designated cichofactin E and F, respectively. The structures were elucidated by HR-MS and NMR experiments.

Zusammenfassung

Lipopeptide bilden eine strukturell vielfältige Gruppe von Stoffwechselprodukten, die von einer Vielzahl von Bakterien produziert werden. Die beträchtliche strukturelle Vielfalt der Lipopeptide lässt vermuten, dass diese Metaboliten unterschiedliche natürliche Funktionen haben, und die vorliegende Arbeit konzentriert sich auf zwei dieser Lipopeptid-Gruppen.

Guanidinhaltige Lipopeptid-Antibiotika bilden eine Gruppe natürlich vorkommender zyklischer Lipopeptide, zu denen Empedopeptin (Emp), Plusbacin (Plus) und Tripropeptin (Tpp) gehören, die eine starke antibakterielle Wirkung gegen eine Vielzahl von Gram-positiven Krankheitserregern aufweisen. Trotz ihrer großen strukturellen Ähnlichkeit weisen diese Lipopeptide erhebliche Unterschiede in ihrer Wirksamkeit auf. In früheren Arbeiten wurden die molekularen Zielstrukturen von Empedopeptin identifiziert und erlaubten erste Einblicke in den Wirkmechanismus. Empedopeptin bindet nachweislich Lipid II als sein primäres Target in Gegenwart von Kalzium in einem 2:1-Komplex.[1]

Das erste Ziel dieser Studie war es, die Wirkmechanismen aller Mitglieder dieser Gruppe genauer zu untersuchen und ein besseres Verständnis bezüglich der Target-Interaktion auf molekularer Ebene zu erlangen. Durch Kultivierung der Produzentenstämmen PB-6250 bzw. ATCC 31962 wurden die Metaboliten Plusbacin und Empedopeptin produziert und chromatographisch isoliert. Tripropeptin wurde uns vom Institute of Microbial Chemistry (BIKAKEN), Japan zur Verfügung gestellt.

Plusbacin A_3, das aktivste Plusbacin-Derivat, wurde in einem Gemisch mit anderen Plusbacin-Derivaten gewonnen, da die chromatograpische Trennung der einzelnen Komponenten nicht realisierbar war. Plus A_2 hingegen konnte als Einzelkomponente, unter Verwendung eines Phosphatpuffers, erhalten werden.

Um die Produktion von Plusbacin A_3 zu steigern, wurden die Produktionsmedien mit Vorläufern der Biosynthese verzweigter Fettsäuren supplementiert. Die Kultivierung in Leinsamenmedium, das mit Vorläufern ergänzt wurde, hatte keinen positiven Effekt auf die Produktion von Plus A_3. Im Gegensatz dazu zeigte die Kultivierung in R2A-Medium, das mit Vorstufen ergänzt wurde, dass die Produktion der Plusbacine A_2/B_2 durch die Zugabe von L-Leucin dosisabhängig signifikant

verbessert wurde. Eine leicht positive Wirkung auf die Produktion von Plus $A_3/A_4/B_3/B_4$ wurde durch die Zugabe von L-Valin beobachtet.

Empedopeptin wurde in ausreichender Menge gewonnen, um die Struktur einschließlich Ringschluss durch HR-MS- und NMR-Experimente zu bestätigen. Das gewonnene Emp wurde für serielle Passage-Experimente zur Verfügung gestellt. Weitere Emp-Derivate konnten unter Einbeziehung der molecular MS networking Methode analysiert und charakterisiert werden.

Für die Bestimmung der Lösungsstruktur von CLPs mit 3-Lipid II durch NMR war ein vollständig ^{15}N-markiertes Lipopeptid erforderlich. ^{15}N-markiertes Plusbacin A_3 konnte nur in einer Mischung von Plusbacin-Derivaten gewonnen werden, während ^{15}N-markiertes Empedopeptin in ausreichender Menge isoliert werden konnte, um die Struktur zu bestätigen. Zwei Emp-Derivate wurden ebenfalls isoliert und ihre Strukturen mittels NMR analysiert.

Die erste Analyse der Interaktionsstudie von ^{15}N-markiertem Emp mit 3-Lipid II ergab, dass die westliche Hemisphäre von Emp und der Pyrophosphatanteil von 3-Lipid II an der Interaktion beteiligt sind.

Der zweite Teil dieser Studie zielte darauf ab, mit Hilfe von Genome Mining neue Lipopeptide in *Pseudomonas*-Bakterien aus der Tübinger Stammsammlung zu finden. Sieben Stämme, die zur Spezies *P. viridiflava* gehören, wurden aufgrund des Vorhandenseins eines Oktapeptid-Genclusters in allen Stämmen für eine eingehende Analyse ausgewählt.

In einem ersten Schritt wurde ein geeignetes Kultivierungsmedium bestimmt, und der beste Produzent für die angestrebten Octalipopeptide wurde bewertet und als *P. viridiflava* P1.A2 identifiziert. Es wurde nachgewiesen, dass diese sieben Stämme die bekannten Verbindungen Cichofactin A und B sowie zwei Derivate produzieren. Die chemischen Strukturen von Cichofactin A und B wurden durch NMR und HR-MS Experimente bestätigt. Die erhaltenen Cichofactine A und B wurden anschließend einem Screening gegen eine Vielzahl humanpathogener Bakterien unterzogen, jedoch sind die beobachtete Aktivitäten lediglich als moderat einzustufen, ebenso die Zytotoxizität.

Es wurden verschiedene Strategien angewandt, um die Produktion der Derivate, Cichofactin C und D, zu steigern. Bei der ersten Strategie wurde das Medium mit Pflanzenextrakten von *Arabidopsis thaliana* angereichert, von denen bekannt ist, dass sie mit *P. viridiflava* Stämmen interagieren, was die Produktivität etwa verdoppelte. Im zweiten Ansatz wurde dem Nährmedium L-Isoleucin zugesetzt, was die Produktionsrate von Cichofactin C und D um das 4-fache erhöhte. Die Strukturen wurden durch HR-MS-Analyse im Vergleich zu den bekannten Cichofactinen A und B identifiziert, da die erhaltenen Mengen für eine vollständige Strukturanalyse mittels NMR nicht

ausreichten. Drittens wurde das Kultivierungsmedium mit L-Leucin ergänzt, was zur Produktion von zwei weiteren Derivaten führte, die als Cichofactin E bzw. F bezeichnet wurden. Die Strukturen wurden durch HR-MS- und NMR-Experimente aufgeklärt.

I Introduction

I.1 Lipopeptides and their Structural Diversity

Lipopeptides (LPs) form a structurally diverse class of natural products and are produced by fungi, algae, plants and a variety of bacterial genera mainly from *Actinomyces* spp., *Actinoplanes* spp., *Bacillus* spp., *Burkholderiae* spp., *Streptomyces* spp., as well as plant-associated *Pseudomonas* spp.[2] The core structure of LPs consists of an oligopeptide ranging from 2 – 25 amino acids which is N-terminally acylated with a fatty acid moiety in the length of 5 – 20 carbon atoms.[3,4] Additionally, the structure of the fatty acids is variable such as β-hydroxylated groups as well as *iso*- and *anteiso*-methyl branched forms (**Figure I-1**).[5] The majority of the native LPs consist of complex cyclic structures. They can form a macrolactam or – lactone ring that is formed between two amino acids in the peptide chain or the C terminus of the peptide and a hydroxyl group of a serine or threonine. The ring size ranges from 4 to 14 amino acid residues. Cyclisation of the peptide moiety increases the *in vivo* stability of the motif compared to linear lipopeptides. The reason for this is a reduced proteolysis resulting from the lack of free C- and N-termini.[6,7]

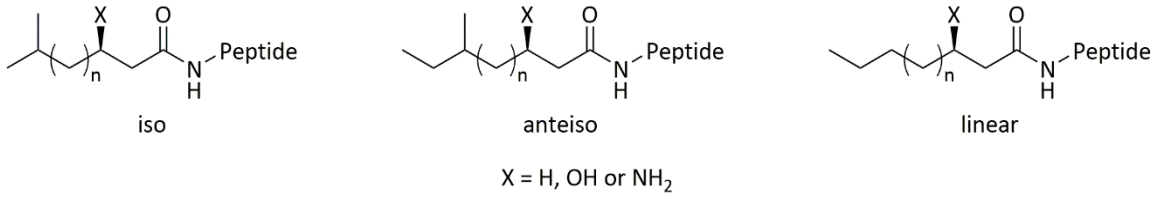

Figure I-1: Examples of lipid tail variations.

The oligopeptide part consists of a mixture of constituents including proteinogenic, modified and non-proteinogenic amino acids. These include D-/*allo*-configurated, *O*-methylated, *N*-methylated, chlorinated, hydroxylated (e.g. 3-hydroxyaspartic acid) or β-amino acids (**Figure I-2**)[8]. These unusual amino acids are incorporated by nonribosomal peptide synthetases (NRPSs) (**Chapter I.3**).

The occurrence of these mixtures of constituents as well as the cyclisation are features that make cyclic lipopeptides (CLPs) less susceptible to ubiquitous peptidases. In addition, the structural nature of lipopeptides, which simultaneously bear a hydrophobic (fatty acid side chain) and a hydrophilic (oligopeptides) moieties, classifies them as amphiphilic molecules.

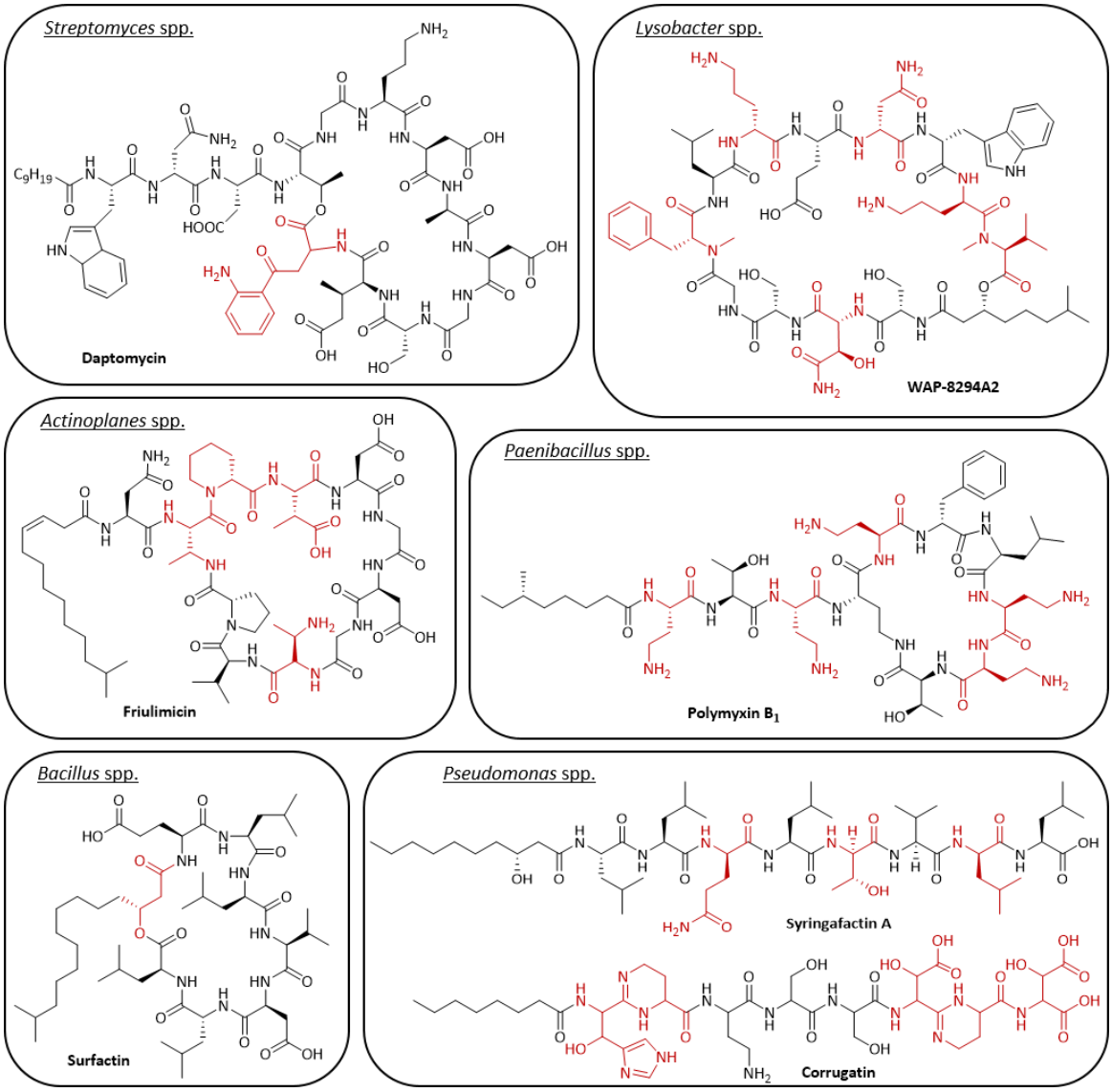

Figure I-2: Structural diversity of lipopeptides.

Depiction of daptomycin, friulimicin, surfactin, WAP-8294A_2, polymyxin B_1, surfactin, syringafactin A and corrugatin, which represent non-ribosomal lipopeptides (NRLPs) from different genera and have unique structural motifs (highlighted in red).

I.2 Lipopeptides and their Natural Functions

The wide structural variety of LPs indicates that these metabolites have distinct functions and different natural roles. Some of these roles may be unique to the biology of the producing organism.[2]

The following chapter provides a detailed overview of the diverse functions of lipopeptides. Pharmaceutically, they are used for the treatment of a variety of diseases including bacterial infections, as antitumor agents, immunosuppressants (e.g. cyclosporine A[9]) as well as surfactants.[2] Further, the physiological functions are discussed like the cell motility, biofilm formation and development as well as the plant pathogenesis.

I.2.1 Pharmaceutical Activities

Cyclic lipopeptides (CLPs) show activity against a wide range of species, including multi-resistant human-pathogenic bacteria such as MRSA and viruses. In general, bactericidal activity of lipopeptides is increased with an appropriate length of the lipid moiety (typically $C_{10} – C_{12}$), while lipopeptides bearing a lipid moiety with higher carbon content (such as $C_{14} – C_{16}$) exhibit enhanced antifungal activity in addition to antibacterial activity.[10,11]

Currently, there are two cyclic lipopeptides on the market which are approved as last resort antibiotics. On the one hand daptomycin which is the only lipopeptide antibiotic approved for clinical use, while two polymyxins are available for human treatment.[12] These two classes amongst others serve as cornerstones in our medical system.[13] The following covers these therapeutically significant CLPs and those which are of interest for clinical trials.

I.2.1.1 Daptomycin

Daptomycin (**Figure I-3**) was first isolated from *Streptomyces roseosporus* in 1987 [14] with a potent bactericidal activity against most Gram-positive pathogens including antibiotic-resistant strains such as methicillin-resistant *Staphylococcus aureus* (MRSA) and vancomycin-resistant *S. aureus* (VRSA).[15] Daptomycin (Cubicin®) was approved in the USA in 2003 for the treatment of complicated skin and skin structure infections caused by certain Gram-positive pathogens.[16,17]

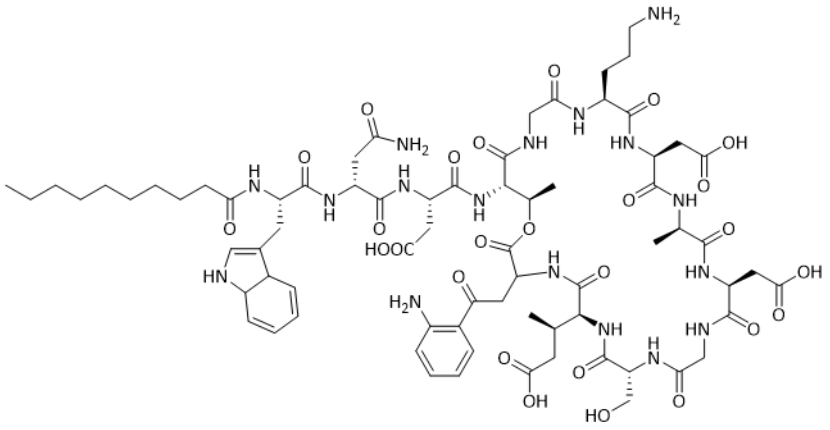

Figure I-3: Structure of daptomycin (Cubicin®).

Notably, there is little or no activity given for daptomycin in the absence of Ca^{2+}, whereas a maximum of antibacterial potency is achieved with a Ca^{2+} concentration of around 50 mg/L (1.25 mM) resulting in aggregation into oligomeric structures (14 to 16-mers).[18–20] This Ca^{2+} concentration corresponds to the concentration which is normally found in human serum.[21] Since its antibacterial activity depends on the presence of calcium ions, daptomycin belongs to the group of calcium-dependent lipopeptide antibiotics. The mode of action of daptomycin was just recently solved, showing that daptomycin targets the cell wall biosynthesis by forming a tripartite complex.[22] This complex is formed in the presence of calcium, the membrane lipid phosphatidylglycerol (PG) and lipid II, important building blocks for cell wall biosynthesis. The complex formation triggers delocalisation of the cell wall biosynthetic machinery, followed by dissolution of the membrane bilayer, finally leading to membrane leakage and cell death.[22]

I.2.1.2 Colistin and the Polymyxins

The polymyxins represent the first class of clinically used lipopeptide antibiotics with polymyxin B first isolated in 1947 and polymyxin E (colistin) identified in 1949 from *Paenibacillus polymyxa* var. *colistinus*.[23–25] Polymyxin B and colistin only differ in one amino acid moiety at position 6 of the peptide backbone, D-phenylalanine instead of a D-leucine group.[26]

This class is highly potent towards various Gram-negative bacteria such as *P. aeruginosa, Klebsiella, Acinetobacter* and *Enterobacter* species which can be explained by their mode of action.[27,28] Polymyxins show a specific electrostatic interaction with lipopolysaccharide (LPS) of the anionic outer membrane, a target structure which is indispensable in Gram-negative bacteria. This results in a destabilisation of the outer membrane as the polymyxins displace the present calcium and magnesium bridges in the outermost leaflet of the cell surface bilayer by competing with them.[29–31] In addition, the short lipophilic side chain of the polymyxin structure interacts with

LPS molecules leading to further damage of the cell surface bilayer and facilitating the insertion of the lipopeptides into the outer membrane. Subsequently, this results in an increase of the cell envelop permeability and leakage of ions, molecules and small proteins which is followed by cell death.[32,33]

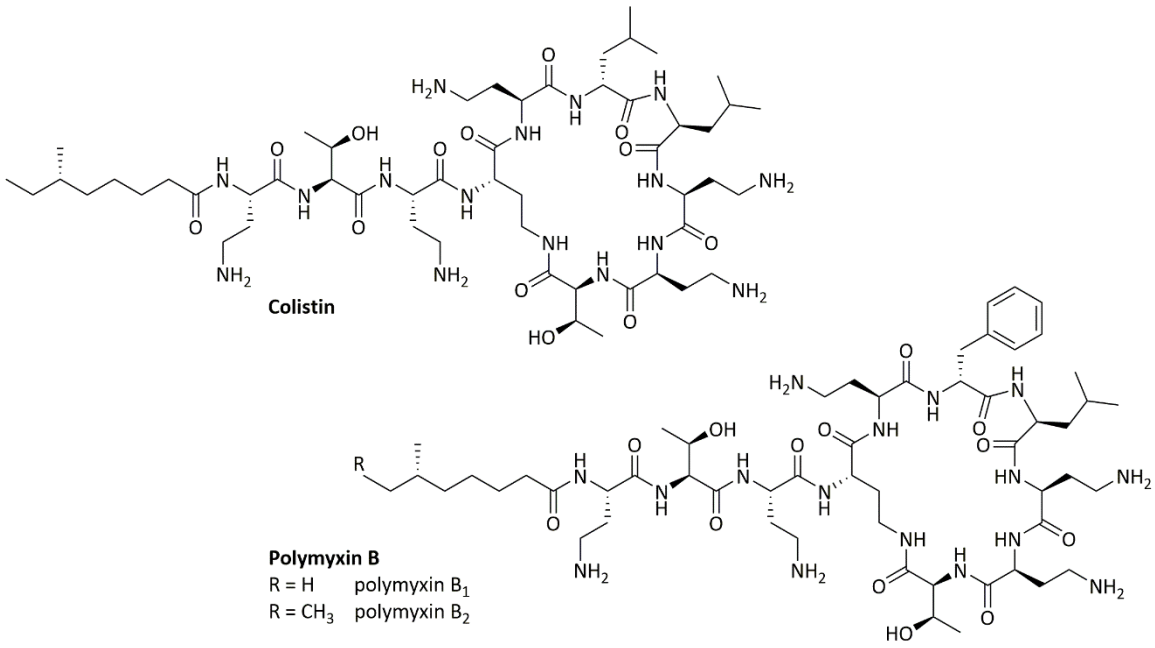

Figure I-4: Structure of Colistin (polymyxin E) and polymyxin B.

I.2.1.3 Guanidine-Containing Cyclic Lipopeptides

Guanidine-containing cyclic lipopeptides are another promising compound class with potent antibacterial activity against Gram-positive bacteria including important antibiotic-resistant strains, such as methicillin-resistant *Staphylococcus aureus* (MRSA), penicillin-resistant streptococci and vancomycin-resistant enterococci (VRE).[34–36] Within this class, the naturally occurring empedopeptin (Emp), plusbacins (Plus) and tripropeptins (Tpp) comprise a type of guanidine-containing cyclic lipopeptides. Characteristic for the guanidine-containing lipopeptides is the presence of an arginine and two hydroxyaspartic acids (OH-Asp).[8] The structure of these CLPs is highly similar and they differ only in three amino acids in the peptide backbone and in the length and branching of the fatty acid side chain (**Figure I-5**).

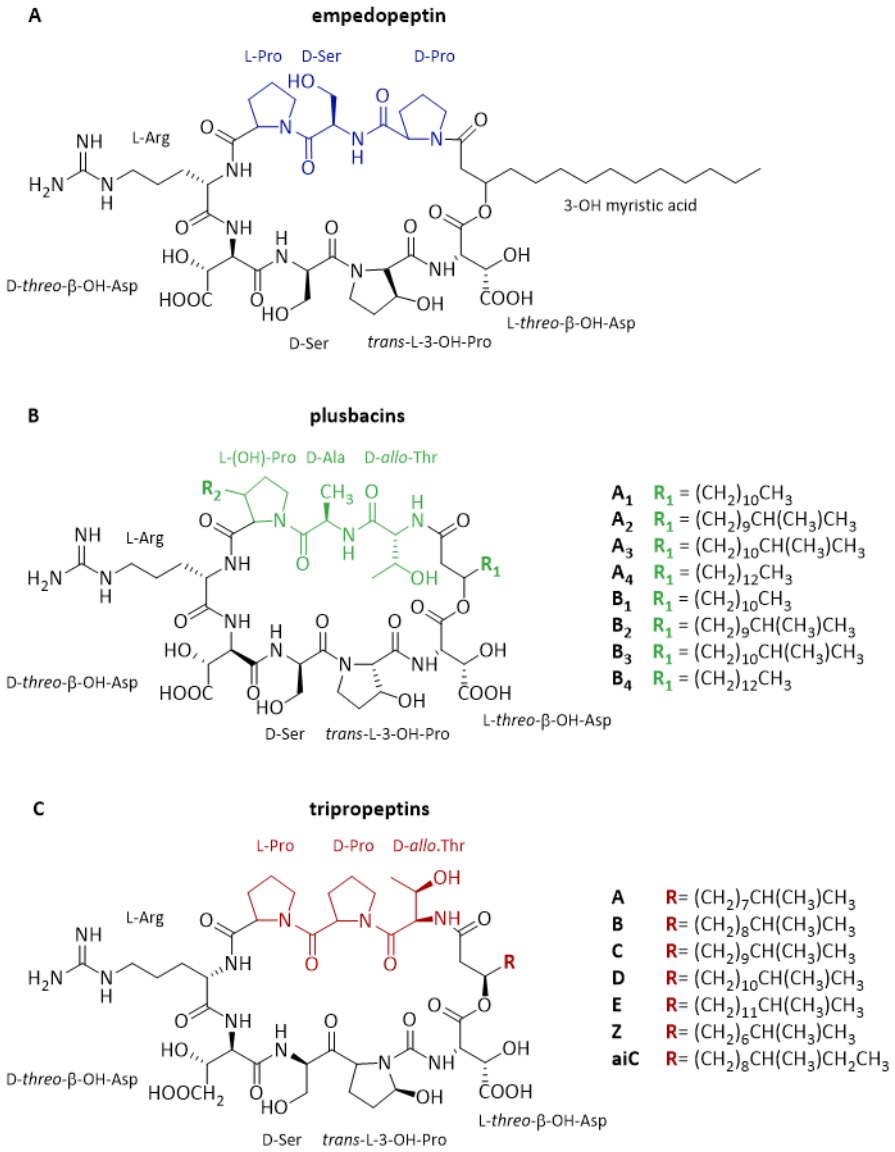

Figure I-5: Chemical structures of empedopeptin, plusbacins and tripropeptins.
The variation in the peptidic backbone as well as the fatty acid side chain is marked in color.

Empedopeptin was isolated for the first time in 1984 from the Gram-negative bacterial strain *Massilia* sp. (formerly *Empedobacter haloabium*) ATCC 31962 as a single derivative without variations in the fatty acid side chain (**Figure I-5 A**).[34,37] Antimicrobial activity was shown against a variety of multi-drug-resistant aerobic and anaerobic Gram-positive pathogens, *in vitro* and *in vivo*. Minimal inhibitory concentrations (MICs) are similar to those of vancomycin, and combined with low acute toxicity and good pharmacokinetic parameters, Emp is a promising compound in light of increasing vancomycin resistance.[34]

Analysis of the molecular mechanism of action showed that Emp targets the peptidoglycan biosynthesis by binding the cell wall building block lipid II as its primary target in a 2:1 complex in presence of calcium.[1] In order to narrow down the binding site of Emp, antagonization assays of

Emp and peptidoglycan precursors were performed (**Table I-1**). These showed that the strongest antagonization effect occurred between Emp and lipid I and lipid II. Antagonization by lipid I congener with truncated peptide side chains, wall teichoic acid precursor lipid III and undecaprenyl pyrophosphate (C_{55}-PP) was slightly less effective. In contrast, no effect was observed with C_{55}-P and the nucleotide-activated peptidoglycan sugars UDP-GlcNAc and UDP-MurNAc-pp. In summary, the binding site of Emp with lipid II involves the pyrophosphate group, the first sugar as well as the first one or two amino acids of the stem peptide and the proximal part of the undecaprenyl chain.[1]

Table I-1: Antagonization assays of different cell wall precursors and their truncated variants with empedopeptin.

Emp at 8x MIC was exposed to the potential antagonists at the indicated molar ratios before being mixed with *B. subtilis* in culture broth containing 1.25 mM Ca^{2+}. The results of two independent experiments are summarized as follows.[1] +: antagonization; -: no antagonization.

Lipid intermediate	Molar ratio of precursors to Emp						
	10x	**5x**	**2.5x**	**1.25x**	**0.625x**	**0.3125x**	**0.156x**
UDP-GlcNAc	-	-	-	-	-	-	-
UDP-MurNAc-pp	-	-	-	-	-	-	-
C_{55}-P	-	-	-	-	-	-	-
C_{15}-PP	+	+	+	-	-	-	-
C_{55}-PP	+	+	+	-	-	-	-
Lipid I (dipeptide)	+	+	+	+	+	-	-
Lipid I (tripeptide)	+	+	+	+	+	-	-
Lipid I (pentapeptide)	+	+	+	+	+	+	-
Lipid II	+	+	+	+	+	+	-
Lipid III	+	+	+	+	-	-	-

Plusbacins were first isolated in 1992 from *Lysobacter firmicutimachus* PB-6250^T, previously *Pseudomonas* sp. and to date, eight different plusbacin derivatives (A_1 – A_4 and B_1 – B_4) have been identified (**Figure I-5 B**).[35,38] The fatty acid side chain can differ in length and branching and also the amino acid 7 can either be proline or hydroxy proline.

Early studies on the mechanism of action of plusbacin A_3, the most active Plus derivative, suggested an interference with the membrane bound steps of peptidoglycan biosynthesis. The incorporation of *N*-acetylglucosamine, a precursor of the cell wall biosynthesis, is inhibited with IC_{50} values (inhibitory concentration of 50%), which correspond to its MIC value.[39] *In vitro* investigations revealed that Plus A_3 inhibited the formation of lipid intermediates as well as nascent peptidoglycan, in contrast to vancomycin, that did not show any effect on the formation of lipid intermediates.[39]

A structure-activity relationship (SAR) study proposed that Plus A_3 interacts with the pentaglycine interpeptide bridge of lipid II, that is specifically bound to the L-lysine of the lipid stem peptide of *S. aureus*. [40] The molecular role of the isotridecanyl side chain remains still elusive. However, this study revealed that the fatty acid side chain is essential for antimicrobial activity. This finding was also corroborated by testing a Plus A_3 derivative, missing the fatty acid side chain, which showed a complete loss of biological activity.[40]

A recent solid-state NMR study did not detect conclusive interactions with lipid-linked peptidoglycan precursors suggesting an alternative mechanism of action involving membrane perturbation by a dual mode of action.[41] This hypothesis was based solely on studies with Plus derivatives and was not verified by experiments analysing the direct interaction of Plus derivatives with the target.

Tripropeptins were isolated from *Lysobacter* sp. BMK333-48F3 and comprises seven derivatives (A-E, Z and aiC) which vary in the fatty acid side chain (**Figure I-5 C**).[42–46] The activity of tripropeptins seems to increase with the length of the fatty acid side chain, while tripropeptin D shows the strongest microbial activity.[36,42] Studies of Tpp C revealed that bactoprenol-pyrophosphate (C_{55}-PP) is kept at the periplasmic site, by formation of a complex with Tpp C in presence of Ca^{2+}, in a similar fashion to bacitracin.[47] Blocking C_{55}-PP prevents recycling of the universal lipid carrier C_{55}-PP, which is only present in limited amounts in the cell. In addition, a recent study of Tpp C with β-lactam antibiotics showed highly synergistic effects against MRSA strains, leading to a potentially effective therapeutic strategy for MRSA infections.[48] However, this effect cannot be explained by binding to prenyl-pyrophosphate, which may indicate the interference with another antibiotic target.

I.2.2 Natural Functions

Natural functions of LPs in microorganisms have received significantly less attention compared to the research on the antimicrobial, antitumor and immunosuppressant activities of lipopeptides.[2] The huge structural diversity of this group already indicates an enormous functional versatility, while certain LPs seem to be unique due to the biology of their producing organism. The following will give an overview of different functions of *Pseudomonas* and *Bacillus* LPs such as cell motility, biofilm formation and colonization as well as the role in plant pathogenesis.

I.2.2.1 Role in Motility

Lipopeptides are often involved in the movement of their producers and there are several mobility mechanisms such as swarming, swimming, twitching, gliding and sliding.[49] Surfactant properties of the LPs are used to lower the tension between the surface and the bacterial cell.[50] The reduction of the surface tension of liquids is enabled by the amphiphilic character of LPs, in a concentration-dependent manner, thereby turning them into biosurfactants. While the hydrophilic part is immersed in the aqueous phase, the hydrophobic part interacts with lipophiles. This includes nonpolar molecules and lipophilic parts of other amphiphiles.[51] The LPs initially form a monolayer on the liquid surface. With increasing surfactant concentration, the surface becomes saturated until the so called critical micelle concentration (CMC) is reached.[52] At this concentration, the minimum of the surface tension of the liquid is reached and addition of further biosurfactants leads to formation of micelles in the liquid phase.

Many LPs produced by *Pseudomonas* spp. are capable of reducing the surface tension of growth media to varying degrees as shown in **Table I-2**, such as viscosin, orfamide A and arthrofactin A to only mention a few of them.[4,53] The combination of the surfactant property and the actively rotating flagella pushes the bacteria forward and spread over solid surfaces. Individual movement of bacterial cells is called swimming, while swarming is the multicellular movement of bacteria over a surface. In order to analyse the effect of LPs on the motility of *Pseudomonas* strains, LP-deficient mutants were generated and subsequently tested *in vitro* on semi-solid agar plates. In most cases, these mutants lost their surface motility. By addition of LPs to the growth medium, motility could be restored, demonstrating that lipopeptide production is necessary for bacterial motility.[54–57]

Table I-2: Surface properties of pseudomonal lipopeptides.

[a] CMC [mg/L] in water. [b] Minimum surface tension between air and water at the CMC [mN/m] at 20 – 25 °C [c] Can the swarming ability of the producing *Pseudomonas* strain be attributed to the corresponding lipopeptide?; n.n. = not determined.[4]

Lipopeptide	CMC[a]	γ_{CMC}[b]	Swarming?[c]
Syringafactins	n.d.	n.d.	Yes
Cichofactins	n.d.	n.d.	Yes
Pseudofactin II	72	32	n.d.
Viscosin	54	28	Yes
WLIP	n.d.	n.d.	Yes
Massetolide A	n.d.	n.d.	Yes
Syringomycin E	1250	33	n.d.
Cormycin A	176	n.d.	n.d.
Nunamycin/nunapeptin	n.d.	n.d.	Yes
Orfamides	n.d.	n.d.	Yes
Orfamide A	~10	38	n.d.
Poaeamide A	15	~40	Yes
Amphisin	n.d.	n.d.	Yes
Anikasin	n.d.	n.d.	Yes
Arthrofactin A	14	24	Yes
Gacamide A	33	29	Yes
Putisolvins	n.d.	n.d.	Yes
Entolysin	n.d.	n.d.	Yes
Xantholysins	n.d.	n.d.	Yes
Tolaasin I/II (mixture)	460	42	No
Sesselins	n.d.	n.d.	No
SP22-A	820	40	n.d.
SP22-B	800	41	n.d.
SP25-A	2160	n.d.	n.d.

I.2.2.2 Role in Biofilm Formation and Development

Biofilms are highly organised microbial matrices that occur as surface-attached communities or suspended aggregates. They consist of bacterial cells embedded in a self-produced matrix composed of polymers such as polysaccharides and protein, forming a hydrated gel-like slime.[58,59] For *Bacillus* and *Pseudomonas* spp., lipopeptides play an important role in surface attachment and biofilm formation, although the outcome depends on the type of LP, as the structural similarity of LPs does not indicate whether they are involved in the formation or inhibition of biofilm formation.[2,4]

An example of the dependence on the type of LP is observed on the one hand with massetolide A, which has a positive effect on biofilm formation, while the closely related CLPs WLIP or viscosin have an inhibitory effect on biofilm formation (**Table I-3**).[55,60,61] Xantholysin and sessilin also support their producer in biofilm formation, whereas arthrofactins, cichofactins, orfamides and putisolvins inhibit the biofilm development.[57,62–65] The basic mechanism of biofilm formation and development is not yet clear, as only a few lipopeptides are known to have different and

sometimes contradictory effects in biofilm regulation.[66] They could be associated to the different physicochemical properties and the potential effect of LPs on the cell surface and substrate.[2]

Table I-3: Involvement of lipopeptides in biofilm formation by *Pseudomonas.*

+ positive effect on biofilm formation; - inhibition of biofilm formation[2,4]

Species	Biosurfactants	Biofilm formation
Pseudomonas cichorii	Cichofactins	-
Pseudomonas fluorescens	Massetolide A	+
Pseudomonas fluorescens	Viscosin	-
Pseudomonas protegens	Orfamides	-
Pseudomonas putida	WLIP	-
Pseudomonas putida	Xantholysin	+
Pseudomonas putida	Putisolvin I/II	-
Pseudomonas sp.	Sessilin	+
Pseudomonas sp.	Arthrofactin	-

I.2.2.3 Role in Plant Interactions

Lipopeptide-producing pseudomonads often colonise in bulk soil, the rhizosphere or in the phyllosphere which is the part of the plant above ground.[67–69] They can either be pathogenic of beneficial for plant growth. Therefore, many investigations were already performed on their capability of biocontrol and biostimulation.

In the following significant plant pathogens are listed that use lipopeptides as virulence factors. The first common known plant pathogen for example is *P. syringae* which produces the cyclic nonapeptide syringomycin that induces canker disease in peach trees (**Figure I-6 B**).[70] Other representatives for plant pathogens are *P. syringae* pv. *atrofaciens* which causes basal glume rot in wheat and other cereals, and *P. fuscovaginae* which induces sheath brown rot in rice. Syringomycin and syringopeptin (**Figure I-6 B** and **D**) as well as syringotoxin and fuscopeptin (**Figure I-6 B** and **D**) are produced by the latter, respectively.[71,72] They all belong to the cyclic pseudomonal lipopeptides with a peptide backbone of 9 to 25 amino acids. Cormycin A (**Figure I-6 B**) and corpeptin (**Figure I-6 D**), cyclic lipopeptides with 9 and 21 amino acids, are produced by *P. corrugata* which lead to induction of tomato pit necrosis.[73] Further known plant pathogens are *P. fluorescens* 5064 which induces broccoli head rot by its produced lipopeptide viscosin (**Figure I-6 C**), and *P. cichorii* SF1-54 that induces lettuce midrib rot.[74,75] The produced lipopeptides of *P. cichorii* are cichofactin (**Figure I-6 A**) and cichopeptin (**Figure I-6 D**). Cichofactin is the only linear lipopeptide listed in this overview and belongs to the group of syringafactins whose members consist of eight amino acids. The only difference to syringafactins is the exchange

of threonine by glutamine at position 5 in the peptide backbone. Cichofactins were first isolated in 2013.[65]

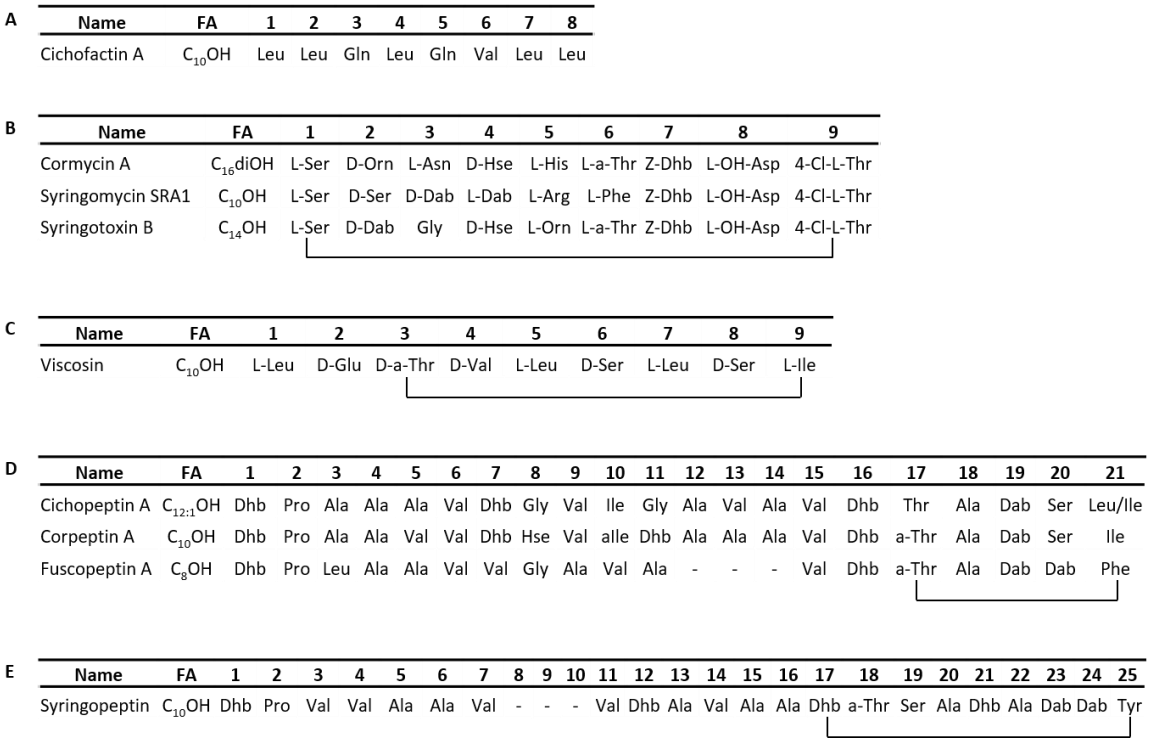

A

Name	FA	1	2	3	4	5	6	7	8
Cichofactin A	C_{10}OH	Leu	Leu	Gln	Leu	Gln	Val	Leu	Leu

B

Name	FA	1	2	3	4	5	6	7	8	9
Cormycin A	C_{16}diOH	L-Ser	D-Orn	L-Asn	D-Hse	L-His	L-a-Thr	Z-Dhb	L-OH-Asp	4-Cl-L-Thr
Syringomycin SRA1	C_{10}OH	L-Ser	D-Ser	D-Dab	L-Dab	L-Arg	L-Phe	Z-Dhb	L-OH-Asp	4-Cl-L-Thr
Syringotoxin B	C_{14}OH	L-Ser	D-Dab	Gly	D-Hse	L-Orn	L-a-Thr	Z-Dhb	L-OH-Asp	4-Cl-L-Thr

C

Name	FA	1	2	3	4	5	6	7	8	9
Viscosin	C_{10}OH	L-Leu	D-Glu	D-a-Thr	D-Val	L-Leu	D-Ser	L-Leu	D-Ser	L-Ile

D

Name	FA	1	2	3	4	5	6	7	8	9	10	11	12	13	14	15	16	17	18	19	20	21
Cichopeptin A	$C_{12:1}$OH	Dhb	Pro	Ala	Ala	Ala	Val	Dhb	Gly	Val	Ile	Gly	Ala	Val	Ala	Val	Dhb	Thr	Ala	Dab	Ser	Leu/Ile
Corpeptin A	C_{10}OH	Dhb	Pro	Ala	Ala	Val	Val	Dhb	Hse	Val	aIle	Dhb	Ala	Ala	Ala	Val	Dhb	a-Thr	Ala	Dab	Ser	Ile
Fuscopeptin A	C_8OH	Dhb	Pro	Leu	Ala	Ala	Val	Val	Gly	Ala	Val	Ala	-	-	-	Val	Dhb	a-Thr	Ala	Dab	Dab	Phe

E

Name	FA	1	2	3	4	5	6	7	8	9	10	11	12	13	14	15	16	17	18	19	20	21	22	23	24	25
Syringopeptin	C_{10}OH	Dhb	Pro	Val	Val	Ala	Ala	Val	-	-	-	Val	Dhb	Ala	Val	Ala	Ala	Dhb	a-Thr	Ser	Ala	Dhb	Ala	Dab	Dab	Tyr

Figure I-6: Overview of prominent plant pathogens.

A: Syringafactin group, linear octalipopeptide; **B:** Syringomycin group, cyclic nonapeptides; **C:** Viscosin group, cyclic nonapeptide; **D:** Tolaasin group; **E:** Syringopeptin group.

The common infection pathway of plant-pathogenic *Pseudomonas* spp. is described as follows. Initially, the leaf or fruit surfaces of plants are colonised by bacteria. Due to the biosurfactant properties of the produced lipopeptides, the bacteria can spread throughout the entire phyllosphere of the plants.[76] Thereby, stomata or cracks in the upper epidermis of leaves and fruits can be reached efficiently. Subsequently, the pathogens invade these open stomata or cracks to colonise the plant apoplast (extracellular space inside plant tissue).[77] After that, the pseudomonads change from an epiphytic (organism that grows on the surface of a plant) to an endophytic (organism that grows inside a plant) lifestyle and proliferate inside the plant tissue.[4] The immune system of the plant is activated and the pathogen starts to produce phytotoxic lipopeptides in order to gain access to nutrients by permeabilisation of plant cells.[78–80] In the end, this lack of resources results in the formation of necrotic plant tissue and in severe cases to death of the plant.

On the other hand, some lipopeptides have positive effects on plants by stimulating their immune system. For example, a plant-beneficial endophytic relationship is established between the *Pseudomonas poae* strain RE*1-1-14 and sugar beets. The cyclic lipopeptide poaeamide A (**Figure I-7**) which is produced by this strain is colonising a biofilm-like matrix on the roots of the plant, so that the strain can invade into the roots and proliferate inside the plant. The plant provides nutrients to the bacterial strain, and in return, the poaeamide produced by the endophyte has antagonistic activity against soil-borne plant pathogens such as the fungus *R. solani* and different oomycetes, including *Phytophthora capsica* and *Pythium ultimum*.[81]

Name	FA	1	2	3	4	5	6	7	8	9	10
Poaeamide A	$C_{10}OH$	L-Leu	D-Glu	D-allo-Thr	D-Leu	L-Leu	D-Ser	L-Leu	L-Leu	D-Ser	L-Ile

Figure I-7: Poaeamide A produced by the plant beneficial strain *Pseudomonas poae.*

Another non-pathogenic strain with beneficial effects on plants by stimulating the immune system of the plant is *Pseudomonas fluorescens.* Massetolide A (**Figure I-8**), a cyclic lipopeptide produced by this strain, resulted in significant protection in tomato leaves against infection by *P. infestans.*[82] Purified fengycins and surfactins, produced by *Bacillus subtilis*, were also able to increase the resistance of bean and tomato leaves to the fungal pathogen *B. cinerea*.[83]

Name	FA	1	2	3	4	5	6	7	8	9
Massetolide A	$C_{10}OH$	L-Leu	D-Glu	D-a-Thr	D-a-Ile	L-Leu	D-Ser	L-Leu	D-Ser	L-Ile

Figure I-8: Massetolide A produced by the non-pathogenic *Pseudomonas fluorescens.*

I.3 Biosynthesis of Lipopeptides

Cyclic as well as linear lipopeptides are produced by nonribosomal peptide synthetases (NRPSs) which are multi-enzyme complexes with a modular organisation. In contrast to ribosomal peptide and protein synthesis, nonribosomally produced peptides (NRPs) are not limited to proteinogenic amino acids. NRPSs can also incorporate non-proteinogenic amino acids including for example D-configurated or hydroxylated amino acids, carboxy acids and fatty acids, as mentioned in **Chapter I.1**.[84–86]

For the synthesis of NRPs a modular concept is used by nature, in which each module of the NRPS assembly line is responsible for the incorporation of one amino acid into the corresponding peptide product. According to this so-called 'colinearity rule', the biosynthesis of an octapeptide consists of eight such modules. The modules can be subdivided into the following three subunits: the adenylation (A) domain, the peptidyl carrier protein (PCP) domain, also referred as thiolation (T) domain, and the condensation (C) domain. Beside these three essential domains, additional modification domains can be integrated into a module including epimerisation (E), heterocyclisation (Cy), methylation (MT), reduction (R), formylation (F) and oxidation (Ox) domains. The termination module contains an additional thioesterase (TE) domain which is responsible to release the mature oligopeptide from the NRPS machinery.

I.3.1 Adenylation (A) Domain

The adenylation (A) domain consists of about 550 amino acid residues and is responsible for substrate recognition and activation. The specific amino (carboxy) acid substrates are selected from the available substrate pool and simultaneously activated as aminoacyl adenylates under consumption of Mg^{2+}-ATP (**Figure I-9 A**). In the next step, the aminoacyl adenylate intermediates are converted into aminoacyl thioesters by covalent attachment to the thiol groups of PCP domains under release of AMP (**Figure I-9 B**).[84]

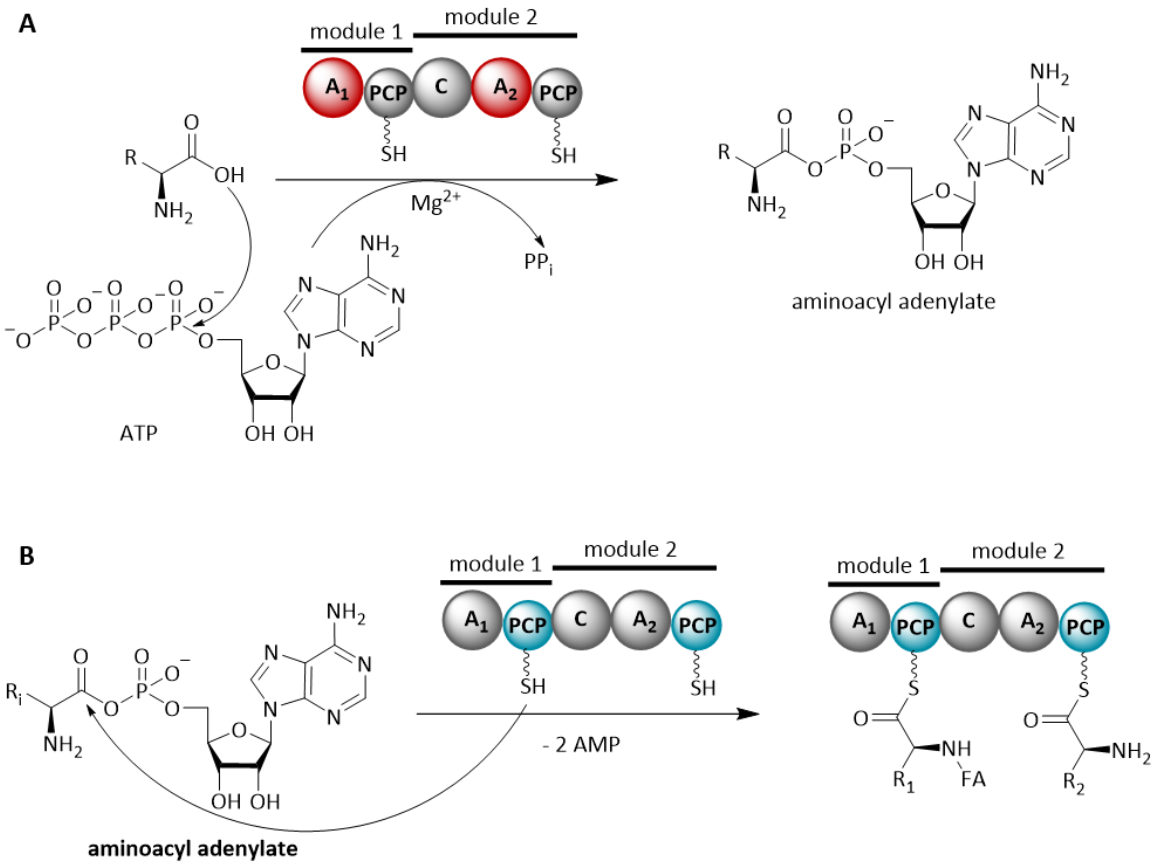

Figure I-9: The adenylation reaction catalysed by the A domains of NRPSs.

The modules consist of peptidyl protein (PCP), adenylation (A) and condensation (C) domains. **A:** The A domain catalyses recognition and activation of substrates under consumption of Mg^{2+}-ATP. **B:** Transfer of the aminoacyl adenylate intermediates to the thiol groups of the PCP domains resulting in aminoacyl thioesters.

The A domains are part of the ANL (Acyl-CoA synthetases, NRPS adenylation domains and Luciferase enzymes) superfamily of adenylating enzymes. Crystallisation and structural analysis of several members of this superfamily have been reported including the acetyl-CoA synthetase (Acs) of primary metabolism,[87] the oxidoreductase luciferase from *Photinus pyralis*,[88] the 2,3-dihydroxybenzoate (DHB) activating A domain (DhbE) from *B. subtilis*,[89] and the phenylalanine activating A domain of the first module of the gramicidin S synthetase (PheA) of *B. brevis*.[90] The protein sequence similarity between these crystal structures is low but they share a highly conserved three dimensional structure. The A domain consists of a small, flexible C-terminal and a large N-terminal subdomain. It was shown that the substrate binding pocket is located at the junction between these two subdomains consisting of up to 10 residues which determine the substrate specificity of A domains and define the non-ribosomal code.[88,91,92] These residues can be used to predict the specificity of biochemically uncharacterised NPRPs by sequence analysis.

In many studies about NRPS A domains, a relaxed substrate specificity of A domains was observed, which seems to be a strategy to increase product diversity of NRPS-producing organisms. This

promiscuity in substrate recognition is depending on the constellation of amino acid side chains in the binding pocket and leads to a certain flexibility, so that not only chemically similar residues such as arginine and lysine can be interchanged, but even chemically different substrates such as arginine and tyrosine.[93,94] Further studies have also indicated that the C domains can directly influence the substrate selectivity of the neighbouring A domains, presumably by stabilisation or destabilisation of specific conformational states within the NRPS catalytic cycle.[88]

I.3.2 Peptidyl Carrier Protein (PCP) Domain / Thiolation (T) Domain

The peptidyl carrier protein (PCP) domain, which is located downstream of the A domain, consists of about 80 – 100 amino acid residues and represents the transport unit for the transfer of the activated amino acid to move between the catalytic centres.

The inactive *apo*-PCP form is activated by adding coenzyme A (CoA). The 4'-phosphopantetheine (4'-PP) cofactor is post-translationally transferred from the CoA to a conserved serine residue of the PCP domain to obtain the active *holo*-form (**Figure I-10**). This conversion from *apo*-to-*holo* form is catalysed by phosphopantetheinyl transferases (PPTases) such as Sfb and Gsp from *B. subtilis* and *B. brevis*, respectively. The activated amino acids and peptides of the A domain are covalently attached to the free thiol moiety of the 4'PP-cofactor of the PCP domain forming an aminoacyl thioester.[84]

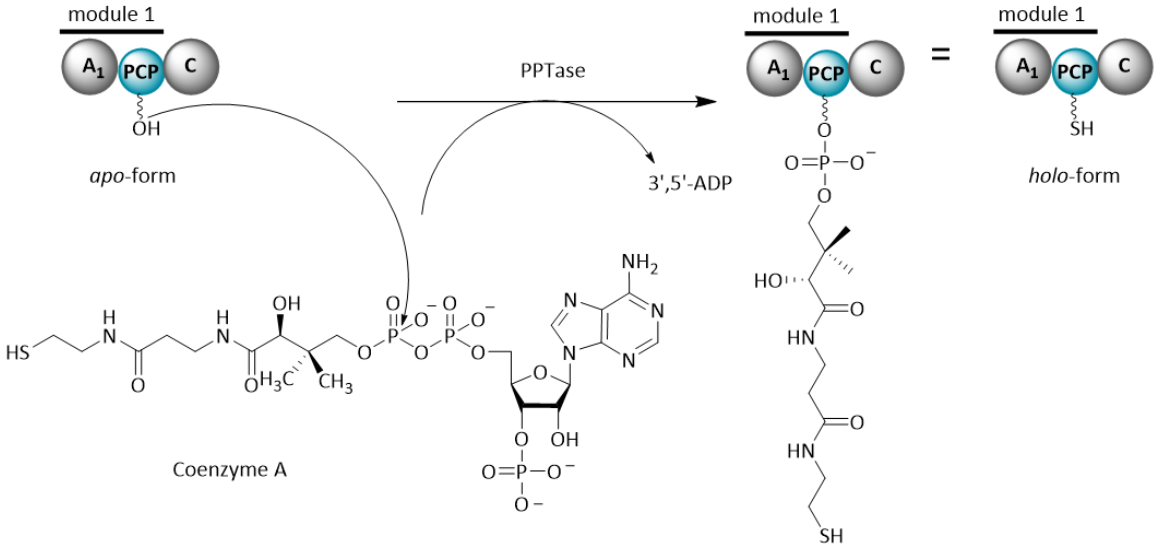

Figure I-10: Activation of PCP domain from *apo*-to-*holo* form.

I.3.3 Condensation (C) Domain

The third subunit is the condensation domain which is located downstream of the PCP domain and consists of about 450 amino acid residues.[95] The C domain catalyses the peptide bond formation via nucleophilic attack of the α-amino group of an aminoacyl thioester bound to the downstream module onto the acyl moiety of the amino acid attached to the corresponding upstream module (**Figure I-11**).[96] Condensation domains exhibit a certain substrate specificity by possessing an acceptor position for the aminoacyl thioester nucleophile with a strong stereo and side chain selectivity while the donor position of the electrophile is strictly stereo selective.[84]

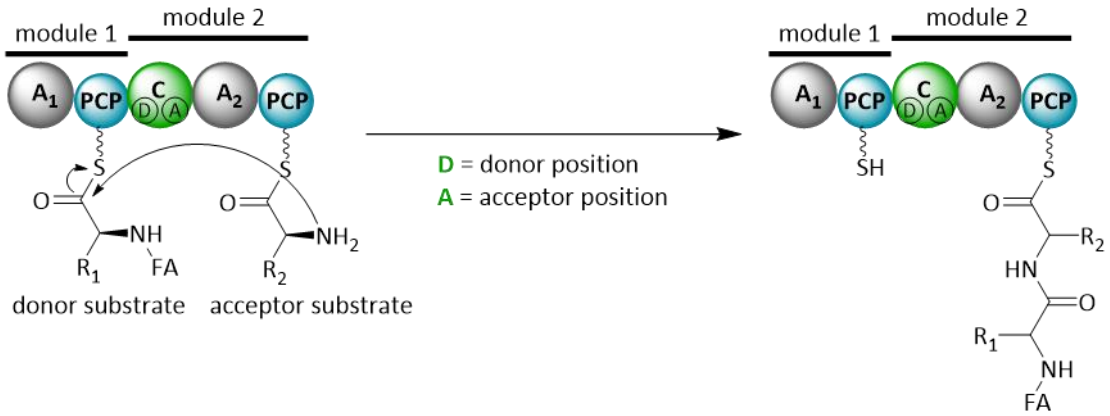

Figure I-11: The condensation domain catalyses the peptide bond formation.

Three different functional subtypes of the C domain exist: $^{L}C_{L}/^{D}C_{L}$, dual E/C and $C_{Starter}$ domains.[97] The $^{L}C_{L}$ domain catalyses the peptide bond formation between two L-amino acids while the $^{D}C_{L}$ domains condensates an activated D-amino acid with an L-amino acid. Similar to the latter is the dual epimerisation/condensation domain, which has an integrated epimerase activity where the L-amino acid is converted into the D-form and subsequently incorporated.[97] The last subtype is the $C_{Starter}$ domain which condensates the first amino acid with a (β-hydroxy-)carboxylic acid, typically a (β-hydroxy) fatty acid, via acylation.[97]

I.3.4 Thioesterase (TE) Domain

The growing peptide chain is transferred to the next module during synthesis, until the PCP domain of the last module is reached which in most cases contains a TE domain with a length of about 250 amino acids. This module is responsible for product release in a two-step process. In the first step, an acyl-*O*-TE-enzyme intermediate is obtained, which is subsequently hydrolysed (**Figure I-12 A**) or attacked by a peptide-internal nucleophile forming either lactam or lactone rings

(**Figure I-12 B** and **C**), resulting in a linear peptide such as syringafactin A (**Figure I-2**) or a macrocyclic product such as colistin (**Figure I-4**) or tripropeptin C (**Figure I-5**).[98]

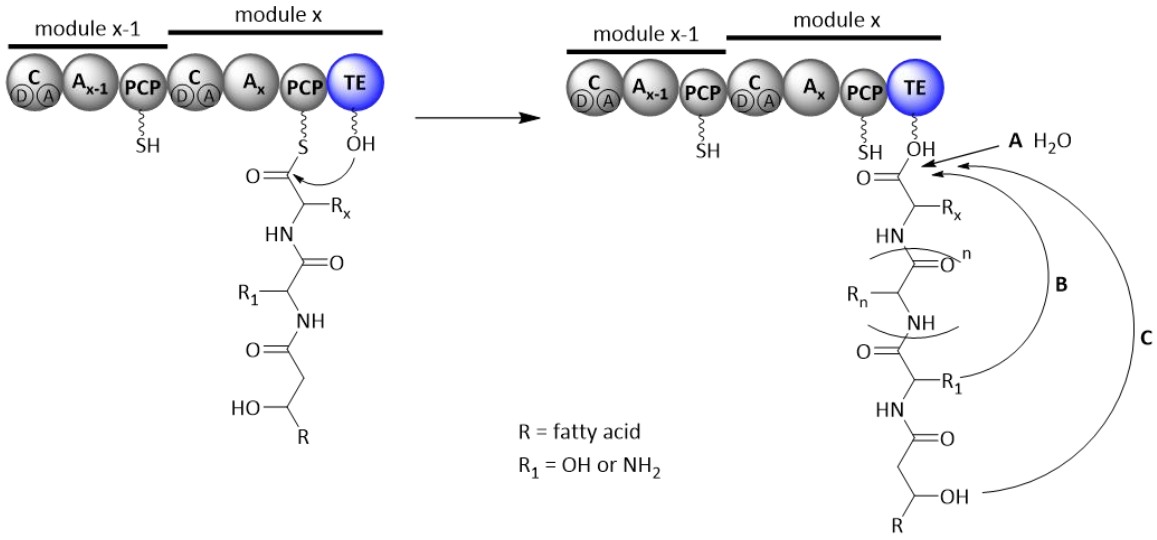

Figure I-12: Release mechanism in NRP lipopeptide biosynthesis.

A: The peptide is released from the TE domain by hydrolysis with water as nucleophile. **B:** Peptide release by nucleophilic attack of the OH or NH_2 group of the amino acid side chain forming a macrolactone or –lactam ring. **C:** Peptide release by nucleophilic attack of 3-OH group of a fatty acid resulting in a macrolactone ring formation.

TE domains can be divided in two functional classes (type I and type II TE proteins). Type I TE domains are responsible for specific recognition, macrocyclisation and product release, while type II TE domains have a function as repair enzymes in order to remove blockages of the 4'-PP cofactor arm caused by misprimed short-chain acyl-Co As.[86] All misprimed PCPs must be reliably recognised by TE II domains and the incorrect acyl or peptidyl group cleaved off without cleaving of the correct growing peptide.[99]

I.3.5 N- and C-Methyltransferase Domains

Amino acids in nonribosomal peptides are often N- and C-methylated which are introduced by methyltransferase (MT) domains.[84] The methyl group is typically transferred to the amino acid from the cofactor (*S*)-adenosyl methionine (SAM) of the MT domain, which is located at the C-terminus of the associated A domain, while the latter is attached to the PPant arm of the PCP domain.[99] This is observed in cyclosporine A where seven of eleven amino acids are N-methylated.[100]

Different to N-methyltransferases which methylate PCP bound amino acids, C-methyltransferases (C-MT) insert the methyl group to precursors leading to the final non-proteogenic amino acids.

For example, the acidic lipopeptides such as daptomycin and calcium-dependent antibiotics (CDA) contain β-methylated glutamate catalysed by a C-MT that is also SAM-dependent.[99]

I.4 Detection and Identification of Lipopeptides

Natural products have played an important role in the discovery of drugs in the past, providing many effective drugs and are promising to provide many more drugs in the future. Their discovery is important because the structure of many isolated compounds is quite complex and a simple synthetic approach is not possible. Traditionally, the search for new drugs from nature was based on systematic and chemotaxonomic analysis of microorganisms, plants and marine animals. Later on, bioassay-guided isolation strategies have been established as standard procedures to obtain new and significantly bioactive compounds. The typical procedure consists of the stepwise separation of the extracted compounds based on their different physicochemical properties and screening for biological activity, followed by the next round of separation and screening.[101,102] This approach has already led to the isolation of several secondary metabolites. However, nowadays this approach leads frequently to the rediscovery of already known natural products. Thus, new approaches are needed to find bioactive compounds hidden in genomes.

I.4.1 Genome Mining

In the last two decades, genomic science has become increasingly important since it enabled the identification of potential drug targets and the search for novel gene clusters for the biosynthesis of natural products. With the advent of genome sequencing techniques, the idea of genome mining was born, making it possible to predict and isolate natural products based on genetic information.[103]

Using sophisticated web-based tools such as antiSMASH, target genome sequences can be compared with known gene clusters to predict their function and structure.[104] Subsequently, the data are evaluated in terms of a potential secondary metabolite. Prediction works very well for biosynthetic enzymes such as NRPS, where the adenylation domains have highly conserved sequences and thus code for a very specific substrate.[105]

Thus, with regard to the colinearity rule, a corresponding amino acid sequence of the expected product can already be predicted which may already give a first indication of the natural product class or of the biological function of the peptide. The presence of certain domains can already allow conclusions about posttranslational modifications of the peptide. In combination with

instrumental analytical methods such as mass spectrometry or magnetic resonance spectroscopy, it is then possible to search specifically for the expected metabolites.[106–108]

Genome mining tools also uncovered a large number of gene clusters, also known as silent gene cluster, that code for the synthesis of potential secondary metabolites which are not detectable under standard laboratory conditions.[103,105] Therefore, recently using this approach, the cyclic lipopeptides orfamides from *Pseudomonas protegens* Pf-5 and poaeamides from *Pseudomonas poae* RE*1-1-14 were identified, both of which represent a new type of cyclic lipopeptide.[81,109]

I.4.2 Molecular Networking

Analysis of genome sequence data has shown that even well-known bacteria have the genetic potential to produce many more secondary metabolites than previous suggested.[110,111] Methods for the identification of known compounds and detection of new ones have been quite inefficient. Therefore, MS-based molecular networking is a technique that allows high-throughput comparisons between multi-strains, a rapid method for de-replication, and identification of new compounds with known structural motifs.[112–116]

For the MS-based molecular networking, compounds of interest characterized by mass spectrometry are subjected to fragmentation by MS/MS measurements. These MS/MS spectra are organised into groups based on the similarities in their fragmentation patterns and the expectations that structurally related molecules will result in similar MS/MS spectra (**Figure I-13 A**). Within these networks, each fragmentation is represented as a node and the similarity between each node is visualised by an edge (lines) (**Figure I-13 B**).[117,118] The thickness of the edge is determined by the degree of similarity between the MS/MS spectra. A series of interconnected nodes generally indicates structurally related molecules or molecular families (MFs).[114]

Molecular networking (MN) is accessible through the Global Social Molecular Networking of Natural Products (GNPS) web platform "https://gnps.ucsd.edu".

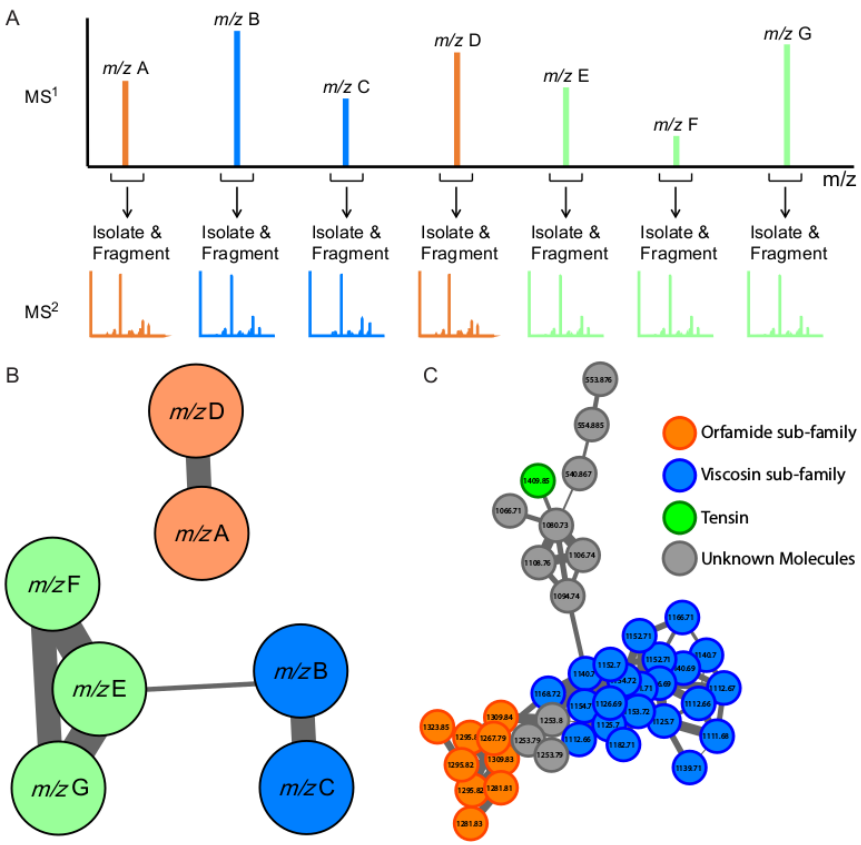

Figure I-13: An overview from mass spectra to molecular networks.

(**A**) The ions of a mass spectra are selected and fragmented by MS/MS measurements. The MS/MS spectra are compared based on their similarity (colour-coded in this case). (**B**) Examples of molecular networks. MS/MS spectra are represented as a node while the similarity between each node is visualised by the thickness of an edge (lines). (**C**) Example of a molecular family grouping molecules that share structural similarities. Orange, blue and green nodes represent known molecules. Grey nodes represent unknown molecules.[119]

I.5 Aims of this Study

The first part of this study was performed within the frame of the Collaborative Research Center Transregional (CRC-TR) 261 “Antibiotic CellMAP” in order to gain a deeper understanding of cellular mechanisms of antibiotic action and production. The goal of the subproject A9 “Binding mode of cyclic lipopeptides to cell wall precursors” was to achieve a detailed understanding of the mode of action of guanidine-containing lipopeptides by determination of their binding modes with lipid II Namely, our hypothesis is that the structurally related lipopeptides Emp, Plus and Tpp all bind to lipid II as their primary target and that the observed differences in potency rely on variations in recognition with lipid II.

Therefore, the antimicrobial cyclic lipopeptides empedopeptin and plusbacin A_3 should be isolated from their producer strains and the chemical structures of all three should be confirmed by NMR and HR-MS. Additionally, the lipopeptides should be uniformly labelled with ^{15}N, due to the low natural abundance of ^{15}N (0.37 %), in order to determine the solution structure of the lipopeptides in complex with lipid II by NMR interaction studies. The chemical shift perturbations should then give insight into the structural features of CLPs and lipid II interactions.

In the second part of this study, putative candidate structures should be identified by *in silico* screening for lipopeptides in genomes of the genus *Pseudomonas* of the strain collection of Tübingen. Subsequently, the targeted lipopeptides should be isolated chromatographically and their chemical structures elucidated by NMR and HR-MS. In order to obtain sufficient amounts for structural analysis, the production rate of the targeted lipopeptides should be improved by different strategies. Furthermore, the bioactivity of these lipopeptides should be investigated.

II Materials and Methods

II.1 Materials

II.1.1 Chemicals

Table II-1: Chemicals used in this study and their supplier. All chemicals were used without further modification.

Chemicals	Abbreviation / Chemical formula	Manufacturer
Acetone	C_3H_6O	Brenntag GmbH, Plochingen, Germany
Acetonitrile HPLC grade	CH_3CN	J. T. Baker® Chemicals, Center Valley, Pennsylvania, USA
Acetonitrile LC-MS grade	CH_3CN	Chemsolute, Th. Geyer GmbH & Co. KG, Renningen, Germany
Agar		Sigma-Aldrich®, St. Louis, Missouri, USA
Ammonium chloride	NH_4Cl	Sigma-Aldrich®, St. Louis, Missouri, USA
Ammonium sulphate	$(NH_4)_2SO_4$	Merck Chemicals GmbH, Darmstadt, Germany
^{15}N-Ammonium sulphate (98 atom % ^{15}N)	$(^{15}NH_4)_2SO_4$	Sigma-Aldrich®, St. Louis, Missouri, USA
Bacto™ Proteose peptone No.3		Difco Becton Dickinson, Franklin Lakes, New Jersey, USA
Bacto™ Peptone		Difco Becton Dickinson, Franklin Lakes, New Jersey, USA
Bacto™ Tryptone		Difco Becton Dickinson, Franklin Lakes, New Jersey, USA
Bacto™ Yeast extract		Difco Becton Dickinson, Franklin Lakes, New Jersey, USA
Boric acid	H_3BO_3	Merck Chemicals GmbH, Darmstadt, Germany
Butanol	BuOH, $C_4H_{10}O$	VWR International GmbH, Darmstadt, Germany
Cafestol	$C_{20}H_{28}O_3$	HPC Standards GmbH, Cunnersdorf, Germany
Calcium carbonate	$CaCO_3$	Chemsolute, Th. Geyer GmbH & Co. KG, Renningen, Germany

Chemicals	**Abbreviation / Chemical formula**	**Manufacturer**
Casamino acids		MP Biomedicals Germany GmbH, Eschwege, Germany
Cobalt chloride hexahydrate	$CoCl_2*6H_2O$	Fluka, Thermo Fisher Scientific, Waltham, Massachusetts, USA
Copper sulphate pentahydrate	$CuSO_4*5H_2O$	AppliChem GmbH, Darmstadt, Germany
Dextrose / D-Glucose	$C_6H_{12}O_6$	Sigma-Aldrich®, St. Louis, Missouri, USA
Dichloromethane	DCM, CH_2Cl_2	Brenntag GmbH, Plochingen, Germany
Difco™ Minimal Broth Davis without Dextrose	DMB	Sigma-Aldrich®, St. Louis, Missouri, USA
d_6-Dimethyl sulfoxide (99.9 %)	d_6-DMSO, $(CD_3)_2SO$	Sigma-Aldrich®, St. Louis, Missouri, USA
Disodium hydrogen phosphate	Na_2HPO_4	Merck Chemicals GmbH, Darmstadt, Germany
Dipotassium hydrogen phosphate	K_2HPO_4	Sigma-Aldrich®, St. Louis, Missouri, USA
D-Leucine	$C_6H_{13}NO_2$	Sigma-Aldrich®, St. Louis, Missouri, USA
D-Valine	$C_5H_{11}NO_2$	Sigma-Aldrich®, St. Louis, Missouri, USA
Ethyl acetate	EtOAc, $C_4H_8O_2$	Brenntag GmbH, Plochingen, Germany
Ethylenediaminetetraacetic acid	EDTA, $C_{10}H_{16}N_2O_8$	Carl Roth GmbH & Co. KG, Karlsruhe, Germany
Formic acid	HCOOH	Sigma-Aldrich®, St. Louis, Missouri, USA
Glycerol (99 %)	Gly, $C_3H_8O_3$	Carl Roth GmbH & Co. KG, Karlsruhe, Germany
HEPES (4-(2-hydroxyethyl)-1-piperazineethanesulfonic acid)	$C_8H_{18}N_2O_4S$	Sigma-Aldrich®, St. Louis, Missouri, USA
Hydrochloric acid	HCl	Brenntag GmbH, Plochingen, Germany
L-Isoleucine	$C_6H_{13}NO_2$	Fluka, Thermo Fisher Scientific, Waltham, Massachusetts, USA
Linseed meal		Topfruits / Megerle Online GmbH, Ubstadt-Weiher, Germany
L-Leucine	$C_6H_{13}NO_2$	Sigma-Aldrich®, St. Louis, Missouri, USA

Chemicals	Abbreviation / Chemical formula	Manufacturer
Magnesium sulphate heptahydrate	$MgSO_4*7H_2O$	AppliChem GmbH, Darmstadt, Germany
Manganese sulphate tetrahydrate	$MnSO_4*4H_2O$	Alfa Aesar, Ward Hill, Massachusetts, USA
Meat extract		Sigma-Aldrich®, St. Louis, Missouri, USA
d_3-Methanol (99.5 %)	d_3-MeOH, CD_3OH	Deutero GmbH, Kastellaun, Germany
d_4-Methanol (≥99.8 %)	d_4-MeOH, CD_3OD	Sigma-Aldrich®, St. Louis, Missouri, USA
Methanol HPLC grade	MeOH, CH_3OH	Sigma-Aldrich®, St. Louis, Missouri, USA
Methanol LC-MS grade	MeOH, CH_3OH	Chemsolute, Th. Geyer GmbH & Co. KG, Renningen, Germany
L-Methionine	$C_5H_{11}NO_2S$	Carl Roth GmbH & Co. KG, Karlsruhe, Germany
3-Methyl-2-oxobutanoic acid	$C_5H_8O_3$	Fluorochem Ltd, Hadfield, Glossop, United Kingdom
NZ Case		Fluka, Thermo Fisher Scientific, Waltham, Massachusetts, USA
Polygoprep™	60-50 C_{18}	Macherey Nagel, Düren, Germany
Potassium dihydrogen phosphate	KH_2PO_4	Sigma-Aldrich®, St. Louis, Missouri, USA
^{15}N-Proline (≥ 95 atom % ^{15}N)	^{15}N-Pro, $C_5H_9{}^{15}NO_2$	Sigma-Aldrich®, St. Louis, Missouri, USA
Sodium chloride	NaCl	Sigma-Aldrich®, St. Louis, Missouri, USA
Sodium dihydrogen phosphate monohydrate	$NaH_2PO_4*H_2O$	Carl Roth GmbH & Co. KG, Karlsruhe, Germany
Sodium hydroxide	NaOH	Honeywell International Inc., Morristown, New Jersey, USA
Sodium molybdate dihydrate	$Na_2MoO_4*2H_2O$	Carl Roth GmbH & Co. KG, Karlsruhe, Germany
Sodium pyruvate	$C_3H_3O_3Na$	AppliChem GmbH, Darmstadt, Germany
Soluble starch	$(C_6H_{10}O_5)n$	Carl Roth GmbH & Co. KG, Karlsruhe, Germany
Sucrose	$C_{12}H_{22}O_{11}$	Merck Chemicals GmbH, Darmstadt, Germany
Trifluoroacetic acid	TFA, CF_3COOH	Sigma-Aldrich®, St. Louis, Missouri, USA

Chemicals	Abbreviation / Chemical formula	Manufacturer
L-Valine	$C_5H_{11}NO_2$	Sigma-Aldrich®, St. Louis, Missouri, USA
Zinc sulphate heptahydrate	$ZnSO_4*7H_2O$	AppliChem GmbH, Darmstadt, Germany

II.1.2 Devices

Table II-2: Devices used in this study.

Device	Specification	Manufacturer
Autoclave	Systec VX-150	Systec GmbH, Linden, Germany
Centrifuges	• Heraeus Multifuge 4KR	Thermo Fisher Scientific Inc., Waltham, Massachusetts, USA
	• Centrifuge 5424 R	Eppendorf AG, Hamburg, Germany
Clean Bench	Safe 2020	Thermo Fisher Scientific Inc., Waltham, Massachusetts, USA
Gel Doc™ Molecular Imager®	System XR+	Bio-Rad Laboratories, Inc., Hercules, California, USA
Freeze Dryer	Christ Alpha 3-4 Lyo-Screen-Control basic	Martin Christ Gefriertrocknungs-anlagen GmbH, Osterode am Harz, Germany
HPLC System	Waters™ 1525 Binary Pump Waters™ 717 plus autosampler Waters™ 2996 photodiode array detector Waters™ Fraction Collector II	Waters Corporation, Milford, Massachusetts, USA
Incubators	Plate incubator IN110 & IPP30	Memmert GmbH + Co.KG, Büchenbach, Germany
Laboratory Shakers	• Infors HT Multitron Pro	Infors AG, Bottmingen, Switzerland
	• Orbital Shaker Incubator (Falcons)	VWR International, Radnor, Pennsylvania, USA
LC-MS System	LC: Agilent 1100/1200 Series	Agilent Technologies, Inc., Santa Clara, California, USA
	MS: QTRAP 3200	AB Sciex GmbH, Darmstadt, Germany
(Micro) Scales	• Sartorius MC210 P ISO9001	Sartorius AG, Göttingen, Germany
	• A&D FZ-2000i	A&D Instruments LTD., Abingdon, Oxfordshire, UK
NanoDrop	BioPhotometer® D30	Eppendorf AG, Hamburg, Germany
NMR	• Bruker Avance III HD 400 MHz Nanobay (5 mm BBO probe head)	Bruker Corporation, Billerica, Massachusetts, USA

Device	Specification	Manufacturer
	• Bruker Avance III HDX 700 MHz (5 mm Prodigy TCI cryo probe head)	
pH Meter	FiveEasy	Mettler Toledo, Columbus, Ohio, USA
Rotary Evaporator	Rotavac Valve Control Heidolph-VAP Precision	Heidolph Instruments GmbH & Co.KG, Schwabach, Germany
	Huber Unichiller	Peter Huber Kältemaschinenbau AG, Offenburg, Germany
SpeedVac Vacuum Concentrator	Concentrator Plus	Enzyscreen B. V., Al Leiden, The Netherlands
Water Purification System	Elga^{TM} Purelab^{TM} Flex	Elga LabWater, Veolia Water Technologies Deutschland GmbH, Celle, Germany

II.1.3 Equipment

Table II-3: Equipment used in this study.

Equipment	Specification	Manufacturer
Beakers	glass, various volumes	VITLAB GmbH, Grossostheim, Germany
Erlenmeyer Flasks	various volumes	VWR, Darmstadt, Germany
Hamilton Syringe	710RN, 100 µL, 1.46 x 60 mm	Hamilton Company, Reno, Nevada, USA
Pipettes	10000 μL, 5000 μL, 1000 μL, 200 μL	Eppendorf AG, Hamburg, Germany
Round Bottom Flasks	various volumes	VWR, Darmstadt, Germany
Pear Shaped Flasks	25 mL, 10 mL, 5 mL	DURAN Group GmbH, Wertheim/Main, Germany
Schott Bottles	1000 mL, 500 mL, 100 mL	DURAN Group GmbH, Wertheim/Main, Germany
Measuring Cylinder	various volumes	DURAN Group GmbH, Wertheim/Main, Germany
NMR Tubes	5 mm, 3 mm	Deutero GmbH, Kastellaun, Germany

Table II-4: HPLC columns used in this study and their supplier.

Column name	Specification	Manufacturer
Aeris™ 3.6 µm Peptide XB-C18 100 Å	250 x 4.6 mm	Phenomenex Inc., Torrance, California, USA
Aeris™ 5 µm Peptide XB-C18 100 Å	250 x 10.0 mm	
Chirex 5 µm 3010 120 Å ((S)-valine and 3,5-dinitroaniline phase)	250 x 4.6 mm	
Kinetex® 5 µm EVO C18 100 Å	250 x 4.6 mm	
Luna® 5 µm C18(2) 100 Å	250 x 2 mm	
Luna® 5 µm C18(2) 100 Å	250 x 4.6 mm	
Luna® 5 µm C18(2) 100 Å	250 x 10.0 mm	
Luna® 5 µm CN 100 Å	250 x 4.6 mm	
Luna® Omega 3 µm Polar C18 100 Å	150 x 3 mm	
Luna® Omega 5 µm Polar C18 100 Å	250 x 4.6 mm	
Xterra® MS C18 5 µm	3.0 x 100 mm	Waters Corporation, Milford, Massachusetts, USA

II.1.4 Consumables

Table II-5: Consumables used in this study.

Consumables	Specification	Manufacturer
Centrifugation Tubes	1000 mL, 50 mL, 15 mL	Sarstedt AG & Co.KG, Nümbrecht. Germany
Cryo Preservation Tubes	1.8 mL	Sarstedt AG & Co.KG, Nümbrecht. Germany
Cuvettes, Uvettes	1 mL	Sarstedt AG & Co.KG, Nümbrecht. Germany
Falcon Tubes	50 mL, 15 mL	Sarstedt AG & Co.KG, Nümbrecht. Germany
Filter Discs	6 mm	GE Healthcare, Chicago, Illinois, USA
HPLC Vials & Caps	1.5 mL, 32 x 11.6 mm	IVA Analysentechnik GmbH & Co.KG, Meerbusch Germany
HPLC Vial Inlays	0.1 mL, 29 x 5.7 mm	IVA Analysentechnik GmbH & Co.KG, Meerbusch Germany
LC-MS Vials & Caps	1 mL, 40 x 8.2 mm	IVA Analysentechnik GmbH & Co.KG, Meerbusch Germany
LC-MS Vial Inlays	0.1 mL, 34 x 5.0 mm	IVA Analysentechnik GmbH & Co.KG, Meerbusch Germany

Consumables	Specification	Manufacturer
Pasteur Pipettes ISO7712	230 mm, 150 mm	Glaswarenfabrik Karl Hecht GmbH & Co. KG, Sondheim vor der Rhön, Germany
Petri Dishes	Ø 14.5 cm; 92 x 16 mm	Sarstedt AG & Co.KG, Nümbrecht. Germany
Pipette Tips	various volumes	Sarstedt AG & Co.KG, Nümbrecht. Germany
Reaction Tubes	2 mL, 1.5 mL	Sarstedt AG & Co.KG, Nümbrecht. Germany
Sterile Filters	Filtropur S 0.2 µm PES-membrane	Sarstedt AG & Co.KG, Nümbrecht. Germany
Syringes	20 mL, 10 mL, 1 mL	Henke-Sass, Wolf GmbH, Tuttlingen, Germany

II.1.5 Bacterial Strains

Table II-6: Bacterial strains used in this study.

Bacterial strain	Relevant characteristics	Reference(s) or source
Bacillus subtilis 168	Indicator strain for bioassays	Brötz-Oesterhelt Lab, University of Tübingen, Germany
Lysobacter firmicutimachus PB-6250^T	Plusbacin producer	IPOD[a]
Massilia sp. (formerly *Empedobacter haloabium*) ATCC 31962	Empedopeptin producer	ATCC[b]
Pseudomonas viridiflava P1.A2	Cichofactin producer	Weigel Lab, University of Tübingen, Germany
Pseudomonas viridiflava P8.B2	Cichofactin producer	Weigel Lab, University of Tübingen, Germany
Pseudomonas viridiflava P8.B3	Cichofactin producer	Weigel Lab, University of Tübingen, Germany
Pseudomonas viridiflava P8.B9	Cichofactin producer	Weigel Lab, University of Tübingen, Germany
Pseudomonas viridiflava P13.F2	Cichofactin producer	Weigel Lab, University of Tübingen, Germany
Pseudomonas viridiflava P22.F1	Cichofactin producer	Weigel Lab, University of Tübingen, Germany
Pseudomonas viridiflava P25.C2	Cichofactin producer	Weigel Lab, University of Tübingen, Germany

[a]IPOD: International Patent Organism Depositary; [b]ATCC: American Type Culture Collection

II.1.6 Bacterial Media Composition

The following media were prepared with demineralised water and the pH value was adjusted with 1 M HCl / 1 M NaOH. Media were sterilised by autoclaving for 20 min at 121 °C and a pressure of 2 bar. Heat sensitive solutions were sterile filtered prior to use. Media were stored at room temperature or 4 °C.

Table II-7: Media used in this study.

Media	Component	Concentration
DMBGly *Pseudomonas* production medium	Difco™ Minimal Broth Davis without Dextrose	10.6 g/L
	Glycerol	1.84 mL/L
Linseed Medium (pH 7) *Lysobacter / Massilia* production medium	Sucrose	30 g/L
	Linseed meal	20 g/L
	$(NH_4)_2SO_4$ or $(^{15}NH_4)_2SO_4$	3 g/L
	$CaCO_3$	5 g/L
LB Medium (pH 7.5) Lysogeny Broth	Bacto tryptone	10 g/L
	Bacto yeast extract	5 g/L
	NaCl	10 g/L
LB Agar (pH 7)	Bacto tryptone	10 g/L
	Bacto yeast extract	5 g/L
	NaCl	10 g/L
	Agar	15 g/L
Massilia Medium	Soluble starch	20 g/L
	Glucose	10 g/L
	Meat extract	2 g/L
	Bacto yeast extract	2 g/L
	NZ case	5 g/L
	$CaCO_3$	2 g/L
Minimal Medium	Difco™ Minimal Broth Davis without Dextrose	5.3 g/L
	EDTA	0.52 mg/L
	HEPES	0.56 g/L
	Sucrose	5.1 g/L
	Trace metal mix A5 + Co	1 mL/L
	L-Methionine	1 mg/L
M9 Minimal Salts Medium	D-Glucose	4.0 g/L
	NH_4Cl	1.0 g/L
	$NaH_2PO_4*H_2O$	3.45 g/L
	Na_2HPO_4	6.78 g/L
	NaCl	0.5 g/L

Media	Component	Concentration
M9 Minimal Salts Medium supplemented with yeast extract	D-Glucose	4.0 g/L
	NH_4Cl	1.0 g/L
	NaH_2PO_4	3.0 g/L
	Na_2HPO_4	6.78 g/L
	NaCl	0.5 g/L
	Bacto yeast extract	1.0 g/L
R2A Medium (pH 7.2) *Lysobacter / Massilia* production medium	Bacto yeast extract	0.5 g/L
	Bacto proteose peptone No.3	0.5 g/L
	Casamino acids	0.5 g/L
	Dextrose	0.5 g/L
	Soluble starch	0.5 g/L
	Sodium pyruvate	0.3 g/L
	KH_2PO_4	0.3 g/L
	$MgSO_4$*7 H_2O	50 mg/L
R2A Medium for ^{15}N labelled compounds (pH 7.2) *Lysobacter / Massilia* production medium	Bacto yeast extract	0.5 g/L
	Bacto proteose peptone No.3	0.5 g/L
	$(^{15}NH_4)_2SO_4$	0.83 g/L
	Dextrose	0.5 g/L
	Soluble starch	0.5 g/L
	Sodium pyruvate	0.3 g/L
	KH_2PO_4	0.3 g/L
	$MgSO_4$*7 H_2O	50 mg/L
SM5	Bacto peptone	2 g/L
	Bacto yeast extract	0.2 g/L
	Glucose	0.2 g/L
	KH_2PO_4	1.9 g/L
	K_2HPO_4	1.0 g/L
	$MgSO_4$	0.49 g/L
Trace element solution for Minimal Medium	$ZnSO_4$*7 H_2O	0.18 g/L
	H_3BO_3	0.1 g/L
	$MnSO_4$*4 H_2O	0.044 g/L
	$CoCl_2$*6H_2O	0.02 g/L
	$CuSO_4$*5 H_2O	0.006 g/L
	Na_2MoO_4*2H_2O	0.02 g/L

***** Linseed meal was allowed to swell in water for 2 h under stirring, followed by centrifugation. The supernatant was decanted and water was added to reach 1 L homogenous medium.

II.1.7 Software

Table II-8: Software used in this study.

Name	Version	Manufacturer
Analyst®	1.6.3	AB Sciex LLC, Framingham, Massachusetts, USA
AntiSMASH[120,121]	3.0 & 4.0	University of Groningen, Netherlands; University of Tübingen, Germany, University of Manchester, UK; University of California, San Francisco, USA
ChemBio Draw	Professional 17.0	PerkinElmer, Waltham, Massachusetts, USA
ClustalOmega[122]	2.1	EMBL-EBI, Hinxton, Cambridgeshire, UK
CytoScape	3.5.1	Bruker Daltonik GmbH, Bremen, Germany
Compass Data Analysis	4.4	Bruker Daltonik GmbH, Bremen, Germany
GNPS[123]		University of San Diego, La Jolla, California, USA
MegaX[124]		Pennsylvania State University, State College, Pennsylvania, USA
MestReNova	12.0.0	Mestrelab Research, S.L., Santiago de Compostela, Spain
MetaboScape®	3.0	Bruker Daltonik GmbH, Bremen, Germany
TopSpin	3.6.1	Bruker Daltonik GmbH, Bremen, Germany

II.2 Biological Methods

II.2.1 Cryogenic Storage of Bacteria

For long term storage at -80 °C, 750 µL of a liquid culture (24 h) was mixed with 750 µL of 50 % glycerol (v/v) in a cryopreservation vial under sterile conditions. Glycerol stocks were vortexed vigorously before freezing at -80 °C.

II.2.2 Preculture of Bacterial Strains

Plusbacins were isolated from *Lysobacter* PB-6250^T, empedopeptin from *Massilia* sp. ATCC 31962 and cichofactins from *Pseudomonas* P1.A2. All precultures were carried out in 50 mL Falcon tubes containing 12 mL R2A, MM or LB medium, respectively, and were inoculated with 80-100 µL cryo culture. The cultures were grown for 24-48 h at 30 °C and 200 rpm.

II.2.3 Cultivation of *Lysobacter* and *Massilia*

II.2.3.1 Production of Secondary Metabolites

For the production of secondary metabolites, cultivation was performed on a 9 L scale. Main cultures were cultivated in linseed or R2A medium in 5 L Erlenmeyer flasks, containing 1.5 L medium, inoculated with 5 mL of preculture and incubated for 3-4 days at 28 °C (*Lysobacter*) or 27 °C (*Massilia*) and 140 rpm.

II.2.3.2 Production of ^{15}N-labelled Secondary Metabolites

For the production of ^{15}N-labelled secondary metabolites, cultivation was performed on a 9 L scale. $(^{15}NH_4)_2SO_4$ was added to the culture medium before sterilisation by autoclaving. Main cultures were cultivated in linseed or R2A medium for labelled compounds (see **Chapter** I.1.6) in 5 L Erlenmeyer flasks, containing 1.5 L medium, inoculated with 5 mL of preculture and incubated for 3-4 days at 28 °C (*Lysobacter*) or 27 °C (*Massilia*) and 140 rpm.

II.2.3.3 Bacterial Growth Curve Determination and Semi-Quantitative Analysis of Plusbacin Production

In order to determine the growth rate, doubling time and the produced amount of plusbacins, a 1.5 L culture was prepared to prevent cultivation differences and to achieve a uniform growth instead of growing many small cultures. The culture was grown in linseed and R2A medium which were each inoculated with 5 mL of preculture and the time of inoculation was set as the starting point.

In the beginning, the samples were taken every 2 hours and subsequently every 4-8 hours over a period of four days. Each time point was tested in duplicates and the samples were processed as followed:

Bacterial growth was determined by measuring the optical density at 600 nm (OD_{600}) of 1 mL culture. Sterile medium was used as reference. This experimental step was not possible with linseed medium due to its turbidity.

In order to determine the dry weight, 1 mL of culture was centrifuged for 5 min at 13000 rpm. The supernatant was discarded. The cells were washed with 1 mL sterile water, centrifuged for 5 min at 13000 rpm and the water discarded. This step was repeated. The cells were dried for 3 days at 70 °C and the dry weight was determined.

For semi-quantification, 1 mL culture was acidified with hydrochloric acid (5 M) to a pH value of 3 and extracted with 1 mL of BuOH (v/v). The organic supernatant was evaporated to dryness using a speed vac (45 °C) and the obtained crude extract was dissolved in 1 mL MeOH LC-MS grade and analysed by LC-MS.

Calculation of the specific growth rate and the doubling time

$$OD = OD_0 \times e^{\mu t}$$

$$\mu = \frac{\ln 2}{t_d}$$

OD = optical density
OD_0 = optical density at t_0
t = time [h]
μ = specific growth rate
t_d = doubling time [h]

II.2.3.4 Production of Plusbacins in Linseed Medium Supplemented with Precursors

Cultivation was carried out in 500 mL of linseed medium which was inoculated with 2 mL preculture. L-Valine was added to the culture medium before sterilisation by autoclaving and 3-methyl-2-oxobutanoic acid was added 8 hours after inoculation. The medium without addition of precursors served as negative control. Cultivation was carried out in duplicates for 3 days at 28 °C and 140 rpm. The culture broth was acidified with hydrochloric acid (5 M) to a pH value of 3 and extracted twice with 500 mL of n-butanol. The organic solvent was evaporated to dryness under reduced pressure. The obtained crude extract was dissolved in 3 mL MeOH LC-MS grade, diluted in the ratio of 1:5 and analysed by LC-MS.

II.2.3.5 Production of Plusbacins in R2A Medium Supplemented with Precursors

Cultivation was carried out in 100 mL of R2A medium which was inoculated with 1 mL of preculture. L-Leucine, D-leucine, L-valine and D-valine were added to the culture medium prior to sterilisation by autoclaving. The medium without addition of precursors served as a negative control. Cultivation was carried out in duplicates for 3 days at 28 °C and 140 rpm. The culture broth was acidified with hydrochloric acid (5 M) to a pH value of 3 and extracted with 100 mL of n-butanol. The organic solvent was evaporated to dryness under reduced pressure. The crude extract was dissolved in 3 mL MeOH and analysed by LC-MS.

II.2.4 Cultivation of *Pseudomonas* Strains

II.2.4.1 Media Screening of *Pseudomonas* Strains

Liquid cultures were inoculated with 1 mL of the corresponding preculture and grown on a small scale (each 100 mL) in DMBGly, DMBGly supplemented with cafestol, R2A, SM5, M9 and M9Y (see **Table II-7**), incubated for 3 days at different temperatures (23 °C and 30 °C) and 140 rpm. For each experiment, the corresponding medium without inoculum served as control.

II.2.4.2 Production of Secondary Metabolites

For the production of secondary metabolites, such as the cichofactins, cultivation was performed on a 9 L scale. Main cultures were cultivated in DMBGly in 5 L Erlenmeyer flasks, containing 1.5 L medium, inoculated with 5 mL of the preculture and incubated for 3 days at 23 °C and 140 rpm.

II.2.4.3 Production of Cichofactins in DMBGly Medium Supplemented with Plant Extracts

Cultivation was carried out in 100 mL of DMBGly medium which was inoculated with 1 mL of preculture. Four different genotypes of the plant *Arabidopsis thaliana* were grown in a plate with media including Col-0 (reference genotype), Ey15-2, ICE153 and Sha. The leaves of each genotype were collected, sliced and blended equally in three aliquots which were sterilised by autoclaving. The medium without addition of plant slices served as a negative control. Cultivation was carried out for 3 days at 23 °C and 140 rpm. The culture broth was acidified with hydrochloric acid (5 M) to a pH value of 3 and extracted with 100 mL of ethyl acetate. The organic solvent was evaporated to dryness under reduced pressure. The crude extract was dissolved in 1 mL MeOH LC-MS grade and analysed by LC-MS.

II.2.4.4 Production of Cichofactins in DMBGly Medium Supplemented with Precursors

Cultivation was carried out in 100 mL of DMBGly medium which was inoculated with 1 mL of preculture. L-Isoleucine and L-leucine were added to the culture medium before sterilisation by autoclaving as well as four and eight hours after inoculation. The medium without addition of precursors served as a negative control. Cultivation was carried out in duplicates for 3 days at 23 °C and 140 rpm. The culture broth was acidified with hydrochloric acid (5 M) to a pH value of 3 and extracted with 100 mL of ethyl acetate. The organic solvent was evaporated to dryness under

reduced pressure. The crude extract was dissolved in 1 mL MeOH LC-MS grade and analysed by LC-MS measurements.

II.2.5 Agar Diffusion Assays (Bioassays)

The antibacterial activity was determined by agar diffusion assays. In this study, *Bacillus subtilis* 168 was used as indicator strain which was cultivated in LB medium overnight at 30 °C and 200 rpm. 1 mL of this preculture was added to 100 mL LB agar (~45 °C) which was distributed into petri dishes. After solidifying, sterile filter discs were placed onto the agar and 10 µL of the obtained fractions and the corresponding solvent as negative control were dropped on the discs. The plates were incubated at 30 °C for 24-48 h. The observation of an inhibition zone indicated the presence of an active compound.

II.3 Chemical Methods

II.3.1 Extraction of Secondary Metabolites

II.3.1.1 Extraction of Large Scale Cultivation of *Lysobacter* and *Massilia* spp.

The culture broth (1.5 L) was acidified with hydrochloric acid (5 M) to a pH value of 3. The acidified cultures were extracted twice with 1 L of n-butanol. The two-phase system was stirred at 70 rpm for 3 hours. The organic supernatant was decanted and evaporated under reduced pressure to dryness. The aqueous layer was discarded and the crude extract was further processed.

II.3.1.2 Extraction of Large Scale Cultivation of *Pseudomonas* spp.

The culture broth was adjusted with hydrochloric acid (5 M) to a pH value of 3 and extracted twice with 1 L of ethyl acetate. The resulting organic supernatant was evaporated under reduced pressure to dryness and the crude extract was used for further purification.

II.3.2 Vacuum Liquid Chromatography

VLC was performed by using a column with a diameter of 6.5 cm filled to height around 20 cm with Polygoprep® 60-50 C_{18} material. The column was equilibrated with 600 mL of the first eluent mixture. The crude extract was dissolved in a small amount of the first eluent mixture and applied to the top of the column. Subsequently, the following stepwise gradient was applied:

Table II-9: Gradient used for VLC purification.

Fraction	Solvent	Ratio
A	MeOH/H_2O	30:70
B	MeOH/H_2O	50:50
C	MeOH/H_2O	65:35
D	MeOH/H_2O	80:20
E	MeOH/H_2O	100:0
F	DCM	100

The volume of solvents was adjusted to the amount of crude and ranged from 600 to 1200 mL. Each fraction was collected and evaporated to dryness under reduced pressure. All fractions, except fraction F were redissolved in MeOH LC-MS grade (~1mg/mL) and analysed by LC-MS.

II.3.3 High Performance Liquid Chromatography

The separation and purification of natural product derivatives was achieved with a Waters HPLC system equipped with a 1525 Binary Pump, a 717 plus auto sampler or a 7725i Rheodyne injector port, a 996 photodiode array detector and a Fraction Collector II and operated by the software Millenium[32] (Version 4.00).

II.3.3.1 Purification of Plusbacin Derivatives

Plusbacin derivatives and ^{15}N-labelled plusbacin derivatives were purified over two steps so far. The following gradients and columns were used.

Purification step 1:

A Phenomenex Aeris™ peptide XB-C18 column (5 µm, 250 x 4.6 mm) was used at a flow rate of 0.7 mL/min and UV monitoring occurred at 220 nm. This HPLC system was equipped with a Fraction Collector II.

Table II-10: Linear gradient used for the first HPLC purification step of plusbacin derivatives.

Time [min]	Methanol [%]	Water [0.1 % TFA]
0	40	60
20	80	20
30	80	20
35	100	0
45	100	0
55	40	60
60	40	60

Purification step 2:

A Phenomenex CN column (5 µm, 250 x 4.6 mm) was used. The fractions were separated under isocratic conditions with a mobile phase of acetonitrile (solvent A) and 50 mM phosphate buffer, pH 2.2 containing 50 mM Na_2SO_4 (solvent B) with a ratio of 25:75, a flow rate of 1 mL/min and UV monitoring occurred at 220 nm.

II.3.3.2 Purification of Empedopeptin Derivatives

Empedopeptin derivatives as well as the ^{15}N-labelled empedopeptin derivatives were purified over three steps. The following gradients and columns were used.

Purification step 1:

A Phenomenex Aeris^{TM} peptide XB-C18 column (5 µm, 250 x 10.0 mm) was used at a flow rate of 2 mL/min and UV monitoring occurred at 220 nm. This HPLC system was equipped with a Fraction Collector II.

Table II-11: Linear gradient used for the first HPLC purification step of empedopeptin derivatives.

Time [min]	Methanol [%]	Water [0.1 % TFA]
0	40	60
20	75	25
30	75	25
35	100	0
45	100	0
55	40	60
60	40	60

Purification step 2:

A Phenomenex Kinetex® EVO C_{18} column (5 μm, 250 x 4.6 mm) was used at a flow rate of 1 mL/min and UV monitoring occurred at 220 nm.

Table II-12: Linear gradient used for the second HPLC purification step of plusbacin derivatives.

Time [min]	Methanol [%]	Water [0.1 % HCOOH]
0	50	50
15	65	35
20	65	35
28	75	25
35	75	25
40	50	50

Purification step 3:

A Phenomenex Luna® C18(2) column (5 µm, 250 x 4.6 mm) was used at a flow rate of 1 mL/min and UV monitoring occurred at 220 nm.

Table II-13: Linear gradient used for the third HPLC purification step of empedopeptin derivatives.

Time [min]	Methanol [%]	Water [0.1 % HCOOH]
0	60	40
5	70	30
30	70	30
35	60	40
38	60	40

II.3.3.3 Purification of Chichofactin Derivatives

Cichofactin derivatives were purified over 2 steps. The following gradients and columns were used.

Purification step 1:

A Phenomenex Luna® C18(2) column (5 μm, 250 x 10.0 mm) was used at a flow rate of 3 mL/min and UV monitoring occurred at 220 nm.

Table II-14: Linear gradient used for the first HPLC purification step of cichofactin derivatives.

Time [min]	Acetonitrile [%]	Water [0.1 % TFA]
0	50	50
20	70	30
35	100	0
38	100	0
43	50	50
45	50	50

Purification step 2:

A Phenomenex Luna® C18(2) column (5 µm, 250 x 4.6 mm) was used at a flow rate of 1 mL/min and UV monitoring occurred at 220 nm.

Table II-15: Linear gradient used for the second HPLC purification step of cichofactin derivatives.

Time [min]	Acetonitrile [%]	Water [0.1 % TFA]
0	50	50
15	60	40
30	70	30
35	70	30
40	50	50
42	50	50

II.3.4 Mass Spectrometry

II.3.4.1 Low Resolution (LR) HPLC-ESI-MS

HPLC-ESI-MS measurements were performed on a Sciex 3200 QT mass spectrometer coupled with an Agilent 1100/1200 Series HPLC including a diode array detector. The samples were dissolved in LC-MS grade methanol and centrifuged to remove small particles prior to analysis. A Phenomenex Luna C18(2) column (5 µm, 250 x 2.0 mm) was used with a flow rate of 0.2 mL/min.

The following gradient and settings were used in the plusbacin and empedopeptin projects using the Q3 MS positive scan mode:

Table II-16: Linear gradient used for LC-MS analytics of plusbacin and empedopeptin.

Time [min]	Methanol [%]	Water [0.1 % TFA]
0	40	60
10	50	50
30	100	0
45	100	0
60	40	60
65	40	60

Table II-17: Parameters used for LC-MS analytics of plusbacin and empedopeptin.

Parameter	Value
Declustering potential [V]	50
Entrance potential [V]	10
Curtain gas [psi]	25
Collision gas [V]	2
Ion Spray Voltage [V]	5500
Temperature [°C]	450
Ion Source Gas 1 [psi]	30
Ion Source Gas 2 [psi]	30

The following gradients and settings were used in the cichofactin project using the Q3 MS positive scan mode. The first gradient was used for identification of cichofactin-containing fractions and the second for the semi-quantitative determination of cichofactin derivatives.

Table II-18: Linear gradient used for LC-MS analytics of cichofactins.

Time [min]	Acetonitrile [%]	Water [0.1 % TFA]
0	10	90
8	30	70
16	50	50
22	100	0
30	100	0
40	10	90
50	10	90

Table II-19: Linear gradient used for LC-MS analytics of semi-quantitative determination of cichofactin derivatives.

Time [min]	Acetonitrile [%]	Water [0.1 % TFA]
0	50	50
20	70	30
35	100	0
38	100	0
43	50	50
45	50	50

Table II-20: Parameters used for LC-MS analytics of cichofactins.

Parameter	Value
Declustering potential [V]	50
Entrance potential [V]	10
Curtain gas [psi]	25
Collision gas [V]	2
Ion Spray Voltage [V]	5500
Temperature [°C]	450
Ion Source Gas 1 [psi]	30
Ion Source Gas 2 [psi]	30

II.3.4.2 High Resolution (HR) HPLC-ESI-MS

High resolution LC-ESI-MS and MS^2 measurements were performed by Dr. Dorothee Wistuba, Department of Organic Chemistry, University of Tübingen using a Bruker Daltonics MaXis 4G connected to a Thermo Scientific Ultimate 3000 system using a reversed-phase Luna Omega polar C18 column (3 µm, 150 x 3 mm) at a flow rate of 0.3 mL/min. A linear gradient from 10 % to 100 % of solvent B in 40 min was used (solvent A: 0.1 % HCOOH in H_2O; solvent B: MeOH), an injection volume of 5 µL and UV monitoring occurred at 210, 254, 280 and 360 nm. The range of MS acquisition was *m/z* 50-1800. A capillary voltage of 4500 V, nebulizer gas pressure (nitrogen) of 2 bar, ion source temperature of 200 °C, a dry gas flow of 9 L/min and spectral rates of 3 Hz for MS^1 and 10 Hz for MS^2 were used.

II.3.5 Nuclear Magnetic Resonance

1D and 2D NMR spectra were recorded on an Avance III HD 400 MHz Nanobay NMR spectrometer equipped with a 5 mm broadband SmartProbe (Bruker BioSpin GmbH, Rheinstetten, Germany) and on a Bruker Avance III HDX 700 MHz NMR equipped with a 5 mm Prodigy TCI cryo probe head. NMR spectra were measured in d_6-DMSO, d_4-MeOH or d_3-MeOH at 293/308 K and were referenced to the corresponding residual solvent signals $\delta_{H/C}$ 2.50/39.5 (d_6-DMSO), $\delta_{H/C}$ 3.31/49.0 (d_4-MeOH, d_3-MeOH) or the internal offset for ^{15}N assigned by the instrument manufacturer (Bruker). Spectra were processed using TopSpin 3.6.1 and MestReNova 12.0. Structure elucidation was achieved by combination of the following NMR experiments:
^{1}H, ^{13}C, DEPT135, ^{1}H-^{1}H COSY, ^{1}H-^{13}C HSQC, ^{1}H-^{13}C HMBC, ^{1}H-^{1}H NOESY, ^{1}H-^{1}H ROESY, ^{1}H-^{13}C HSQC-TOCSY, ^{1}H-^{15}N HSQC, ^{1}H-^{15}N HMBC and band selective ^{1}H-^{13}C HMBC.

II.3.5.1 Interaction Studies

A full set of 1D and 2D NMR spectra was recorded on a Bruker Avance III HDX 700 MHz NMR equipped with a Prodigy TCI cryo probe head at 308 K in d_6-DMSO of uniformly ^{15}N-labelled Emp and unlabelled 3-lipid II to assign all chemical shifts. The Emp-3-lipid II complex was prepared by mixing molar amounts in a 2:1 ratio in methanol/water (50:50). The solvent was evaporated and the complex was lyophilised and subsequently dissolved in perdeuterated d_6-DMSO. For measurements in presence of calcium, a stock solution of $CaCl_2$*$2H_2O$ (125 mM) was prepared in d_6-DMSO and added to the complex solution to reach a final concentration of 1.25 mM. The following experiments were performed for interaction analysis: ^{1}H, ^{31}P, ^{1}H-^{1}H NOESY, ^{1}H-^{1}H TOCSY, ^{1}H-^{13}C HSQC, ^{1}H-^{15}N HSQC and HMBC.

II.3.6 Linearisation of Empedopeptin Derivatives

Pure empedopeptin and its possible derivatives (1 mg) were dissolved in 200 µL methanol and hydrolysed with 1N NaOH (400 µL) overnight at room temperature. After neutralisation with 1 N HCl (400 µL) the solvent was evaporated and the residue was dissolved in 500 µL methanol and analysed by LC-MS.

II.4 Bioinformatic Methods

II.4.1 Identification and Phylogenetic Analysis of NRPS Genes and Domains

For detection of relevant biosynthetic gene clusters encoding secondary metabolites, the online software antiSMASH 3.0 and 4.0 were used as well as for the automated prediction of adenylation and condensation domain specificity.[120,121]

For a more detailed phylogenetic analysis of the A and C domains in *Pseudomonas*, amino acid sequences of around 200 A and C domains of known NRPS and NRPS-PKS natural products were aligned using the software package MegaX with default settings (algorithm: MUSCLE). Trees were inferred by neighbour-joining using Jones-Taylor-Thornton (JTT) model with 1000 bootstrap replicates. The phylogenetic tree was visualised using Interactive Tree of Life (iTOL: https://itol.embl.de/).

For a phylogenetic analysis of TE domains, amino acid sequences of 46 TE domains of known NRPS natural products from *Lysobacter*, *Pseudomonas, Paenibacillus* and *Streptomyces* were aligned using the neighbour-joining method. The phylogenetic tree was created with ClustalOmega using the software available at https://www.ebi.ac.uk/Tools/msa/clustalo/ and visualised using Interactive Tree of Life (iTOL: https://itol.embl.de/).

II.4.2 MS Networking

HR-MS data processing was performed using Compass Data Analysis 4.4 and MetaboScape 3.0 was used for molecular features selection. Raw data files were imported into MetaboScape 3.0 for the complete data treatment and pre-processing in which the T-ReX 3D (Time aligned Region Complete eXtraction) algorithm is integrated for retention time alignment with an automatic detection to decompose fragments, isotopes and adducts intrinsic to the same compound into one single feature. A bucket table was generated for the obtained ions with their corresponding retention time, measured *m/z*, molecular weight, detected ions and their intensity within in the sample. The bucket table was prepared using the following settings for Emp_ring closed and Emp_ring open:[123]

Table II-21: Parameters used for bucket list.

	Emp_ring closed	Emp_ring open
Intensity threshold [counts]	100000.0	10000.0
Minimum peak length [spectra]	3	3
Minimum peak length (recursive) [spectra]	1	1
Minimum # Features for Extraction	1	1
Presence of features in minimum # of analyses	1	1
Lock mass calibration	false	false
Mass calibration	true	true
Primary Ion	$[M+H]^+$	
Seed Ions	$[M+Na]^+$, $[M+K]^+$, $[2M+H]^+$, $[2M+Na]^+$, $[M+2H]^{2+}$, $[M+H+Na]^{2+}$	
Common Ions	$[M-H_2O+H]^+$, $[M+H_2O+H]^+$, $[2M+H_2O+H]^+$, $[2M-H_2O+H]^+$	
EIC correlation	0.8	0.8
Mass range: Start [*m/z*]	500.0	500.0
Mass range: End [*m/z*]	1500.0	1500.0
Retention time range: Start [min]	15.0	15.0
Retention time range: End [min]	25.0	25.0
Perform MS/MS import	true	true
Group by collision energy	true	true
MS/MS import method	average	average

The feature list of the pre-processed retention time range was exported from MetaboScape as a single MFG file which in turn was uploaded to the GNPS online platform where a Feature-Based Molecular Network (FBMN) was performed. The precursor ion mass tolerance was set to 0.03 Da and a MS/MS fragment ion tolerance of 0.03 Da. Subsequently, a network was created where edges were filtered to have a cosine score above 0.7 and more than 6 matched peaks. Further, edges between two nodes were kept in the network if and only if each of the nodes appeared in each other's respective top 10 most similar nodes. Finally, the maximum size of a molecular family was set to 100, and the lowest scoring edges were removed from molecular families until the molecular family size was below this threshold. CytoScape was used for molecular network visualisation.[123]

Emp_ring closed:
https://gnps.ucsd.edu/ProteoSAFe/status.jsp?task=b0c65f6cdda34f31ba395dadb761379c
Emp_ring open:
https://gnps.ucsd.edu/ProteoSAFe/status.jsp?task=c4b7415e353a4139b63b423fb1b7ccbe

III Results

III.1 Recognition Mechanisms of Guanidine-Containing Lipopeptide Antibiotics

The family of guanidine-containing lipopeptide antibiotics is formed by empedopeptin, plusbacins and tripropeptins (**Chapter I.2.1.3**). Their structure is highly similar varying only in the northern hemisphere (R-6 to R-8) of the peptide moiety as well as in the terminal part of the fatty acid (**Figure III-1**). Despite their similarity, they differ significantly in potency. Empedopeptin (Emp), plusbacin A_3 (Plus A_3) and tripropeptin C (Tpp C) are the most active compounds of each class. Therefore, the focus of this study was put on these three compounds.

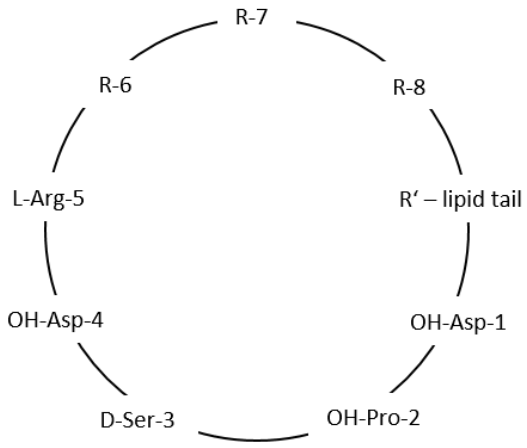

	R-6	R-7	R-8	R' – lipid tail
empedopeptin	Pro	Ser	Pro	$(CH_2)_{10} - CH_3$
plusbacin A_3	OH-Pro	Ala	Thr	$(CH_2)_{10} - CH(CH_3)CH_3$
tripropeptin C	Pro	Pro	Thr	$(CH_2)_9 - CH(CH_3)CH_3$

Figure III-1: Schematic structure of the cyclic lipopeptides of interest.

Empedopeptin, plusbacin A_3 and tripropeptin C consist of a depsi-octapeptide backbone and a lipid tail. Their structure is highly similar since variation occurs in the northern hemisphere (R6 – R8) and they differ in the lipid tail (R') which is either linear (Emp) or iso-branched (Plus A_3 and Tpp C).

This study was divided into two parts. In the first part, the focus was put on the isolation and purification of the cyclic lipopeptides, plusbacin A_3 and empedopeptin. The second goal was to obtain uniformly labelled CLPs to determine the solution structure of Emp, Plus A_3 and Tpp C in complex with 3-lipid II.

III.1.1 Isolation of Plusbacin A_3

Plusbacins were first isolated from *Pseudomonas* sp. PB-6250 in 1991 from Shionogi Research Laboratories, Osaka, Japan.[35] This strain was later reclassified as *Lysobacter firmicutimachus* sp. PB-6250^T.[38] Eight different derivatives are produced which are highly similar and are difficult to separate (**Figure III-2**). Plusbacins can be divided in an A and B series and the difference is a hydroxyl group on the proline at position 6. Additionally, there are variations in the lipid side chain. As plusbacin A_3 shows the highest bioactivity, this compound was prioritised.

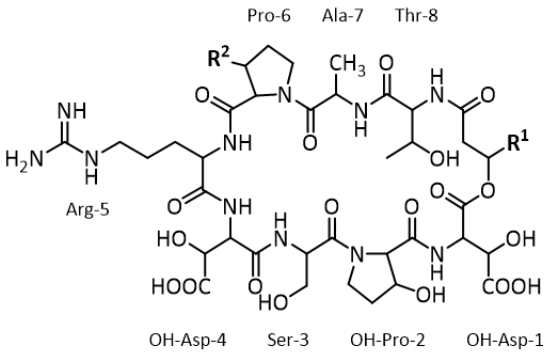

Plusbacin	R^1	R^2	*m/z* [Da]
A_1	$(CH_2)_{10}CH_3$	OH	1130.7
A_2	$(CH_2)_9CH(CH_3)CH_3$	OH	1144.7
A_3	$(CH_2)_{10}CH(CH_3)CH_3$	OH	1158.7
A_4	$(CH_2)_{12}CH_3$	OH	1158.7
B_1	$(CH_2)_{10}CH_3$	H	1114.7
B_2	$(CH_2)_9CH(CH_3)CH_3$	H	1128.7
B_3	$(CH_2)_{10}CH(CH_3)CH_3$	H	1142.7
B_4	$(CH_2)_{12}CH_3$	H	1142.7

Figure III-2: Plusbacin derivatives with their structural features and molecular weights.

Structure of plusbacin (left), the variations and the corresponding masses are shown in the table (right). Plusbacin A_{1-4} contain an OH-Pro at position 6 while B_{1-4} bears a regular proline at this position. Derivatives 1 – 4 of each series differ in length as well as branching of the fatty acid side chain.

Cultivation conditions were adopted from Henrike Miess[125] and are described in **Chapters II.2.2** and **II.2.3.1**. Large scale cultivations were performed due to the low production rate of plusbacins. At the beginning of this study, the cultivation was performed in linseed medium and was later on switched to R2A medium which generates less medium by-products. In general, the culture broth was acidified with HCl (5 M) and extracted twice with n-BuOH. The crude extract was separated by vacuum liquid chromatography (VLC) (**Chapter II.3.2**) and the active fractions were further purified by HPLC chromatography (**Chapter II.3.3.1**). All fractions were analysed by LC-MS (**Chapter II.3.4.1**) and an additional bioassay using *B. subtilis* 168 (**Chapter II.2.5**) was performed to identify the active fractions. The fractionation scheme is shown in **Figure III-3**.

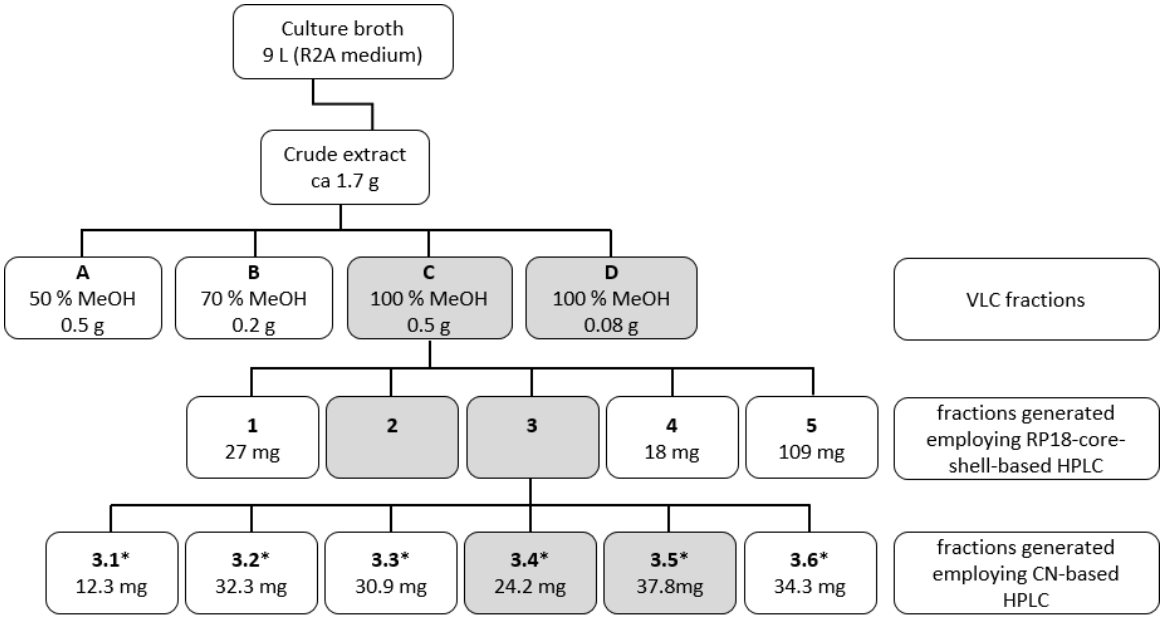

Figure III-3: Fractionation scheme for plusbacin A_3.

Cultivation of PB-6250 in 9 L R2A medium where 1.7 g of crude extract was obtained and subsequently, separated by RP-VLC (**A – F**). VLC fraction C was further fractionated using an HPLC system equipped with a Phenomenex Aeris peptide column (**1 – 5**). Fraction 2 and 3 were further purified by HPLC using a Phenomenex CN column (**3.1 – 3.6**). Highlighted in grey are fractions containing plusbacin A_3/A_4 (*m/z* 1158.8 $[M+H]^+$) confirmed by LC-MS. *The amount of these fractions was analysed in presence of phosphate salts due to the use of phosphate buffer in the last purification step.

All fractions containing plusbacin A_3 are highlighted in grey. After VLC separation, the active fraction C was further purified by a HPLC system equipped with a Phenomenex Aeris peptide column, followed by separation on a Phenomenex CN column using acetonitrile – phosphate buffer mixture as mobile phase. This last purification step was performed according to the published isolation protocol of plusbacins to obtain the single components.[126] LC-MS analysis revealed single components of plusbacin A_1 (*m/z* 1130.7) and A_2 (*m/z* 1144.7) as shown in **Figure III-4 A** and **C**, respectively. The corresponding B-series, B_1 (*m/z* 1114.7) and B_2 (*m/z* 1128.8), was only obtained as a mixture (**Figure III-4 B** and **D**).

Plusbacin A_3 (*m/z* 1158.8 Da, marked in green) was not obtained as a pure compound as shown in **Figure III-4 D** (fraction 3.4) and **E** (fraction 3.5). These fractions gave a peak at 31.53 (**D**) or 31.66 min (**E**) with masses of *m/z* 1128.8, 1142.8, 1144.8 and 1158 $[M+H]^+$ belonging to plusbacins B_2, B_3/B_4, A_2 and A_3/A_4, respectively, while the prioritised mass is marked in green. Separation of plusbacin A_3 from A_4 and B_3 from B_4 was not apparent from the LC-MS analysis, as they have the same mass but vary only in the constitution of their fatty acid side chain (branched fatty acid – 3 series, linear fatty acid – 4 series).

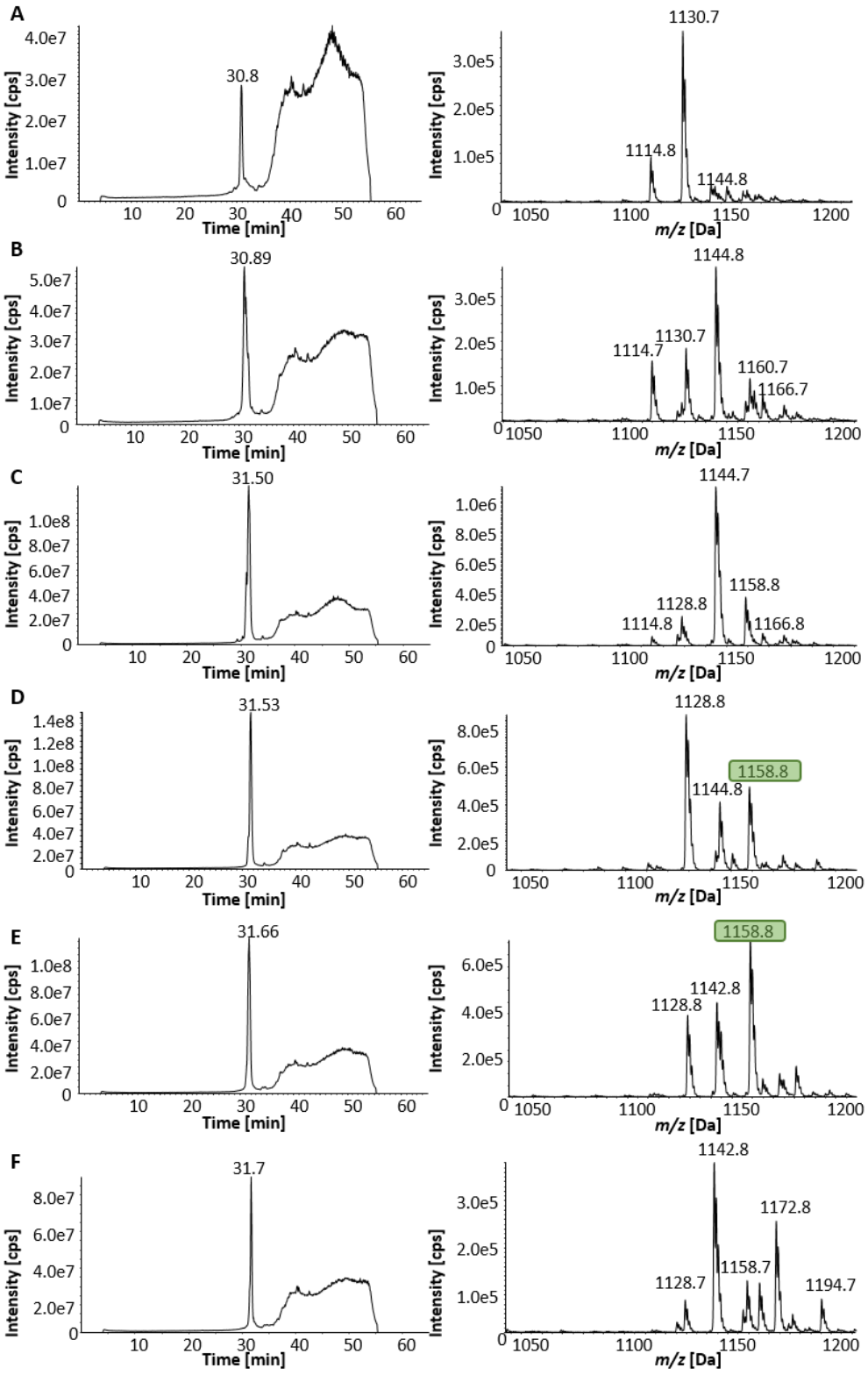

Figure III-4: LC-MS analysis of the fractions obtained after purification of fraction 3 using a CN column.

Total ion chromatogram (TIC) of each fraction is shown on the left side and the resulting molecular ions are shown on the right side. **A-F** showed the different fractions of 3.1 to 3.6 after purification by HPLC on a CN column. Fractions **D** (3.4) and **E** (3.5) showed the mass of interest highlighted in a green box (1158.8 Da, A_3/A_4), but in a mixture with the masses of 1128.8 (B_2), 1142.8 (B_3/B_4) and 1144.8 Da (A_2). The constitution of the fatty acid A_3 (branched) or A_4 (linear) is not apparent from the LC-MS analysis.

In order to achieve pure plusbacin A_3, different purification strategies were performed. On the one hand, various columns and different gradients were applied like a Phenomenex Luna Omega Polar, EVO and a chiral column (see **Table II-4**). On the other hand, different cultivation and extraction methods were tested. Cultivation was performed on solid linseed and R2A media but no improvement was observed. The extraction method with acetone according to Yoshida and co-workers was conducted but the separated fractions contained more compounds than the extracts with butanol.[126]

All in all, plusbacin A_3 was obtained in mixtures with other plusbacin derivatives, but isolation of single components was not achievable. Therefore, further purification methods need to be applied to get pure plusbacin A_3 to perform mode of action tests. Plusbacin A_2 could be obtained as single component in phosphate buffer. However, the amount was not sufficient for a complete structure elucidation.

III.1.1.1 Growth Curve of *Lysobacter firmicutimachus* PB-6250 and Determination of Plusbacin Production in Different Media

A bacterial growth curve of *L. firmicutimachus* and a semi-quantitative analysis of plusbacin production were conducted in different media as described in **Chapter II.2.3.3** to determine the optimal time for extraction as well as for feeding precursors to the cultivation medium.

First, cultivation was performed in linseed medium which was used as production medium in the beginning of the study. Therefore, a 1.5 L culture was prepared to prevent cultivation differences and the time of inoculation was set as the starting point. Due to turbidity of this medium, determination of bacterial growth by measuring the optical density at 600 nm was not appropriate. It was also not possible to calculate the dry weight owing to the large amount of calcium carbonate in the medium which interfered with the cell dry weight. The production of plusbacins was determined by semi-quantitative analysis because no standard was available. Production of plusbacins started 28 hours after inoculation as shown in **Figure III-5**. The production rate was analysed from plusbacin A_2/B_2 (peak 1) and plusbacins $A_3/A_4/B_3/B_4$ (peak 2). The highest production was achieved after 82 hours (**Figure III-5 B**). Therefore, the time for extraction was chosen between 72 and 82 hours due to a decreasing production of plusbacin after this time point. The feeding time for precursors was defined to be 26 hours because no significant production was observed before this time point.

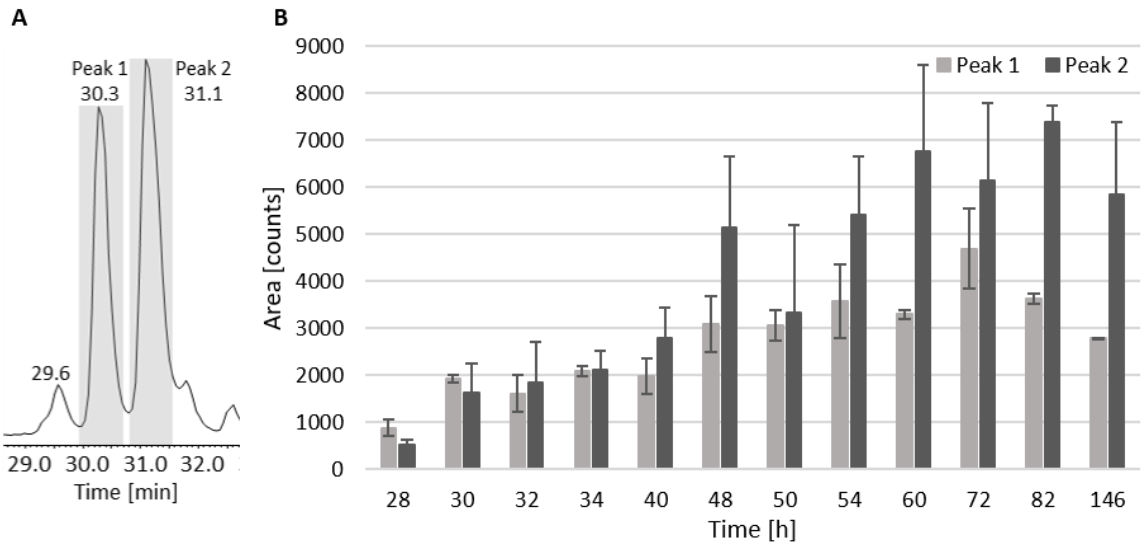

Figure III-5: Production of plusbacins by *Lysobacter firmicutimachus* in linseed medium.

A: TIC of crude extract after 72 hours of cultivation. Plusbacins A_1/B_1 gave a peak at 29.6 min and their production was not analysed due to the low amount. Plusbacins A_2/B_2 gave a peak (1) at 30.3 min and plusbacins $A_3/A_4/B_3/B_4$ a peak (2) at 31.1 min. **B:** Plusbacin production started after 28 hours and the maximum was achieved at around 72 hours. The production of Plusbacin A_2/B_2 is shown in light grey and the produced amount of plusbacin $A_3/A_4/B_3/B_4$ is shown in dark grey. Each time point was tested as duplicate.

Next, the bacterial growth curve and the production rate of PB-6250 were determined in R2A medium which was also a suitable production medium with low nutrient concentration. The growth curve (**Figure III-6 A**) showed a lag-phase of 7 hours where bacteria adjust their metabolism to the nutrients present and produce the corresponding enzymes. The exponential phase (also called log phase) lasted till ~18 hours where bacteria exhibit fast cell growth, which was followed by the stationary phase up to 98 hours of cultivation. The inoculation was performed with too little preculture, therefore the lag phase lasted quite long. The specific growth rate was determined by plotting the logarithm of cell density of the exponential phase against the time resulting in a straight line and gave a value of 0.3019 1/h. The doubling time was calculated as described in **Chapter II.2.3.3** with a value of 2.29 hours (**Figure III-6 B**).

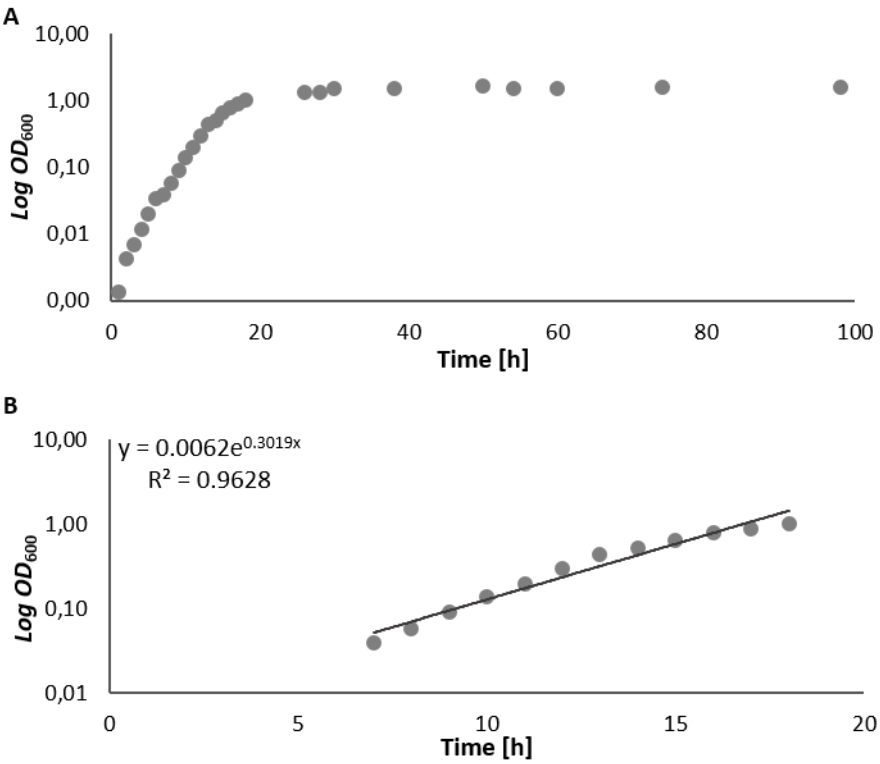

Figure III-6: Growth curve and determination of the doubling time of *Lysobacter firmicutimachus* PB-6250 in R2A medium.

A: Growth curve of *Lysobacter* PB-6250 by plotting the logarithm of optical density (OD_{600}) against the time of cultivation. The curve revealed a lag phase of 7 hours, followed by the log phase up to 18 hours to reach the stationary phase. **B:** The specific growth rate was determined by plotting the logarithm of cell density (OD_{600}) of the exponential phase against the time producing a straight line. The slope of this line gave the value for the specific growth rate of 0.3019. The doubling time was calculated as described previously and was determined with 2.29 hours.

The production of plusbacins by PB-6250 in R2A medium was also determined by semi-quantitative analysis. Production was observed after 14 hours of inoculation as depicted in **Figure III-7**. The produced amount was calculated for plusbacin A_2/B_2 (peak 1) and plusbacins $A_3/A_4/B_3/B_4$ (peak 2). There was a continuous increase in plusbacin production and the maximum was achieved between 32 and 50 hours. Therefore, the harvesting time was reduced to 50 hours due to a decreasing production of plusbacin after this time point. The feeding time for precursors was set to 12 hours after inoculation because no significant production was observed before this time point.

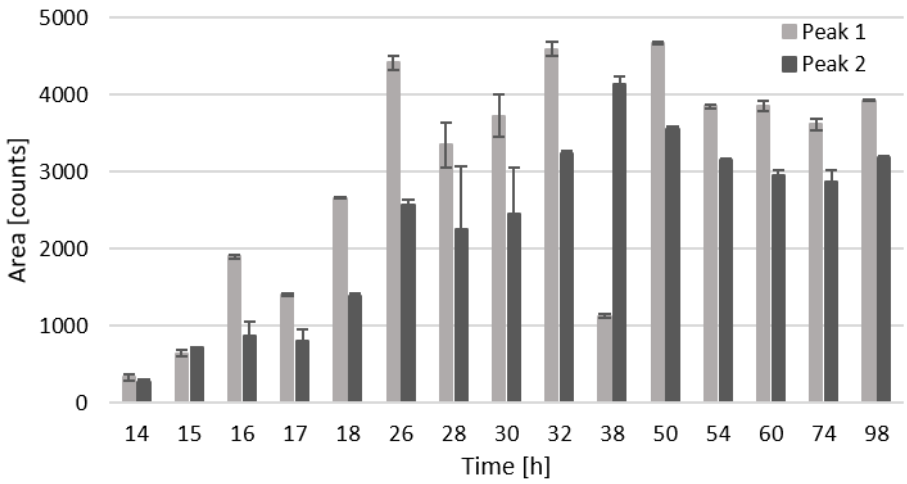

Figure III-7: Production of plusbacins by *Lysobacter* PB-6250 in R2A medium.

In R2A medium, plusbacin production started after 14 hours and the maximum was achieved between 38 to 50 hours. The production of plusbacin A_2/B_2 is shown in light grey (peak 1) and the produced amount of plusbacin $A_3/A_4/B_3/B_4$ is shown in dark grey (peak 2). Each time point was tested as duplicate.

III.1.1.2 Improvement of the Production Rate of Plusbacins in Media Supplemented with Precursors

In order to improve the production efficiency of plusbacin A_3, the most effective component, cultivation was first performed in linseed media supplemented with precursors of the biosynthesis of branched chain fatty acids. The synthetic pathway of branched fatty acids was already clarified in detail by Massey *et al*.[127] The biosynthetic precursors are the branched amino acids leucine and valine as shown in **Figure III-8**. Intermediates of this pathway are 4-methyl-2-oxo-butanoic acid and 3-methyl-2-oxo-butanoic acid, leading to the production of iso-fatty acids with odd and even number of carbon atoms, respectively. Cultivations supplemented with branched amino acids and their intermediates are known to enhance the productivity of established cyclic lipopeptide antibiotics bearing an acyl side chain.[128–130]

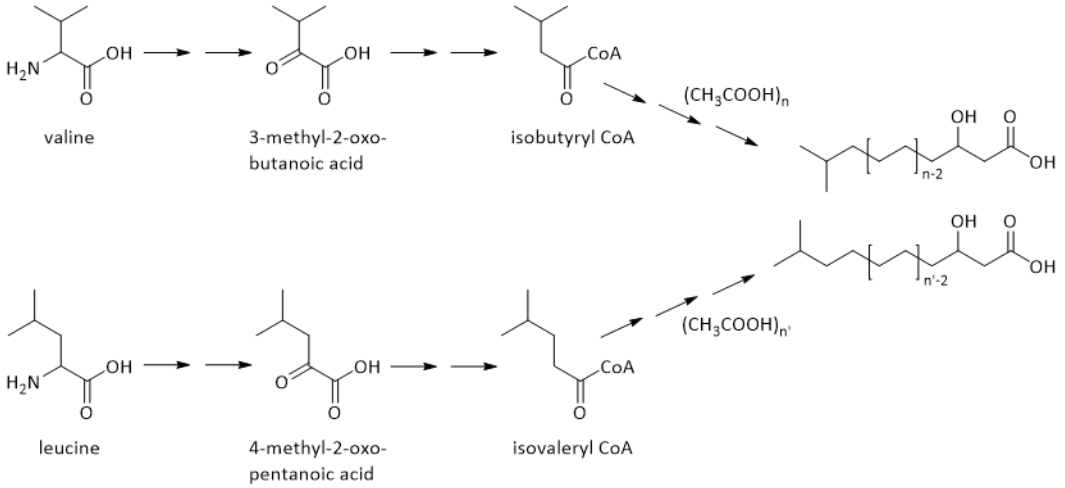

Figure III-8: Biosynthetic pathway of branched fatty acids with even and odd number of carbon atoms.

The biosynthetic precursors of branched fatty acids are valine and leucine. The intermediates are 4-methyl-2-oxo-butanoic acid and 3-methyl-2-oxo-butanoic acid to obtain iso-fatty acid with odd and even number of carbon atoms, respectively.[130]

Plusbacin A_3 is bearing an iso-fatty acid with even number of carbon atoms. Therefore, to improve the productivity of plusbacin A_3, cultivations were performed by adding L-valine (2 mg/mL) and 3-methyl-2-oxo-butanoic acid (2.5 mg/mL) to the culture media. These concentrations were chosen in accordance to the production enhancement of tripropeptins.[130] The addition of 3-methyl-2-oxo-butanoic acid to the cultivation medium 8 hours after inoculation did not significantly affect the production of plusbacin A_3 (32.9 min), as shown in **Figure III-9**. On the other hand, the production was completely abolished by adding valine to the culture medium. Therefore, large scale cultivations were conducted without addition of precursors.

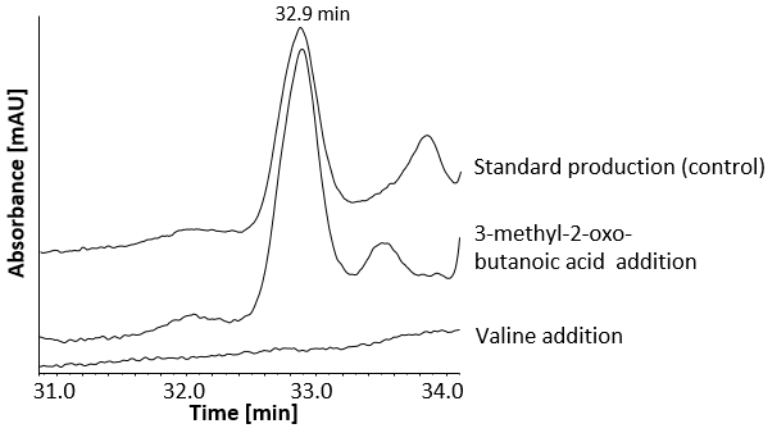

Figure III-9: UV chromatograms of plusbacin A_3 production in linseed medium supplemented with precursors.

Standard cultivation (top), addition of 3-methyl-2-oxo-butanoic acid (2.5 mg/mL, 8 hours after inoculation, middle) and L-valine (2 mg/mL, directly before inoculation, bottom) to the culture medium. The produced amount under standard conditions was comparable to the production in media supplemented with 3-methyl-2-oxo-butanoic acid. The production was abolished in media supplemented with L-valine.

During this study, the culture medium was changed from linseed medium to R2A medium since it contains the lower nutrient concentration and therefore generates fewer medium by-products. Precursor supplementation was also performed in R2A media at the end of this study, but this time, in order to simplify the process only inexpensive precursors were used. The production ratio of plusbacins was determined by addition of different branched amino acids like D- and L-leucine and D- and L-valine at different concentrations. Under standard conditions, plusbacins A_2/B_2 (peak 1 eluting at 30.30 min) and plusbacins $A_3/A_4/B_3/B_4$ (peak 2 eluting at 31.13 min) are produced in a ratio of 1:1 as shown in **Figure III-10 A**. The concentration of each branched amino acid which significantly affected (positive or negative) the production of plusbacins is shown in **Figure III-10 A**.

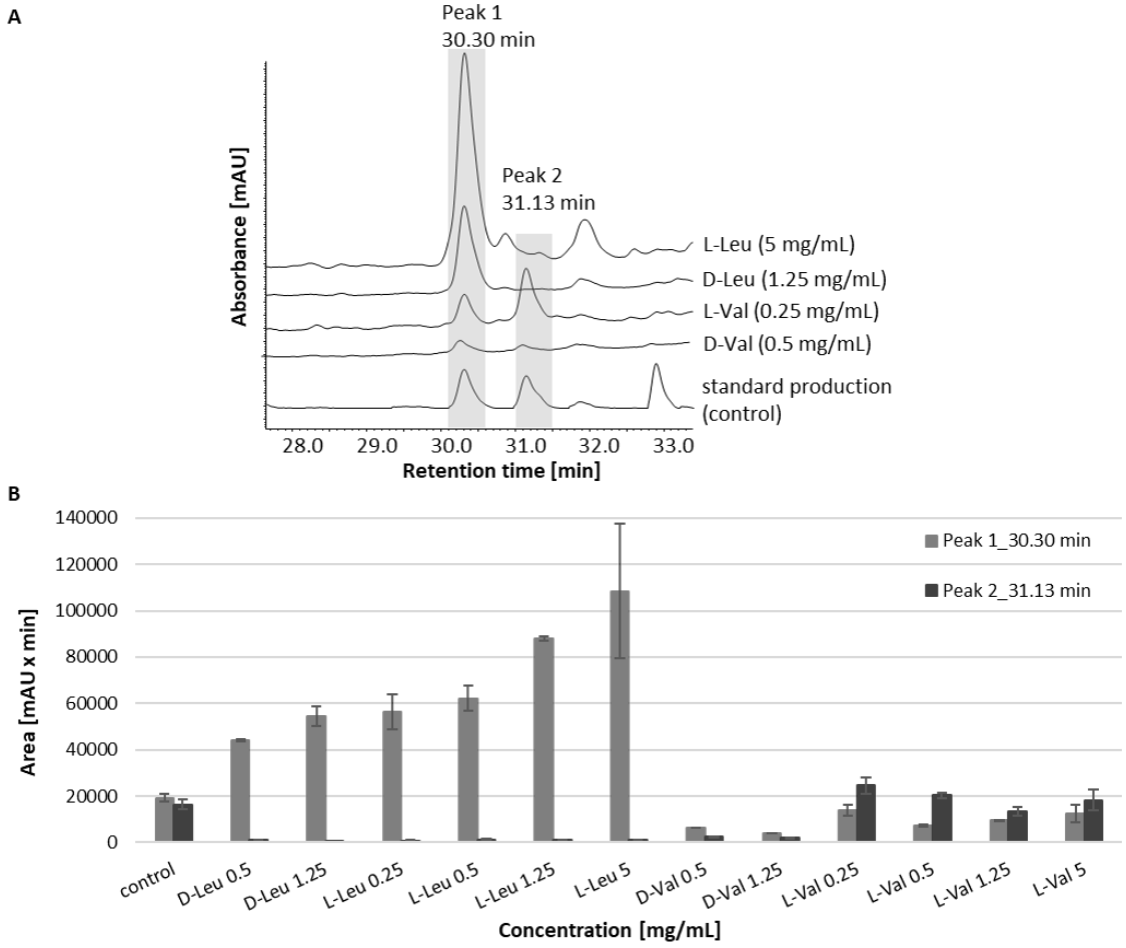

Figure III-10: Effect of plusbacin production in R2A medium supplemented with branched amino acids.

A: Comparison of UV chromatograms of plusbacin production in media supplemented with different branched amino acid. The concentration of each amino acid which significantly affected (positive or negative) the production is shown. Plusbacins A_2/B_2 gave a peak (1) at 30.30 min and plusbacins $A_3/A_4/B_3/B_4$ gave a peak (2) at 31.13 min.

B: The production of plusbacin A_2/B_2 is shown in light grey (peak 1) and the produced amount of plusbacin $A_3/A_4/B_3/B_4$ is shown in dark grey (peak 2). The addition of D- and L- leucine to the culture medium increased the production of plusbacins A_2/B_2 in a dose-dependent manner while the production of plusbacins $A_3/A_4/B_3/B_4$ was almost abolished under these conditions. The production of all plusbacins was remarkably decreased in media supplemented with D-valine. The production of plusbacins $A_3/A_4/B_3/B_4$ was slightly enhanced by addition of L-valine.

The production of plusbacins A_2/B_2 was improved in a dose-dependent manner by addition of D- and L-leucine to the culture medium as shown in **Figure III-10 B**. The maximum production was achieved to 3.25-fold at a concentration of 5 mg/mL of L-leucine. The produced amount of plusbacins $A_3/A_4/B_3/B_4$ was decreased significantly under these conditions. In culture media supplemented with D-valine at concentrations of 0.5 and 1.25 mg/mL, the production of all plusbacins was reduced. The addition of L-valine revealed a slight positive effect on the production of plusbacins $A_3/A_4/B_3/B_4$ while the highest production was achieved at 1.5 fold at 0.25 mg/mL of L-valine. The production of plusbacins A_2/B_2 was slightly decreased compared to the control under these conditions.

Surprisingly, cultivation of PB-6250 in R2A medium supplemented with branched amino acids had a positive effect on the production of plusbacins while the production was completely prevented in linseed media supplemented with L-valine.

III.1.2 Isolation and Purification of Empedopeptin

Empedopeptin was first isolated from Konishi *et al.* in 1984 in Japan.[34] Large scale cultivations of *Massilia* sp. ATCC 31962[37], formerly known as *Empedobacter haloabium* ATCC 31962, were performed to achieve sufficient amounts for serial passaging experiments. These experiments were performed in the working group of Prof. Dr. Tanja Schneider (University of Bonn, Germany) as project within the frame of the Collaborative Research Centre Transregional 261 (CRC-TR). Therefore, 18 litres of linseed medium were cultivated and purified as described in **Chapter II.2.3.1** and **II.3.3.2** and around 4 mg were obtained. Further cultivations of *Massilia sp. ATCC 31962* in linseed medium did not lead to any production. Cultivation in different media (R2A, Massilia medium (MM) (preculture medium of Emp) and minimal media; **Table II-7**) was performed and the crude extracts were analysed by LC-MS. In MM medium, the linear form of empedopeptin was produced as major compound however R2A medium was proven to be the most efficient medium for further production of empedopeptin (data not shown). Thus, 54 litres of R2A medium were cultivated and the culture broth was acidified with HCl to pH 3 – 4 and extracted twice with n-butanol. The established procedures are described in **Chapters II.2.3.1** and **II.3.1.1**. Subsequently, the crude extract was separated first by vacuum liquid chromatography (see **Chapter II.3.2**) and VLC fractions D, E and F were further purified by HPLC according to **Chapter II.3.3.2**. The purification workflow of empedopeptin from R2A medium is visualised in **Figure III-11**. All fractions were analysed by LR LC-MS measurements to confirm the presence of empedopeptin.

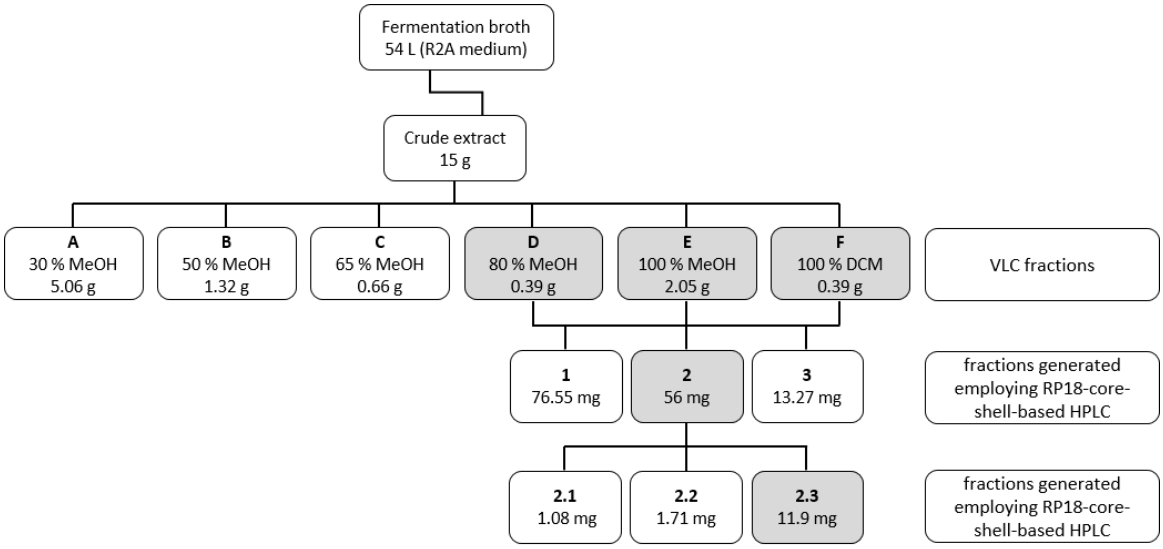

Figure III-11: Fractionation scheme for empedopeptin.

Crude extract was obtained from 54 L of R2A medium and subsequently separated by RP-VLC (A – F). VLC fractions D, E and F were further fractionated using an HPLC system equipped with a Phenomenex Aeris peptide column (1 – 3). Fraction 2 was further purified by HPLC using a Kinetex EVO column (2.1 – 2.3). Highlighted in grey are fractions containing empedopeptin confirmed by LC-MS.

The mass of empedopeptin (1126.7 Da $[M+H]^+$) was present in fractions highlighted in grey. In addition to the mass of Emp, other fractions showed masses of 1140.7 Da (fraction 2.1) and 1158.7 Da (fraction 2.2). The observed mass difference of 14 and 32 Da, respectively, could correspond to one methylene group or a methylene group and the addition of water (18 Da), leading to the assumption of new derivatives. Detailed analysis was performed by a MS networking approach to verify this hypothesis (**Chapter III.1.2.1**).

Altogether, around 16 mg of empedopeptin was obtained from 72 litres of fermentation broth (linseed and R2A medium). The compound was confirmed by HR-MS (**Figure III-12**) and NMR analysis (see **Chapter III.1.5.1**). Empedopeptin gave a peak at 18.3 min and revealed masses of *m/z* 1126.5636 $[M+H]^+$ and 563.7860 $[M+2H]^{2+}$, related to a molecular formula of $C_{49}H_{80}N_{11}O_{19}$ (calcd. for 1126.5626; Δ +0.9 ppm) and $C_{49}H_{81}N_{11}O_{19}$ (calcd. for 563.7850; Δ +1.8 ppm). MS/MS analysis revealed information about the peptide sequence as well as the attached fatty acid. The produced b- and y-series fragment ions of empedopeptin and all relevant fragments of the $[M+H]^+$ form are listed in **Table VIII-1**.

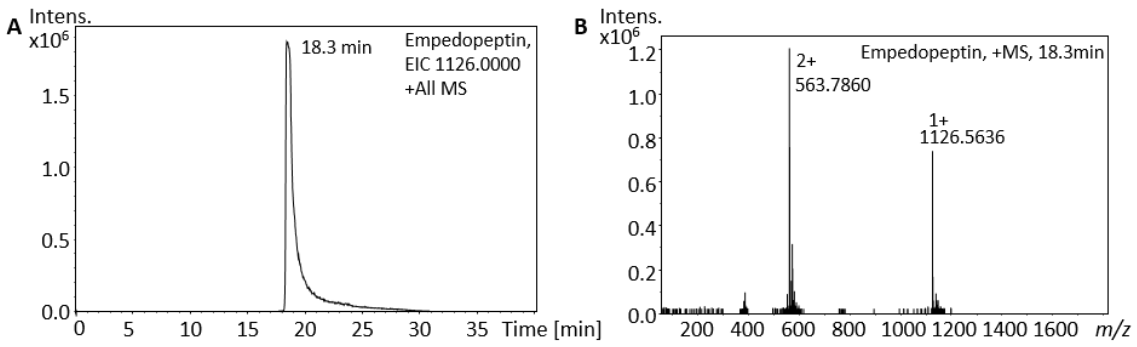

Figure III-12: HR-MS analysis of empedopeptin.

Mass analysis of purified empedopeptin. **A:** Extracted ion chromatogram (EIC) and **B:** MS^1 of empedopeptin (*m/z* 1126.5636 $[M+H]^+$ and 563.7860 $[M+2H]^{2+}$).

III.1.2.1 Molecular MS Networking

In order to illustrate the relation of empedopeptin to the new masses obtained in the other fractions, a molecular network (MN) was generated. Cultivations of ATCC 31962 performed in linseed media and isolation of Emp by using the Kinetex EVO column caused six different fractions with masses similar to Emp, of which fractions 3 and 4 contained Emp. The MN was developed from the fractions 3.1, 3.2, 3.5 and 3.6 from production in linseed medium as well as from the fractions 2.1 and 2.2 from cultivation performed in R2A. Each fraction was treated with sodium hydroxide as described in **Chapter II.3.6** to linearize the compounds in order to achieve a better fragmentation pattern. Every fraction was profiled by HR LC-MS (positive mode) before and after linearisation. The data were analysed by DataAnalysis. A molecular network was generated for all untreated and one for all treated (linearised) fractions. The MN of the treated fractions is shown in **Figure III-13** and the cluster in the grey rectangle was selected and annotated.

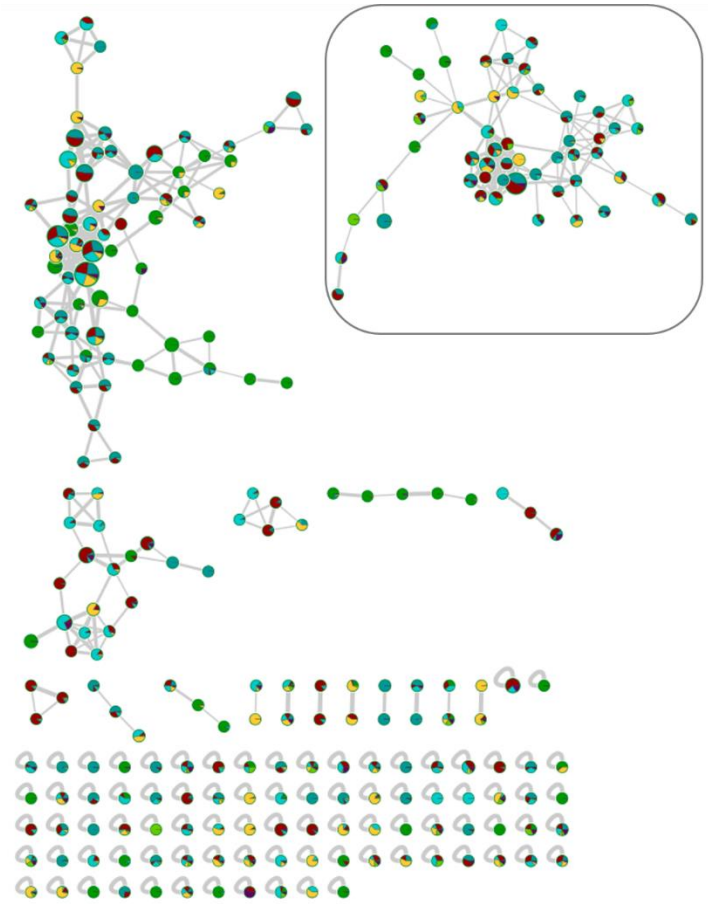

Figure III-13: Molecular Networking of linear empedopeptin and the related derivatives.
Minimum cluster size 1. Nodes are labelled with pepmass; edge thickness represents the cosine similarity score.

The colour of the nodes in **Figure III-13** and **Figure III-14** showed the major abundance of the masses in the different fractions. Structural annotation of the compounds was done by analysis of HR-LC-MS and MS/MS data. The fragments of the derivatives revealed similarity to the fragmentation pattern of empedopeptin. The nodes in the grey rectangles were analysed (**Figure III-14**). Linearization of Emp did not work completely, therefore node (a) revealed $[M+2H]^{2+}$ of the cyclised Emp. Node (b) was analysed and represented the linear form of empedopeptin. The analysed fragments are shown and listed in **Table VIII-2**. Node (c) and (d) showed masses which are 14 and 28 Da larger than empedopeptin. The analysis of the MS^2 spectra indicated an extension by CH_2 groups on the 3-hydroxy aspartic acids. Node (c) revealed the addition at the aspartic acid 1 and node (d) showed an extension on aspartic acid 1 and 3. The obtained fragments of node (c) and (d) are shown and listed in **Table VIII-3** and **Table VIII-4**, respectively. The amino acid can either be extended by a CH_2 group or the amino acid is methylated probably on the carboxylic acid. The analysis of node (e) predicted a peptide sequence of Ser-OH-Pro-Ser-Gly-Arg-Pro-Ser-Pro-myristic FA and is presented in **Table VIII-5**. In contrast to Emp, the amino acid 1 is a serine and amino acid 4 is a glycine instead of 3-hydroxy aspartic acids.

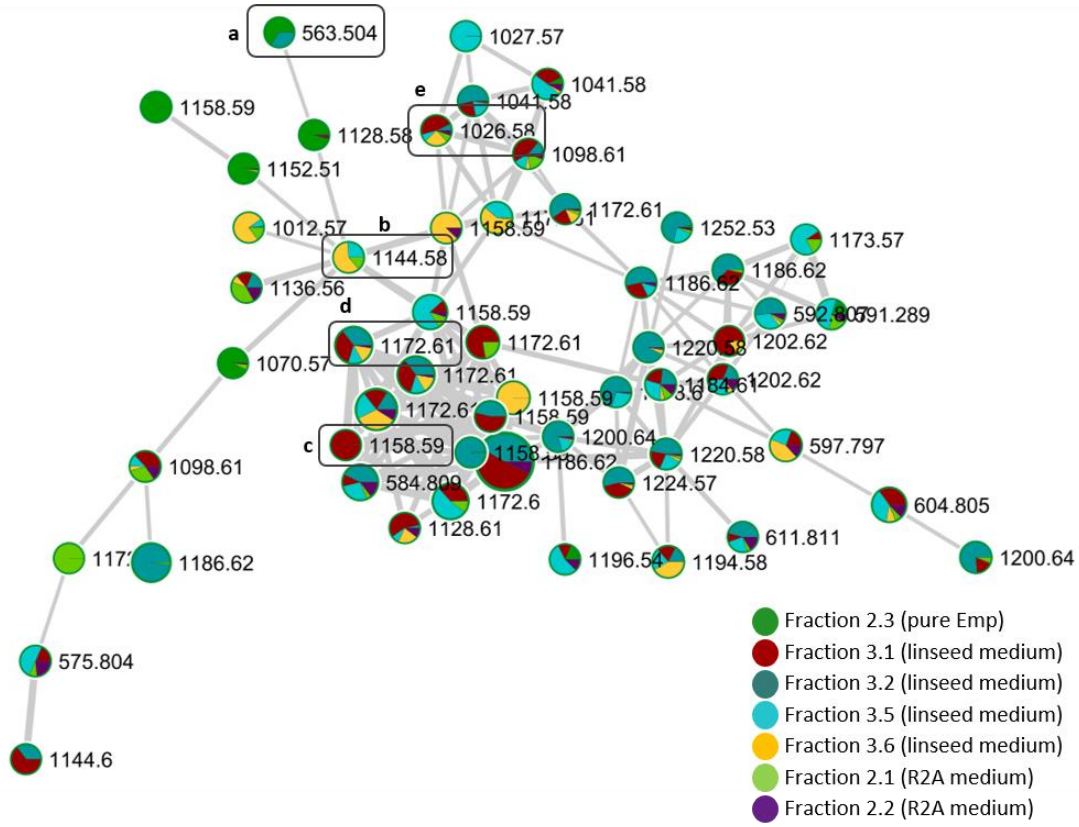

Figure III-14: Cluster from the previous figure analysed in detail.

Nodes in the grey rectangles were analysed. The colour of the nodes shows the major abundance of the masses in the different fractions.

The molecular network of the untreated compounds is not shown. However, the following compounds were analysed and are shown in **Table III-1**. The analysed fragments of compounds 4 – 7 are shown and listed in **Table VIII-6** to **Table VIII-9**. Derivative 4 possesses a methylated/extended 3-hydroxy aspartic acid at position 4 compared to empedopeptin. Derivative 5 and 6 revealed a methylated threonine at position 3 as well as methylated/extended 3-hydroxy aspartic acids. For derivative 7 a peptide sequence of Gly-OH-Pro-Ser-Me-OH-Asp-Arg-Pro-Ser-Pro was predicted. In all derivatives the *m/z* value of a myristic fatty acid (209 Da $[M+H]^+$) was observed.

Table III-1: Structural annotation of untreated compounds.

Cmp	Sequence	*m/z* [Da]; $[M+2H]^{2+}$
4	OH-Asp – OH-Pro – Ser – Me-OH-Asp – Arg – Pro – Ser – Pro	570.7937
5	OH-Asp – OH-Pro – Me-Thr – di-Me-OH-Asp – Arg – Pro – Ser – Pro	591.8161
6	Me-OH-Asp – OH-Pro – Me-Thr – di-Me-OH-Asp – Arg – Pro – Ser – Pro	598.8239
7	Gly – OH-Pro – Ser – Me-OH-Asp – Arg – Pro – Ser – Pro	542.7984

All in all, the isolated compounds with masses 14 and 28 Da larger than empedopeptin contain probably methylated 3-hydroxy aspartic acids or an extended OH-Asp resulting in a 3-OH-Glu. In the HR-LC-MS data, derivatives were observed with a different amino acid sequence, but there was no variation in the fatty acid like in the plusbacin or tripropeptin family. For further evidence, the compounds need to be analysed in more detail.

III.1.3 Cultivation of Uniformly Labelled Cyclic Lipopeptides

In order to determine the solution structure of CLPs in complex with 3-lipid II by NMR, a uniformly labelled cyclic lipopeptide is required due to the low natural abundance of nitrogen-15 isotope (0.37 %). Consequently, ^{15}N-labelled ammonium sulphate was established as an efficient precursor for uniformly labelled compounds. In linseed medium, the contained ammonium sulphate was exchanged in a 1:1 ratio with ^{15}N-labelled ammonium sulphate to achieve a similar production of cyclic lipopeptides. In R2A medium, the ingredient casamino acids was replaced by ammonium sulphate in a 1:1 ratio leading to an equal production rate. The amount of ^{15}N-labelled ammonium sulphate was increased to 1.6 fold due to the better isotope distribution pattern (data not shown). LC-MS revealed the incorporation of labelled nitrogen atoms by a stepwise increase of isotopic mass peaks. The isotope distribution pattern of plusbacin showed a bell shape and was shifted up to 11 isotopic mass peaks indicating that all 11 nitrogen atoms of the compound were labelled (*m/z* 1158 $[M+11+H]^+$; **Figure III-15 B)**. The isotope distribution pattern of empedopeptin revealed a shift up to 8 isotopic mass peaks (*m/z* 1126 $[M+8+H]^+$; **Figure III-15 D**). The distribution patterns of the unlabelled compounds, plusbacin and empedopeptin, are shown in comparison to the labelled compounds (**Figure III-15 A** and **C**).

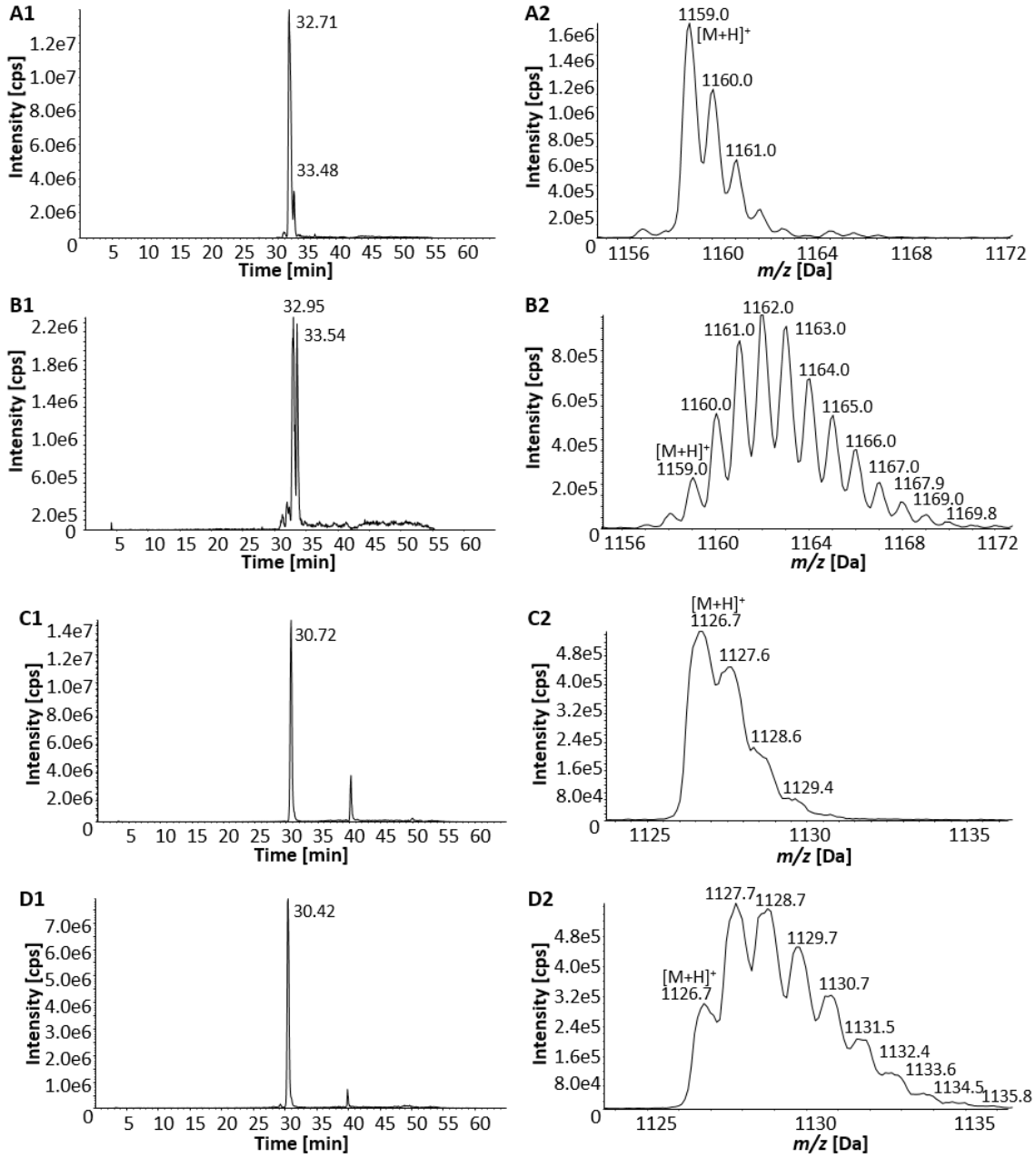

Figure III-15: Confirmation of production of ^{15}N –labelled plusbacin and ^{15}N-labelled empedopeptin.

LR LC-MS analysis of crude extracts from cultivations of PB-6250 (**A** & **B**) and *Massilia sp. ATCC 31962* (**C** & **D**) in media with and without supplementation of isotope-labelled $(^{15}NH_4)_2SO_4$. Extracted ion chromatogram (EIC) of unlabelled Plus A_3 (*m/z* 1158 – 1159) is shown in the top panel (**A1**) next to the resultant MS isotope distribution pattern of the peak eluting at 32.71 min (**A2**). In comparison, the EIC (**B1**) as well as the resultant MS isotope distribution pattern (**B2**) of labelled Plus A_3 are shown in the second panel. The distribution pattern of the peak eluting at 32.95 min of Plus A_3 was shifted and showed a bell shape. EIC and the resultant MS isotope distribution pattern of labelled and unlabelled empedopeptin is shown in panel **C** (unlabelled Emp) and **D** (labelled Emp). The distribution patterns of the peaks eluting at 30.72 and 30.42 min, respectively, are displayed.

III.1.4 Isolation and Purification of ^{15}N-labelled Plusbacin A_3

The cultivation and purification methods of ^{15}N-labelled plusbacin were adopted from the unlabelled plusbacins (see **Chapter III.1.1**). 9 Litres of linseed medium and 9 litres of R2A medium supplemented with ^{15}N-labelled ammonium sulphate were cultivated. Purification of crude extract from linseed medium was conducted by HPLC using a Phenomenex Aeris peptide column followed by a CN-based column. The purification of labelled plusbacin dealt with the same separation issues as in the case of unlabelled plusbacin. Therefore, the fraction of interest (plusbacin A_3) contained also other plusbacin derivatives and possibly methylated plusbacin A_3. Crude extract obtained from R2A medium was purified first by VLC, followed by HPLC using a Phenomenex Aeris peptide column (10 mm) and then employing a Kinetex EVO column as shown in **Figure III-16**.

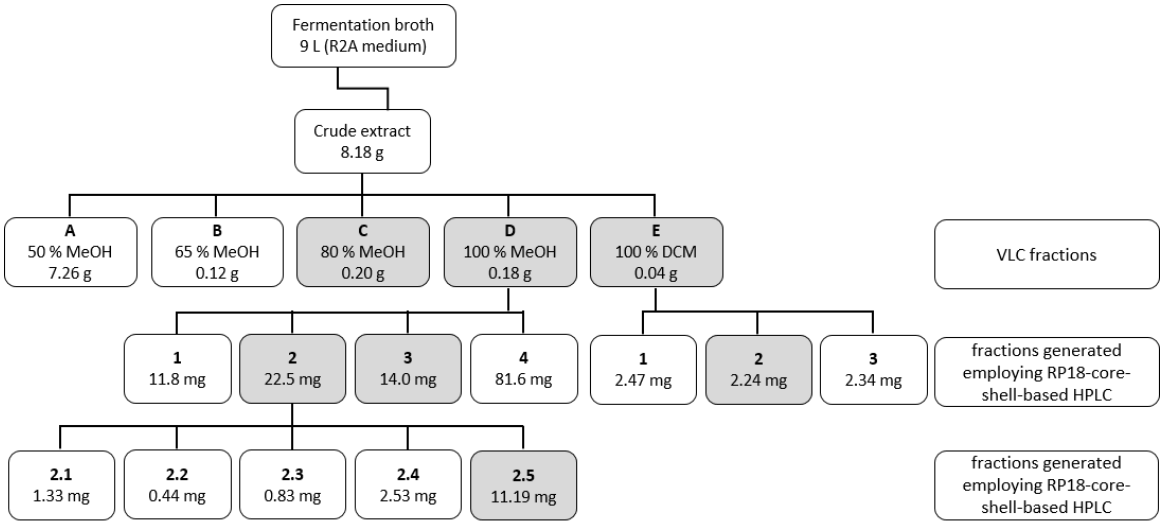

Figure III-16: Fractionation scheme of ^{15}N-labelled plusbacin produced in R2A medium.

9 L of R2A medium supplemented with ^{15}N-labelled ammonium sulphate was cultivated and the obtained crude extract was separated by VLC. The fractions C, D and E were further purified by HPLC on an Aeris peptide column. Fraction D2 was separated on a Kinetex EVO column. Fractions containing labelled plusbacin are highlighted in grey.

The fractions highlighted in grey contained the mass of plusbacin A_3 (*m/z* 1158.9 $[M+H]^+$) with a stepwise increase of the isotopic mass peak which was confirmed by LC-MS measurements. Fraction 2.5 contained mainly the mass of plusbacin A_3/A_4 (*m/z* 1158.9 $[M+H]^+$) and B_3/B_4 (*m/z* 1142.9 $[M+H]^+$) as shown in **Figure III-17**. The additional *m/z* value of 1172.9 was pointing to the N- or O-methylated form of plusbacin A_3/A_4 or the incorporation of glutamic acid instead of aspartic acid as the value is 14 Da larger. In the other fractions, *m/z* values of 1156.8 were observed with a stepwise increase of the isotopic mass peak leading to the assumption that

plusbacin B_3/B_4 are methylated or plusbacin B_2 is dimethylated due to the use of methanol as HPLC solvent. However, this assumption was not confirmed.

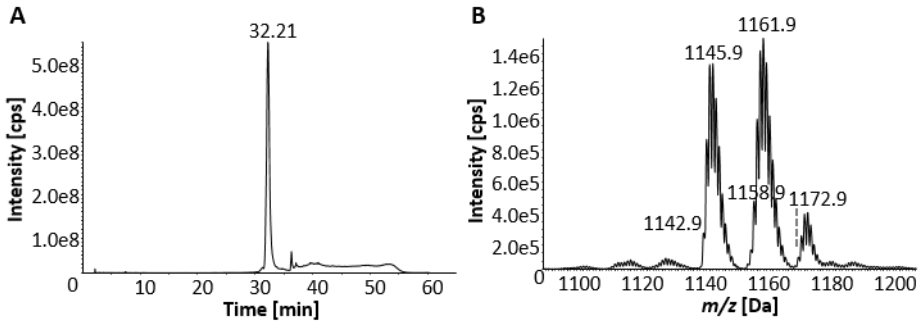

Figure III-17: LC-MS analysis of ^{15}N-labelled plusbacin A_3 after purification on a Kinetex EVO column.

A: Total ion chromatogram (TIC) of fraction **2.5** gave a peak at 32.21 min. **B:** Resulting molecular ions of plusbacin B_3/B_4 (*m/z* 1142.9 $[M+H]^+$) and plusbacin A_3/A_4 (*m/z* 1142.9 $[M+H]^+$)) with a stepwise increase of the isotopic mass peaks. An additional molecular ion of *m/z* 1172.8 was pointing to the methylated form of plusbacin A_3/A_4 or that glutamic acid was incorporated instead of aspartic acid.

III.1.5 Isolation and Purification of ^{15}N-labelled Empedopeptin

In order to obtain a sufficient amount of labelled empedopeptin for structure analysis and for the interaction studies, 67 litres of R2A medium supplemented with ^{15}N-labelled ammonium sulphate were cultivated and the fermentation broth was acidified with HCl (5 M) to pH 3 and extracted twice with n-butanol. The purification was performed according to the procedures of unlabelled Emp which are described in **Chapter II.2.3.2** and **II.3.1.1**. Subsequently, the obtained extract was separated first by vacuum liquid chromatography (see **Chapter II.3.2**) and VLC fractions D, E and F were further purified by HPLC chromatography according to **Chapter II.3.3.2**. The purification workflow of ^{15}N-labelled extracts from R2A medium supplemented with labelled ammonium sulphate is visualised in **Figure III-18**. All fractions were analysed by LR LC-MS measurements to confirm the presence of labelled empedopeptin.

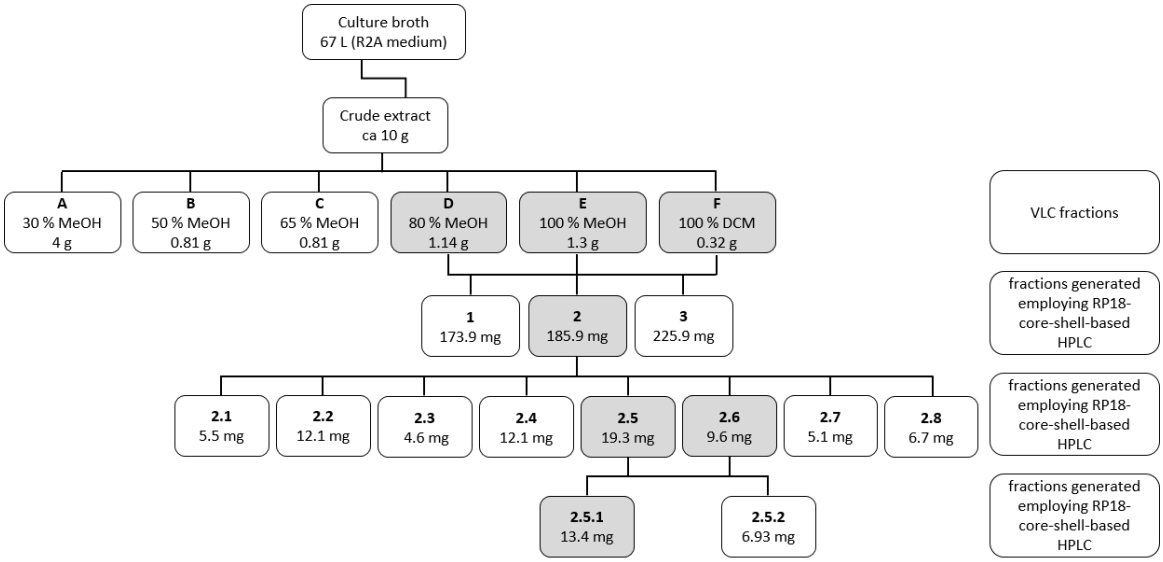

Figure III-18: Fractionation scheme of ^{15}N-labelled empedopeptin.

Cultivation of *Massilia sp. ATCC 31962* in 67 L of R2A medium supplemented with ^{15}N-labelled ammonium sulphate where around 10 g of crude extract was obtained. Fractionation by RP-VLC led to fractions A-F. Fractions D, E and F were further purified by HPLC using a Phenomenex Aeris peptide column (**1 – 3**), followed by fractionation using a Kinetex EVO column (2.1 – 2.8) The final purification step was performed by using a Phenomenex C_{18} column and 13.4 mg of ^{15}N-labelled Emp was obtained (2.5.1). Fractions containing labelled Emp are highlighted in grey which was confirmed by LC-MS.

In the purification workflow, the fractions containing empedopeptin are highlighted in grey and they revealed a mass of *m/z* 1126.7 $[M+H]^+$ with a shifted isotope distribution pattern as presented in **Figure III-15**. In accordance with the purification of unlabelled Emp, additional masses were observed after fractionation with a Kinetex EVO column. Six compounds were observed and showed masses of 1154.7 Da (2.1, 5.5 mg), 1140.7 Da (2.2, 12.1 mg and 2.5.2, 6.9 mg), 1172.7 Da (2.3, 4.6 mg), 1158.7 Da (2.4, 12.1 mg and 2.7, 5.1 mg) and 1144.7 Da (2.8, 6.7 mg). The mass of 1144.7 Da is related to the linear form of empedopeptin. The other masses showed a difference of 14 or 28 Da indicating an additional one or two methylene groups plus a mass difference of 18 Da corresponding to the mass of water. The addition of 18 Da could result from linearization of the peptide moiety through hydrolysis. From the MS^2 analysis of the unlabelled Emp (**Chapter III.1.2.1**), it is known that the alteration occurred at the 3-hydroxy aspartic acids. Therefore, NMR experiments (^{1}H, ^{1}H-^{13}C HSQC-TOCSY and ^{1}H-^{13}C HSQC) were conducted of the compounds with the masses of 1154.7 Da (2.1) and 1140.7 Da (2.2) to verify if new derivatives of Emp were obtained or if *N*- or *O*-methylation occurred in the presence of methanol (see **Chapter III.1.5.1**).

All in all, ^{15}N-labelled empedopeptin was obtained in a sufficient amount (13.4 mg) to fully elucidate the structure and to perform interaction studies with its primary target 3-lipid II.

III.1.5.1 Structure Elucidation of Empedopeptin

The structure of Emp was determined by Sugawara *et al.* by acid hydrolysis and mass spectral analysis.[131] Emp was partially analysed by NMR[132] but no full assignment was published so far. In this study, the structure of ^{15}N-labelled empedopeptin was fully analysed based on NMR experiments as described in **Chapter II.3.5**. The following experiments were performed: ^{1}H, ^{13}C, DEPT135, ^{1}H-^{1}H COSY, ^{1}H-^{13}C HSQC, ^{1}H-^{13}C HSQC-TOCSY, ^{1}H-^{13}C HMBC, ^{1}H-^{13}C band selective HMBC, ^{1}H-^{15}N HSQC and HMBC. Due to low quality of the NMR spectra at 293 K, the temperature was set to 308 K.

The ^{1}H NMR spectrum of empedopeptin (**Figure III-19**) as well as the ^{13}C NMR spectrum (**Figure VIII-1**) revealed resonances which are typical for the peptidic nature. A ^{1}H-^{13}C HSQC spectrum was recorded to assign all protons and their directly bonded carbons (**Figure VIII-3**).

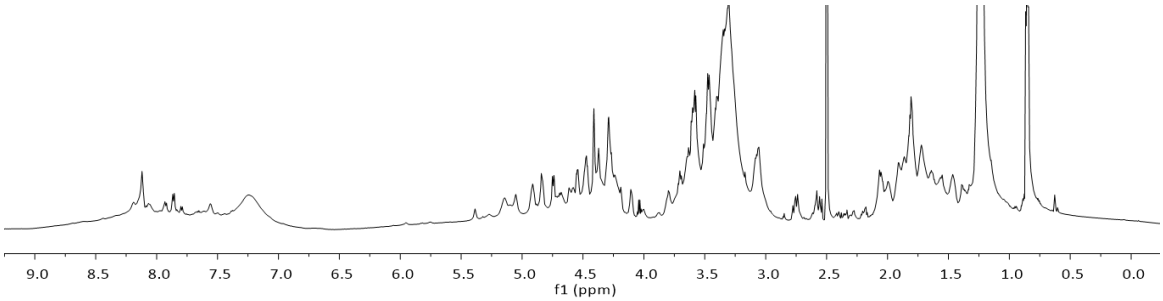

Figure III-19: ^{1}H NMR spectrum of empedopeptin in d_6-DMSO (700 MHz, 308 K).

The analysis of the ^{1}H-^{13}C HSQC-TOCSY represented the typical spin systems of an arginine, two serine residues, two 3-hydroxy aspartic acids, two proline moieties as well as one 3-hydroxy proline and 3-hydroxy fatty acid. The sequence of the peptide was determined by using a combination of the different 2D NMR spectra mentioned above. The identified sequence is comparable to the structure determination published by Sugawara *et al*.[131] The carbonyl atoms were assigned by band selective ^{1}H-^{13}C HMBC. The final structure and all key correlations of empedopeptin are shown in **Figure III-20**. The NMR spectroscopic data of empedopeptin are summarised in **Table III-2**.

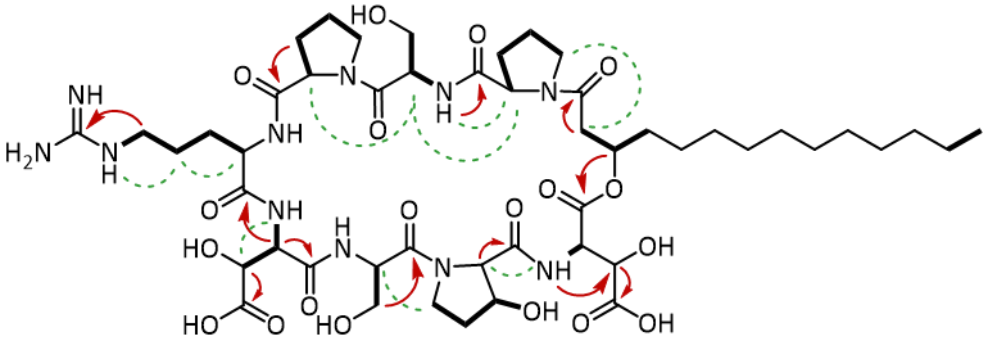

Figure III-20: Complete structure of empedopeptin and the obtained key correlations.

Bold lines indicate ^{1}H-^{1}H COSY correlations. Red arrows represent the ^{1}H-^{13}C HMBC correlations and dashed green lines depict the ^{1}H-^{1}H NOESY through space correlations.

Furthermore, two of the isolated compounds potentially related to empedopeptin (compound 2.1 and 2.2) were analysed by NMR. A comparison of the molecular masses of the compounds suggested a difference of one or two methylene groups leading to an extended amino acid (e.g., Glu instead of Asp) or *N*- or *O*-methylation of the amino acid. A typical range of a methoxy group in NMR spectra is defined at 3.5 - 4.0 ppm of ^{1}H and 50.0 – 55.0 ppm for ^{13}C.[133] The ^{1}H-^{13}C HSQC spectrum of both compounds revealed a cross peak in this area. The cross peak for compound 2.1 was observed at δ_H = 3.61 / δ_C = 51.7 and compound 2.2 at δ_H = 3.61 / δ_C = 51.6. The ^{1}H-^{13}C HSQC-TOCSY spectrum of the congeners did not show an additional spin system correlated to a glutamic acid or any other extended amino acid and the cross peak in the range of a methoxy group did not depict any correlation potentially due to the isolated position. Thus, it can be suggested, that compound 2.2 is methylated at one of the carboxylic acid moieties, whereas in compound 2.1, methylation occurred on both carboxylic acid moieties (**Figure III-21 A**). Compounds 2.4 and 2.3 are suggested to be the linear forms of compounds 2.2 and 2.1 (**Figure III-21 B**). The masses of *m/z* 1140.7 Da and 1158.7 Da were also observed in fractions 2.5.2 and 2.7, respectively, indicating that the methylation can also occur on the other aspartic acid. Compound 2.8 was suggested to be the linear form of empedopeptin with a molecular ion of *m/z* 1144.7 Da (**Figure III-21 B**).

A

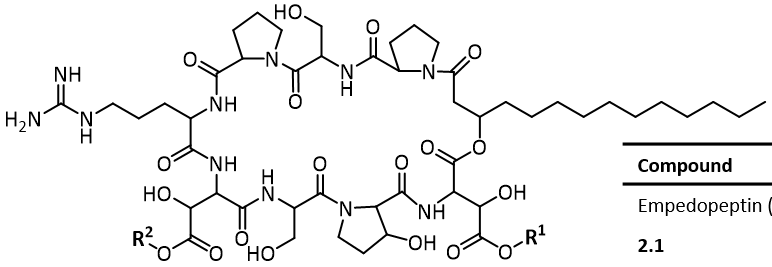

Compound	R^1	R^2	*m/z* [Da]
Empedopeptin (**2.5.1**)	H	H	1126.7
2.1	Me	H	1140.7
2.5.2	H	Me	1140.7
2.2	Me	Me	1154.7

B

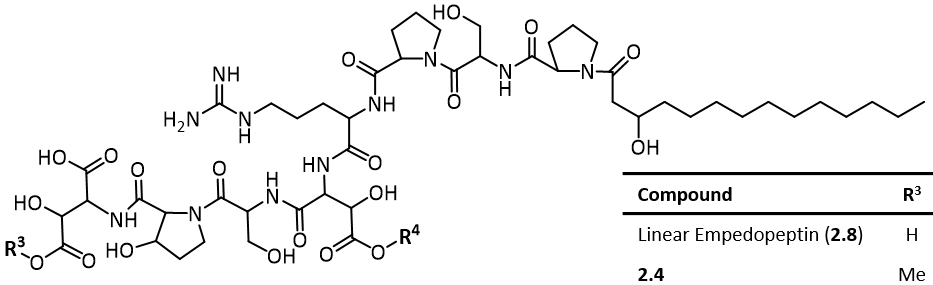

Compound	R^3	R^4	*m/z* [Da]
Linear Empedopeptin (**2.8**)	H	H	1144.7
2.4	Me	H	1158.7
2.7	H	Me	1158.7
2.3	Me	Me	1172.7

Figure III-21: Proposed structures of congeners of empedopeptin.

A: Ring closed form of empedopeptin and the related methylated congeners. **B:** Ring opened form of empedopeptin and the methylated relatives.

Table III-2: NMR spectroscopic data of ^{15}N-labelled empedopeptin (700 MHz, 308 K)**.**

residue	position	$\delta_{C/N}$[a]	δ_H (*J* in Hz)[b]	residue	position	$\delta_{C/N}$[a]	δ_H (*J* in Hz)[b]
3-HMA	CO	168.2 C_q		**Arg 5**	α	52.2 CH	4.23
	2	37.5 CH_2	2.57		β	28.8 CH_2	1.70
			2.76		γ	24.4 CH_2	1.39
	3	72.4 CH	4.91				1.47
	4	33.12 CH_2	1.64		δ	40.4 CH_2	3.07
	5-12	31.2 CH_2			ε	156.8 C_q	
		28.9 CH_2			α-CO	171.5 C_q	
		23.8 CH_2			α-NH	n.d.	n.d.
	13	22.0 CH_2	1.26		δ-NH	85.6 NH	7.56
	14	13.9 CH_2	0.85		ε-NH	74.7 NH_2	7.02 – 7.40
OH-Asp 1	α	54.9 CH	4.74	**Pro 6**	α	59.8 CH	4.83
	β	69.9 CH	4.37		β	31.6 CH_2	2.06
	α-CO	168.8 C_q			γ	22.3 CH_2	1.74
	α-NH	111.3 NH	7.86		δ	46.5 CH_2	3.30
	β-CO	174.0 C_q					3.36
	β-OH		n.d.		α-CO	172.3 C_q	
	OH		n.d.		α-NH	n.d.	n.d.
OH-Pro 2	α	67.2 CH	4.40	**Ser 7**	α	53.4 CH	4.10
	β	69.9 CH	4.41		β	60.6 CH_2	3.47
	γ	32.5 CH_2	1.81				3.59
			1.91		β -OH		n.d.
	δ	43.8 CH_2	3.26		α-CO	169.36 C_q	
			3.46		α-NH		8.12
	β-OH		5.05	**Pro 8**	α	58.3 CH	4.47
	α-CO	169.4 C_q			β	29.3 CH_2	1.72
	α-N	n.d.					2.03
Ser 3	α	52.3 CH	4.49		γ	23.9 CH_2	1.80
	β	60.1 CH_2	3.40		δ	47.1 CH_2	3.47
			3.70				3.59
	β-OH		n.d.		α-CO	171.0 C_q	
	α-CO	169.8 C_q			α-NH	n.d.	n.d.
	α-NH	n.d.	n.d.				
OH-Asp 4	α	57.3 CH	4.54				
	β	70.2 CH	4.29				
	α-CO	169.6 C_q					
	α-NH	109.2 NH	8.13				
	β-CO	172.9 C^q					
	β-OH		n.d.				

3-HMA: 3-hydroxy myristic acid. [a] Recorded at 176/101 MHz for ^{13}C and ^{15}N values were extracted from the corresponding ^{1}H-^{15}N HSQC and DEPT135 NMR spectrum. Multiplicity determined by an edited ^{1}H-^{13}C HSQC NMR experiment. [b] Recorded at 700/400 MHz. n.d. not detectable

III.1.5.2 Interaction Study of Emp and 3-Lipid II in Complex

From previous studies it was known, that empedopeptin binds lipid II as its primary target in a 2:1 complex in presence of calcium.[1] Moreover, antagonization assays of Emp and peptidoglycan precursors were conducted by Müller *et al.* and revealed interactions of the region of the pyrophosphate group, the MurNAc-moiety as well as the proximal regions of the stem peptide and the undecaprenyl chain.[1] However, the interaction on a molecular level was not analysed so far. Therefore, the solution structure of uniformly ^{15}N-labelled Emp in a 2:1 complex with lipid II was determined by NMR. The experiment was conducted by using a lipid II variant (3-lipid II, **Figure III-22**) which exhibits a shortened prenyl tail of only three isoprene units ((*E, E*)-farnesyl lipid II). Natural lipid II consists of eleven isoprene units, resulting in a poor solubility and a number of intense NMR signals arising from these units which can overlap important signals. 3-Lipid II was synthesized in a two-step synthesis by collaboration partners of the CRC-TR 261 from the University of Bonn (Prof. Dr. Dirk Menche and Prof. Dr. Tanja Schneider).[134] Each reaction partner was measured separately and the complex was measured with and without addition of calcium (1.25 mM, corresponding to the Ca^{2+} concentration in human serum) as described in **Chapter II.3.5.1.**

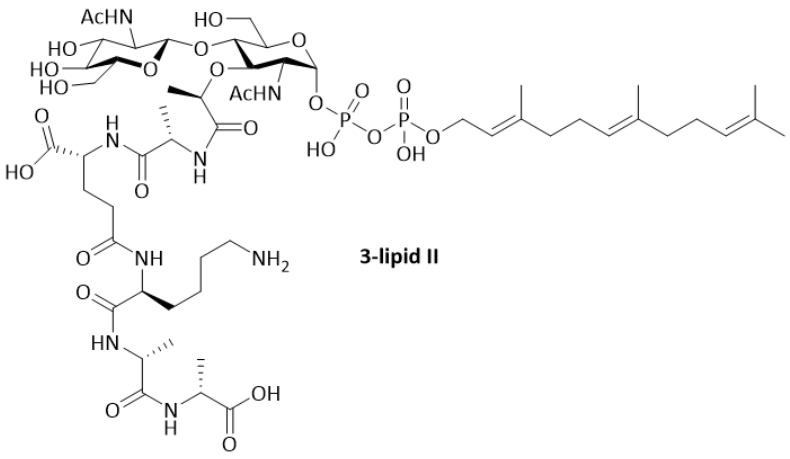

Figure III-22: Structure of 3-lipid II.

3-Lipid II consists of a disaccharide GlcNAc and MurNAc moiety where a pentapeptide (typical sequence: L-Ala-D-Glu-L-Lys-D-Ala-D-Ala) is attached and an isoprenyl tail of three units is linked via a pyrophosphate group.

In **Figure III-23** ^{31}P NMR spectra of the pyrophosphate group are compared. The pyrophosphate group of free 3-lipid II (black) is compared with Emp in complex with 3-lipid II in presence of calcium ions (red) and without addition of calcium ions (green). The spectra of free 3-lipid II revealed two major peaks at δ_P -12.0 (B) and δ_P -13.6 (A) which are comparable to published values and the shape of the peaks is identical to published lipid I variants.[135] Therefore, the signals A and

B would correlate to the two phosphates attached to either the part of the MurNAc or the prenyl tail, respectively, which need to be confirmed by a ^{1}H-^{31}P HMBC. The spectra of Emp in complex with 3-lipid II did not give a clear picture due to the low quality of these spectra. The peaks of the pyrophosphate group in the complex without supplementation of calcium showed a potential upfield shift to $\delta P_{A/B}$ -13.9 ($\Delta\delta P_A$ = -0.3 and $\Delta\delta P_B$ = -1.9, green line). Such an upfield shift was also observed in the results of nisin in complex with 3-lipid II.[136] An upfield shift was also observed in the ^{31}P NMR spectrum of the Emp:3-lipid II complex in presence of calcium ions at δP_A -13.8 and δP_B -12.9 ($\Delta\delta P_A$ = -0.2 and $\Delta\delta P_B$ = -0.9, red line). These potential shifts are indicating an interaction between Emp and the pyrophosphate moiety of 3-lipid II. The direct interaction side needs to be analysed further. Grey asterisks indicate impurities that probably originate from the enzymatic reaction. These probably also interact with Emp resulting in a chemical shift which are marked with green asterisks.

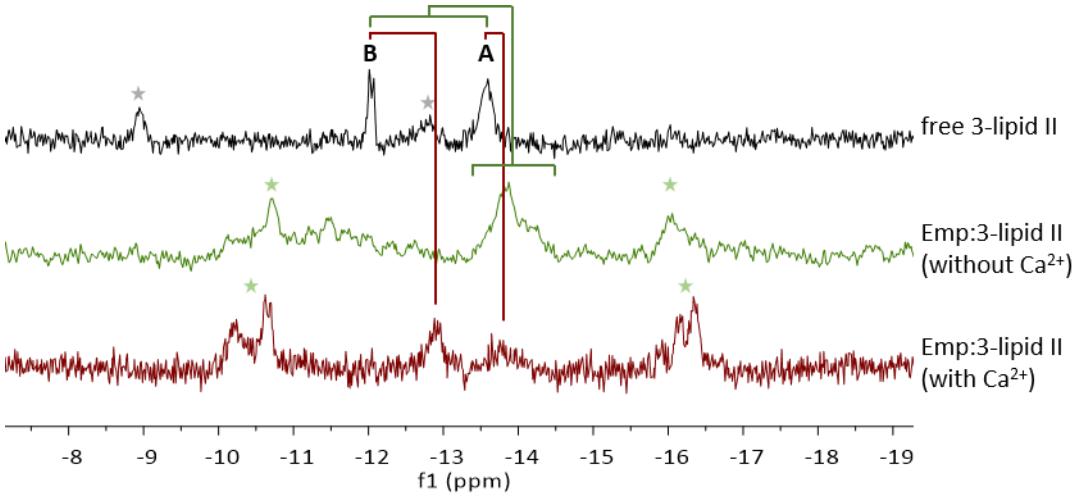

Figure III-23: ^{31}P NMR spectra of free 3-lipid II and in complex with Emp (600 MHz, 308 K).

The pyrophosphate group of 3-lipid II in the free (black), in complex with Emp without addition of Ca^{2+} (green) and in complex with Emp with addition of Ca^{2+} (red). Grey asterisks indicate impurities of the enzymatic reaction.

The stacked ^{1}H-^{15}N HMBC spectra of free ^{15}N-labelled Emp (black) and in complex with 3-lipid II (green) without addition of Ca^{2} (**Figure III-24**) presented a shifted signal of the amine group of the 3-hydroxy aspartic acid at position 4 which is marked by a red line ($\Delta\delta_H$ = 0.25). The other peak obtained (3-hydroxy aspartic acid at position 1) was not affected. An additional cross peak at δ_H 5.38 / δ_N 76.3 was observed in the spectra of the 3-lipid II bound Emp without addition of calcium. However, the assignment of this signal was not possible, but it can be suggested that this signal arises from the guanidinium group of arginine at position 5. This is due to the ^{15}N value of δ_N 76.3 which is comparable to the ^{15}N value of free Emp (δ_N 74.7 obtained from ^{1}H-^{15}N HSQC NMR spectra **Figure VIII-9**) whereas the proton value is shifted by a value of $\Delta\delta_H$ = -1.83. The

^{1}H-^{15}N HMBC spectra of Emp in complex with 3-lipid II with supplementation of calcium showed the same result, but the quality of these spectra is quite low and therefore not shown. The first analysis of the NMR measurements of the complex unveiled contacts of the western hemisphere (3-hydroxy aspartic acid 4 and arginine 5) of Emp with 3-lipid II. Significant intramolecular NOE signals could not be observed due to the low quality of the spectra.

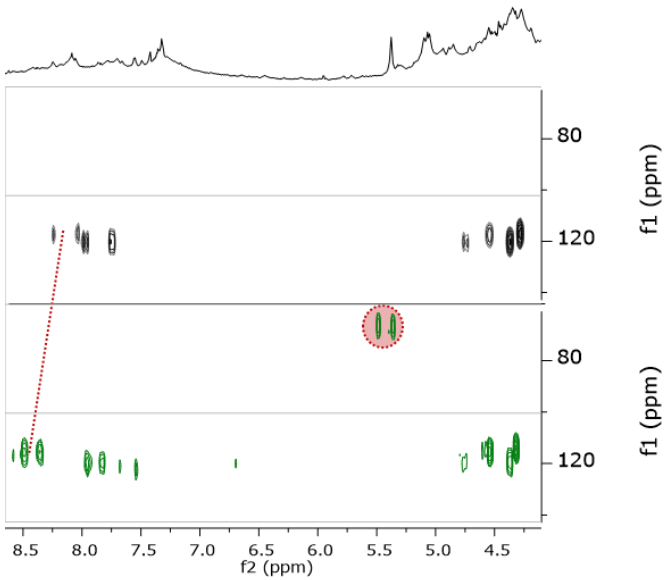

Figure III-24: Stacked ^{1}H-^{15}N HMBC spectra of free ^{15}N-labelled Emp (black) and in complex with 3-lipid II (green) without addition of Ca^{2+}

Red line indicates a change in the chemical shift of 3-OH Asp-4 and the red circle presents the presence of an additional cross peak, possibly the guanidinium group of arginine at position 5.

III.1.6 Analysis of the Cyclisation Scheme of CLPs

The cyclisation schemes of the CLPs empedopeptin, plusbacins and tripropeptins were suggested to be different than published in literature.[43,126,131] Therefore, the tandem TE domains were phylogenetically analysed and compared with TE domains identified in known NRPS biosynthetic gene clusters from *Bacillus, Lysobacter, Pseudomonas* and *Streptomyces* (**Figure III-25**).

The analysed TE domains can be grouped in two functional classes (type I and type II TE proteins) which are further divided into subclasses (**Chapter I.3.4**). The type II TE proteins are classified in two subgroups. The first subgroup belongs to bacilli and showed a repair function to regenerate misacylated NRPS enzymes (TE 2, in blue).[137] The second subgroup revealed an integrated function and is part of gram-negative pseudomonads (TE 2, in red). The type I TE domains are separated in three subclasses. The type I TE domains from bacilli are shown in blue and the macrocyclisation is performed between the fatty acid side chain bearing either an amine (NHFA) or a hydroxyl group and the C-terminal amino acid. In the two other type I subclasses, the TE domains are either from

pseudomonads (green) or actinomycetes (purple) and the ring closure occurs between the C-terminal amino acid and the hydroxyl group of serine or threonine or the amino group of 2,3-diaminobutyric acid (Dab), respectively.

The TE domains from the CLPs of interest, empedopeptin, plusbacins and tripropeptins, are highlighted in bold and cluster into the type I and type II TE domains of pseudomonads. Therefore, the ring closure should occur between the C-terminal amino acid and the hydroxyl group of serine or threonine. However, in the published structures, cyclisation occurs between the C-terminal amino acid and the hydroxyl group of the fatty acid.[34,43,126] NMR analysis was performed to clarify the cyclisation scheme.

Figure III-25: Phylogenetic analysis of TE domains.

Phylogenetic analysis of amino acid sequences of 46 TE domains identified in known NRPS CLP biosynthetic gene clusters (BGC) from *Bacillus*, *Lysobacter*, *Pseudomonas* and *Streptomyces*. The abbreviations in the tree indicate the gene cluster name (see **Table VIII-10**) and the amino acid or moiety through which the cyclisation occurred. The TE number is assigned, whenever a gene cluster contained more than one TE domain and reflects also its sequential arrangement in the gene cluster. Clusters comprising the TE domains of Emp, Plus and Tpp are highlighted in bold. TE: thioesterase; Emp: empedopeptin; Plus: plusbacin; Tpp: tripropeptin; Dab, 2,4-diaminobutyric acid; FA, fatty acid; NHFA: amine group of fatty acid; Ser: serine; Thr: threonine; Tyr: tyrosine.[138]

The structures of empedopeptin and tripropeptin were analysed by NMR experiments. Pure tripropeptin C (11 mg) was obtained from the Microbial Chemistry Research Foundation (MCRF, Japan). The structure was elucidated by NMR and the determined values of tripropeptin C (**Table VIII-11**) are comparable to the published NMR data by Hashizume *et al.*[43]

The ^{1}H-^{13}C HMBC NMR spectrum of empedopeptin revealed a long-range coupling between the α-carbonyl of OH-Asp-1 (δ_C 168.8) and H-3 of the fatty acid (δ_H 4.91), as shown in **Figure III-26 A**. This observation clearly indicated the cyclisation between the fatty acid and the C-terminal amino acid OH-Asp. This long range correlation was not visible in the Tpp ^{13}C NMR data. However, the ^{1}H-^{13}C HSQC TOCSY as well as the ^{1}H-^{1}H TOCSY NMR spectra of tripropeptin C showed a correlation of the β-OH group of threonine (δ_H 4.63) with the spin system of threonine (γ-Thr, δ_C 18.6), as presented in **Figure III-26 B**. The observed free hydroxyl moiety of threonine indicated that the lactone linkage did not occur between the C-terminal amino acid and the hydroxyl group of threonine. This suggests that the cyclisation was also formed between the fatty acid and the C-terminal 3-hydroxy aspartic acid. This cyclisation scheme is identical with the published structure of tripropeptin C. Hashizume *et al*. observed a long range coupling between the carbonyl of OH-Asp-1 (C-1, δ_C 168.6) and the H-3 of the fatty acid (H-39, δ_H 5.06) by decoupled HMBC.[43]

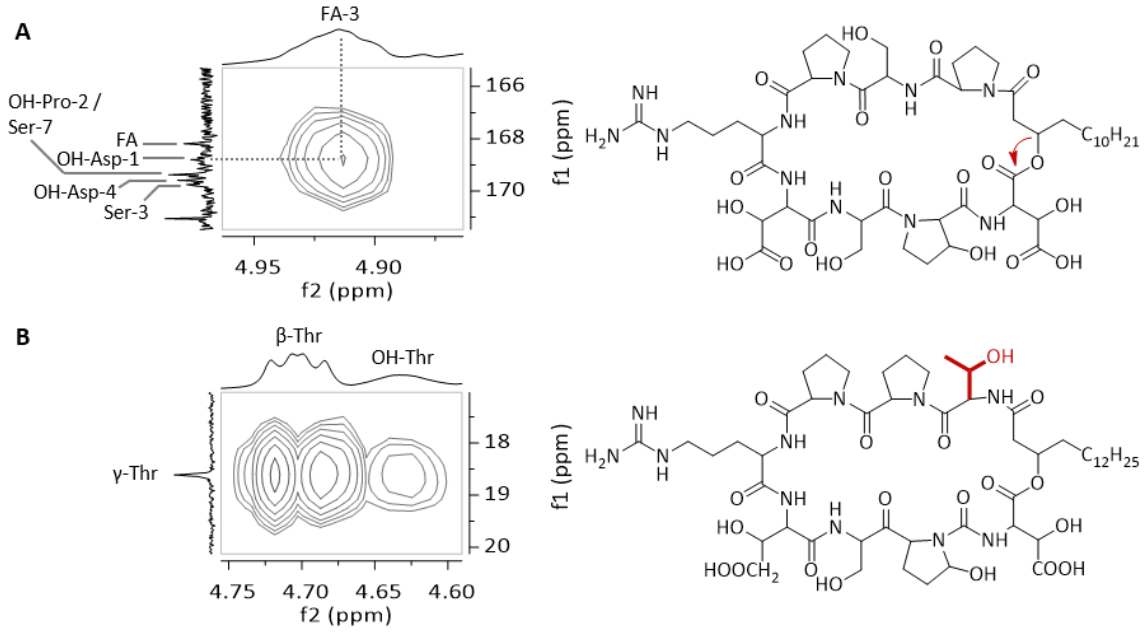

Figure III-26: Proof of the cyclisation scheme of Emp (**A**) and Tpp (**B**).

A: A long-range coupling (^{1}H-^{13}C HMBC) was observed between the α-carbonyl of OH-Asp-1 (δ_C 168.8) and H-3 of the fatty acid (δ_H 4.91). **B:** A correlation of the free β-OH group of threonine (δ_H 4.63) with the spin system of threonine (γ-Thr, δ_C 18.6) (^{1}H-^{13}C HSQC TOCSY) was visible. Both correlations indicated that the lactone linkage occurred between the hydroxyl group of the fatty acid and the C-terminal 3-hydroxy aspartic acid.

III.2 Genome Mining in the Plant Pathogenic Bacterium *Pseudomonas viridiflava*

III.2.1 *In silico* Screening for Lipopeptides in *Pseudomonas*

At the beginning of the study, genome sequences of the genus *Pseudomonas* of the strain collection of Tübingen were subjected to an *in silico* screening for lipopeptides. Initially, seven strains belonging to the species *Pseudomonas viridiflava* were prioritised and analysed (see **Table II-6**). Alejandra Duque from the Weigel group (Max Planck Institute for Developmental Biology, Tübingen) was investigating the interactions between *Arabidopsis thaliana* and *Pseudomonas viridiflava* and she kindly provided these seven strains. These strains had four gene clusters in common and with the help of antiSMASH[120,121], these BGCs were identified as a NAGGN gene cluster (N-acetyl-glutaminyl-glutamine amide), a NRPS-PKS hybrid biosynthetic gene cluster, one was predicted to code for a pyoverdine and the last one encoded an octalipopeptide.

The putative octalipopeptide gene cluster is shown as schematic representation of the strain *P. viridiflava* P1.A2 and is located on the genes *Ctg7_838* and *Ctg7_839* (see **Figure III-27**).

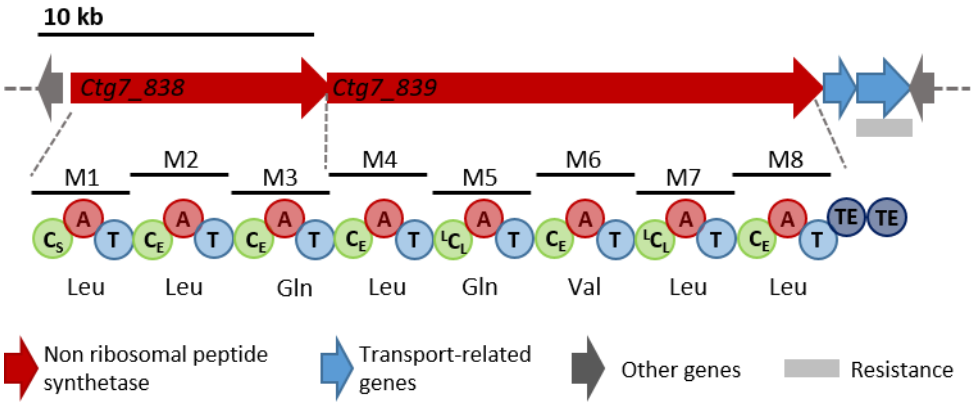

Figure III-27: Schematic representation of the lipopeptide gene cluster identified in *Pseudomonas viridiflava* P1.A2.

Colours of genes indicate putative functions of encoded proteins: red, NRPS; blue, transporter; grey, others; grey box, resistance. Module and domain organisation are indicated below the genes *Ctg7_838* and *Ctg7_839*. Domains were grouped into modules and are represented by a bar and module number. The domains are labelled by C_S = starter condensation domain; C_E = dual-function condensation-epimerisation domain; ^LC_L = condensation domain catalysing a peptide bond between two L-amino acids; A = adenylation domain; T = thiolation domain; and TE = thioesterase domain. Underneath the modules the predicted amino acid specificity is represented.

Bioinformatic analysis of the amino acid sequence using antiSMASH revealed that the proteins *Ctg7_838* and *Ctg7_839* consist of three and five NRPS modules, respectively, each comprising of a C, A and T domain. A starter condensation domain is located at the beginning of *Ctg7_838* and a dual TE domain terminally in *Ctg7_839*. The starter C domain is important for attachment of a fatty acid. The C-domains of modules 5 and 7 are predicted to have a ^LC_L chirality in peptide bond

formation, while modules 2 – 4, 6 and 8 belong to the family of dual-function condensation-epimerisation domains. The A domain specificity was analysed by antiSMASH[120,121] and predicted to activate leucine in position 1, 2, 4, 7 and 8, and valine in position 6. In order to verify the specificity of the A domains and to analyse the A domains in position 3 and 5, a phylogenetic analysis of the A domains of various known *Pseudomonas* lipopeptides was performed (see **Figure III-28**).

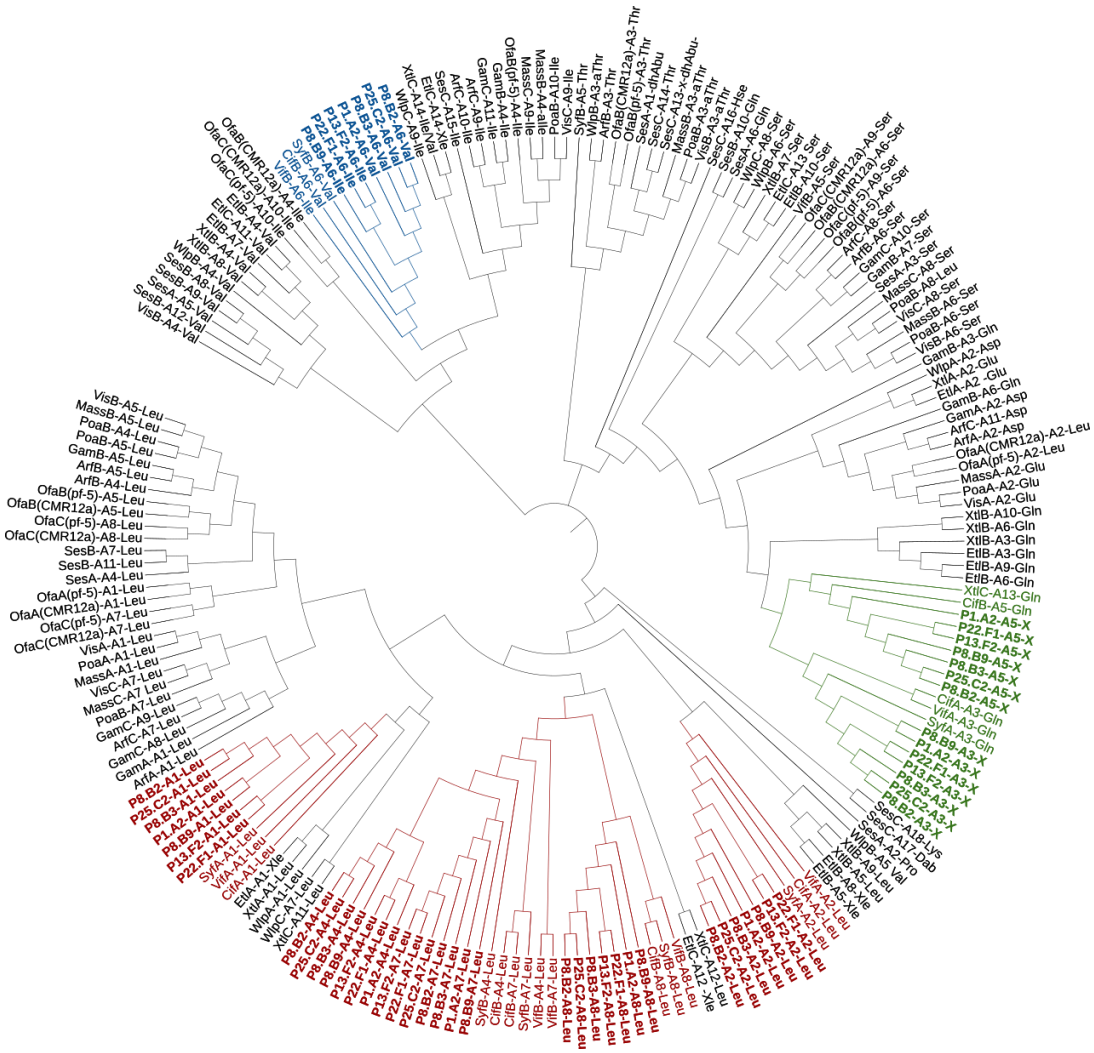

Figure III-28: Phylogenetic analysis of A domains of Pseudomonas lipopeptides.

Phylogenetic analysis of the A domains extracted from the modules of lipopeptide gene clusters encoding synthetases involved in arthrofactin (Arf, *Pseudomonas* sp. MIS38), cichofactin (Cif, *Pseudomonas cichorii* SF1-54), entolysin (Etl, *Pseudomonas entomophila* L48), gacamide (Gam, *Pseudomonas fluorescens* Pf0-1), massetolide (Mass, *Pseudomonas fluorescens* SS101), orfamide (Ofa, *Pseudomonas* sp. CMR12a; *Pseudomonas* protegens Pf-5), poaeamide (Poa, *Pseudomonas poae* RE*1-1-14), sessilin (Sess, *Pseudomonas* sp. CMR12a), syringafactin (Syf, *Pseudomonas syringae* DC3000), virginiafactin (Vif, *Pseudomonas* sp. QS1027), viscosin (Vis, *Pseudomonas fluorescens* SBW25), white-line-inducing principle WLIP (Wlp, *Pseudomonas putida* RW 10S2) and xantholysin (Xtl, *Pseudomonas putida* BW 11M1) synthesis. The A domains of the seven *Pseudomonas viridiflava* strains (P1.A2, P8.B2, P8.B3, P8.B9, P13.F2, P22.F1 and P25.C2) are highlighted in bold font. For each domain the substrate specificity is indicated using the standard amino acid three-letter code. X indicates A domains for which the specificity was not predictable by antiSMASH.

The initial predicted substrate specificity was verified and the five A domains in position 1, 2, 4, 7 and 8 cluster with the clade of leucine (red), whereas the A domain in position 6 clusters with the clade between valine and isoleucine (blue). The two A domains which were not predictable by antiSMASH cluster into the clade of glutamine (green). Application of both approaches was leading to the following proposed composition of the peptide moiety Leu-Leu-Gln-Leu-Gln-Val-Leu-Leu (see **Figure III-27**).

Hence, the predicted peptide sequence of the octalipopeptide is identical to the family of cichofactins[65] and similar to syringafactins[139] and virginiafactins[140] (see **Table III-3**). They all share the same amino acid (L-Leu or D-Leu) in positions 1, 2, 4, 7 and 8 and in position 3 D-glutamine. In position 6, there is either L-valine or L-isoleucine present. Amino acids in position 5 are either D-glutamine (cichofactins), D-*allo*-threonine (syringafactins) or D-serine (virginiafactins), depending on their family affiliation.

Table III-3: Structures of the lipooctapeptides cichofactins, syringafactins and virginiafactins.

Amino acids in positions 1, 2, 4, 7 and 8 are identical (L-Leu or D-Leu, red). Amino acids in position 3 are D-Gln (green). Amino acids in position 6 are either L-Val or L-Ile (blue). Amino acids in position 5 are either D-Gln, D-*a*Thr or D-Ser (green), depending on the family they belong to.[140]

Name	Chain length	AA1	AA2	AA3	AA4	AA5	AA6	AA7	AA8
Cichofactin A	10	L-Leu	L-Leu	D-Gln	L-Leu	D-Gln	L-Val	D-Leu	L-Leu
Cichofactin B	12	L-Leu	L-Leu	D-Gln	L-Leu	D-Gln	L-Val	D-Leu	L-Leu
Syringafactin A	10	L-Leu	L-Leu	D-Gln	L-Leu	D-*a*Thr	L-Val	D-Leu	L-Leu
Syringafactin C	10	L-Leu	L-Leu	D-Gln	L-Leu	D-*a*Thr	L-Ile	D-Leu	L-Leu
Syringafactin D	12	L-Leu	L-Leu	D-Gln	L-Leu	D-*a*Thr	L-Val	D-Leu	L-Leu
Syringafactin F	12	L-Leu	L-Leu	D-Gln	L-Leu	D-*a*Thr	L-Ile	D-Leu	L-Leu
Virginiafactin A	10	L-Leu	L-Leu	D-Gln	L-Leu	D-Ser	L-Val	D-Leu	L-Leu
Virginiafactin B	10	L-Leu	L-Leu	D-Gln	L-Leu	D-Ser	L-Ile	D-Leu	L-Leu
Virginiafactin C	12	L-Leu	L-Leu	D-Gln	L-Leu	D-Ser	L-Val	D-Leu	L-Leu
Virginiafactin D	12	L-Leu	L-Leu	D-Gln	L-Leu	D-Ser	L-Ile	D-Leu	L-Leu

In order to get further insight into the octalipopeptide gene cluster, all C domains were analysed by antiSMASH and a phylogenetic analysis (see **Figure III-29**). Bioinformatic analysis of the C domains suggested the sequence D-Leu-D-Leu-D-Gln-L-Leu-D-Gln-L-Val-D-Leu-L-Leu. The phylogenetic analysis showed that the condensation domain C1 of the first module is a typical starter C domain ($C_{Starter}$) (red) for the acylation of the first amino acid (here: L-Leu) normally with a β-hydroxy fatty acid (3OH-FA). The C domains in position 5 and 7 were identified as $^{L}C_{L}$ domains (green), whereas the other C domains cluster into the clade of dual-function condensation-epimerisation domains (C/E; blue). The predicted locations of dual C/E domains of the octalipopeptides are identical to those of cichofactins, syringafactins and virginiafactins although this prediction is not in accordance with the published structures of the syringafactin family.

Marfey's analysis of virginiafactins showed the presence of three D- and five L-configured amino acids which was also proven by comparison of isolated and synthetic lipooctapeptides of all three families.[140] Several examples have been reported in literature in which dual C domains were not in agreement with the chemical analyses, in contrast to the bioinformatic prediction.[109,141,142] Based on the high similarity of the new biosynthetic gene cluster compared to the syringafactin family, it is presumed that the configuration is identical but requires experimental validation.

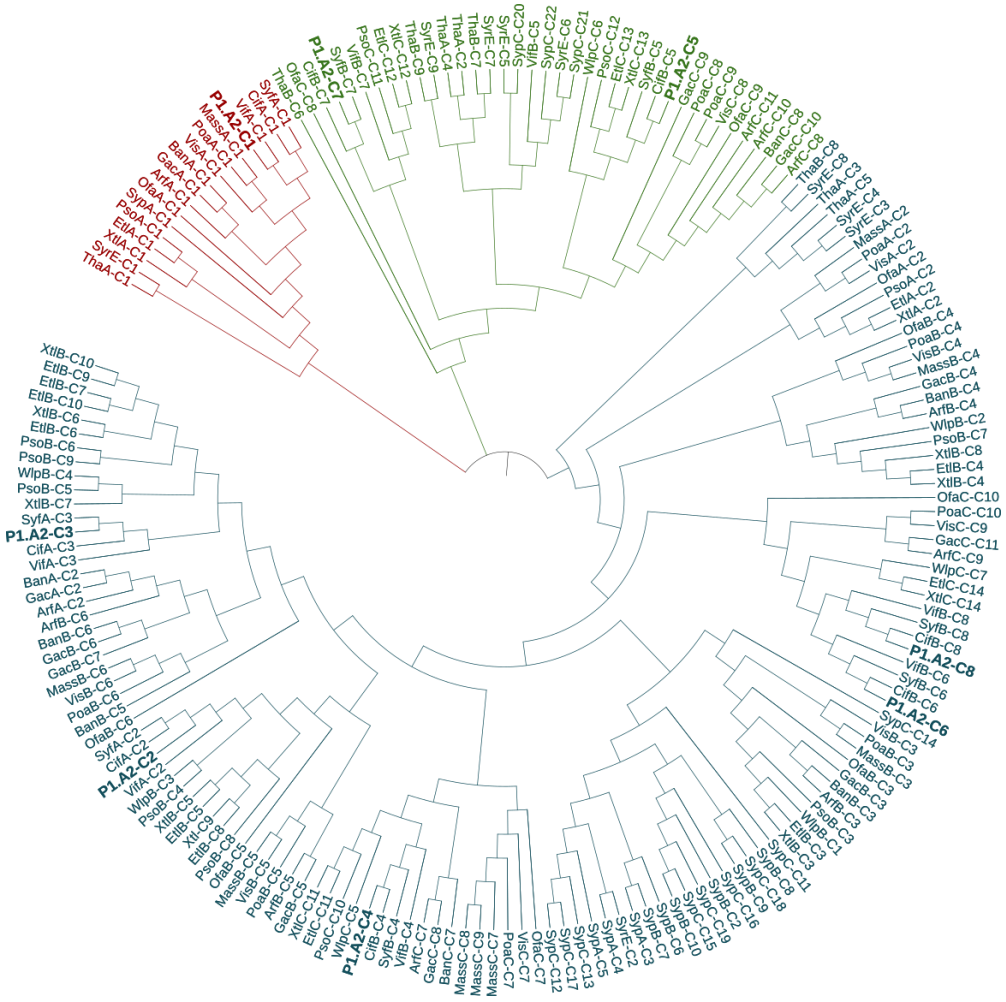

Figure III-29: Phylogenetic analysis of the C domains of Pseudomonas.

Phylogenetic analysis of the C domains extracted from modules of lipopeptide gene clusters encoding synthetases involved in arthrofactin (Arf, *Pseudomonas* sp. MIS38), cichofactin (Cif, *Pseudomonas cichorii* SF1-54), entolysin (Etl, *Pseudomonas entomophila* L48), gacamide (Gam, *Pseudomonas fluorescens* Pf0-1), massetolide (Mass, *Pseudomonas fluorescens* SS101), orfamide (Ofa, *Pseudomonas* sp. CMR12a; *Pseudomonas* protegens Pf-5), poaeamide (Poa, *Pseudomonas poae* RE*1-1-14), putisolvin (Pso, *Pseudomonas putida* PCL1445), syringfactin (Syf, *Pseudomonas syringae* DC3000), syrinogmycin (Syr, *Pseudomonas syringae* pv *syringae* B301D), syringopeptin (Syp, *Pseudomonas syringae* pv *syringae* B301D), virginiafactin (Vif, *Pseudomonas* sp. QS1027), viscosin (Vis, *Pseudomonas fluorescens* SBW25), white-line-inducing principle WLIP (Wlp, *Pseudomonas putida* RW 10S2) and xantholysin (Xtl, *Pseudomonas putida* BW 11M1) synthesis. The C domains of *Pseudomonas viridiflava* P1.A2, which were used as representative for the seven strains, are highlighted in larger bolt font. For each domain the position is indicated at the end.

III.2.2 Media Screening of *Pseudomonas viridiflava* strains

In order to prove the production of the octalipopeptide, the seven *Pseudomonas viridiflava* strains were cultivated at 30 and 23 °C and extracted with ethyl acetate (1:1). The obtained crude extracts were dissolved in 1 mL of MeOH, subsequently subjected to LC-MS analysis (see **Chapter II.3.4.1**) and the secondary metabolite spectrum was compared. In case of cultivation at 30 °C, the LC-MS analysis showed the absence of secondary metabolites whereas in the chromatogram of the cultivation at 23 °C two major peaks were present compared to the media control (see **Figure III-31**, cultivation of *P. viridiflava* P1.A2 is shown exemplarily).

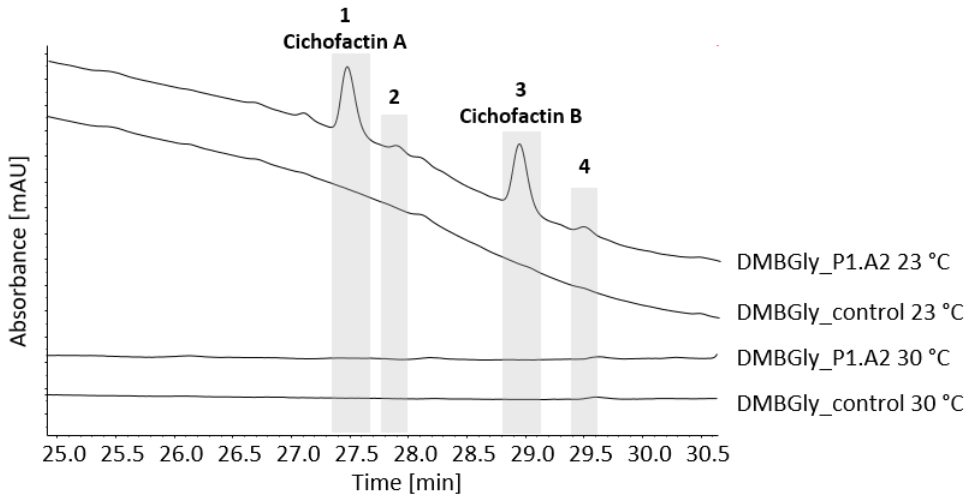

Figure III-30: Comparison of cultivation conditions at different temperatures of *P. viridiflava* P1.A2.

UV chromatogram of LC-MS analysis of ethyl acetate extracts from *P. viridiflava* P1.A2 is shown as representative of the seven strains. Two major and two minor peaks can be detected in the cultivation medium of *P. viridiflava* P1.A2 at 23 °C while they are absent in the medium controls and cultivation at 30 °C. The cultivation was performed in DMBGly medium.

The peak at t_R = 27.5 min gave a mass of *m/z* 1109.9 $[M+H]^+$ and the peak at t_R = 28.9 min gave a mass of *m/z* 1137.9 $[M+H]^+$ which are identical as for cichofactins A and B. There are also two minor peaks visible next to the major ones. The peak at t_R = 27.9 min gave a mass of *m/z* 1124.0 and the peak at t_R = 29.5 min a mass of *m/z* 1152.0 (see **Figure III-31**). Both are 14 Da bigger than its major peak leading to the assumption that the fatty acid or one of the amino acids is extended by a CH_2 group.

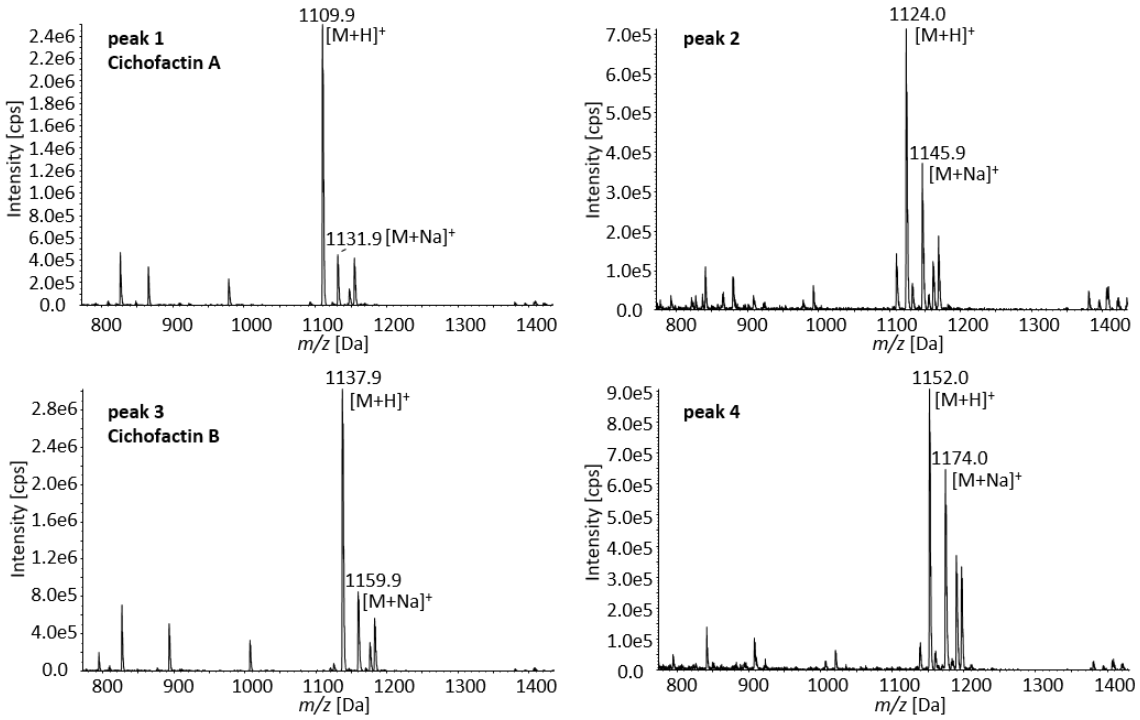

Figure III-31: Masses of secondary metabolites produced by *P. viridiflava* P1.A2.

The resulting molecular ions of the four peaks shown in Figure III-30 revealed peak 1 (cichofactin A) *m/z* 1109.9 $[M+H]^+$, peak 2 *m/z* 1124.0 $[M+H]^+$, peak 3 (cichofactin B) *m/z* 1137.9 $[M+H]^+$ and peak 4 *m/z* 1152.0 $[M+H]^+$.

In order to select the best producer strain for the octalipopeptides and to find the most suitable medium for this strain, a medium screening was performed according to the procedure in **Chapter II.2.4.1**. Various media known to produce secondary metabolites in *Pseudomonas* were tried out. Furthermore, cafestol was added because it can act as an elicitor for secondary metabolism.[143] **Figure III-32** demonstrates the produced amount of the masses 1109.8 Da and 1137.8 Da, respectively, in the different strains and media. All four octalipopeptides were produced by each strain (data not shown for minor peaks).

Following the screening results, the strain *P. viridiflava* P1.A2 was determined to be the best producer for the LPs. The DMBGly medium supplemented with cafestol was the first choice to use for cultivation. Since cafestol is quite expensive and the production in DMBGly medium without supplementation was the second choice, the large scale cultivations were conducted in this medium.

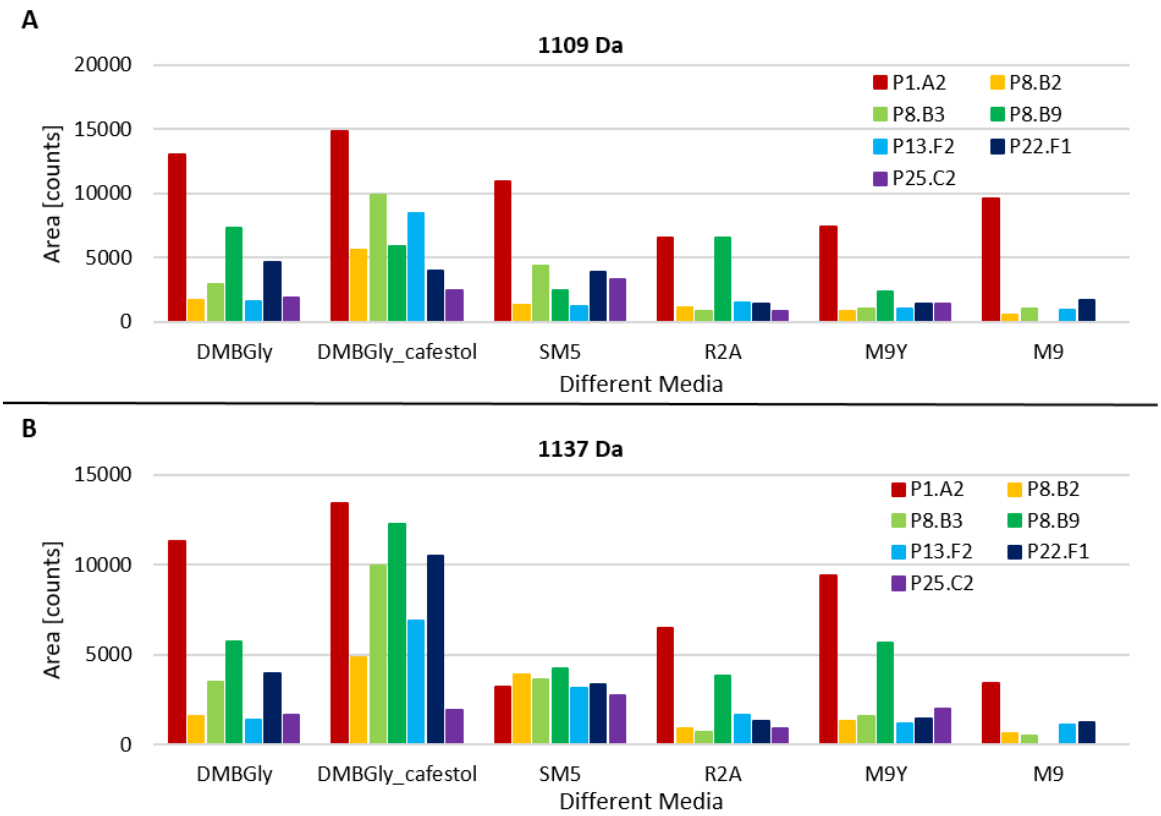

Figure III-32: Results of the media screening of the different *P. viridiflava* strains.

Following media were used: DMBGly, DMBGly supplemented with cafestol, SM5, R2A, M9 supplemented with yeast (M9Y) and M9. Figure **A** shows the produced amount of mass 1109.9 Da for each strain in the different media and **B** reveals the produced amount of mass 1137.9 Da. Media screening was not performed as duplicates.

As a gene cluster was identified producing two known compounds as well as two new derivatives in a suitable medium, this project was considered to be a suitable project for a master thesis. Therefore, the cultivation, separation and also the improvement of production was set as a goal for the thesis. The structure analyses of cichofactin A-D were conducted in cooperation. These tasks were assigned to Marlene Vogt who worked on this project from November 2020 to April 2021.

III.2.3 Isolation and Structure Elucidation of Cichofactins A & B

In order to isolate the four octalipopeptides, *P. viridiflava* P1.A2 was cultivated nine times on a nine litre scale, due to the low amount of the minor peaks, and extracted with ethyl acetate (see **Chapter II.2.4.2**). Subsequently, the crude extract was separated roughly by vacuum liquid chromatography and VLC fractions D and E were further purified by HPLC according to **Chapters II.3.2** and **II.3.3.3**. The four peaks of interest were collected with yields of 11.5 mg of peak 1, 0.2 mg of peak 2, 10.4 mg of peak 3 and 0.1 mg of peak 4. The amount of peak 1 and 3,

designated as cichofactin A and B, respectively, were sufficient for structure elucidation by NMR. The compounds of peak 2 and 4 are named as cichofactin C and D, respectively.

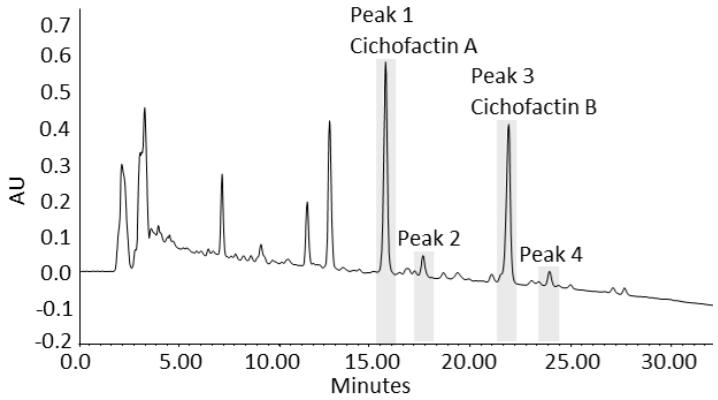

Figure III-33: HPLC profile of fraction E.

The four peaks of interest are labelled. UV detection at 210 nm.

For structure elucidation, HR ESI-MS, MS/MS and NMR measurements were conducted (see **Chapters II.3.4.2** and **II.3.5**). The major compound, cichofactin A, revealed a mass of *m/z* 1109.7537 $[M+H]^+$ in the HR ESI-MS (**Figure VIII-11**), including a molecular formula of $C_{55}H_{101}N_{10}O_{13}$ (calcd. for 1109.7544; Δ -0.7 ppm). Cichofactin B showed a mass of *m/z* 1137.7869 $[M+H]^+$ in the HR ESI-MS (**Figure VIII-11**), consistent with a molecular formula of $C_{57}H_{105}N_{10}O_{13}$ (calcd. for 1137.7857; Δ +1.1 ppm).

MS/MS analysis revealed information about the peptide sequence as well as the attached fatty acid. Based on this analysis, the predicted peptide sequence of Leu-Leu-Gln-Leu-Gln-Val-Leu-Leu was confirmed by the fragmentation pattern. The produced b- and y-series fragment ions of cichofactin A are shown in **Figure III-34** and **Figure VIII-12**. The last amino acid from the C terminus cannot be analysed separately. All relevant fragments of the $[M+H]^+$ form of cichofactin A and B are shown in **Table VIII-13**. The *m/z* values of b fragments of cichofactin B were 28 Da larger, indicating that the fatty acid is two methylene groups longer which is also supported by the detection of an ion at *m/z* 312 belonging to the fragment of FA-Leu (**Figure VIII-12**).

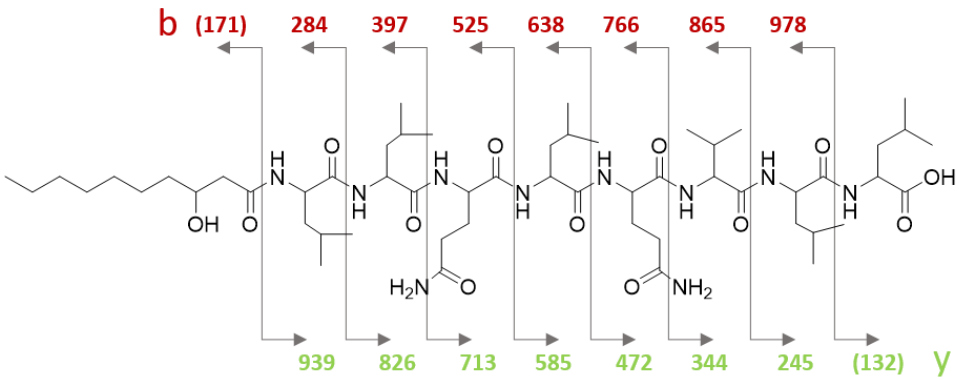

Figure III-34: Fragmentation scheme of cichofactin A.

b-Ions (red) and y-ions (green) obtained from the $[M+H]^+$ form of cichofactin A formed in the HR ESI-MS/MS analysis. The numbers in brackets are not visible in the spectra.

Furthermore, the structure was confirmed by NMR experiments. The following experiments were performed ^{1}H, ^{13}C, DEPT135, ^{1}H-^{1}H COSY, ^{1}H-^{13}C HSQC, ^{1}H-^{13}C HSQC-TOCSY, ^{1}H-^{13}C HMBC, ^{1}H-^{1}H ROESY, ^{1}H-^{15}N HSQC, band selective ^{1}H-^{13}C HSQC and HMBC as well as a ^{1}H-^{15}N HSQC-TOCSY.

The ^{1}H NMR spectrum of cichofactin A (**Figure III-35**; **Figure VIII-13**) displayed resonances typical for a lipopeptide, like the downfield amide resonances (δ_H 6.8 – 8.3) and signals of α-protons in the range of 4.1 to 4.5 ppm. The upfield resonances of 0.9 ppm and 1.5 – 2.5 ppm are characteristic for methyl and methylene groups of the amino acid side chain, respectively, as well as several signals for a fatty acid moiety (δ_H 0.9 and 1.3). The carbonyl resonances in the ^{13}C spectrum (δ_C 173 – 178 ppm) provided further evidence for the peptidic nature just like the signals of the α-carbons (δ_C 52 – 61 ppm) which are shown in **Figure VIII-14**.

A ^{1}H-^{13}C HSQC experiment was recorded to assign the directly bonded proton and carbon pairs (**Figure VIII-15**). The region of the α-carbons showed an overlap of the cross peaks. Therefore, a band selective ^{1}H-^{13}C HSQC experiment between 37 and 58 ppm was performed (**Figure VIII-16**) to facilitate the assignment of the α-carbons and their attached protons.

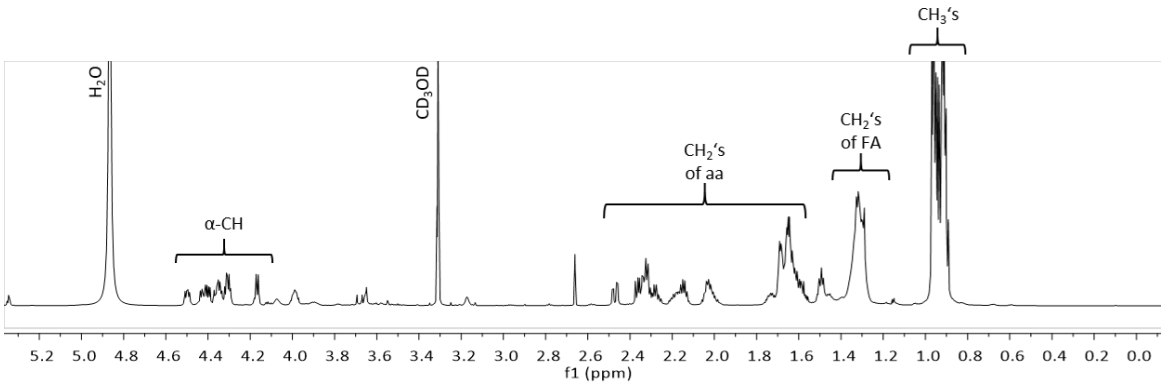

Figure III-35: ^{1}H NMR spectrum of cichofactin A in d_4-MeOH (700 MHz).

This spectrum indicates the different types of protons.

Furthermore, complete spin systems of each amino acid of cichofactin A are depicted in a ^{1}H-^{13}C HSQC-TOCSY spectrum (**Figure III-36**). This spectrum corroborated the presence of eight amino acids and a 3-OH-decanoic acid (HDA). This experiment combines a ^{1}H-^{1}H TOCSY with signals of ^{1}H-^{13}C HSQC experiment resulting in correlations between a ^{13}C-attached proton to all other protons (horizontal line) as well as all carbons which are coupled to this proton (vertical line). The spin systems of the five different leucine residues are shown in red, the two spin systems of the glutamines are marked in green, while valine is labelled in blue and the fatty acid in purple. The different spin systems were also confirmed by a ^{1}H-^{15}N HSQC-TOCSY experiment shown in **Figure VIII-17**.

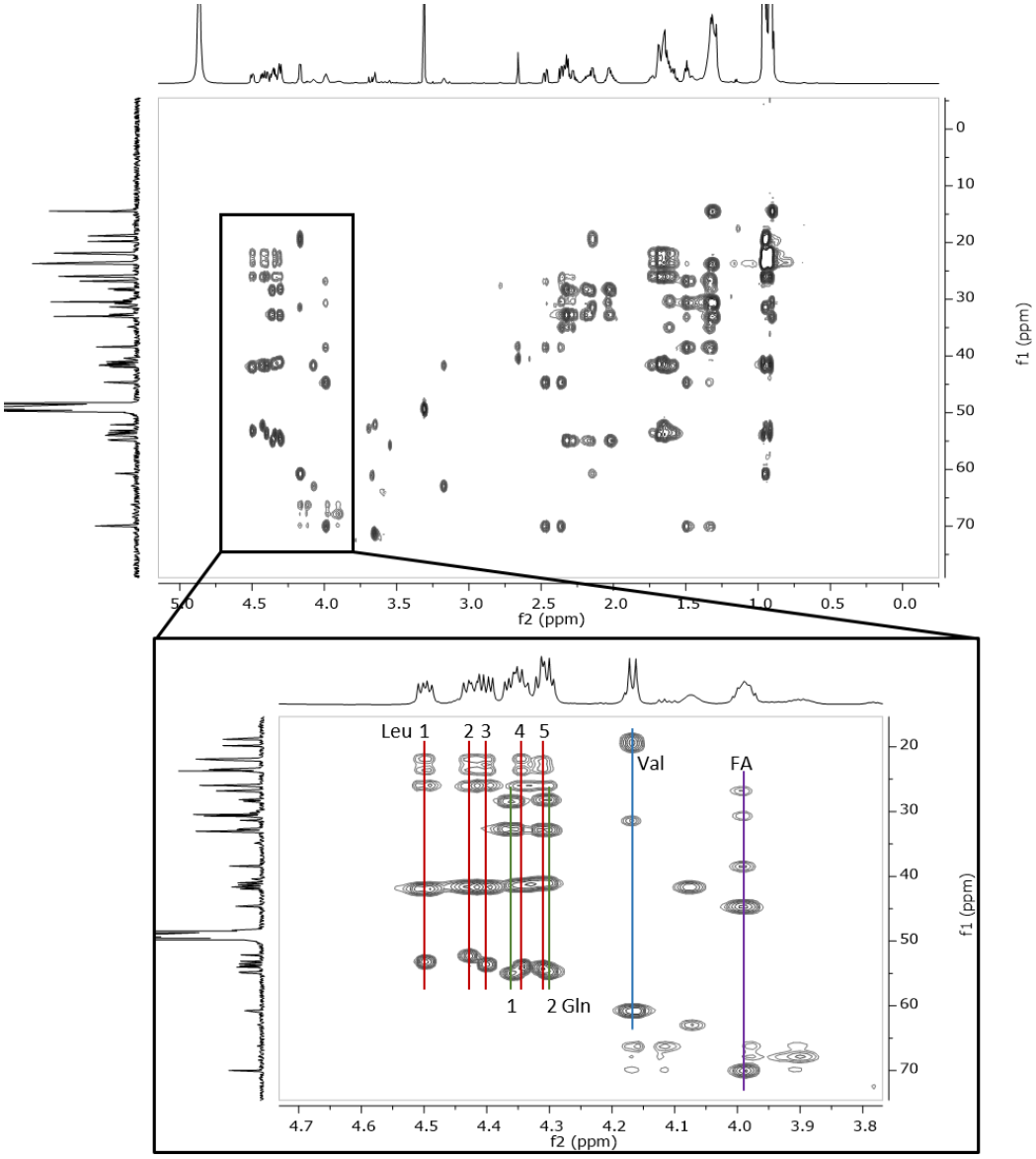

Figure III-36: ^{1}H-^{13}C HSQC-TOCSY spectrum of cichofactin A in d_4-MeOH (700 MHz).

There is shown an overview of the ^{1}H-^{13}C HSQC-TOCSY spectrum of cichofactin A (top) and the section of the α-protons and FA-2 (bottom). The lines indicate the different spin systems of the amino acids. Leucine in red, glutamine in green, valine in blue and the fatty acid in purple.

These spin systems were connected using a combination of different 2D NMR spectra (^{1}H-^{1}H COSY, ^{1}H-^{1}H ROESY, ^{1}H-^{13}C HMBC, a band selective ^{1}H-^{13}C HMBC (160 – 190 ppm) as well as a ^{1}H-^{15}N HSQC; **Figure VIII-18** – **Figure VIII-22**). The primary assembled linear sequence of chichofactin A (HDA-Leu-Leu-Gln-Leu-Gln-Val-Leu-Leu) was confirmed and all key correlations are shown in **Figure III-37**. The NMR spectroscopic data of cichofactin A are shown in **Table VIII-14**. The determined values are comparable to the NMR data published by Götze *et al.*[140] but the chemical shifts were not assigned in their structure elucidation. Götze *et al.* analysed the structure by comparison of synthetic and isolated compounds.

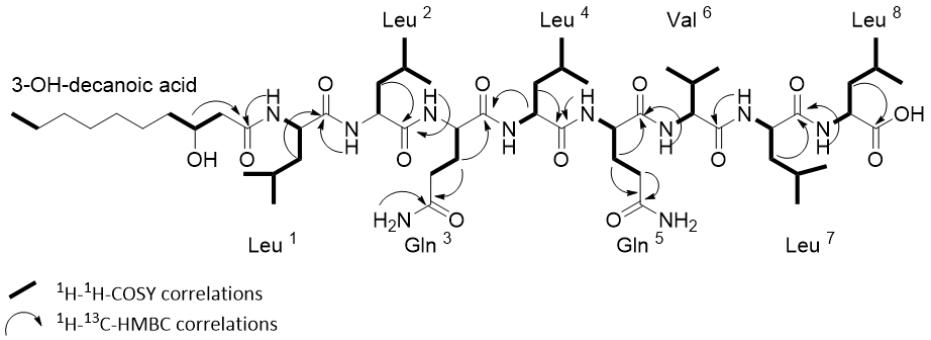

Figure III-37: 2D NMR key correlations of cichofactin A.

Bold lines indicate the ^{1}H-^{1}H COSY correlations and arrows represent the ^{1}H-^{13}C HMBC correlations.

In order to confirm the structure of cichofactin B, the ^{1}H NMR spectra of cichofactins A and B were superimposed and no additional peak was observed. This result in combination with HR-MS/MS analysis confirmed the extension of the fatty acid because the additional peaks in the ^{1}H NMR spectrum are overlapped with the remaining signals of the fatty acid between 1.25 and 1.36 ppm (grey box). The proton spectrum of cichofactin B was also in accordance with the data of Götze *et al.*[140]

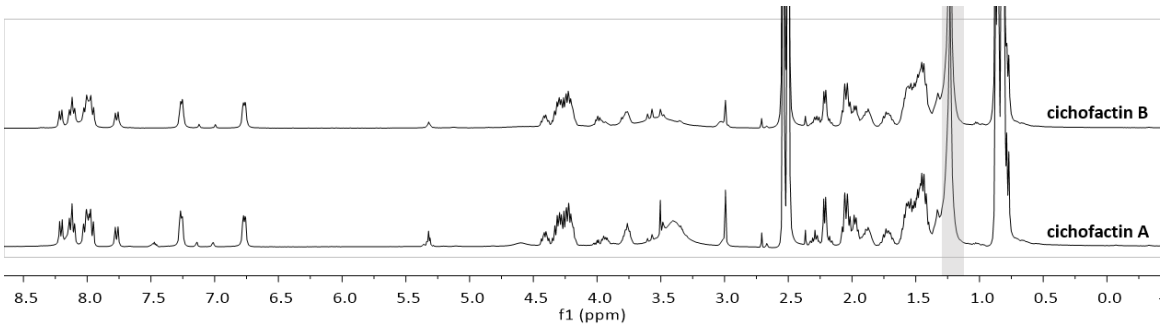

Figure III-38: Overlay of ^{1}H NMR spectra of cichofactins A and B in d_6-DMSO (400 MHz).

III.2.3.1 Biological Activity of Cichofactins A & B

The biological activity of cichofactins A and B were tested against a variety of human pathogenic bacteria shown in **Table III-4**. The bioactivity as well as cytotoxicity tests were performed in the group of Prof. Dr. Heike Brötz-Oesterhelt (Interfaculty Institute of Microbiology and Infection Medicine, University of Tübingen).

The determined MIC values (all >32 µg/mL) of cichofactins A and B did not show any significant antibacterial activity against the tested Gram-positive and Gram-negative bacteria.

Table III-4: Analysis of the biological activity of cichofactin A and B against human pathogens and cytotoxic assays.

Organisms	Cichofactin A	Cichofactin B
	MIC in µg/mL	
Acinetobacter baumanii 09987	>32	>32
Bacillus subtilis 168	>32	>32
Enterobacter aerogenes ATCC 13048	>32	>32
Echerichia coli ATCC 25922	>32	>32
Enterococcus faecium BM 4147-1	>32	>32
Klebsiella pneumonia ATCC 12657	>32	>32
Mycobacterium smegmatis mc^2 155	>32	>32
Pseudomonas aeruginosa ATCC 27853	>32	>32
Staphylococcus aureus ATCC 29213	>32	>32
Cell line	IC_{50} in µg/mL	
HeLa (human cervical tumor cells)	32 – 64	16 – 32

The cytotoxicity of cichofactins was tested in the HeLa cell line. The IC_{50} value for cichofactin B in HeLa cells was 16 to 32 µg/mL, whereas the value for cichofactin A is slightly higher (32 to 64 µg/mL). In comparison, doxorubicin, a cytostatic drug on the market, has an IC_{50} value of 1.15 µg/mL in HeLa cells.[144] These values indicated a minimal cytotoxicity of cichofactins A and B.

III.2.4 Experiments to Improve the Production Rate of Cichofactins

The produced amount of the new derivatives (peak 2 and 4, **Figure III-33**) was initially not sufficient to elucidate their structure. In order to enhance the production rate of these minor compounds, different strategies were applied. The production rate of secondary metabolites can be increased for example by plant signal molecules like arbutin or phenyl-β-D-glucopyranoside on syringomycin production[145], by co-cultivation of neighbouring microbes,[146,147] as well as by supplementation of biosynthetic precursors like amino acids to the cultivation medium.[130,148]

III.2.4.1 Production of Cichofactins in Media Supplemented with Plant Extracts

Pseudomonas viridiflava is pathogenic on *Arabidopsis thaliana* causing disease symptoms of water-soaked, translucent spots which became later chlorotic and necrotic lesions.[149,150] Plant extracts of *Arabidopsis thaliana* were added to the media to explore synergistic effects on cichofactin production by *P. viridiflava*. Plant cultures of four different genotypes (Col-0, Sha, EylS-2 and ICE 153) of *A. thaliana* (**Figure III-39 A**) were kindly provided by Alejandra Duque.

Hereby, Col-0 represents the reference genotype and they all differ in their susceptibility for infections. The cultivation procedure is described in **Chapter II.2.4.3**. The crude extracts were analysed by LC-MS and the produced amounts of derivative 1 (named as cichofactin C, 1123 Da) and derivative 2 (named as cichofactin D, 1151 Da) were calculated by the peak area. The results are shown in **Figure III-39 B**.

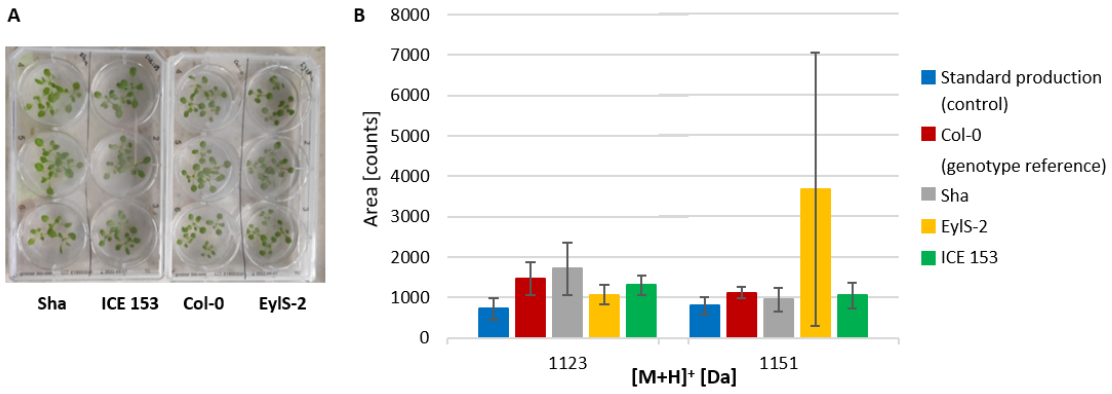

Figure III-39: Effect of plant extracts of *A. thaliana* on cichofactin C and D production.

A: Plant cultures of the four different genotypes Sha, ICE 153, Col-0 and EylS-2 which differ in their susceptibility for infections. **B:** *P. viridiflava* P1.A2 was cultured for 72 h with plant extracts of different genotypes of *A. thaliana*. After cultivation, production ratios of cichofactin C (1123 Da) and D (1151 Da) in media supplemented with plant extracts (reference: blue; Col-0: red; Sha: grey; EylS-2: yellow and ICE 153: green) were calculated by the peak area. Values were determined as average of triplicates.

A slight improvement in cichofactin C and D productivity by adding plant extracts of the different genotypes was observed. The maximum effect on cichofactin C was achieved to 2.3 fold by adding plant extracts of the genotype Sha (grey bar). At the first sight, the best improvement on cichofactin D was achieved to 4.6 fold by adding the plant extracts of EylS-2 (yellow bar) but this effect was just attributed to one of the replicates. All in all, the effect of plant extracts of *A. thaliana* on the production of cichofactin derivatives was not sufficient to continue this approach.

III.2.4.2 Production of Cichofactins in Media Supplemented with Isoleucine

The improvement in the productivity of cichofactin was further investigated by addition of different amino acids. First, the amino acid L-isoleucine was chosen due to the assumption that the amino acid at position 6 is an isoleucine instead of valine. Other members of the syringafactin family were already known having either valine or isoleucine at this position as shown in **Table III-3**. The cultivation was performed as described in **Chapter II.2.4.4**.

On closer inspection, in cultivations under standard conditions four different cichofactin derivatives were produced while one major peak with a mass of 1123 Da at 17.5 min and one with a mass of 1151 Da at 27.6 min were observed. The two minor peaks at 16.5 and 27.0 min exhibited the same masses like their major peaks (1123 and 1151 Da, respectively). With addition of L-isoleucine to the culture medium, the production of the minor peaks significantly increased (**Figure III-40 A**).

L-Isoleucine was added in different concentrations (125, 250, 500 and 1000 mg/L) before autoclaving the medium. The crude extracts were analysed by LC-MS and the produced amounts of the derivatives were calculated by the peak area. The results are shown in **Figure III-40 B**.

The analysis of the peak areas was not straightforward since the peak areas of the reference of the mass 1123 Da (peak A and B) were not baseline-separated. Therefore, the peak area of peak A was not quantifiable while the peak area of peak B is probably too high. The maximum production of peak A was achieved at 125 mg/L and increasing doses of isoleucine caused growth inhibition and lowered the production. The addition of L-isoleucine had a minimal to no effect on the production of peak B but also showed less production at higher concentrations of L-isoleucine. The peak areas of the mass 1151 Da (peak C and D) were not baseline-separated thus they were analysed together. The maximum production of peak C and D was achieved at 125 mg/L L-isoleucine but the effect was minimal.

At high concentrations of L-isoleucine (500 and 1000 mg/L), the productivity of cichofactin derivatives was decreased. Therefore, cultivations were performed adding L-isoleucine (125 and 250 mg/L) to the culture 4 and 8 hours after inoculation to prevent intoxication.

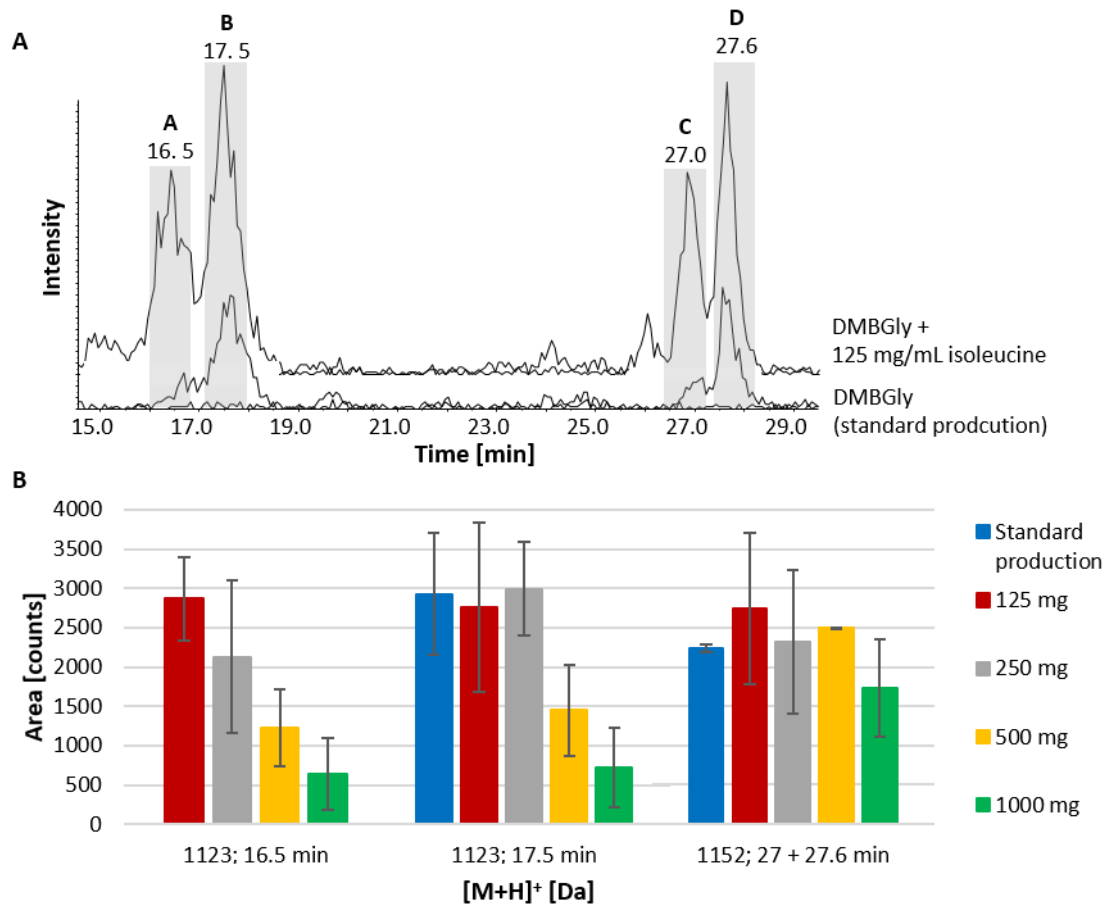

Figure III-40: Effect of L-isoleucine on cichofactin derivative production directly added to the media.

A: Overview of production of cichofactin derivatives (1123 and 1151 Da) in DMBGly (reference) and DMBGly supplemented with 125 mg/mL L-isoleucine. After cultivation in DMBGly media supplemented with isoleucine, two additional peaks with the same masses of 1123 Da (16.5 min) and 1151 Da (27.0 min) were observed in comparison to the reference without supplementation.

B: *P. viridiflava* P1.A2 was cultivated for 72 h with L-isoleucine at different concentrations (125, 250, 500 and 1000 mg/L) added before autoclaving. After cultivation, production ratios of peak A (1123 Da at 16.5 min), B (1123 Da at 17.5 min) as well as C and D (1151 Da at 27.0 and 27.6 min) in media supplemented with L-isoleucine (reference: blue; 125 mg/L: red; 250 mg/L: grey; 500 mg/L: yellow and 1000 mg/L: green) were calculated by the peak area. Values were calculated as average of triplicates.

Next, the effect of the addition of L-isoleucine 4 and 8 hours after inoculation was examined. The cultivation procedure was performed as described previously. The results are shown in **Figure III-41**. The maximum production of peak A (14.5 min) was achieved to 4.5 fold by addition of 250 mg/L of L-isoleucine after 4 hours of inoculation. The production of peak C was improved in a dose-dependent manner up to 250 mg/L after 4 hour of inoculation but the reference peak was not quantifiable. Otherwise, the addition of L-isoleucine to the culture medium had no significant effect on the production of peak B and D.

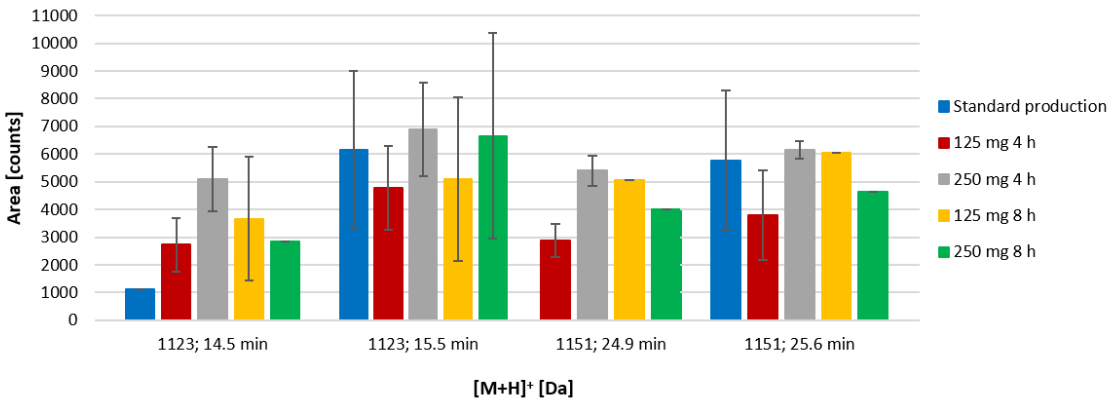

Figure III-41: Effect of L-isoleucine on cichofactin derivative production added 4 and 8 hours after inoculation.

The cichofactins producing organism was cultivated for 72 h with L-isoleucine at different concentrations (125 and 250 mg/L) 4 and 8 h after inoculation. After cultivation, production ratios of peak A (1123 Da at 14.5 min), B (1123 Da at 15.5 min), C (1151 Da at 24.9 min) and D (1151 Da at 25.6 min) in media supplemented with L-isoleucine (reference: blue; 125 mg/L 4 h: red; 250 mg/L 4 h: grey; 125 mg/L 8 h: yellow and 250 mg/L 8 h: green) were calculated by the peak area. Values were determined as average of triplicates.

The addition of L-isoleucine to the cultivation medium showed an improvement of the production of chichofactin derivatives at 14.5 min (cichofactin A) and 24.9 min (cichofactin C). Therefore, a large scale cultivation of 24 L of *P. viridiflava* P1.A2 was performed in medium supplemented with L-isoleucine (250 mg/L 4 h after inoculation) and the crude extract was measured by LC-MS. The analysis of this large scale experiment revealed low production of the cichofactin derivatives.

III.2.4.3 Production of Cichofactins in Media Supplemented with L-Leucine

In the next step, the effect of L-leucine on the cichofactin production was investigated because cichofactins contain five leucine residues which could represent a bottle neck in the biosynthesis. Therefore, cultivation was performed as described previously and L-leucine was added at different concentrations (125, 250, 500 and 1000 mg/L) and two different time points (before autoclavation and 4 hours after inoculation). The crude extracts were analysed by LC-MS, the produced amounts of the derivatives were calculated by the peak area and the results are shown in **Figure III-42**.

In cultivations supplemented with L-leucine, four compounds were produced with the same intensity as shown in **Figure III-42 A**. Peak 5 and 7 revealed masses of 1109 Da and 1123 Da consistent with cichofactin A and B, respectively. Peak 6 and 8 showed masses of 1123 Da (named as cichofactin E) and 1151 Da (named as cichofactin F), respectively, but no additional peaks with the same masses were observed.

All in all, the addition of L-leucine to the cultivation medium significantly improved the production of cichofactin derivatives. The maximum effect of peak 6 was achieved to 3.4 fold by the addition

of L-leucine at 250 mg/L and four hours after inoculation. The best improvement of peak 8 was obtained to 6.3 fold at a concentration of 1000 mg/L four hours after inoculation. To have a positive effect on both compounds (1123 and 1151 Da), a concentration of 125 mg/L directly added to the cultivation medium was set as suitable condition to perform large scale cultivations.

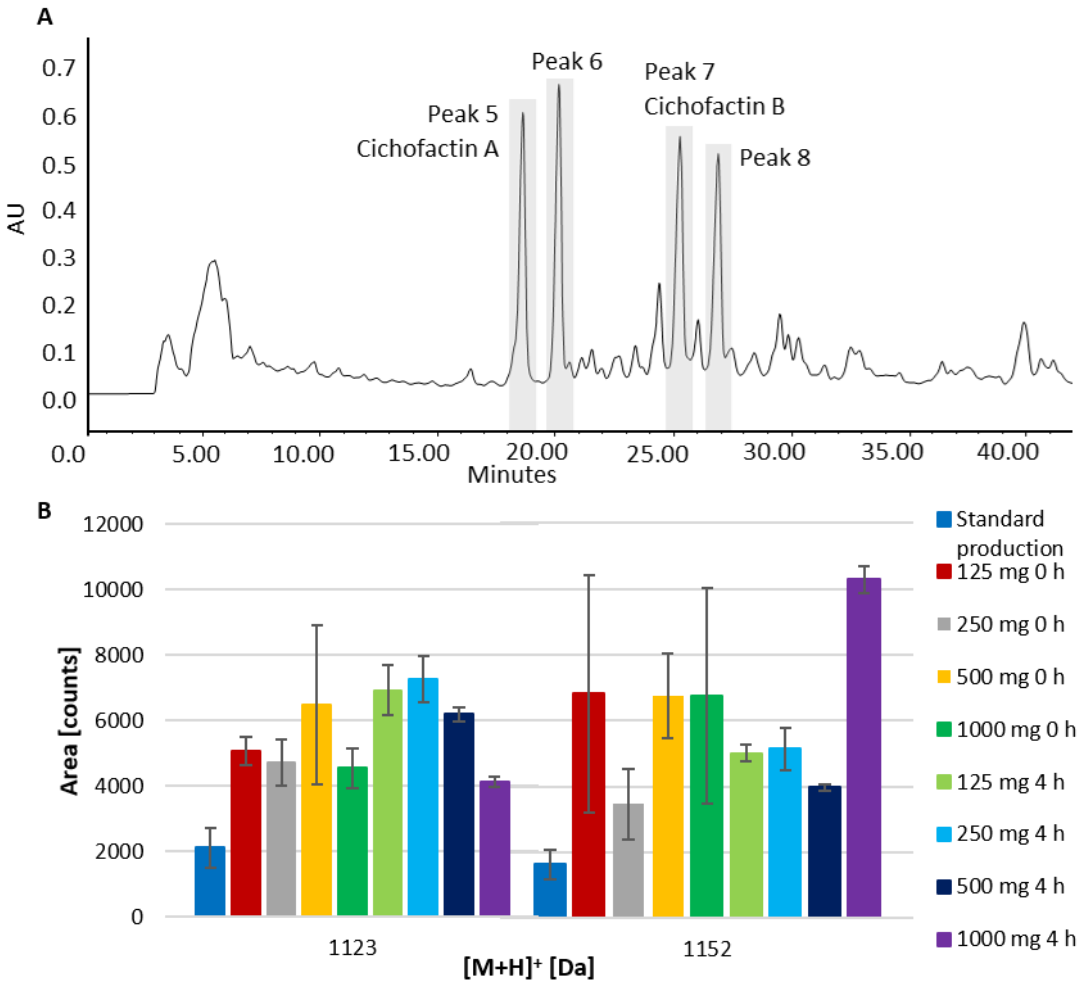

Figure III-42: Effect of L-leucine on cichofactin derivative production added before inoculation as well as 4 hours after.

A: HPLC profile of VLC fraction E. The four peaks of interest are labelled. UV detection at 210 nm.

B: *P viridiflava* P1.A2 was cultured for 72 h with L-leucine at different concentrations (125, 250, 500 and 1000 mg/L) before autoclaving and 4 h after inoculation. After cultivation, production ratios of cichofactin E (1123 Da) and F (1151 Da) in media supplemented with L-leucine (reference: blue; 125 mg/L 0 h: red; 250 mg/L 0 h: grey; 500 mg/L 0 h: yellow;1000 mg/L 0 h: dark green; 125 mg/L 4 h: light green; 250 mg/L 4 h: light blue; 500 mg/L 4 h: dark blue and 1000 mg/L 4 h: purple) were calculated by the peak area. Values were determined as average of triplicates.

In order to isolate the two new cichofactin derivatives, cichofactin E and F, *P. viridiflava* P1.A2 was cultivated on a 24 litre scale and extracted with ethyl acetate. Subsequently, the crude extract was separated roughly by vacuum liquid chromatography and VLC fraction E was further purified by HPLC according to **Chapters II.3.2** and **II.3.3.3**. Four peaks of interest were collected with yields of 2.45 mg of peak 5 (cichofactin A), 3.98 mg of peak 6 (cichofactin E), 3.51 mg of peak 7

(cichofactin B) and 3.13 mg of peak 8 (cichofactin F). The amounts were sufficient to elucidate their structures by NMR in comparison with the measured NMR data of cichofactin A.

III.2.5 Structure Elucidation of Cichofactin Derivatives C & D

The obtained amount of cichofactin C and D was not sufficient for a complete structure elucidation (0.2 mg of peak 2 (cichofactin C) and 0.1 mg of peak 4 (cichofactin D) see **Chapter III.2.3**). Therefore, HR ESI-MS and MS/MS measurements were conducted to analyse the structure.

The HR ESI-MS experiment of cichofactin C (peak 2) gave a major peak 2 **B** and minor peak 2 **A** (cichofactin C2) and both revealed a mass of *m/z* 1123.7691 and 1123.7700, respectively, including a molecular formula of $C_{56}H_{103}N_{10}O_{13}$ (calcd. for 1123.7701; Δ -0.9 ppm and -0.1 ppm) shown in **Figure VIII-23**.

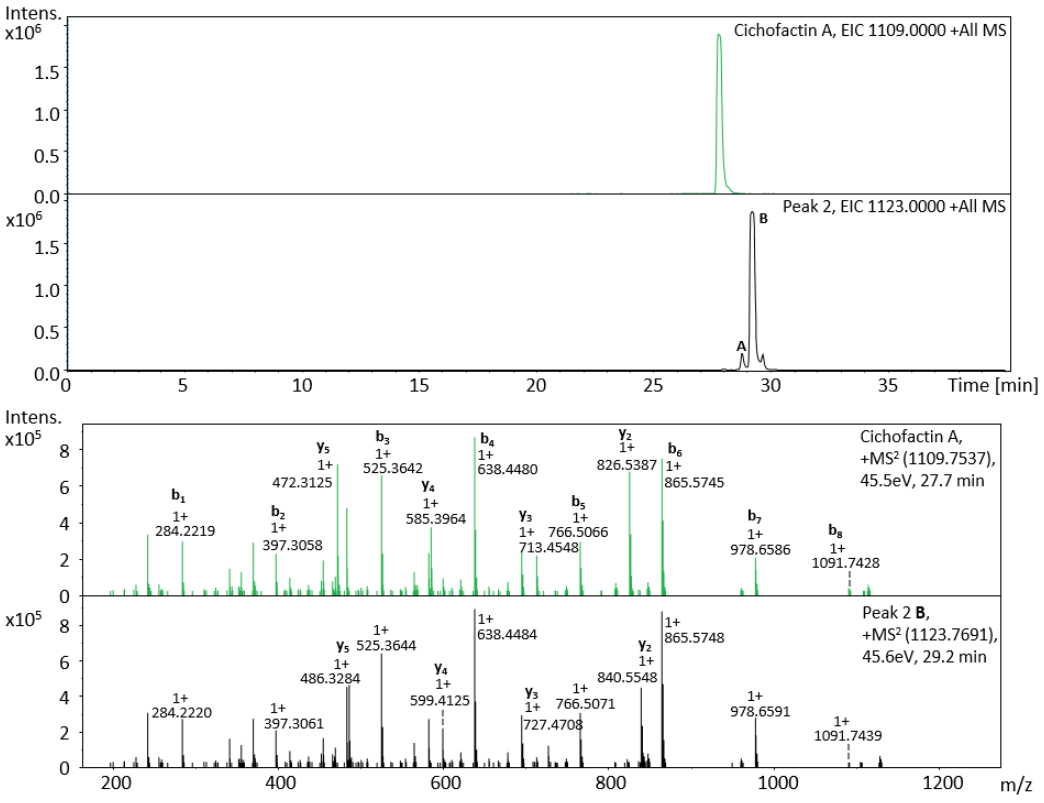

Figure III-43: Superimposed HR ESI-MS (top) and MS/MS (bottom) spectra of cichofactin A and C (peak 2 **B**).

MS/MS analysis was performed to get further information about the peptide sequence and was compared with the fragmentation pattern of cichofactin A (**Figure III-43**). The produced b-series fragment ions of cichofactin C were identical to the fragments of cichofactin A indicating the same amino acid sequence and fatty acid. The difference occurred at the last amino acid (AA8) proposing a methylation of the carboxylic moiety of amino acid 8 (Leu). The produced y-series

fragment ions are 14 Da larger compared to cichofactin A also leading to the assumption that the extension occurs at the C-terminus of the peptide. All relevant fragments are shown in **Table VIII-15**.

In order to confirm the methylation of the carboxylic moiety of amino acid 8, a proton spectrum was recorded and compared to cichofactin A. The superimposed spectra displayed an additional resonance at δ_H = 3.69 ppm which is typical for a methoxy moiety as shown in **Figure III-44**. 2D NMR spectra to confirm the position of the methoxy group were not possible due to the low amount of cichofactin C.

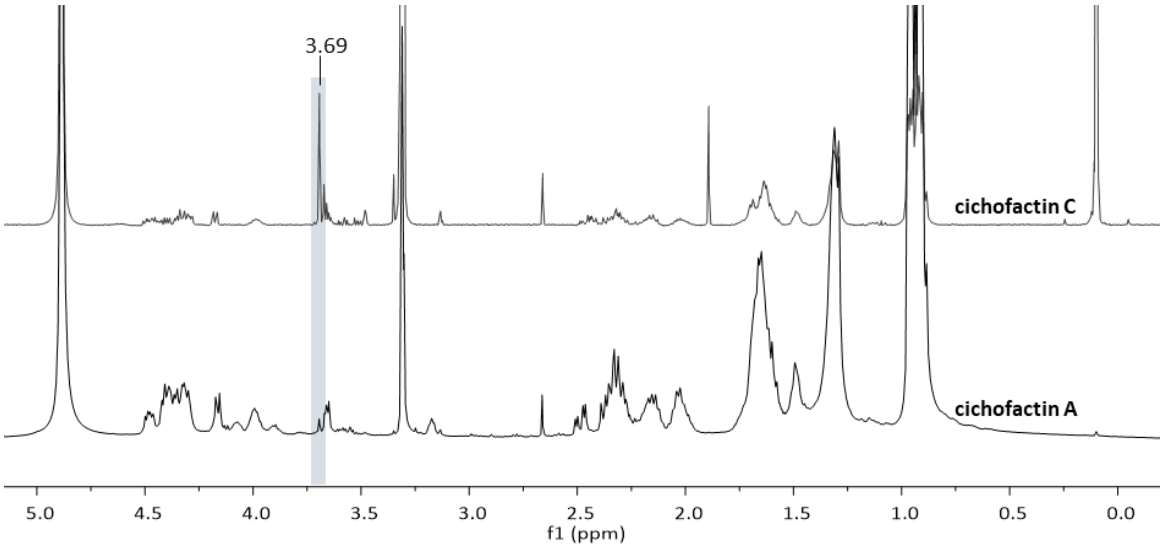

Figure III-44: Superimposed proton spectra of cichofactin A (bottom) and C (top) in d_6-DMSO (400 MHz).
The main difference is displayed in an additional resonance at δ_H = 3.69 ppm which is typical for a methoxy group (grey box).

To elucidate the structure of the minor compound (cichofactin C2, peak 2 **A**), the MS^2 spectra of cichofactin C and C2 were superimposed (**Figure III-45**). The produced b-series fragment ions were identical up to amino acid five and then 14 Da larger indicating that amino acid six contains a CH_2 group more. This result leads to the assumption that amino acid six could either be an isoleucine or a leucine. Complete structure elucidation was not possible due to the low amount.

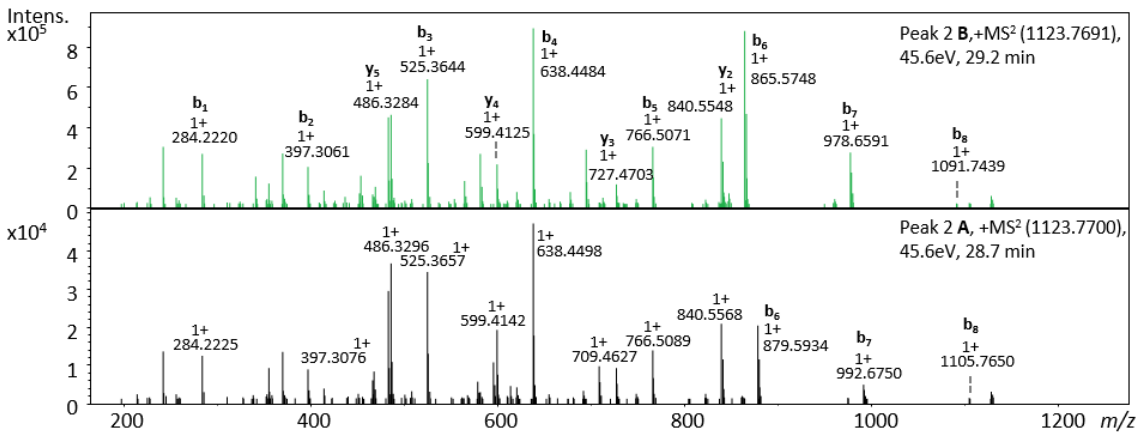

Figure III-45: Comparative MS^2 of peak 2 at 28.7 (cichofactin C2, bottom) and 29.2 min (cichofactin C, top) (1123 Da $[M+H]^+$).

The HR ESI-MS experiment of cichofactin D (peak 4) also gave a major peak 4 **D** and minor peak 4 **C** (cichofactin D2) and both revealed a mass of *m/z* 1151.8023 and 1151.8006, respectively, including a molecular formula of $C_{58}H_{107}N_{10}O_{13}$ (calcd. for 1151.8014; Δ +0.8 ppm and -0.7 ppm) shown in **Figure VIII-24**. MS/MS experiments of cichofactin D and D2 were performed (**Figure VIII-25**), also leading to the assumption that amino acid six is extended by a CH_2 group. The relevant fragments are presented in **Table VIII-16**.

III.2.5.1 Proof of Methylation

Methylation of lipopeptides can occur through methyltransferase (MT) domains present in NRPS gene clusters.[151] The analysis of the gene cluster of *P. viridiflava* P1.A2 did not reveal such a domain. Methylation can also arise in presence of methanol and the isolated compounds were dissolved in methanol for LC-MS analysis and methanol was also used as solvent during VLC separation. In order to analyse if the lipopeptides get methylated during biosynthesis or if it is an artefact of the solvent, another cultivation was performed where no methanol was used as solvent. The cultivation broths were acidified and then extracted with ethyl acetate. The crude extract was either dissolved in methanol as positive control or in acetonitrile and subsequently analysed by LC-MS. The extracted ion chromatogram (1123 Da) of crude extract dissolved in methanol revealed two peaks (27.5 and 28.2 min, **Figure III-46 A** bottom) whereas the peak at 28.2 min was absent in the crude extract dissolved in acetonitrile (top). Both peaks A and B showed the masses of 1123 Da $[M+H]^+$ and 1145 Da $[M+Na]^+$. The absence of peak B in acetonitrile indicated that the lipopeptide got methylated in presence of methanol. To confirm this assumption, MS/MS measurements were performed.

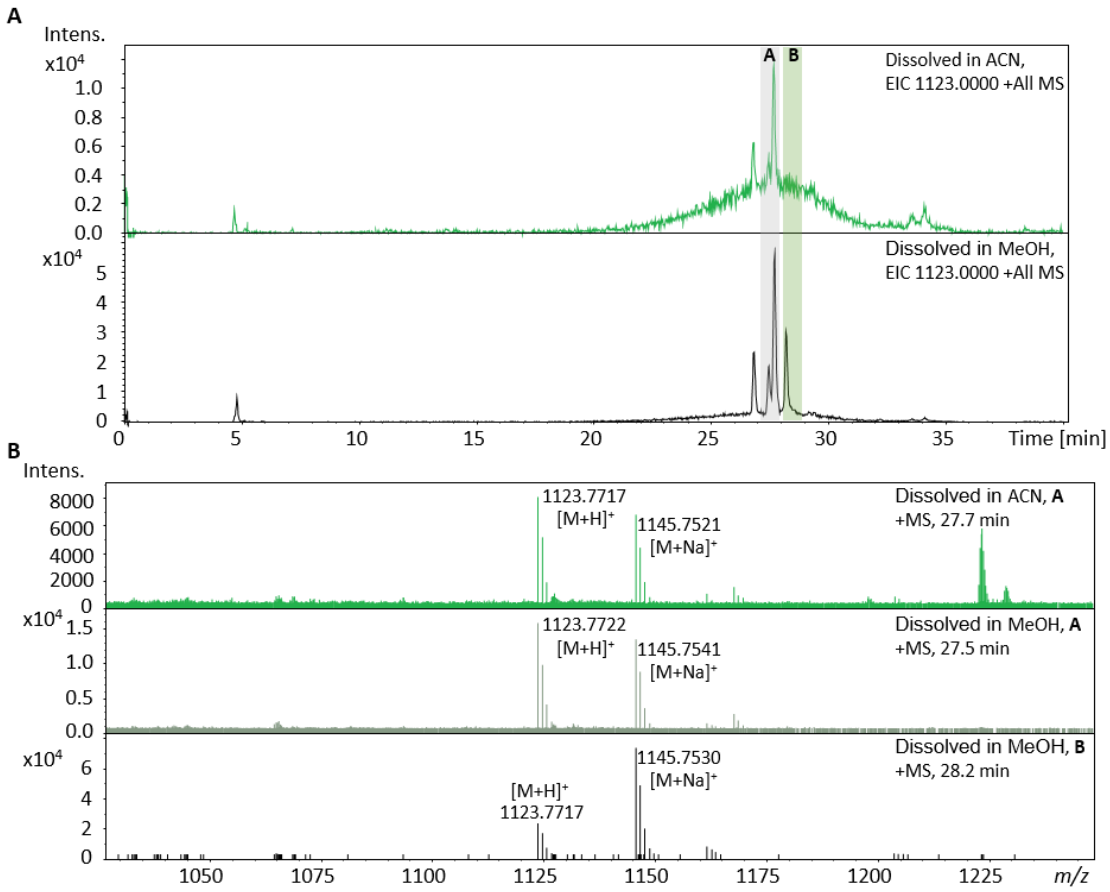

Figure III-46: Proof of methylation arising from methanol.

A: Extracted ion chromatogram (*m/z* 1123 Da) of crude extracts dissolved in methanol (bottom) and acetonitrile (top). There were two peaks present in methanol whereas peak B was absent in acetonitrile (green box).

B: MS^1 showed the masses of *m/z* 1123 Da $[M+H]^+$ and *m/z* 1145 Da $[M+Na]^+$ for each peak.

The produced b-series fragment ions from amino acid 5 to 7 of the HR-MS/MS experiment are shown in **Figure III-47**. The fragmentation pattern of peak A in both solvents showed the incorporation of either an isoleucine or leucine at position 6 (top and middle). Peak B in methanol showed valine at this position leading to the assumption that the lipopeptide is methylated at the C-terminus (Leu8).

All in all, *P. viridiflava* produced a lipopeptide containing either an isoleucine or leucine at position 6. The methylation of the lipopeptide is an artefact due to the presence of methanol during the purification process.

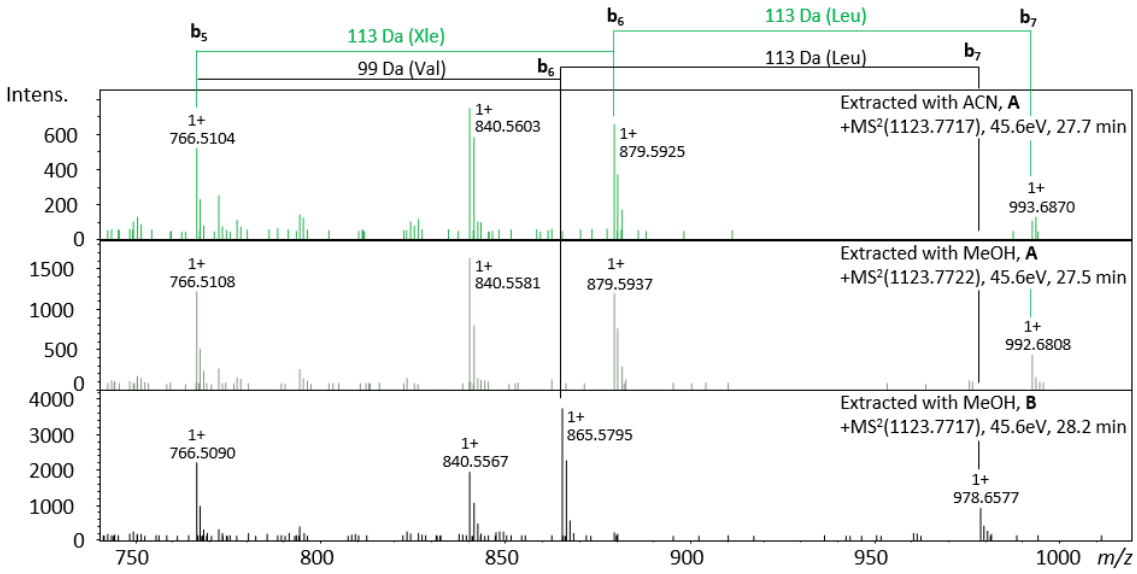

Figure III-47: Comparative MS^2 of crude extracts dissolved in methanol or acetonitrile.

Peak A showed the incorporation of Xle at position 6 in both solvents (top and middle). Peak B revealed a valine at position 6 (bottom). Therefore, the methylation occurred at the carboxylic moiety of Leu8.

III.2.6 Structure Elucidation of Cichofactin Derivatives E & F

In cultivations supplemented with L-leucine, four different compounds were produced. For structure elucidation, HR ESI-MS, MS^2 and NMR measurements were recorded as described previously.

Peak 5 (**Figure III-42**) showed a mass of 1109.7538 Da, consistent with a molecular formula of $C_{55}H_{101}N_{10}O_{13}$ (calcd. for 1109.7544; Δ -0.5 ppm) (data not shown), indicating a high identity to cichofactin A. Superimposed MS/MS spectra of peak 5 (top) and cichofactin A (bottom) from regular production revealed the identical fragmentation pattern as shown in **Figure III-48**. Therefore, these compounds were combined for structure elucidation (see **Chapter III.2.3**).

Peak 7 revealed a mass of 1137.7841 Da which is identical to cichofactin B demonstrated by HR-MS and MS/MS measurements (data not shown). Also these two compounds were combined for structure analysis and further biological activity testing.

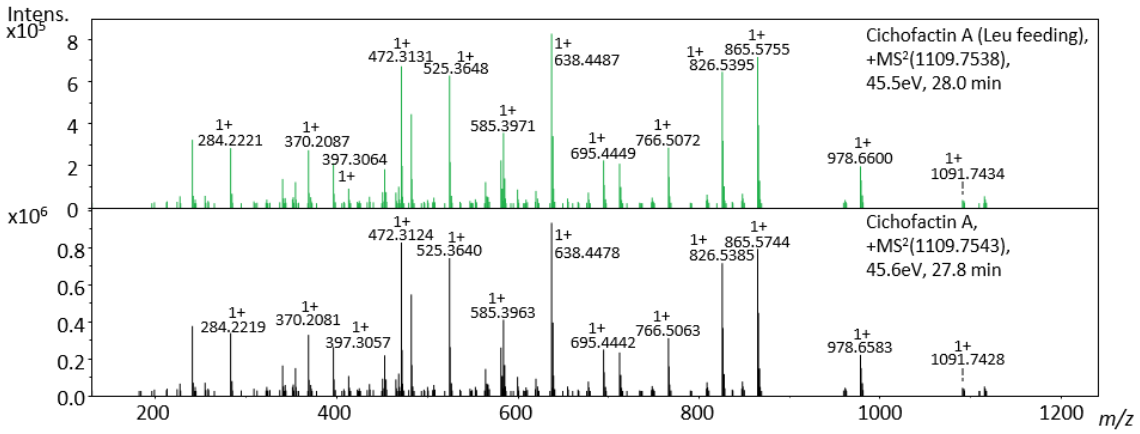

Figure III-48: Comparative MS^2 of cichofactin A produced regularly (bottom) and in media supplemented with leucine (top) (*m/z* 1109 Da $[M+H]^+$).

The major compound, cichofactin E (peak 6), showed a peak at 1123.7712 $[M+H]^+$ in the HR ESI-MS (**Figure VIII-26**), corresponding to a molecular formula of $C_{56}H_{103}N_{10}O_{13}$ (calcd. for 1123.7701; Δ +0.9 ppm). The analysis of the MS/MS spectra revealed the predicted peptide sequence of Leu-Leu-Gln-Leu-Gln-Xle-Leu-Leu indicating that amino acid 6 is either a leucine or isoleucine instead of valine. The produced b- and y-series fragment ions of cichofactin E are shown in **Figure VIII-27**and **Table VIII-15**.

Furthermore, the structure was confirmed by NMR and the following experiments were recorded: ^{1}H, ^{13}C, ^{1}H-^{1}H COSY, ^{1}H-^{13}C HSQC, ^{1}H-^{13}C HSQC-TOCSY, ^{1}H-^{13}C HMBC, ^{1}H-^{15}N HSQC, band selective ^{1}H-^{13}C HSQC and HMBC.

The proton spectrum of cichofactin E (**Figure III-49**; **Figure VIII-30**) revealed typical resonances for a lipopeptide such as the amide signals between 8.0 and 8.5 ppm, the resonances of α-protons in the range of 4.1 to 4.6 ppm as well as the methylene groups of the amino acid side chain between 1.6 and 2.4 ppm. The characteristic resonances of the fatty acid appeared at 4.0 (hydroxyl group bearing position), 1.3 (methylene groups) and 0.9 (methyl group) ppm. The typical resonances for peptides were also present in the carbon spectrum like the carbonyl region (173 – 178 ppm) and the region of the α-protons (52 – 55 ppm) as shown in **Figure VIII-31**.

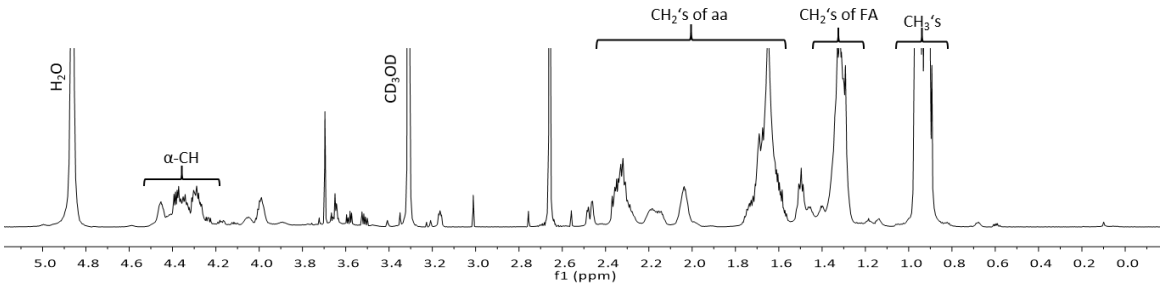

Figure III-49: ^{1}H NMR spectrum of cichofactin E in d_4-MeOH (700 MHz).

This spectrum indicates the different types of protons.

A ^{1}H-^{13}C HSQC experiment was performed to correlate the carbons with their directly bound protons (**Figure VIII-32**). The cross peaks of the α-carbons are overlapped but even a band selective ^{1}H-^{13}C HSQC experiment focussing on the range from 40 to70 ppm could not provide any further information.

Additionally, a ^{1}H-^{13}C HSQC-TOCSY spectrum was recorded and complete spin systems of each amino acid of cichofactin E are depicted in **Figure III-50**. This spectrum corroborated the absence of a spin system for valine (blue box) but revealed spin systems of leucines, glutamines and a fatty acid. Leucine spin systems are shown in the red box, two spin systems of glutamine are labelled in green and the fatty acid in purple. The presence of an isoleucine spin system was also not confirmed indicating the incorporation of another leucine at position 6. The six spin systems of the amino acid leucine are not separated well so the proof for the presence of six leucines was shown in another spectrum.

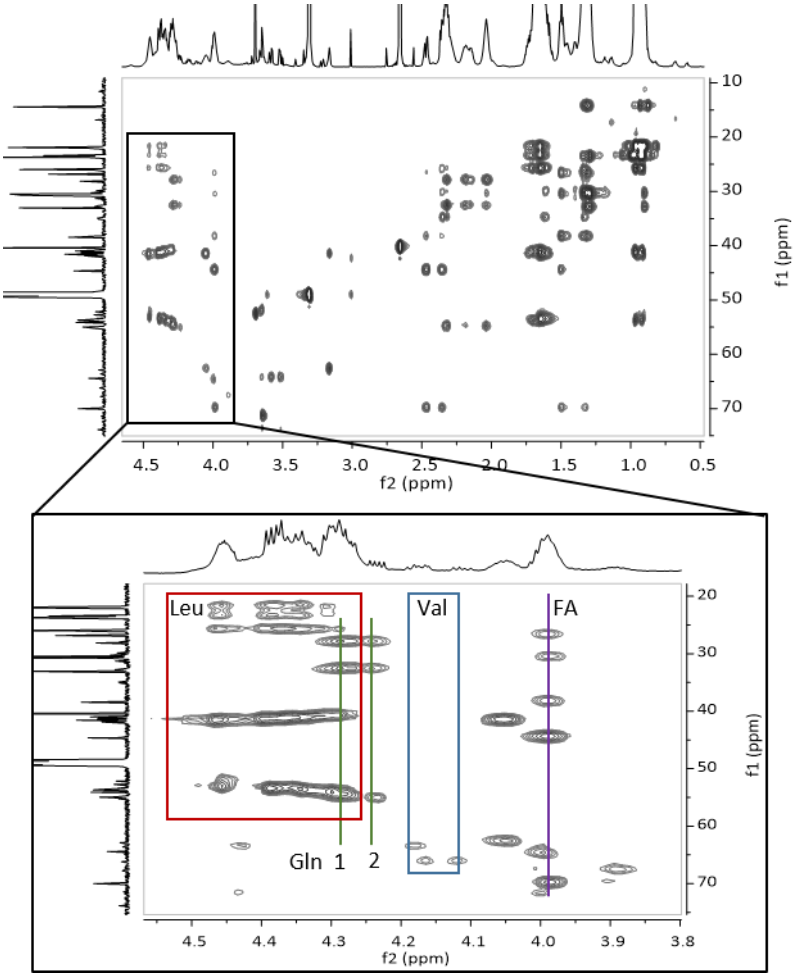

Figure III-50: ^{1}H-^{13}C HSQC-TOCSY spectrum of cichofactin E in d_4-MeOH (700 MHz).

An overview of the ^{1}H-^{13}C HSQC-TOCSY spectrum of cichofactin E (top) is shown and a detailed region of the α- protons and fatty acid (bottom). The lines indicate the different spin systems of the amino acids; glutamine in green and fatty acid in purple. The leucine spin systems are shown in a red box. The blue box presents the absence of valine.

In order to confirm the presence of an additional leucine in the lipopeptide and to connect the spin systems, a combination of different 2D NMR spectra (^{1}H-^{1}H COSY, ^{1}H-^{13}C HMBC, ^{1}H-^{15}N HSQC and a band selective ^{1}H-^{13}C HMBC) was performed. The presence of six leucine residues was confirmed by ^{1}H-^{1}H COSY correlations between the alpha and beta protons of the amino acids (**Figure III-51 A**) and by ^{1}H-^{13}C HSQC correlations between the α-protons and their directly bound carbons (**Figure III-51 B**).

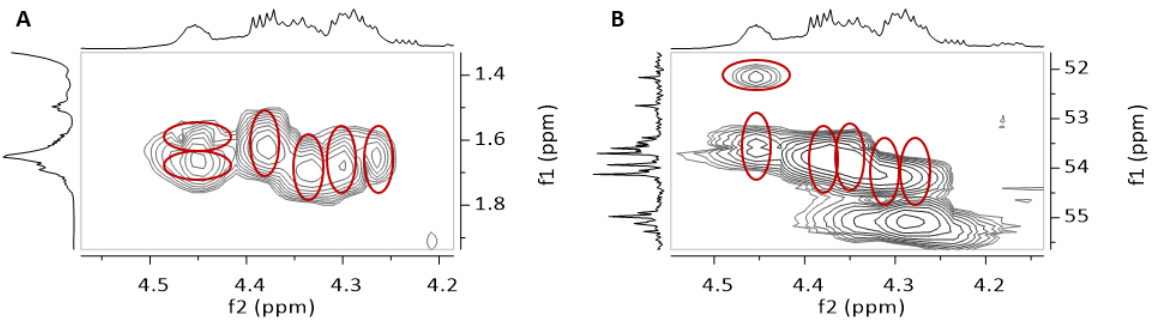

Figure III-51: Proof of the presence of a sixth leucine in cichofactin E.

A: Detail region of ^{1}H-^{1}H COSY spectrum of correlation between α-protons (δ_H = 4.2 – 4.5 ppm) of six leucines and their β-protons (δ_H = 1.6 – 1.7 ppm). **B:** Detail region of ^{1}H-^{13}C HSQC spectrum of correlation between α-protons (δ_H = 4.2 – 4.5 ppm) of six leucines and their directly bonded carbon (δ_C = 53 – 55 ppm).

The sequence of cichofactin E was determined in comparison with the NMR data of cichofactin A due to the low amount of cichofactin E and six identical amino acids. The key correlations are shown in **Figure III-52**. The determined chemical shifts of cichofactin E are presented in **Table III-5**. The NMR data corroborated the HR ESI-MS and MS/MS findings.

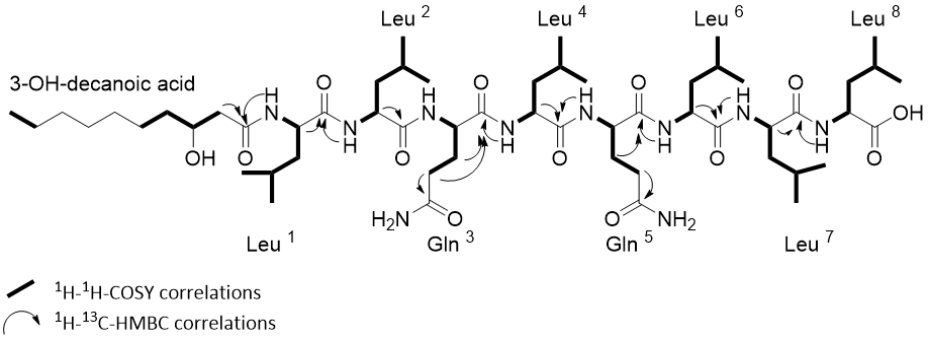

Figure III-52: 2D NMR key correlations of cichofactin E.

Bold lines indicate the ^{1}H-^{1}H COSY correlations and arrows represent the ^{1}H-^{13}C HMBC correlations

Cichofactin F was determined by HR ESI-MS which gave a major peak (8 G) with a mass of *m/z* 1151.8003 corresponding to a molecular formula of $C_{58}H_{107}N_{10}O_{13}$ (calcd. for 1151.8014; Δ --0.9 ppm), as shown in **Figure VIII-29**. The fragmentation pattern revealed an additional leucine at position 6 instead of valine and an extension of the fatty acid by 28 Da compared to cichofactin E. All relevant fragments are listed in **Table VIII-16**. A ^{1}H-^{13}C HSQC-TOCSY spectrum corroborated the absence of valine (data not shown), leading to another derivative of cichofactins.

Table III-5: NMR spectroscopic data of cichofactin E (700 MHz, 298 K).

residue	pos.	$\delta_{C/N}$[a]	δ_H (*J* in Hz)[b]	residue	pos.	$\delta_{C/N}$[a]	δ_H (*J* in Hz)[b]
HDA	CO	174.9 C_q		**Leu 4**	α	54.1 CH	4.33
	2	44.6 CH_2	2.36		β	41.1 CH_2	1.68
			2.47		γ[c]	25.9-26.0 CH	1.63 – 1.75
	3	70.1 CH	3.99		δ_1[d]	23.4-23.7 CH_3	0.93 – 0.98
	4	38.5 CH_2	1.5		δ_2[e]	21.8-22.0 CH_3	0.90 – 0.94
	5 - 8	33.0 CH_2	1.30		α-CO	175.1 C_q	
		30.7 CH_2	1.39		α-NH	n.d.	8.23 (d, 7.3 Hz)
		30.5 CH_2	1.32	**Gln 5**	α	55.1 CH	4.24
		26.8 CH_2	1.34		β	28.1 CH_2	2.04
			1.48				2.18
	9	23.7 CH_2	1.32		γ[f]	32.7 CH_2	2.28
	10	14.5 CH_3	0.90		α-CO	173.9 C_q	
Leu 1	α	53.7 CH	4.39		α-NH	117.7 NH	8.28
	β	41.5 CH_2	1.63		γ-CO	177.7 C_q	
	γ[c]	25.9-26.0 CH	1.63 – 1.75		γ-NH_2	107.3 NH_2	6.83 + 7.60
	δ_1[d]	23.4-23.7 CH_3	0.93 – 0.98	**Leu 6**	α	53.9 CH	4.35
	δ_2[e]	21.8-22.0 CH_3	0.90 – 0.94		β	41.2 CH	1.70
	α-CO	175.7 C_q			γ	25.9-26.0 CH	1.63 – 1.75
	α-NH	125.0 NH	8.19		δ_1[d]	23.4-23.7 CH_3	0.93 – 0.98
Leu 2	α	54.1 CH	4.29		δ_2[e]	21.8-22.0 CH_3	0.90 – 0.94
	β	41.0 CH_2	1.66		α-CO	174.4 C_q	
	γ[c]	25.9-26.0 CH	1.63 – 1.75		α-NH	118.3 NH	8.03 (d, 7.4 Hz)
	δ_1[d]	23.4-23.7 CH_3	0.93 – 0.98	**Leu 7**	α	53.6 CH	4.45
	δ_2[e]	21.8-22.0 CH_3	0.90 – 0.94		β	41.6 CH_2	1.66
	α-CO	175.4 C_q			γ[c]	25.9-26.0 CH	1.63 – 1.75
	α-NH	118.8 NH	8.25		δ_1[d]	23.4-23.7 CH_3	0.93 – 0.98
Gln 3	α	55.0 CH	4.30		δ_2[e]	21.8-22.0 CH_3	0.90 – 0.94
	β	28.1 CH_2	2.04		α-CO	174.5 C_q	
			2.20		α-NH	n.d.	8.09 (d, 8.1 Hz)
	γ[f]	32.8 CH_2	2.32	**Leu 8**	α	52.2 CH	4.48
	α-CO	174.3 C_q			β	41.6 CH_2	1.64
	α-NH	118.7 NH	8.42		γ[c]	25.9-26.0 CH	1.63 – 1.75
	γ-CO	177.7 C_q			δ_1[d]	23.4-23.7 CH_3	0.93 – 0.98
	γ-NH_2	107.3 NH_2	6.83 + 7.60		δ_2[e]	21.8-22.0 CH_3	0.90 – 0.94
					α-CO	n.d.	
					α-NH	n.d.	8.12 (d, 8.0 Hz)

[a] Recorded at 176 MHz for ^{13}C and ^{15}N values were extracted from the corresponding ^{1}H-^{15}N HSQC NMR spectrum. Multiplicity determined by an edited ^{1}H-^{13}C HSQC NMR experiment. [b] Recorded at 700 MHz. [c] The γ-Leu values are interchangeable. [d] The δ_1-Leu values are interchangeable. [e] The δ_2-Leu values are interchangeable. [f] The γ-Gln values are interchangeable. n.d.: not detectable

IV Discussion & Outlook

IV.1 Guanidine-Containing Lipopeptides

This project was investigated within in the framework of the transregional collaborative research centre TRR 261 'Cellular Mechanisms of Antibiotic Action and Production' and was a subproject of project A09 'Recognition mechanisms of guanidine-containing lipopeptide antibiotics for cell wall precursor targets'. The overall goal of this project was to gain a detailed understanding of the antibiotic action of the guanidine-containing lipopeptides. On the one hand, this subproject aimed to isolate the cyclic lipopeptides plusbacin A_3 and empedopeptin in order to enable collaboration partners to determine the modes of action of the CLPs and to perform serial passaging experiments. On the other hand, the solution structure of the CLPs in complex with lipid II should be determined by NMR.

In the following chapters, both the difficulties and the achieved goals of this project are discussed, as well as an outlook on the possible future prospects.

IV.1.1 Investigations on Plusbacin A_3

The antimicrobial cyclic lipopeptide plusbacin A_3 should be isolated from the strain *Lysobacter firmicutimachus* PB-6250 unlabelled on the one side (goal 1) and ^{15}N-labelled on the other hand (goal 2).

Plusbacins A_1-A_4 and B_1-B_4 were first isolated in 1992 from a strain of *Pseudomonas* sp. PB-6250^T which was reclassified as *Lysobacter firmicutimachus* sp. nov.[35,38] The isolation, structural characterisation as well as the antibacterial activity *in vitro* and *in vivo* of these compounds was investigated by Shoji *et al*.[35,126] Thereby, plusbacins showed strong activity against Gram-positive bacteria including strains of methicillin-resistant *Staphylococcus aureus* as well as inhibitory effects on the cell wall synthesis.[35,39] A specific target could not be identified in these initial studies so far.

The structures of the eight components were only determined by HR-MS measurements and Edman degradation of the deacylated products as the recorded proton NMR spectra were of low quality.[126] In order to determine the solution structure of Plus A_3 in complex with 3-lipid II, a full assignment of the NMR values is necessary to analyse observed shift alterations.

In order to isolate a sufficient amount of plusbacin A_3, fermentation was performed on large scale cultivation in linseed medium and later in R2A medium due to less media by-products. Separation of each analogue was rather challenging as the culture broth contains highly similar products. Shoji *et al*. described the isolation of each plusbacin component in sufficient amounts. However, the NMR spectroscopic measurements of plusbacin A_2 did not reveal sharp signals, indicating the presence of multiple conformers in solution.[126] This suggests that the isolated compounds were not sufficiently purified at that time. In our study, multiple purification steps, with different columns varying in their stationary phase, were performed, however, all tested options were insufficient for an adequate separation of plusbacin A_3 from the very similar derivatives. In addition, the extraction method described by *Shoji et al.* was accessed, but did not lead to a satisfying result as even more impurities were present.[35] According to Zachow *et al.* many *Pseudomonas* species are known to grow on agar medium and most of them are also soil bacteria.[152] Therefore, based on the pigment production in *P. aeruginosa* which was increased on agar medium supplemented with cetrimide,[153] cultivation on solid medium (linseed and R2A medium) was performed to reduce impurities and to improve the production. However, this strategy also did not lead to a satisfactory result.

Nevertheless, plusbacin A_1 and A_2 were isolated in a highly purified form, although phosphate salts from the last purification step were still present, so that no valid amount could be determined. The phosphate buffer was used as plusbacins contain acidic and basic functional groups and in order to reduce pH fluctuation. The ionisation of these groups was employed to obtain a better separation. Thus, at low pH, components with acidic functional groups will be more retained.[154] These compounds were provided to the collaborations partner in order to determine the modes of action of the CLPs.

The cultivation media was modified by supplementation of precursors in order to improve the production of plusbacin A_3 or to favour the production of this certain derivative, and is described in the following **Chapter IV.1.1.1**.

^{15}N-labelled plusbacins were produced straightforward as described for uniformly ^{15}N-labelled nisin in ^{15}N-enriched growth medium as nitrogen source.[136,155] For production of ^{15}N-labelled plusbacins in linseed medium, the containing ammonium sulphate as nitrogen source was replaced by ^{15}N-labelled ammonium sulphate in a 1:1 ratio. By switching the cultivation of *L. firmicutimachus* from linseed medium to R2A medium, the ingredient casamino acids as nitrogen source have been replaced by ammonium sulphate in 1:1.6 ratio. Cultivation in both media resulted in the production of uniformly ^{15}N-labelled plusbacins. The isolation and

purification of the ^{15}N-labelled plusbacins revealed the same issues as for the unlabelled plusbacins.

IV.1.1.1 Improvement of Plusbacin Production Rate

The production of plusbacins can be controlled by supplementation of branched amino acids to the cultivation medium (R2A medium) which are biosynthetic precursors of branched fatty acids (**Figure III-8**). The production of plusbacin A_2 was significantly increased by the addition of D- and L-leucine, but not by addition of D- and L-valine. The productivity of plusbacin A_3, the component of interest, was only affected slightly by supplementation of L-valine, but not by adding the other branched amino acids. These results suggest that α-keto acids are produced specifically on leucine, but not on valine by the transaminases of the producing organism. This also inidcates that 3-methyl-2-oxo-butanoic acid, a precursor of iso-type fatty acid with an even carbon content could be produced from other amino acids than valine via an alternative metabolic pathway.[130] The L-form of amino acids is the natural form and is therefore better accepted, as shown for L- and D-leucine and L- and D-valine. The steric hindrance of D-valine is closer to the stereocentre of the amino acid than for leucine. Therefore, the synthesis of the fatty acid starting with D-valine is less preferred and results in a lowered productivity of the precursor. Previous studies already showed improved productivities of lipopeptides by biosynthetic precursors. A similar effect on the proportion of the variants was observed on the production of tripropeptins in media supplemented with precursors by Hashizume *et al*.[130] Tripropeptin C, which exhibits the same odd β-hydroxy fatty acid as plusbacin A_2, was mainly produced by supplementation of L- and D-leucine, 4-methyl-2-oxo-pentanoic acid or 3-methyl-butanoic acid. In contrast, the production of Tpp D, which has the same even β-hydroxy fatty acid as plusbacin A_3, was affected by addition of 3-methyl-2-oxo-butanoic acid or 3-hydroxy-14-methylpentanoic acid, but was not enhanced by addition of L- and D-valine or L-homoleucine.[130] An increased productivity also appeared on surfactin variants by the addition of different amino acids.[148] The production of surfactin variants with even β-hydroxy fatty acids was significantly enhanced when Arg, Gln or Val was added to the culture medium whereas the supplementation of Cys, His, Ile, Leu, Met, Ser or Thr affected surfactin variants with odd β-hydroxy fatty acids.[148]

IV.1.2 Investigations on Empedopeptin

The antimicrobial cyclic lipopeptide empedopeptin should be also isolated unlabelled and ^{15}N-labelled from the strain *Massilia* sp. ATCC31962, formerly *Empedobacter haloabium*, in order

to perform serial passaging experiments by our collaborative partner and to determine the interaction site in complex with 3-lipid II, respectively.

The production, isolation, structure determination as well as the antibacterial activity *in vitro* and *in vivo* of empedopeptin was first published in 1984 in two consecutive papers.[34,131] Thereby, empedopeptin showed a potent antimicrobial activity against a variety of aerobic and anaerobic Gram-positive bacteria including clinical important pathogens like *Staphylococcus aureus, Staphylococcus epidermidis* and *Clostridioides* (formerly *Clostridium) difficile*.[34] Due to the promising profile of empedopeptin such as minimal inhibitory concentrations (MIC) in the low *µ*g/mL range, antibiotic-resistant isolates and good pharmacokinetic parameters, the molecular mechanism of action was further investigated by Müller *et al*.[1] This study revealed that empedopeptin interferes with the late stages of the cell wall biosynthesis by preventing the incorporation of *N*-acetylglucosamine into the cell wall and thereby interrupting peptidoglycan biosynthesis.[1] Further distinct assays showed that Emp binds lipid II (undecaprenyl pyrophosphate-*N*-acetylmuramic acid (pentapeptide)-*N*-acetylglucosamine) as its primary target in a 2:1 complex as well as that calcium ions at a concentration similar to human serum strongly influenced their interaction.[1] The analysis of antagonization assays demonstrated that the regions of the pyrophosphate group, the first sugar as well as contiguous parts of stem peptide and undecaprenyl chain are involved as shown in **Table IV-1**.[1]

Table IV-1: Antagonization assays with various cell wall precursors and shortened variants thereof.[1]

Different lipid precursors were used to narrow down the interaction region with Emp (concentration of Emp 8x MIC). +: antagonization, -: no antagonization.

lipid intermediate	**molar ratio of precursor to EMP**						
	10 x	**5 x**	**2.5 x**	**1.25 x**	**0.625 x**	**0.3125 x**	**0.156 x**
UDP-GlcNAc	-	-	-	-	-	-	-
UDP-MurNAc-pp	-	-	-	-	-	-	-
C_{55}-P	-	-	-	-	-	-	-
C_{15}-PP	+	+	+	-	-	-	-
C_{55}-PP	+	+	+	-	-	-	-
lipid I-(dipeptide)	+	+	+	+	+	-	-
lipid I-(tripeptide)	+	+	+	+	+	-	-
lipid I-(pentapeptide)	+	+	+	+	+	+	-
lipid II	+	+	+	+	+	+	-
lipid III	+	+	+	+	-	-	-

In order to arrive at a detailed understanding of the antibiotic action of empedopeptin, further analysis is necessary. Therefore, a sufficient amount of empedopeptin (16 mg) was isolated to

enable the collaborative group to perform serial passaging experiments which are still ongoing. The cultivation and purification procedure of Emp was adapted from previous studies.[125]

For the second goal, the particular focus was on primary contact events of the antibiotic Emp with its primary target lipid II. Antagonization assays revealed already the involved regions[1], but were not confirmed by structural methods. Therefore, the interaction side should be determined by NMR experiments. Due to the low natural abundance of ^{15}N, uniformly ^{15}N labelled empedopeptin was produced by cultivations in media supplemented with ^{15}N-labelled ammonium sulphate and a sufficient amount of ^{15}N-labelled empedopeptin was isolated (13.4 mg).

First, the structure of ^{15}N-labelled empedopeptin was confirmed by NMR and the NMR values were fully assigned. In previous studies, the structure was only characterised based on partial hydrolysis and LC-MS analysis[131] and the peptide sequence was corroborated by NMR, but no full assignment was possible.[132]

IV.1.2.1 New Derivatives of Empedopeptin

During the purification procedures of unlabelled and labelled empedopeptin, new congeners of empedopeptin were isolated or at least new variants were discovered by mass spectrometry. The consanguinity of empedopeptin variants of the unlabelled form was illustrated by MS networking (**Figure III-14**). The isolates are suggested to represent a linear form or methylated variants of the linear and cyclised empedopeptin. The additional congeners which were detected in the HR-MS spectrum are proposed to exhibit an alteration at the 3-hydroxy aspartic acids. The new derivatives were confirmed by HR-MS and MS/MS measurements so far. Another molecular network was conducted by Yang and co-workers who identified 44 empedopeptin analogues, including 17 cyclic lipopeptides and 27 linear variants.[156] Their analysis of the analogues revealed that they consist of the identical amino acid sequences but have hydroxyl modifications in different amino acids and variants in the length of the 3-hydroxy fatty acid side chain.[156] However, in this study of Yang and co-workers, no methylated empedopeptin variants and no incorporation of different amino acids were observed, although the empedopeptin extracts were dissolved in methanol for LC-MS analysis. The extraction of the culture broth was performed with EtOAc and butanol while acetonitrile was used as LC-MS solvent. Therefore, the extracts were probably not exposed to methanol for a long time, so that methylation could occur.[156]

In the present study, the isolates were treated with sodium hydroxide to linearize the compounds and thus get better MS fragmentation, therefore it was not surprising to observe the linear form of empedopeptin. However, the linear form was also visible in the untreated extracts as minor

compound which might be due to the different separation step using numerous solvents at a low pH leading to hydrolysis of the compound. Another possible explanation is that the cyclisation through the TE tandem domain has not occurred as it was observed in the biosynthesis of syringafactins.[139]

The suggested structures of empedopeptin derivatives 1, 2 and 4 revealed an additional methyl or methylene group at the 3-hydroxy aspartic acids which could either result from an extension (Glu instead of Asp) or methylation of the amino acid as N-methylation, ether methoxy or ester methoxy (**Figure IV-1**). The incorporation of glutamic acid instead of aspartic acid can occur based on the certain promiscuity of non-ribosomal peptide synthetases (NRPSs), especially the A domains responsible for the recognition and activation of amino acids, which is biosynthetically the most probable explanation. The promiscuity of A domains was already observed in the biosynthesis of different lipopeptides as for example in fusaricidins[157] or the amphisin group[158] where the A domain can either activate an Asn/Asp or a Gln/Glu. The incorporation of a 3-hydroxy glutamic acid would generate a ^{1}H NMR shift of around 2.4 (dd) and 2.6 (dd) ppm and a ^{13}C NMR shift of around 38 ppm.[159–161] However, the lack of a glutamic acid spin system in the NMR spectra speaks against this possibility. The other option is methylation of the amino acid, which can be carried out by an independent methyltransferase domain within the NRPS cluster with S-adenosyl-methionine (SAM) as a co-substrate, which catalyse the transfer of a methyl group from SAM to an acceptor substrate.[162] Additionally, O-methylation can occur by additional enzymes. Within the biosynthesis of kutznerides, O-methylated serine was incorporated by an adenylation domain interrupted by the SAM-binding part of a methyltransferase, in combination with a MbtH-like protein.[163]

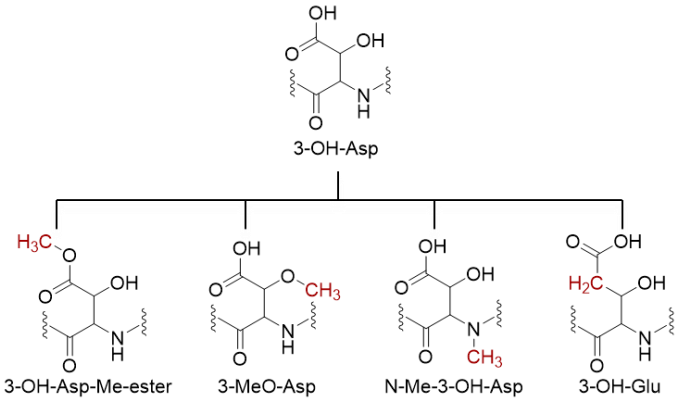

Figure IV-1: Different variants of an additional methyl or methylene group in aspartic acid.

However, no methyltransferase or SAM was found in or adjacent to the biosynthetic gene cluster of empedopeptin indicating that the addition of a methyl or methylene group occurred by using methanol as solvent. Since a sufficient amount of the ^{15}N-labelled empedopeptin variants was isolated, methylation should be detected by NMR measurements. The recorded NMR experiments of two empedopeptin derivatives did not reveal a spin system for glutamic acid, but an additional cross peak in the region of methoxy groups (δ_H = 3.61 / δ_C = 51.7) was observed. With the observed NMR shifts a N-methylation can be excluded, as the NMR shifts for N-methylated compounds typically occur in the range of δ_H = 2.6 – 3.2 and δ_C = 31 – 37.[164] O-Methylation can either occur on the 3-hydroxyl group or on the carboxylic moiety of Asp. ^{13}C NMR shifts of ether methoxy are typically between 55 to 62 ppm,[165] while ester methoxy is around δ_C = 52[166] leading to the assumption that Asp contains an ester methoxy based on the observed cross-peak. Neither a ^{1}H NMR shift around 5 ppm for the hydroxyl group of 3-OH group of Asp nor a ^{1}H-^{13}C HMBC NMR spectrum could support the ester methoxy. The amount of Emp was not sufficient to perform a ^{1}H-^{13}C HMBC NMR spectrum. However, methylation of the carboxyl moiety is more likely in an acidic environment with methanol.

Furthermore, empedopeptin congeners were discovered by HR-MS measurements that exhibited a change in the hydroxy aspartic acid. In this study, it was proposed for derivative 3 that a serine and a glycine were incorporated instead of the two 3-hydroxy aspartic acids while derivatives 5 and 6 contained a methylated threonine at position 3 instead of serine as well as methylated 3-hydroxy aspartic acids. These variants were solely confirmed by MS^2 fragmentation. In order to confirm these hypotheses further NMR or HR-MS studies need to be conducted. As mentioned above, no enzymatic system for OH-methylation was identified in the biosynthetic gene cluster and the methylation was attributable to methanol as solvent. A methylation system could have indicated a protective mechanism of the bacteria. Antibacterial activity studies of plusbacin and tripropeptin derivatives have shown that the hydroxyl groups of the aspartic acids play an important role in the antibacterial activity.[167,168] Both, the lack of the hydroxy groups of the 3-hydroxy aspartic acids in plusbacin and the methyl ester of the aspartic acids in tripropeptin led to a significant reduction in their antibacterial activity.[167,168]The incorporation of various amino acids could be based on the certain promiscuity of the A domains, as described previously. However, all empedopeptin variants revealed strictly conserved amino acids on position 5 (Arg) to 8 (Pro). The specificity of these modules could, for example, result from the strict specificity of the A domain or from the specificity of the C domains involved.

Surprisingly, no empedopeptin analogues with variations in the fatty acid side chain were observed. The structural highly similar classes of plusbacin and tripropeptin mainly include

derivatives that vary in the fatty acid side chain both in length and branching such as plusbacins A_1 to A_4 and B_1 to B_4 as well as tripropeptins A to E and Z.[36,42,126] Since the responsible $C_{Starter}$-domain has a broad substrate specificity, different fatty acid moieties are a common variation in the biosynthesis of lipopeptides from *Pseudomonas* or *Bacillus* species[169] and the origin can be traced to the primary metabolism of the organisms. The fatty acid composition of lipopeptides is controlled by the amount of fatty acid precursors in the cell, which may be present in low amounts during the biosynthesis of empedopeptin in *Massilia sp.* ATCC 31962, resulting in the production of only one fatty acid variant.[170]

IV.1.2.2 Interaction Study of Emp in Complex with 3-Lipid II

In order to understand the antibacterial activity on a structural basis, a solution NMR study of ^{15}N-labelled empedopeptin in complex with shortened lipid II was performed. Such comprehensive structural details on molecular interactions of antibiotics with lipid II are rare due to the challenging physicochemical properties of this unusual target structure. The target molecule has a long lipophilic isoprene tail on the one hand and a polar disaccharide-pentapeptide moiety on the other, resulting in poor solubility and formation of micelles. Therefore, structural information on antibiotics in complex with lipid II is currently limited to the lantibiotics nisin, lacticin 3147 and mersacidin, the tridecaptin A_1 ($TriA_1$) as well as the fungal defensin plectasin (**Figure IV-2**).[136,171–174]

The structure of the nisin and lipid II complex was investigated by high-resolution NMR spectroscopy.[136] The structure reveals that the N-terminal residues of nisin form a unique cage in which the pyrophosphate moiety of the lipid II molecule is bound via amide intermolecular hydrogen bonds, while the interactions with the first sugar are crucial for target-mediated pore formation (**Figure IV-2 1**).[136,175–177]

Similar studies with LtnA1, the Type-B-like component of lacticin 3147, showed that this lantibiotic also forms a pyrophosphate cage with lipid II, but with its C-terminal residues, using additional π-interactions besides amide-mediated hydrogen bonding to bind to the pyrophosphate of lipid II (**Figure IV-2 2**).[171]

Mersacidin, which also belongs to Type-B lantibiotics, showed a similar NMR solution structure in dodecylphosphocholine (DPC) micelles as LtnA1 by binding lipid II through the C-terminal residues (**Figure IV-2 3**).[172]

NMR binding studies for plectasin in complex with native full-length lipid II, supported by computational modelling, revealed that lipid II binds into a pocket with the bactoprenol tail

attached to the hydrophobic part of plectasin near the membrane. In addition to the interaction with the pyrophosphates and the first sugar, the studies showed that the binding of defensin involves crucial interactions with D-Glu2 of the lipid II stem peptide (**Figure IV-2 5**).[174]

Consistent with the structural data, plectasin does not bind to the WTA precursor lipid III, and a reduction in binding affinity is observed *in vivo* and *in vitro* when this critical interaction site is amidated.[178] In contrast, NMR analysis of tridecaptin A_1 in complex with lipid II in dodecylphosphocholine (DPC) micelles showed that the pyrophosphate moiety of lipid II is not involved in binding (**Figure IV-2 4**).[173] Chemical shifts of D-Glu2, D-Ala4 and D-Ala5 in lipid II indicated relevant interactions with the stem peptide.

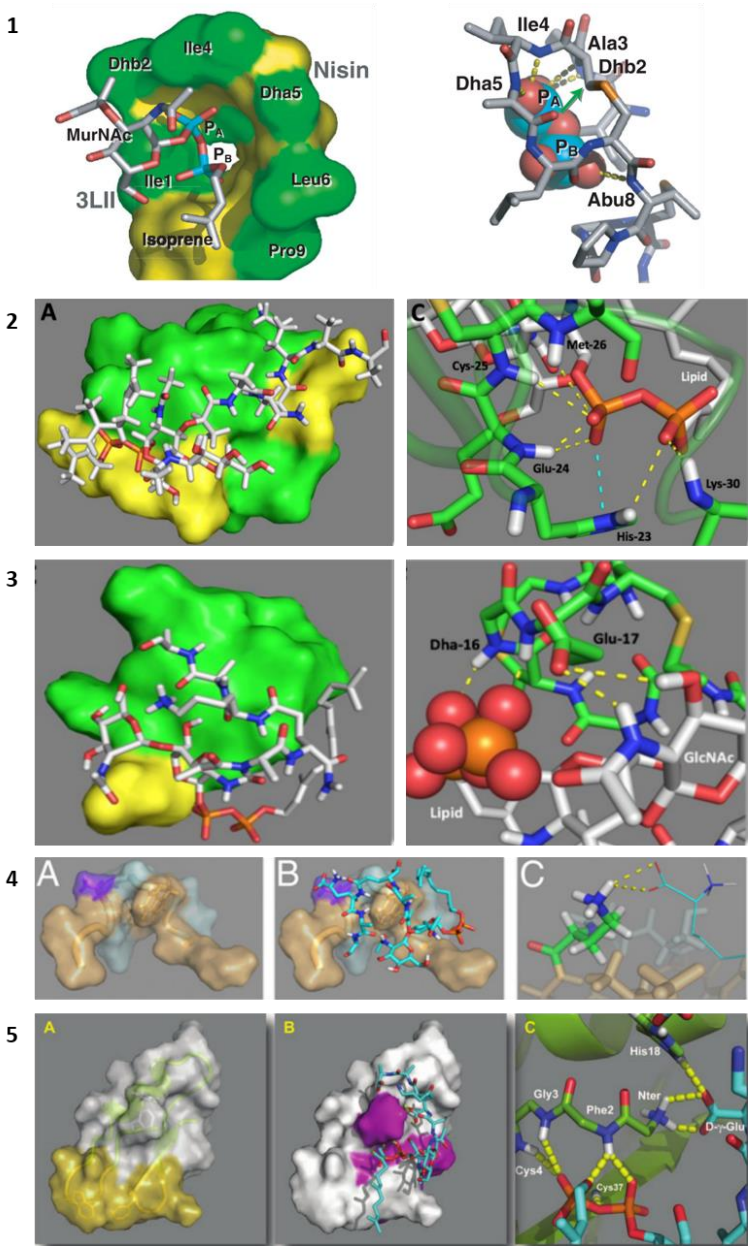

Figure IV-2: Molecular interactions of different antibiotics with lipid II.

1: Structure of the nisin-3-lipid II complex. Left: The N-terminal portion of nisin (residues 1-12 are shown in the van der Waals surface, with the backbone and side chain atoms in yellow and green, respectively) encages the pyrophosphate moiety of 3-lipid II. Right: Nisin backbone – 3-lipid II pyrophosphate intermolecular hydrogen bond network.[136] **2:** Model of the LtnA1-3-lipid II complex. Left: Surface representation with hydrophobic residues green and hydrophilic residues yellow. Lipid II is illustrated as a stick model. Right: Key binding interactions between the C-terminal residues of Ltn1A and pyrophosphate of lipid II. Yellow dash: hydrogen bonds; turquoise dash: possible π-anion interaction.[171] **3:** NMR solution structure of mersacidin bound to lipid II in DPC micelles. Left: Mersacidin adopts a globular structure and binds to lipid II through its C-terminal residues. Right: A model of the proposed mersacidin-lipid II intermolecular bonds.[171] **4:** Left: NMR solution structure of $TriA_1$ in DPC micelles containing 3-lipid II. Middle: 3-Lipid II docked into $TriA_1$. Hydrophobic residues interact with the lipid II terpene tail, and the pentapeptide occupies the binding pocket. Right: Modelled hydrogen bond interactions.[173] **5:** NMR-based model of the plectasin/lipid II complex. Left: Surface representation of plectasin, with the residues that form micelles upon binding to DPC shown in yellow. Middle: Surface representation of plectasin, with the residues that show significant chemical shift perturbations upon lipid II titration shown in magenta. Right: Detailed view of the pyrophosphate-binding pocket with the hydrogen bonds as yellow dashes.[174]

The interaction study of Emp with 3-lipid II was performed according to the NMR-based studies of nisin with soluble 3-lipid II and was depending on the structural information already obtained from previous studies.[1,136] Therefore, the solution structure was determined in a complex of a 2:1 ratio (Emp : 3-lipid II) as well as in absence and presence of calcium ions. The quality of the recorded spectra was quite low. However, the analysis of the phosphorus spectra revealed that the pyrophosphate group of 3-lipid II is involved in the binding motif with empedopeptin which was also shown in previous antagonization assays.[1] ^{31}P NMR spectra of 3-lipid II with Emp in the absence and presence of calcium ions showed an upfield shift. This upfield shift was also observed in studies of the lantibiotics nisin and lacticin 3147 LtnA1 with 3-lipid II in the absence of calcium ions (**Figure IV-3**).[136,171] In contrast, no chemical shift was observed in the ^{31}P NMR of lipid II after addition of tridecaptin A_1, confirming that the pyrophosphate is not involved in binding (**Figure IV-3 C**).[173]

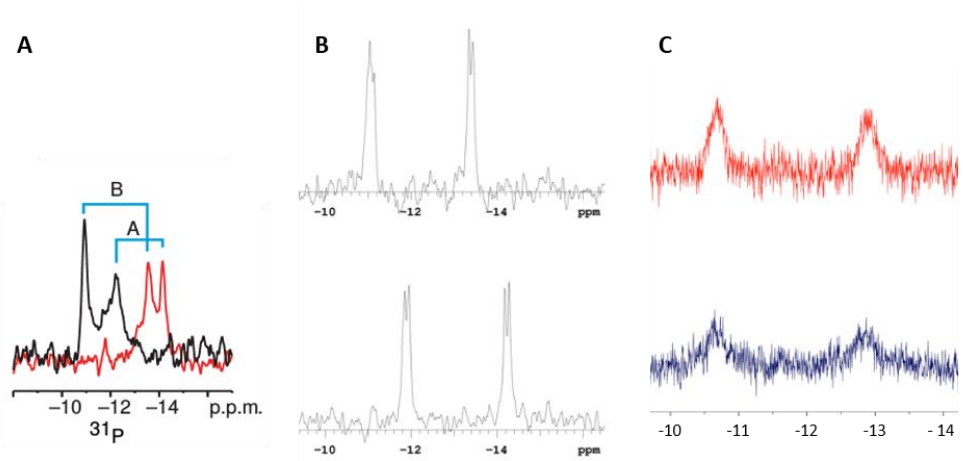

Figure IV-3: ^{31}P NMR spectra of various antibiotics in complex with 3-lipid II.

A: ^{31}P NMR spectra of the pyrophosphate group of 3-lipid II in the free (black) and nisin-bound (red) forms. Signals A and B correspond to the individual phosphates bound to the MurNAc moiety and the prenyl chain, respectively.[136]
B: ^{31}P-NMR chemical shift perturbation of lacticin 3147 LtnA1 and 3-lipid II. Top: free 3-lipid II. Bottom: In complex.[171]
C: ^{31}P-NMR spectra of lipid II in DPC micelles (red) and lipid II in DPC micelles with tridecaptin A_1 (blue). No chemical shift of the phosphorus atoms was observed, indicating that the pyrophosphate moiety is not involved in the binding.[173]

From the ^{1}H-^{15}N HMBC spectrum it could be deduced, that in empedopeptin the 3-hydroxy aspartic acid at position 4 and the neighbouring arginine 5 are probably engaged in the interaction with 3-lipid II indicating an interaction with the western hemisphere of Emp. The guanidinium group in the side chain of arginine is known to interfere with negatively charged groups as for example an interaction between a guanidinium moiety and a phosphate group was identified in the active centre of *Staphylococcus nucleases*, that catalyse the hydrolysis of DNA and RNA.[179,180] The binding motif of a guanidinium group and a phosphate moiety is schematically depicted in **Figure IV-4**. Possibly, in a complex of Emp with 3-lipid II in absence of calcium ions, a direct salt

bridge between the positively charged side of Arg-5 in Emp and the negatively charged pyrophosphate group in lipid II is formed.

Furthermore, the data of the antagonization assays indicated that the direct interaction of Emp with its target was promoted by calcium.[1] It is likely that calcium ions are important to build a complex between the 3-OH Asp-4 or Arg-5 side chain and the negatively charged pyrophosphate group of 3-lipid II. A similar complex was shown for bacitracin A and undecaprenyl pyrophosphate with zinc ions which was proven by the analysis of a crystal structure.[156]

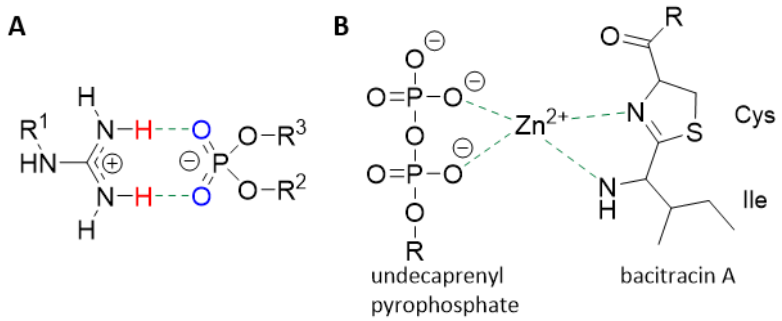

Figure IV-4: Binding modes of nitrogenous compounds and a phosphate moiety.

A: Schematic binding motif of a guanidinium group and a phosphate moiety.[180] **B:** Binding motif of bacitracin A and undecaprenyl pyrophosphate in presence of zinc ions.[156]

Investigation of a plusbacin analogue which was lacking the two hydroxy groups of the aspartic acids revealed that these residues are essential for the antibacterial activity.[167] The conformation of the backbone was dramatically changed without these residues, resulting in a loss of binding to its target and causing therefore a reduction in antibacterial activity.[167] A correlation of these residues with 3-lipid II was not observed by NMR so far. Further analysis on the interaction of Emp and 3-lipid II is still ongoing to get a complete understanding of the binding motif.

IV.1.3 Proof of Ring Closure of the Guanidine-Containing Lipopeptides

In previous studies, the structures of plusbacins and empedopeptin were determined merely by partial hydrolysis and mass spectrometric analysis. As NMR measurements were of poor quality, only the structures of tripropeptins were fully characterized by mass spectrometric analysis and NMR experiments.[43,126,131] In order to verify the cyclisation scheme of this compound class, first a phylogenetic analysis was performed and in the second step the ring closure of Emp and Tpp was proven by NMR.

The phylogenetic analysis of the TE domains of the three CLPs revealed a cyclisation scheme which was similar to the majority of cyclic lipopeptides and where cyclisation occurs within the peptide

moiety. The TE domains clustered in the type I TE domains of pseudomonads which typically cyclise between the C-terminal amino acid and the hydroxyl group of serine or threonine. The analysis of the recorded NMR spectra of empedopeptin and tripropeptin gave the evidence that the published cyclisation scheme is correct. The guanidine-containing lipopeptides cyclise into the hydroxy group of the fatty acid side chain and the phylogenetic prediction was not in agreement with the obtained results. Phylogenetic analysis can be used to explore the evolutionary relationship between organisms. A possible explanation, that the TE domains of the guanidine-containing lipopeptides cluster into the group of pseudomonads, is that they are also gram-negative bacteria (*Lysobacter*, *Massilia*) and thus they are more similar to each other. This similarity is also demonstrated by the fact that the producer strain of plusbacin was previously assigned to the genus of *Pseudomonas*. Nevertheless, the guanidine-containing lipopeptides form a clade of their own into which another lipopeptide (lysobactin) produced by *Lysobacter* clusters. The cyclisation between the fatty acid bearing a hydroxyl group and the C-terminal amino acid is catalysed by type I TE domains belonging to the bacilli, which are gram-positive bacteria. Within the frame of this study, it was not possible to isolate a sufficient amount of plusbacin, therefore the proof for the cyclisation of this compound with the natural product itself. However, total synthesis studies proved to generate functional antibiotics.[181,182]

IV.1.4 Future Perspectives

Isolation of guanidine-containing lipopeptides, elucidation of their structure, and the insight into the molecular interactions with their target are significant advances in this project. Nevertheless, there are still subprojects that need to be completed.

Within this study, it was not possible to isolate sufficient amount of pure plusbacin A_3, the most effective component of this class, to confirm the structure and to determine the solution structure in complex with 3-lipid II. However, the present study revealed that plusbacin A_2 was mainly produced by addition of L- and D-leucine. Therefore, the focus should be on the isolation of plusbacin A_2 since only the fatty acid side chain is shorter by a CH_2 group and then the structure could be elucidated by NMR as well as the molecular interaction with lipid II.

Another suggestion for the purification of cyclic lipopeptides is to change the solvent in the HPLC separation from methanol to acetonitrile, since methylated derivatives were found during the isolation process of both empedopeptin and plusbacin simply due to the exposure of the solvent.

Furthermore, the solution structure of empedopeptin with its target 3-lipid II needs to be fully elucidated. For this purpose, both intra- and intermolecular NOEs need to be analysed and the observed shift perturbations visualised using modelling experiments.

To complete the picture of guanidine-containing lipopeptides, the solution structure of tripropeptin should be also determined. Therefore, ^{15}N-labelled tripropeptin has already been prepared by the Microbial Chemistry Research Foundation (MCRF, Japan) and will be provided for further analysis.

IV.2 Cichofactin Lipopeptides Obtained from *Pseudomonas*

In the second project, new lipopeptides were discovered from the species *Pseudomonas* by genome mining and a sufficient amount should be isolated to determine their structures as well as their antibacterial activity. In order to reach this goal, several strategies were applied to improve the production. The following chapter will discuss the approaches used in the study and the resulting successes as well as provide insight into possible future prospects.

IV.2.1 Genome Mining Approach

In this study, the concept of genome mining was used to identify strains for the isolation of new lipopeptides. To this end, an *in silico* screening for NRPS-derived lipopeptides was performed by using AntiSMASH and seven potential strains with a common gene cluster belonging to the species of *Pseudomonas viridiflava* were discovered. Subsequently, the resulting gene clusters of the different strains were subjected to phylogenetic analysis of the respective A and C domains whereby the peptide backbone of the gene cluster could be correctly predicted and was found to be identical to the cichofactin family and similar to the syringafactin and virginiafactin family.[65,140] The peptide backbone derived from *Pseudomonas* NRPS systems can be precisely determined while the prediction of the fatty acids and the absolute configuration is still challenging. $C_{Starter}$-domains exhibit broad substrate specificity and are therefore not predictable, so that different fatty acid moieties are produced during the biosynthesis of lipopeptides from *Pseudomonas* species.[169] It was possible to predict the stereochemistry of Leu-4 and Val/Ile-6 to be L-configured due to the identified $^{L}C_{L}$ domains of the modules 5 and 7 in comparison with the published structures of the syringafactin family.[140] However, the analysis of dual-function condensation-epimerisation domains revealed a much more complicated picture. The dual C/E domains of modules 2 and 3 are probably inactive as the configuration of Leu-1 and Leu-2 was not inverted as shown in the published data.[140] This effect has already been reported several times in literature.[141]

IV.2.2 Isolation of Cichofactins A & B

The production, isolation and structure elucidation of cichofactins A and B from *P. cichorii* SF1-54 was first published in 2013 and later it was shown that these compounds could be also produced by other *Pseudomonas* species including *P. asturiensis* and *P. viridiflava*.[183,184]

In this study, in order to determine the optimal production conditions and to identify the best producer strain, cultivation of the seven strains was performed in several media at two different temperatures (23 °C and 30 °C). According to the screening results, cultivation of the strain *P. viridiflava* P1.A2 in DMBGly medium at 23 °C gave the best production rate for the lipopeptides.

The analysed crude extract obtained from cultivations at 30 °C revealed the absence of secondary metabolites. The temperature effects in plant-associated bacteria were already studied in more detail and most of them showed an increased expression of gene encoding virulence factors at lower temperatures such as 16 – 24 °C.[185] This phenomenon is not fully understood, but a possible explanation is that water films or aerosols are essential for most plant pathogenic bacteria to efficiently infect their host plants and these occur primarily when the temperature of the plant surface or the air temperature is low.[185] Another interesting aspect is that the virulence of these plant pathogenic bacteria is stronger at lower temperatures even though the optimal growth temperature is usually between 25 °C and 30 °C.[185] The two phytotoxins coronatine and phaseolotoxin for example are produced by the pathogen *P. syringae* in a temperature-dependent manner while the highest production is achieved at 18 °C.[186,187]

Sufficient amounts of cichofactin A and B were isolated from *P. viridiflava* P1.A2, cultivated in DMBGly medium at 23 °C, and the structures were fully assigned by NMR analysis and HR-MS and MS^2 measurements. In previous studies, the structures of cichofactin A and B were solely analysed by HR-MS measurements and later by comparison of NMR data of isolated and synthesised compounds.[65,140]

IV.2.2.1 Bioactivity of Cichofactins A & B

Lipopeptides produced by the genus *Pseudomonas* have different natural roles, such as antimicrobial activity, biofilm formation, swarming, attachment to and colonisation of (plant) surfaces, and act as virulence factors.[2,65,188] Cichofactin A and B were first isolated from *Pseudomonas cichorii* SF1-54. Pauwelyn *et al*. investigated the biological activity as well as the biological role of cichofactins.[65] The two cichofactins were tested on the one hand for surfactant activity and on the other hand for antimicrobial activity and phytotoxicity. Cichofactin A and B caused drop collapse which is typical for biosurfactant lipopeptides and both compounds inhibited the growth of *Rhodotorula mucilaginosa* (a yeast) and *Bacillus megaterium* (a Gram-positive bacterium) which are indicator microorganisms according to the antimicrobial activity spectrum of *P. syringae* pv. *syringae* toxins.[189] However, they were not phytotoxic to chicory.

In order to investigate the biological role of cichofactins and their importance in pathogenicity for *P. cichorii* SF1-54, Pauwelyn *et al*. constructed a cichofactin-deficient mutant.[65] The production of both cichofactins was completely prevented in this mutant. The comparison of these two strains showed that cichofactins are essential for swarming motility and that they have a negative influence on biofilm formation. This study also revealed that cichofactins are involved in virulence of *P. cichorii* SF1-54 on lettuce but are not phytotoxic in general. The analysis proposed that they are relevant for the spread of *P. cichorii* in planta.[65]

In this study, the bioactivity and the cytotoxicity of the isolated cichofactins were investigated in more detail, but both compounds showed minimal effects on the organisms tested, human pathogens and cell lines.

Most CLPs produced by *Pseudomonas* species exhibit antifungal and antibacterial activity, and some possess antioomycete, antiviral, antiprotozoan, and antitumor activities. Cyclic lipopeptides exert their antimicrobial effect by targeting either cell wall biosynthesis or cell membrane integrity.[66] *Pseudomonas* CLPs such as syringopeptins, cormycin, and massetolides exert their antibiotic effect by interfering with the integrity of the membrane.[190,191] In a biomedical context, the linear MDN-0066 was found to be cytotoxic to certain cancer cell lines and to induce apoptosis below the cytotoxic threshold.[192]

In addition to antimicrobial activity, many CLPs produced by *Pseudomonas* spp. are involved in a variety of other biological functions, such as motility, biofilm formation, and virulence (see **Chapter I.2.2**). Most CLPs produced by *Pseudomonas* spp. affect bacterial motility and biofilm formation as biosurfactants.[2] Syringomycin and syringopeptin contribute to the virulence of *P. syringae* pv. *syringae* in cherry fruits.[193] The CLP sessilin inhibits orfamide production in *Pseudomonas* sp. CMR12a.[63] The lipopeptides syringafactins represent the major surfactants produced by *P. syringae* pv. *syringae* B728a and contribute to fitness on leaves under fluctuating humidity and are involved in swarming motility.[194,195]

IV.2.3 Improvement of the Production Rate by Feeding Precursors

The overproduction of lipopeptides or to favour the production of certain isoforms can be achieved by modifying media and fermentation conditions. On one hand, secondary metabolite production can be induced in presence of neighbouring microbes, where microbes are co-cultivated (also called mixed or dixenic fermentation). Research to date indicates that competition and antagonism during co-cultivation could lead to a significantly enhanced production, as the microbes interact through signalling or defence molecules.[146,147] The

production of the cyclic lipopeptides emericellamides A and B, for example, were enhanced 100-fold in a mixed fermentation setup.[196] On the other hand, the addition of amino acids can improve the production of secondary metabolites. Supplementation of different amino acids significantly influences the proportion of lipopeptide variants with different fatty acids and replaces those that have been depleted during growth.[130,148]

To study the effects of co-cultivation on the production rate of cichofactins, cultivation of *P. viridiflava* was performed by addition of plant extracts of *Arabidopsis thaliana* of different genotypes. The plant extracts should serve as signalling molecules and co-cultivation was performed in order to mimic the bacterium-plant association. Analysis of the mixed fermentation showed a slight improvement in the production of cichofactin C (1123 Da) and D (1151 Da), but too low to pursue this approach further. Additional considerations for co-cultivation would need to include the optimum timing of inoculation as well as the concentration of the cultivation partner.

In a second approach, the production of cichofactins was performed by supplementation of different amino acids to the cultivation medium (DMBGly medium). The production of cichofactins was increased significantly by the addition of L-isoleucine and L-leucine in a dose-dependent manner. The amino acid L-isoleucine was selected to be present in excess in the cultivation medium so that L-isoleucine is preferentially incorporated at position 6 of the peptide backbone. L-Leucine was chosen to obtain an excess in the cultivation medium as leucine is the most abundant amino acid in cichofactins and therefore could represent a putative bottleneck of the biosynthesis.

Cichofactins are synthesized by NRPSs and the specificity of the amino acid is principally controlled by the binding pocket of the adenylation domain (see **Chapter I.3.1**). However, previous studies have shown that the adenylation domain is promiscuous in the amino acid recognition, especially for hydrophobic amino acids.[92,197] The analysis of the binding pocket for substrates with hydrophobic side chains revealed that the residues involved in recognition are all hydrophobic and therefore variations in substrate are tolerated.[92] Due to the high amount of L-isoleucine or L-leucine in the cultivation medium, the adenylation domain of module six, whose specificity was predicted to incorporate valine, seemed to be also tolerable for these two amino acids. This promiscuity of A domains was also observed in the biosynthesis of MDN-0066, a cyclic octa-lipopeptide, which differs in position 8 by either L-leucine or L-valine in its peptide moiety, although this structural variation could be attributed to the addition of L-valine to the culture medium during liquid fermentation.[198] Promiscuity of A domains is also known from the

biosynthesis of surfactin, where the adenylation domains of modules 2, 4, and 7 can accept either leucine, valine or isoleucine.[199]

Branched amino acids like valine, isoleucine and leucine are biosynthetic precursors for branched fatty acids and are known to improve the production of lipopeptides. The production of tripropeptins and surfactins was affected by supplementation of different amino acids in the cultivation medium.[130,148] However in the present study, no product was observed containing a branched fatty acid.

IV.2.4 Structure Elucidation of Cichofactin Derivatives

Large scale productions supplemented with branched amino acids L-isoleucine and L-leucine, respectively, were performed in order to obtain a sufficient amount for structure elucidation. Purification of the detected compounds and subsequent HR-MS analysis identified six masses with corresponding molecular formulas consistent with possible cichofactin derivatives (**Figure IV-5**). Three isolates each showed the same mass but different retention times, indicating that different derivatives occurred. 1D and 2D NMR as well as MS/MS experiments, and the comparison with the NMR data of cichofactin A lead to the structure elucidation of cichofactin E and F, which were obtained from cultivation employing a medium supplemented with L-leucine. Due to the presence of six leucines within the lipopeptide, the structure analysis was quite challenging since the NMR values were highly similar.

Full NMR analysis of the other products was not possible as the obtained amounts were not sufficient. These products were obtained from cultivations supplemented with L-isoleucine. The structure of the derivatives, which were named cichofactin C and D, were analysed by MS/MS measurements and their methoxy groups were confirmed by proton spectra. The products named as cichofactins C2 and D2 could not be identified completely. MS/MS analysis confirmed that the variation occurred at amino acid 6, but not whether leucine or isoleucine was incorporated. As the cultivation medium was supplemented with L-isoleucine and the highly similar syringafactins and virginiafactins contain an isoleucine at this position, a hypothetical structure for these derivatives can be speculated. However, without sufficient data for complete structure elucidation, the structures of cichofactins C2 and D2 are only hypothetical.

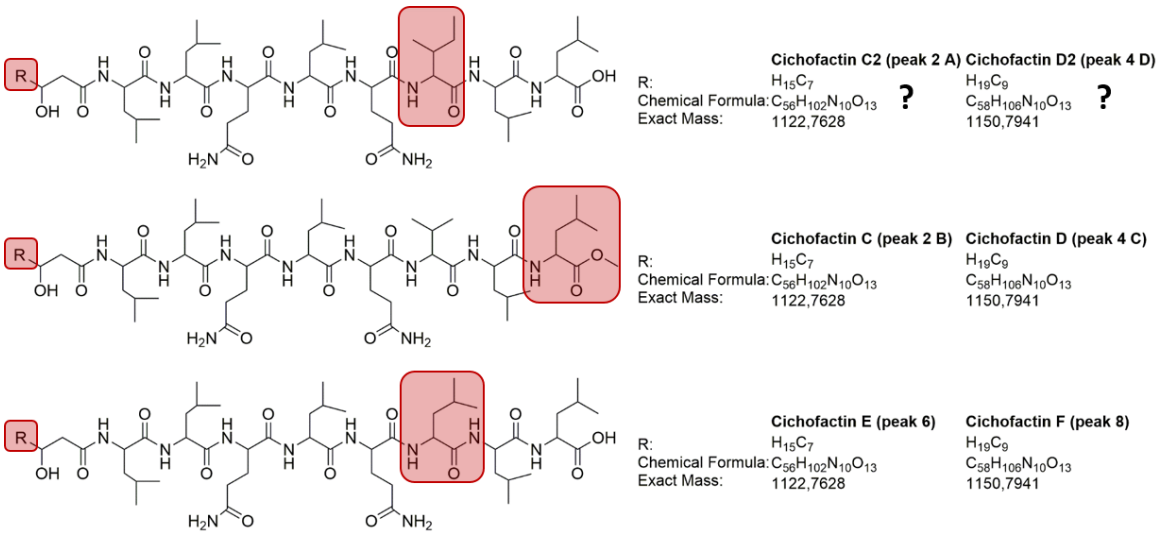

Figure IV-5: Speculated structures for derivatives cichofactins C2 and D2 based on HR-MS analysis and the confirmed structures of cichofactins C, D, E and F. The red boxes indicate the variations in the structure.

The addition of the methyl group to the amino acid was analysed in more detail. Methylation can occur through methyltransferases with S-adenosyl-methionine (SAM) as a co-substrate catalysing the transfer of a methyl group from SAM to an acceptor substrate.[162] Since no methyltransferase was found in the biosynthetic gene cluster of *P. viridiflava*, cultivation and extraction was performed in presence and absence of methanol in order to confirm if auto-methylation occurred non-enzymatically simply by using methanol as solvent. This experiment revealed that the methylation of the lipopeptides represents indeed an artefact due to the presence of the solvent methanol during the purification process.

IV.2.5 Future Perspectives

Within this study, new linear lipopeptide derivatives of *P. viridiflava* were identified by genome mining and their structures were elucidated. Nevertheless, a re-isolation of the cichofactins C2 and D2 is essential in order to proof the presence of an isoleucine at position six of the peptide backbone.

Furthermore, the additional obtained products could also be used to determine the absolute configuration of the amino acids and the fatty acid of the new derivatives. Up to date, the absolute configuration was only investigated of the known cichofactins A and B by Marfey's analysis.[140]

Another purpose for the obtained cichofactin derivatives is the investigation of potential bioactivity. Within this study, cichofactin A and B showed only minimal effects on the organism tested.

In addition, further insights into the interaction of compounds isolated from *P. viridiflava* with *Arabidopsis thaliana* should complete the picture. Therefore, the purified compounds were provided to Alejandra Duque from the Weigel group (Max Planck Institute for Developmental Biology, Tübingen) to investigate the effect of the isolated compounds on *Arabidopsis thaliana*.

V Bibliography

(1) Müller, A.; Münch, D.; Schmidt, Y.; Reder-Christ, K.; Schiffer, G.; Bendas, G.; Gross, H.; Sahl, H.-G.; Schneider, T.; Brötz-Oesterhelt, H. Lipodepsipeptide Empedopeptin Inhibits Cell Wall Biosynthesis through Ca2+-Dependent Complex Formation with Peptidoglycan Precursors. *J. Biol. Chem.* **2012**, *287* (24), 20270. https://doi.org/10.1074/JBC.M112.369561.

(2) Raaijmakers, J. M.; de Bruijn, I.; Nybroe, O.; Ongena, M. Natural Functions of Lipopeptides from Bacillus and Pseudomonas: More than Surfactants and Antibiotics. *FEMS Microbiol. Rev.* **2010**, *34* (6), 1037–1062. https://doi.org/10.1111/j.1574-6976.2010.00221.x.

(3) Schneider, T.; Müller, A.; Miess, H.; Gross, H. Cyclic Lipopeptides as Antibacterial Agents - Potent Antibiotic Activity Mediated by Intriguing Mode of Actions. *Int. J. Med. Microbiol.* **2014**, *304* (1), 37–43. https://doi.org/10.1016/j.ijmm.2013.08.009.

(4) Götze, S.; Stallforth, P. Structure, Properties, and Biological Functions of Nonribosomal Lipopeptides from Pseudomonads. *Nat. Prod. Rep.* **2020**, *37* (1), 29–54. https://doi.org/10.1039/c9np00022d.

(5) Cochrane, S. A.; Vederas, J. C. Lipopeptides from Bacillus and Paenibacillus Spp.: A Gold Mine of Antibiotic Candidates. *Med. Res. Rev.* **2016**, *36* (1), 4–31. https://doi.org/10.1002/MED.21321.

(6) Hill, T. A.; Shepherd, N. E.; Diness, F.; Fairlie, D. P. Constraining Cyclic Peptides to Mimic Protein Structure Motifs. *Angew. Chem. Int. Ed. Engl.* **2014**, *53* (48), 13020–13041. https://doi.org/10.1002/ANIE.201401058.

(7) Hamley, I. W. Lipopeptides: From Self-Assembly to Bioactivity. *Chem. Commun.* **2015**, *51* (41), 8574–8583. https://doi.org/10.1039/c5cc01535a.

(8) Hashizume, H.; Nishimura, Y. Cyclic Lipopeptide Antibiotics. *Stud. Nat. Prod. Chem.* **2008**, *35* (C), 693–751. https://doi.org/10.1016/S1572-5995(08)80016-6.

(9) Survase, S. A.; Kagliwal, L. D.; Annapure, U. S.; Singhal, R. S. Cyclosporin A — A Review on Fermentative Production, Downstream Processing and Pharmacological Applications. *Biotechnol. Adv.* **2011**, *29* (4), 418–435. https://doi.org/10.1016/J.BIOTECHADV.2011.03.004.

(10) Meena, K. R.; Kanwar, S. S. Lipopeptides as the Antifungal and Antibacterial Agents: Applications in Food Safety and Therapeutics. *Biomed Res. Int.* **2015**, *2015*, 1–9. https://doi.org/10.1155/2015/473050.

(11) Mandal, S. M.; Sharma, S.; Pinnaka, A. K.; Kumari, A.; Korpole, S. Isolation and Characterization of Diverse Antimicrobial Lipopeptides Produced by Citrobacter and Enterobacter. *BMC Microbiol.* **2013**, *13* (1), 1–9. https://doi.org/10.1186/1471-2180-13-152/TABLES/1.

(12) Ledger, E. V. K.; Sabnis, A.; Edwards, A. M. Polymyxin and Lipopeptide Antibiotics: Membrane-Targeting Drugs of Last Resort. *Microbiology* **2022**, *168* (2), 1136. https://doi.org/10.1099/MIC.0.001136.

(13) Kleijn, L. H. J.; Martin, N. I. The Cyclic Lipopeptide Antibiotics. In *Topics in Medicinal Chemistry*; Springer Verlag, 2018; Vol. 26, pp 27–53. https://doi.org/10.1007/7355_2017_9.

(14) Debono, M.; Barnhart, M.; Carrell, C. B.; Hoffmann, J. A.; Occolowitz, J. L.; Abbott, B. J.; Fukkuda, D. S.; Hamill, R. L.; Biemann, K.; Herlihy, W. C. A21978C, a Complex of New Acidic Peptide Antibiotics. Isolation, Chemistry, and Mass Spectral Structure Elucidation. *J. Antibiot. (Tokyo).* **1987**, *40* (6), 761–777. https://doi.org/10.7164/antibiotics.40.761.

(15) Steenbergen, J. N.; Alder, J.; Thorne, G. M.; Tally, F. P. Daptomycin: A Lipopeptide Antibiotic for the Treatment of Serious Gram-Positive Infections. *J. Antimicrob. Chemother.* **2005**, *55* (3), 283–288. https://doi.org/10.1093/jac/dkh546.

(16) Baltz, R. H.; Miao, V.; Wrigley, S. K. Natural Products to Drugs: Daptomycin and Related Lipopeptide Antibiotics. *Nat. Prod. Rep.* **2005**, *22* (6), 717–741. https://doi.org/10.1039/B416648P.

(17) Beiras-Fernandez, A.; Vogt, F.; Sodian, R.; Weis, F. Daptomycin: A Novel Lipopeptide Antibiotic against Gram-Positive Pathogens. *Infect. Drug Resist.* **2010**, *3*, 95. https://doi.org/10.2147/IDR.S6961.

(18) Eliopoulos, G. M.; Willey, S.; Reiszner, E.; Spitzer, P. G.; Caputo, G.; Moellering, R. C. In Vitro and in Vivo Activity of LY 146032, a New Cyclic Lipopeptide Antibiotic. *Antimicrob. Agents Chemother.* **1986**, *30* (4), 532–535. https://doi.org/10.1128/AAC.30.4.532.

(19) Rotondi, K. S.; Gierasch, L. M. A Well-Defined Amphipathic Conformation for the Calcium-Free Cyclic Lipopeptide Antibiotic, Daptomycin, in Aqueous Solution. *Biopolymers* **2005**, *80* (2–3), 374–385. https://doi.org/10.1002/BIP.20238.

(20) Ho, S. W.; Jung, D.; Calhoun, J. R.; Lear, J. D.; Okon, M.; Scott, W. R. P.; Hancock, R. E. W.; Straus, S. K. Effect of Divalent Cations on the Structure of the Antibiotic Daptomycin. *Eur. Biophys. J.* **2008**, *37* (4), 421–433. https://doi.org/10.1007/S00249-007-0227-2.

(21) Silverman, J. A.; Oliver, N.; Andrew, T.; Tongchuan, L. I. Resistance Studies with Daptomycin. *Antimicrob. Agents Chemother.* **2001**, *45* (6), 1799–1802. https://doi.org/10.1128/AAC.45.6.1799-1802.2001.

(22) Grein, F.; Müller, A.; Scherer, K. M.; Liu, X.; Ludwig, K. C.; Klöckner, A.; Strach, M.; Sahl, H. G.; Kubitscheck, U.; Schneider, T. Ca2+-Daptomycin Targets Cell Wall Biosynthesis by Forming a Tripartite Complex with Undecaprenyl-Coupled Intermediates and Membrane Lipids. *Nat. Commun. 2020 111* **2020**, *11* (1), 1–11. https://doi.org/10.1038/s41467-020-15257-1.

(23) Ainsworth, G. C.; Brown, A. M.; Brownlee, G. Aerosporin, an Antibiotic Produced by Bacillus Aerosporus Greer. *Nature* **1947**, *159* (4060), 263. https://doi.org/10.1038/160263A0.

(24) Choi, S. K.; Park, S. Y.; Kim, R.; Kim, S. Bin; Lee, C. H.; Kim, J. F.; Park, S. H. Identification of a Polymyxin Synthetase Gene Cluster of Paenibacillus Polymyxa and Heterologous Expression of the Gene in Bacillus Subtilis. *J. Bacteriol.* **2009**, *191* (10), 3350–3358. https://doi.org/10.1128/JB.01728-08.

(25) Tambadou, F.; Caradec, T.; Gagez, A. L.; Bonnet, A.; Sopéna, V.; Bridiau, N.; Thiéry, V.; Didelot, S.; Barthélémy, C.; Chevrot, R. Characterization of the Colistin (Polymyxin E1 and E2) Biosynthetic Gene Cluster. *Arch. Microbiol.* **2015**, *197* (4), 521–532. https://doi.org/10.1007/S00203-015-1084-5.

(26) Velkov, T.; Thompson, P. E.; Nation, R. L.; Li, J. Structure-Activity Relationships of Polymyxin Antibiotics. *J. Med. Chem.* **2010**, *53* (5), 1898–1916. https://doi.org/10.1021/jm900999h.

(27) Landman, D.; Georgescu, C.; Martin, D. A.; Quale, J. Polymyxins Revisited. *Clin. Microbiol. Rev.* **2008**, *21* (3), 449–465. https://doi.org/10.1128/CMR.00006-08.

(28) Zavascki, A. P.; Goldani, L. Z.; Li, J.; Nation, R. L. Polymyxin B for the Treatment of Multidrug-Resistant Pathogens: A Critical Review. *J. Antimicrob. Chemother.* **2007**, *60* (6), 1206–1215. https://doi.org/10.1093/JAC/DKM357.

(29) Hermsen, E. D.; Sullivan, C. J.; Rotschafer, J. C. Polymyxins:: Pharmacology, Pharmacokinetics, Pharmacodynamics, and Clinical Applications. *Infect. Dis. Clin. North Am.* **2003**, *17* (3), 545–562. https://doi.org/10.1016/S0891-5520(03)00058-8.

(30) Evans, M. E.; Feola, D. J.; Rapp, R. P. Polymyxin B Sulfate and Colistin: Old Antibiotics for Emerging Multiresistant Gram-Negative Bacteria. *Ann. Pharmacother.* **1999**, *33* (9), 960–967. https://doi.org/10.1345/APH.18426.

(31) Hancock, R. E. W. Peptide Antibiotics. *Lancet* **1997**, *349* (9049), 418–422. https://doi.org/10.1016/S0140-6736(97)80051-7.

(32) Tam, V. H.; Schilling, A. N.; Vo, G.; Kabbara, S.; Kwa, A. L.; Wiederhold, N. P.; Lewis, R. E. Pharmacodynamics of Polymyxin B against Pseudomonas Aeruginosa. *Antimicrob. Agents Chemother.* **2005**, *49* (9), 3624. https://doi.org/10.1128/AAC.49.9.3624-3630.2005.

(33) Falagas, M. E.; Kasiakou, S. K. Colistin: The Revival of Polymyxins for the Management of Multidrug-Resistant Gram-Negative Bacterial Infections. *Clin. Infect. Dis.* **2005**, *40* (9), 1333–1341. https://doi.org/10.1086/429323.

(34) Konishi, M.; Sugawara, K.; Hanada, M.; Tomita, K.; Tomatsu, K.; Miyaki, T.; Kawaguchi, H.; Buck, R. E.; More, C.; Rossomano, V. Z. Empedopeptin (BMY-28117), a New Depsipeptide Antibiotic. I. Production, Isolation and Properties. *J. Antibiot. (Tokyo).* **1984**, *37* (9), 949–957.

https://doi.org/10.7164/ANTIBIOTICS.37.949.

(35) Shoji, J.; Hinoo, H.; Katayama, T.; Matsumoto, K.; Tanimoto, T.; Hattori, T.; Higashiyama, I.; Miwa, H.; Motokawa, K.; Yoshida, T. Isolation and Characterization of New Peptide Antibiotics, Plusbacins A1~A4 and B1~B4. *J. Antibiot. (Tokyo).* **1992**, *45* (6), 817–823. https://doi.org/10.7164/antibiotics.45.817.

(36) Hashizume, H.; Igarashi, M.; Hattori, S.; Hori, M.; Hamada, M.; Takeuchi, T. Tripropeptins, Novel Antimicrobial Agents Produced by Lysobacter Sp. I. Taxonomy, Isolation and Biological Activities. *J. Antibiot. (Tokyo).* **2001**, *54* (12), 1054–1059. https://doi.org/10.7164/ANTIBIOTICS.54.1054.

(37) Miess, H.; Arlt, P.; Apel, A. K.; Weber, T.; Nieselt, K.; Hanssen, F.; Czemmel, S.; Nahnsen, S.; Gross, H.; Rasko, D. The Draft Whole-Genome Sequence of the Antibiotic Producer Empedobacter Haloabium ATCC 31962 Provides Indications for Its Taxonomic Reclassification. *Microbiol. Resour. Announc.* **2019**, *8* (45). https://doi.org/10.1128/MRA.01120-19.

(38) Miess, H.; Trappen, S. van; Cleenwerck, I.; Vos, P. De; Gross, H. Reclassification of Pseudomonas Sp. PB-6250T as Lysobacter Firmicutimachus Sp. Nov. *Int. J. Syst. Evol. Microbiol.* **2016**, *66* (10), 4162–4166. https://doi.org/10.1099/IJSEM.0.001329.

(39) Maki, H.; Miura, K.; Yamano, Y. Katanosin B and Plusbacin A3, Inhibitors of Peptidoglycan Synthesis in Methicillin-Resistant Staphylococcus Aureus. *Antimicrob. Agents Chemother.* **2001**, *45* (6), 1823–1827. https://doi.org/10.1128/AAC.45.6.1823-1827.2001.

(40) Kim, S. J.; Singh, M.; Wohlrab, A.; Yu, T. Y.; Patti, G. J.; O'Connor, R. D.; Vannieuwenhze, M.; Schaefer, J. Isotridecanyl Side Chain of Plusbacin-A3 Is Essential for the Transglycosylase Inhibition of Peptidoglycan Biosynthesis. *Biochemistry* **2013**, *52* (11), 1973. https://doi.org/10.1021/BI4000222.

(41) O'Connor, R. D.; Singh, M.; Chang, J.; Kim, S. J.; VanNieuwenhze, M.; Schaefer, J. Dual Mode of Action for Plusbacin A3 in Staphylococcus Aureus. *J. Phys. Chem. B* **2017**, *121* (7), 1499–1505. https://doi.org/10.1021/ACS.JPCB.6B11039/SUPPL_FILE/JP6B11039_SI_001.PDF.

(42) Hashizume, H.; Hattori, S.; Igarashi, M.; Akamatsu, Y. Tripropeptin E, a New Tripropeptin Group Antibiotic Produced by Lysobacter Sp. BMK333-48F3. *J. Antibiot. (Tokyo).* **2004**, *57* (6), 394–399. https://doi.org/10.7164/ANTIBIOTICS.57.394.

(43) Hashizume, H.; Hirosawa, S.; Sawa, R.; Muraoka, Y.; Ikeda, D.; Naganawa, H.; Igarashi, M. Tripropeptins, Novel Antimicrobial Agents Produced by Lysobacter Sp. II. Structure Elucidation. *J. Antibiot. (Tokyo).* **2004**, *57* (1), 52–58. https://doi.org/10.7164/ANTIBIOTICS.57.52.

(44) Hashizume, H.; Hirosawa, S.; Sawa, R.; Muraoka, Y.; Ikeda, D.; Naganawa, H.; Igarashi, M. Corrigendum: Tripropeptins, Novel Antimicrobial Agents Produced by Lysobacter Sp. II. Structure Elucidation. *J. Antibiot. (Tokyo).* **2016**, *69* (12), 889–891. https://doi.org/10.1038/JA.2016.104.

(45) Hashizume, H.; Igarashi, M.; Sawa, R.; Adachi, H.; Nishimura, Y.; Akamatsu, Y. A New Type of Tripropeptin with Anteiso-Branched Chain Fatty Acid from Lysobacter Sp. BMK333-48F3. *J. Antibiot. (Tokyo).* **2008**, *61* (9), 577–582. https://doi.org/10.1038/ja.2008.78.

(46) Hashizume, H.; Igarashi, M.; Sawa, R.; Adachi, H.; Nishimura, Y.; Akamatsu, Y. Corrigendum: A New Type of Tripropeptin with Anteiso-Branched Chain Fatty Acid from Lysobacter Sp. BMK333-48F3. *J. Antibiot. (Tokyo).* **2016**, *69* (12), 892–893. https://doi.org/10.1038/JA.2016.105.

(47) Hashizume, H.; Sawa, R.; Harada, S.; Igarashi, M.; Adachi, H.; Nishimura, Y.; Nomoto, A. Tripropeptin C Blocks the Lipid Cycle of Cell Wall Biosynthesis by Complex Formation with Undecaprenyl Pyrophosphate. *Antimicrob. Agents Chemother.* **2011**, *55* (8), 3821. https://doi.org/10.1128/AAC.00443-11.

(48) Hashizume, H.; Takahashi, Y.; Harada, S.; Nomoto, A. Natural Lipopeptide Antibiotic Tripropeptin C Revitalizes and Synergistically Potentiates the Activity of Beta-Lactams against Methicillin-Resistant Staphylococcus Aureus. *J. Antibiot. 2015 686* **2015**, *68* (6), 373–378. https://doi.org/10.1038/ja.2014.169.

(49) Kearns, D. B. A Field Guide to Bacterial Swarming Motility. *Nat. Rev. Microbiol.* **2010**, *8* (9), 634–644. https://doi.org/10.1038/nrmicro2405.

(50) Xu, J.; Platt, T. G.; Fuqua, C. Regulatory Linkages between Flagella and Surfactant during Swarming Behavior: Lubricating the Flagellar Propeller? *J. Bacteriol.* **2012**, *194* (6), 1283–1286.

https://doi.org/10.1128/JB.00019-12/ASSET/BDB1FFB6-2E76-48BC-B6A5-A546FE40568F/ASSETS/GRAPHIC/ZJB9990913180001.JPEG.

(51) Langmuir, I. The Constitution and Fundamental Properties of Solids and Liquids. II. Liquids. *J. Am. Chem. Soc.* **1917**, *39* (9), 1848–1906. https://doi.org/10.1021/JA02254A006/ASSET/JA02254A006.FP.PNG_V03.

(52) Santos, D. K. F.; Rufino, R. D.; Luna, J. M.; Santos, V. A.; Sarubbo, L. A. Biosurfactants: Multifunctional Biomolecules of the 21st Century. *Int. J. Mol. Sci.* **2016**, *17* (3), 401. https://doi.org/10.3390/IJMS17030401.

(53) Fechtner, J.; Koza, A.; Sterpaio, P. Dello; Hapca, S. M.; Spiers, A. J. Surfactants Expressed by Soil Pseudomonads Alter Local Soil–Water Distribution, Suggesting a Hydrological Role for These Compounds. *FEMS Microbiol. Ecol.* **2011**, *78* (1), 50–58. https://doi.org/10.1111/J.1574-6941.2011.01141.X.

(54) Andersen, J. B.; Koch, B.; Nielsen, T. H.; Sørensen, D.; Hansen, M.; Nybroe, O.; Christophersen, C.; Sørensen, J.; Molin, S.; Givskov, M. Surface Motility in Pseudomonas Sp. DSS73 Is Required for Efficient Biological Containment of the Root-Pathogenic Microfungi Rhizoctonia Solani and Pythium Ultimum. *Microbiology* **2003**, *149* (Pt 1), 37–46. https://doi.org/10.1099/MIC.0.25859-0.

(55) De Bruijn, I.; De Kock, M. J. D.; De Waard, P.; Van Beek, T. A.; Raaijmakers, J. M. Massetolide A Biosynthesis in Pseudomonas Fluorescens. *J. Bacteriol.* **2008**, *190* (8), 2777. https://doi.org/10.1128/JB.01563-07.

(56) Gross, H.; Loper, J. E. Genomics of Secondary Metabolite Production by Pseudomonas Spp. *Nat. Prod. Rep.* **2009**, *26* (11), 1408–1446. https://doi.org/10.1039/b817075b.

(57) Roongsawang, N.; Hase, K. I.; Haruki, M.; Imanaka, T.; Morikawa, M.; Kanaya, S. Cloning and Characterization of the Gene Cluster Encoding Arthrofactin Synthetase from Pseudomonas Sp. MIS38. *Chem. Biol.* **2003**, *10* (9), 869–880. https://doi.org/10.1016/j.chembiol.2003.09.004.

(58) Coenye, T. Biofilms. *Ref. Modul. Life Sci.* **2022**. https://doi.org/10.1016/B978-0-12-822563-9.00068-8.

(59) Stewart, P. S.; Franklin, M. J. Physiological Heterogeneity in Biofilms. *Nat. Rev. Microbiol. 2008 63* **2008**, *6* (3), 199–210. https://doi.org/10.1038/nrmicro1838.

(60) Rokni-Zadeh, H.; Li, W.; Sanchez-Rodriguez, A.; Sinnaeve, D.; Rozenski, J.; Martins, J. C.; De Mot, R. Genetic and Functional Characterization of Cyclic Lipopeptide White-Line-Inducing Principle (WLIP) Production by Rice Rhizosphere Isolate Pseudomonas Putida RW10S2. *Appl. Environ. Microbiol.* **2012**, *78* (14), 4826–4834. https://doi.org/10.1128/AEM.00335-12/SUPPL_FILE/AEM00335-12_SUPPLEMENTAL.PDF.

(61) Bonnichsen, L.; Svenningsen, N. B.; Rybtke, M.; de Bruijn, I.; Raaijmakers, J. M.; Tolker-Nielsen, T.; Nybroe, O. Lipopeptide Biosurfactant Viscosin Enhances Dispersal of Pseudomonas Fluorescens SBW25 Biofilms. *Microbiol. (United Kingdom)* **2015**, *161* (12), 2289–2297. https://doi.org/10.1099/MIC.0.000191/CITE/REFWORKS.

(62) Li, W.; Rokni-Zadeh, H.; De Vleeschouwer, M.; Ghequire, M. G. K.; Sinnaeve, D.; Xie, G. L.; Rozenski, J.; Madder, A.; Martins, J. C.; De Mot, R. The Antimicrobial Compound Xantholysin Defines a New Group of Pseudomonas Cyclic Lipopeptides. *PLoS One* **2013**, *8* (5), e62946. https://doi.org/10.1371/journal.pone.0062946.

(63) D'aes, J.; Kieu, N. P.; Léclère, V.; Tokarski, C.; Olorunleke, F. E.; De Maeyer, K.; Jacques, P.; Höfte, M.; Ongena, M. To Settle or to Move? The Interplay between Two Classes of Cyclic Lipopeptides in the Biocontrol Strain Pseudomonas CMR12a. *Environ. Microbiol.* **2014**, *16* (7), 2282–2300. https://doi.org/10.1111/1462-2920.12462.

(64) Kuiper, I.; Lagendijk, E. L.; Pickford, R.; Derrick, J. P.; Lamers, G. E. M.; Thomas-Oates, J. E.; Lugtenberg, B. J. J.; Bloemberg, G. V. Characterization of Two Pseudomonas Putida Lipopeptide Biosurfactants, Putisolvin I and II, Which Inhibit Biofilm Formation and Break down Existing Biofilms. *Mol. Microbiol.* **2004**, *51* (1), 97–113. https://doi.org/10.1046/J.1365-2958.2003.03751.X.

(65) Pauwelyn, E.; Huang, C. J.; Ongena, M.; Leclère, V.; Jacques, P.; Bleyaert, P.; Budzikiewicz, H.; Schäfer, M.; Höfte, M. New Linear Lipopeptides Produced by Pseudomonas Cichorii SF1-54 Are Involved in Virulence, Swarming Motility, and Biofilm Formation. *Mol. Plant-Microbe Interact.* **2013**,

26 (5), 585–598. https://doi.org/10.1094/MPMI-11-12-0258-R.

(66) Geudens, N.; Martins, J. C. Cyclic Lipodepsipeptides from Pseudomonas Spp. - Biological Swiss-Army Knives. *Front. Microbiol.* **2018**, *9* (AUG), 1867. https://doi.org/10.3389/FMICB.2018.01867/BIBTEX.

(67) Berry, C.; Fernando, W. G. D.; Loewen, P. C.; de Kievit, T. R. Lipopeptides Are Essential for Pseudomonas Sp. DF41 Biocontrol of Sclerotinia Sclerotiorum. *Biol. Control* **2010**, *55* (3), 211–218. https://doi.org/10.1016/J.BIOCONTROL.2010.09.011.

(68) Lindow, S. E.; Brandl, M. T. Microbiology of the Phyllosphere. *Appl. Environ. Microbiol.* **2003**, *69* (4), 1875–1883. https://doi.org/10.1128/AEM.69.4.1875-1883.2003.

(69) Nielsen, T. H.; Sørensen, J. Production of Cyclic Lipopeptides by Pseudomonas Fluorescens Strains in Bulk Soil and in the Sugar Beet Rhizosphere. *Appl. Environ. Microbiol.* **2003**, *69* (2), 861. https://doi.org/10.1128/AEM.69.2.861-868.2003.

(70) Sinden, S. L.; DeVay, J. E.; Backman, P. A. Properties of Syringomycin, a Wide Spectrum Antibiotic and Phytotoxin Produced by Pseudomonas Syringae, and Its Role in the Bacterial Canker Disease of Peach Trees. *Physiol. Plant Pathol.* **1971**, *1* (2), 199–213. https://doi.org/10.1016/0048-4059(71)90029-4.

(71) Bobrova, V. K.; Milyutina, I. A.; Troitskii, A. V. Genetic Diversity in Pseudomonads Associated with Cereal Cultures Infected with Basal Bacteriosis. *Microbiology* **2005**, *74* (4), 463–470. https://doi.org/10.1007/S11021-005-0090-Z/METRICS.

(72) Ballio, A.; Bossa, F.; Camoni, L.; Di Giorgio, D.; Flamand, M. C.; Maraite, H.; Nitti, G.; Pucci, P.; Scaloni, A. Structure of Fuscopeptins, Phytotoxic Metabolites of Pseudomonas Fuscovaginae. *FEBS Lett.* **1996**, *381* (3), 213–216. https://doi.org/10.1016/0014-5793(96)00043-9.

(73) Roongsawang, N.; Washio, K.; Morikawa, M. Diversity of Nonribosomal Peptide Synthetases Involved in the Biosynthesis of Lipopeptide Biosurfactants. *Int. J. Mol. Sci.* **2011**, *12* (1), 141. https://doi.org/10.3390/IJMS12010141.

(74) Hildebrand, P. D.; Braun, P. G.; McRae, K. B.; Lu, X. Role of the Biosurfactant Viscosin in Broccoli Head Rot Caused by a Pectolytic Strain of Pseudomonas Fluorescens. *Can. J. Plant Pathol.* **1998**, *20* (3), 296–303. https://doi.org/10.1080/07060669809500396.

(75) Cottyn, B.; Heylen, K.; Heyrman, J.; Vanhouteghem, K.; Pauwelyn, E.; Bleyaert, P.; Van Vaerenbergh, J.; Höfte, M.; De Vos, P.; Maes, M. Pseudomonas Cichorii as the Causal Agent of Midrib Rot, an Emerging Disease of Greenhouse-Grown Butterhead Lettuce in Flanders. *Syst. Appl. Microbiol.* **2009**, *32* (3), 211–225. https://doi.org/10.1016/j.syapm.2008.11.006.

(76) Xin, X. F.; He, S. Y. Pseudomonas Syringae Pv. Tomato DC3000: A Model Pathogen for Probing Disease Susceptibility and Hormone Signaling in Plants. *Annu. Rev. Phytopathol.* **2013**, *51*, 473–498. https://doi.org/10.1146/ANNUREV-PHYTO-082712-102321.

(77) Faulkner, C.; Robatzek, S. Plants and Pathogens: Putting Infection Strategies and Defence Mechanisms on the Map. *Curr. Opin. Plant Biol.* **2012**, *15* (6), 699–707. https://doi.org/10.1016/J.PBI.2012.08.009.

(78) Block, A.; Alfano, J. R. Plant Targets for Pseudomonas Syringae Type III Effectors: Virulence Targets or Guarded Decoys? *Curr. Opin. Microbiol.* **2011**, *14* (1), 39–46. https://doi.org/10.1016/J.MIB.2010.12.011.

(79) Xin, X. F.; Kvitko, B.; He, S. Y. Pseudomonas Syringae: What It Takes to Be a Pathogen. *Nat. Rev. Microbiol.* **2018**, *16* (5), 316–328. https://doi.org/10.1038/NRMICRO.2018.17.

(80) Carpaneto, A.; Dalla Serra, M.; Menestrina, G.; Fogliano, V.; Gambale, F. The Phytotoxic Lipodepsipeptide Syringopeptin 25A from Pseudomonas Syringae Pv Syringae Forms Ion Channels in Sugar Beet Vacuoles. *J. Membr. Biol.* **2002**, *188* (3), 237–248. https://doi.org/10.1007/S00232-001-0187-X/METRICS.

(81) Zachow, C.; Jahanshah, G.; De Bruijn, I.; Song, C.; Ianni, F.; Pataj, Z.; Gerhardt, H.; Pianet, I.; Lämmerhofer, M.; Berg, G.; Gross, H.; Raaijmakers, J. M. The Novel Lipopeptide Poaeamide of the Endophyte Pseudomonas Poae RE*1-1-14 Is Involved in Pathogen Suppression and Root Colonization. *Mol. Plant-Microbe Interact.* **2015**, *28(7)* (7), 800. https://doi.org/10.1094/MPMI-12-14-0406-R.

(82) Tran, H.; Ficke, A.; Asiimwe, T.; Höfte, M.; Raaijmakers, J. M. Role of the Cyclic Lipopeptide Massetolide A in Biological Control of Phytophthora Infestans and in Colonization of Tomato Plants by Pseudomonas Fluorescens. *New Phytol.* **2007**, *175* (4), 731–742. https://doi.org/10.1111/J.1469-8137.2007.02138.X.

(83) Ongena, M.; Jourdan, E.; Adam, A.; Paquot, M.; Brans, A.; Joris, B.; Arpigny, J. L.; Thonart, P. Surfactin and Fengycin Lipopeptides of Bacillus Subtilis as Elicitors of Induced Systemic Resistance in Plants. *Environ. Microbiol.* **2007**, *9* (4), 1084–1090. https://doi.org/10.1111/J.1462-2920.2006.01202.X.

(84) Schwarzer, D.; Finking, R.; Marahiel, M. A. Nonribosomal Peptides: From Genes to Products. *Natural Product Reports*. The Royal Society of Chemistry June 13, 2003, pp 275–287. https://doi.org/10.1039/b111145k.

(85) Marahiel, M. A. A Structural Model for Multimodular NRPS Assembly Lines. *Natural Product Reports*. Royal Society of Chemistry February 1, 2016, pp 136–140. https://doi.org/10.1039/c5np00082c.

(86) Süssmuth, R. D.; Mainz, A. Nonribosomal Peptide Synthesis—Principles and Prospects. *Angewandte Chemie - International Edition*. Wiley-VCH Verlag March 27, 2017, pp 3770–3821. https://doi.org/10.1002/anie.201609079.

(87) Gulick, A. M.; Starai, V. J.; Horswill, A. R.; Homick, K. M.; Escalante-Semerena, J. C. The 1.75 Å Crystal Structure of Acetyl-CoA Synthetase Bound to Adenosine-5′-Propylphosphate and Coenzyme A. *Biochemistry* **2003**, *42* (10), 2866–2873. https://doi.org/10.1021/bi0271603.

(88) Challis, G. L.; Ravel, J.; Townsend, C. A.; Conti, E.; Franks, N. P.; Brick, P.; Stachelhaus, T.; Mootz, H. D.; Marahiel, M. A. Crystal Structure of Firefly Luciferase Throws Light on a Super-Family of Adenylate-Forming Enzymes. *Structure* **1996**, *4* (3), 287–298. https://doi.org/10.1016/S0969-2126(96)00033-0.

(89) May, J. J.; Kessler, N.; Marahiel, M. A.; Stubbs, M. T. Crystal Structure of DhbE, an Archetype for Aryl Acid Activating Domains of Modular Nonribosomal Peptide Synthetases. *Proc. Natl. Acad. Sci. U. S. A.* **2002**, *99* (19), 12120–12125. https://doi.org/10.1073/pnas.182156699.

(90) Conti, E.; Stachelhaus, T.; Marahiel, M. A.; Brick, P. Structural Basis for the Activation of Phenylalanine in the Non-Ribosomal Biosynthesis of Gramicidin S. *EMBO J.* **1997**, *16* (14), 4174–4183. https://doi.org/10.1093/emboj/16.14.4174.

(91) Stachelhaus, T.; Mootz, H. D.; Marahiel, M. A. The Specificity-Conferring Code of Adenylation Domains in Nonribosomal Peptide Synthetases. *Chem. Biol.* **1999**, *6* (8), 493–505. https://doi.org/10.1016/S1074-5521(99)80082-9.

(92) Challis, G. L.; Ravel, J.; Townsend, C. A. Predictive, Structure-Based Model of Amino Acid Recognition by Nonribosomal Peptide Synthetase Adenylation Domains. *Chem. Biol.* **2000**, *7* (3), 211–224. https://doi.org/10.1016/S1074-5521(00)00091-0.

(93) Müller, S.; Garcia-Gonzalez, E.; Mainz, A.; Hertlein, G.; Heid, N. C.; Mösker, E.; Van Den Elst, H.; Overkleeft, H. S.; Genersch, E.; Süssmuth, R. D. Paenilamicin: Structure and Biosynthesis of a Hybrid Nonribosomal Peptide/Polyketide Antibiotic from the Bee Pathogen Paenibacillus Larvae. *Angew. Chem. Int. Ed. Engl.* **2014**, *53* (40), 10821–10825. https://doi.org/10.1002/ANIE.201404572.

(94) Kaljunen, H.; Schiefelbein, S. H. H.; Stummer, D.; Kozak, S.; Meijers, R.; Christiansen, G.; Rentmeister, A. Structural Elucidation of the Bispecificity of A Domains as a Basis for Activating Non-Natural Amino Acids. *Angew. Chem. Int. Ed. Engl.* **2015**, *54* (30), 8833–8836. https://doi.org/10.1002/ANIE.201503275.

(95) Schwarzer, D.; Marahiel, M. A. Multimodular Biocatalysts for Natural Product Assembly. *Naturwissenschaften*. Naturwissenschaften 2001, pp 93–101. https://doi.org/10.1007/s001140100211.

(96) Condurso, H. L.; Bruner, S. D. Structure and Noncanonical Chemistry of Nonribosomal Peptide Biosynthetic Machinery. *Nat. Prod. Rep.* **2012**, *29* (10), 1099–1110. https://doi.org/10.1039/C2NP20023F.

(97) Rausch, C.; Hoof, I.; Weber, T.; Wohlleben, W.; Huson, D. H. Phylogenetic Analysis of Condensation Domains in NRPS Sheds Light on Their Functional Evolution. *BMC Evol. Biol.* **2007**, *7* (1), 1–15. https://doi.org/10.1186/1471-2148-7-78/FIGURES/5.

(98) Finking, R.; Marahiel, M. A. Biosynthesis of Nonribosomal Peptides. *Annual Review of Microbiology*. Annu Rev Microbiol 2004, pp 453–488. https://doi.org/10.1146/annurev.micro.58.030603.123615.

(99) Hur, G. H.; Vickery, C. R.; Burkart, M. D. Explorations of Catalytic Domains in Non-Ribosomal Peptide Synthetase Enzymology. *Nat. Prod. Rep.* **2012**, *29* (10), 1074. https://doi.org/10.1039/C2NP20025B.

(100) Weber, G.; Schörgendorfer, K.; Schneider-Scherzer, E.; Leitner, E. The Peptide Synthetase Catalyzing Cyclosporine Production in Tolypocladium Niveum Is Encoded by a Giant 45.8-Kilobase Open Reading Frame. *Curr. Genet. 1994 262* **1994**, *26* (2), 120–125. https://doi.org/10.1007/BF00313798.

(101) Waksmundzka-Hajnos, M.; Sherma, J. *Chromatographic Sciences Series Volume 102: High Performance Liquid Chromatography in Phytochemical Analysis*; CRC Press, Taylor and Francis Group, 2010. https://doi.org/https://doi.org/10.1201/b10320.

(102) Malviya, N.; Malviya, S. Bioassay Guided Fractionation-an Emerging Technique Influence the Isolation, Identification and Characterization of Lead Phytomolecules. *Int. J. Hosp. Pharm.* **2017**, *2*. https://doi.org/10.28933/IJHP-2017-07-0901.

(103) Ziemert, N.; Alanjary, M.; Weber, T. The Evolution of Genome Mining in Microbes-a Review. *Nat. Prod. Rep.* **2016**, *33* (8), 988–1005. https://doi.org/10.1039/c6np00025h.

(104) Boddy, C. N. Bioinformatics Tools for Genome Mining of Polyketide and Non-Ribosomal Peptides. *J. Ind. Microbiol. Biotechnol.* **2014**, *41* (2), 443–450. https://doi.org/10.1007/S10295-013-1368-1.

(105) Zerikly, M.; Challis, G. L. Strategies for the Discovery of New Natural Products by Genome Mining. *ChemBioChem* **2009**, *10* (4), 625–633. https://doi.org/10.1002/cbic.200800389.

(106) Wilkinson, B.; Micklefield, J. Mining and Engineering Natural-Product Biosynthetic Pathways. *Nat. Chem. Biol.* **2007**, *3* (7), 379–386. https://doi.org/10.1038/NCHEMBIO.2007.7.

(107) Challis, G. L. Mining Microbial Genomes for New Natural Products and Biosynthetic Pathways. *Microbiology* **2008**, *154* (Pt 6), 1555–1569. https://doi.org/10.1099/MIC.0.2008/018523-0.

(108) Corre, C.; Challis, G. L. New Natural Product Biosynthetic Chemistry Discovered by Genome Mining. *Nat. Prod. Rep.* **2009**, *26* (8), 977–986. https://doi.org/10.1039/B713024B.

(109) Gross, H.; Stockwell, V. O.; Henkels, M. D.; Nowak-Thompson, B.; Loper, J. E.; Gerwick, W. H. The Genomisotopic Approach: A Systematic Method to Isolate Products of Orphan Biosynthetic Gene Clusters. *Chem. Biol.* **2007**, *14* (1), 53–63. https://doi.org/10.1016/J.CHEMBIOL.2006.11.007.

(110) Cimermancic, P.; Medema, M. H.; Claesen, J.; Kurita, K.; Wieland Brown, L. C.; Mavrommatis, K.; Pati, A.; Godfrey, P. A.; Koehrsen, M.; Clardy, J.; Birren, B. W.; Takano, E.; Sali, A.; Linington, R. G.; Fischbach, M. A. Insights into Secondary Metabolism from a Global Analysis of Prokaryotic Biosynthetic Gene Clusters. *Cell* **2014**, *158* (2), 412–421. https://doi.org/10.1016/J.CELL.2014.06.034.

(111) Bentley, S. D.; Chater, K. F.; Cerdeño-Tárraga, A. M.; Challis, G. L.; Thomson, N. R.; James, K. D.; Harris, D. E.; Quail, M. A.; Kieser, H.; Harper, D.; Bateman, A.; Brown, S.; Chandra, G.; Chen, C. W.; Collins, M.; Cronin, A.; Fraser, A.; Goble, A.; Hidalgo, J.; Hornsby, T.; Howarth, S.; Huang, C. H.; Kieser, T.; Larke, L.; Murphy, L.; Oliver, K.; O'Neil, S.; Rabbinowitsch, E.; Rajandream, M. A.; Rutherford, K.; Rutter, S.; Seeger, K.; Saunders, D.; Sharp, S.; Squares, R.; Squares, S.; Taylor, K.; Warren, T.; Wietzorrek, A.; Woodward, J.; Barrell, B. G.; Parkhill, J.; Hopwood, D. A. Complete Genome Sequence of the Model Actinomycete Streptomyces Coelicolor A3(2). *Nature* **2002**, *417* (6885), 141–147. https://doi.org/10.1038/417141A.

(112) Koehn, F. E. High Impact Technologies for Natural Products Screening. *Prog. Drug Res.* **2008**, *65*, 176–210. https://doi.org/10.1007/978-3-7643-8117-2_5.

(113) Krug, D.; Müller, R. Secondary Metabolomics: The Impact of Mass Spectrometry-Based Approaches on the Discovery and Characterization of Microbial Natural Products. *Nat. Prod. Rep.* **2014**, *31* (6), 768–783. https://doi.org/10.1039/C3NP70127A.

(114) Duy Nguyen, D.; Wu, C.-H.; Moree, W. J.; Lamsa, A.; Medema, M. H.; Zhao, X.; Gavilan, R. G.; Aparicio, M.; Atencio, L.; Jackson, C.; Ballesteros, J.; Sanchez, J.; Watrous, J. D.; Phelan, V. V; van de Wiel, C.; Kersten, R. D.; Mehnaz, S.; De Mot, R.; Shank, E. A.; Charusanti, P.; Nagarajan, H.; Duggan, B. M.; Moore, B. S.; Bandeira, N.; Ø Palsson, B.; Pogliano, K.; Gutiérrez, M.; Dorrestein, P. C.; analyzed data, P. MS/MS Networking Guided Analysis of Molecule and Gene Cluster Families. **2013**, *110* (28),

E2611–E2620. https://doi.org/10.1073/pnas.1303471110.

(115) Winnikoff, J. R.; Glukhov, E.; Watrous, J.; Dorrestein, P. C.; Gerwick, W. H. Quantitative Molecular Networking to Profile Marine Cyanobacterial Metabolomes. *J. Antibiot. (Tokyo).* **2014**, *67* (1), 105–112. https://doi.org/10.1038/JA.2013.120.

(116) Yang, J. Y.; Sanchez, L. M.; Rath, C. M.; Liu, X.; Boudreau, P. D.; Bruns, N.; Glukhov, E.; Wodtke, A.; De Felicio, R.; Fenner, A.; Wong, W. R.; Linington, R. G.; Zhang, L.; Debonsi, H. M.; Gerwick, W. H.; Dorrestein, P. C. Molecular Networking as a Dereplication Strategy. *J. Nat. Prod.* **2013**, *76* (9), 1686–1699. https://doi.org/10.1021/NP400413S.

(117) Bandeira, N. Spectral Networks: A New Approach to de Novo Discovery of Protein Sequences and Posttranslational Modifications. *Biotechniques* **2007**, *42* (6), 687–697. https://doi.org/10.2144/000112487.

(118) Watrous, J.; Roach, P.; Alexandrov, T.; Heath, B. S.; Yang, J. Y.; Kersten, R. D.; Van Der Voort, M.; Pogliano, K.; Gross, H.; Raaijmakers, J. M.; Moore, B. S.; Laskin, J.; Bandeira, N.; Dorrestein, P. C. Mass Spectral Molecular Networking of Living Microbial Colonies. *Proc. Natl. Acad. Sci. U. S. A.* **2012**, *109* (26), E1743–E1752. https://doi.org/10.1073/PNAS.1203689109/-/DCSUPPLEMENTAL/SAPP.PDF.

(119) Applications in Mass Spectrometry and Molecular Networking: The Pseudomonas Specialized Metabolome and Algal Biofuels https://escholarship.org/uc/item/84p4v4ms (accessed Apr 17, 2023).

(120) Weber, T.; Blin, K.; Duddela, S.; Krug, D.; Kim, H. U.; Bruccoleri, R.; Lee, S. Y.; Fischbach, M. A.; Müller, R.; Wohlleben, W.; Breitling, R.; Takano, E.; Medema, M. H. AntiSMASH 3.0-A Comprehensive Resource for the Genome Mining of Biosynthetic Gene Clusters. *Nucleic Acids Res.* **2015**, *43* (W1), W237–W243. https://doi.org/10.1093/nar/gkv437.

(121) Blin, K.; Wolf, T.; Chevrette, M. G.; Lu, X.; Schwalen, C. J.; Kautsar, S. A.; Suarez Duran, H. G.; De Los Santos, E. L. C.; Kim, H. U.; Nave, M.; Dickschat, J. S.; Mitchell, D. A.; Shelest, E.; Breitling, R.; Takano, E.; Lee, S. Y.; Weber, T.; Medema, M. H. AntiSMASH 4.0 - Improvements in Chemistry Prediction and Gene Cluster Boundary Identification. *Nucleic Acids Res.* **2017**, *45* (W1), W36–W41. https://doi.org/10.1093/nar/gkx319.

(122) Sievers, F.; Wilm, A.; Dineen, D.; Gibson, T. J.; Karplus, K.; Li, W.; Lopez, R.; McWilliam, H.; Remmert, M.; Söding, J.; Thompson, J. D.; Higgins, D. G. Fast, Scalable Generation of High-Quality Protein Multiple Sequence Alignments Using Clustal Omega. *Mol. Syst. Biol.* **2011**, *7*, 539. https://doi.org/10.1038/msb.2011.75.

(123) Wang, M.; Carver, J. J.; Phelan, V. V.; Sanchez, L. M.; Garg, N.; Peng, Y.; Nguyen, D. D. D.-T. T.; Watrous, J.; Kapono, C. A.; Luzzatto-Knaan, T.; Porto, C.; Bouslimani, A.; Melnik, A. V.; Meehan, M. J.; Liu, W.-T. T.; Crüsemann, M.; Boudreau, P. D.; Esquenazi, E.; Sandoval-Calderón, M.; Kersten, R. D.; Pace, L. A.; Quinn, R. A.; Duncan, K. R.; Hsu, C.-C. C.; Floros, D. J.; Gavilan, R. G.; Kleigrewe, K.; Northen, T.; Dutton, R. J.; Parrot, D.; Carlson, E. E.; Aigle, B.; Michelsen, C. F.; Jelsbak, L.; Sohlenkamp, C.; Pevzner, P.; Edlund, A.; McLean, J.; Piel, J.; Murphy, B. T.; Gerwick, L.; Liaw, C.-C. C.; Yang, Y.-L. L.; Humpf, H.-U. U.; Maansson, M.; Keyzers, R. A.; Sims, A. C.; Johnson, A. R.; Sidebottom, A. M.; Sedio, B. E.; Klitgaard, A.; Larson, C. B.; Boya, C. A. P.; Torres-Mendoza, D.; Gonzalez, D. J.; Silva, D. B.; Marques, L. M.; Demarque, D. P.; Pociute, E.; O'Neill, E. C.; Briand, E.; Helfrich, E. J. N.; Granatosky, E. A.; Glukhov, E.; Ryffel, F.; Houson, H.; Mohimani, H.; Kharbush, J. J.; Zeng, Y.; Vorholt, J. A.; Kurita, K. L.; Charusanti, P.; McPhail, K. L.; Nielsen, K. F.; Vuong, L.; Elfeki, M.; Traxler, M. F.; Engene, N.; Koyama, N.; Vining, O. B.; Baric, R.; Silva, R. R.; Mascuch, S. J.; Tomasi, S.; Jenkins, S.; Macherla, V.; Hoffman, T.; Agarwal, V.; Williams, P. G.; Dai, J.; Neupane, R.; Gurr, J.; Rodríguez, A. M. C.; Lamsa, A.; Zhang, C.; Dorrestein, K.; Duggan, B. M.; Almaliti, J.; Allard, P.-M. M.; Phapale, P.; Nothias, L.-F. F.; Alexandrov, T.; Litaudon, M.; Wolfender, J.-L. L.; Kyle, J. E.; Metz, T. O.; Peryea, T.; Nguyen, D. D. D.-T. T.; VanLeer, D.; Shinn, P.; Jadhav, A.; Müller, R.; Waters, K. M.; Shi, W.; Liu, X.; Zhang, L.; Knight, R.; Jensen, P. R.; Palsson, B.; Pogliano, K.; Linington, R. G.; Gutiérrez, M.; Lopes, N. P.; Gerwick, W. H.; Moore, B. S.; Dorrestein, P. C.; Bandeira, N.; Duy Nguyen, D.; Watrous, J.; Kapono, C. A.; Luzzatto-Knaan, T.; Porto, C.; Bouslimani, A.; Melnik, A. V.; Meehan, M. J.; Liu, W.-T. T.; Crüsemann, M.; Boudreau, P. D.; Esquenazi, E.; Sandoval-Calderón, M.; Kersten, R. D.; Pace, L. A.; Quinn, R. A.; Duncan, K. R.; Hsu, C.-C. C.; Floros, D. J.; Gavilan, R. G.; Kleigrewe, K.; Northen, T.; Dutton, R. J.; Parrot, D.; Carlson, E. E.; Aigle, B.; Michelsen, C. F.; Jelsbak, L.; Sohlenkamp, C.; Pevzner,

P.; Edlund, A.; McLean, J.; Piel, J.; Murphy, B. T.; Gerwick, L.; Liaw, C.-C. C.; Yang, Y.-L. L.; Humpf, H.-U. U.; Maansson, M.; Keyzers, R. A.; Sims, A. C.; Johnson, A. R.; Sidebottom, A. M.; Sedio, B. E.; Klitgaard, A.; Larson, C. B.; Boya P, C. A.; Torres-Mendoza, D.; Gonzalez, D. J.; Silva, D. B.; Marques, L. M.; Demarque, D. P.; Pociute, E.; O, E. C.; Briand, E.; N Helfrich, E. J.; Granatosky, E. A.; Glukhov, E.; Ryffel, F.; Houson, H.; Mohimani, H.; Kharbush, J. J.; Zeng, Y.; Vorholt, J. A.; Kurita, K. L.; Charusanti, P.; McPhail, K. L.; Fog Nielsen, K.; Vuong, L.; Elfeki, M.; Traxler, M. F.; Engene, N.; Koyama, N.; Vining, O. B.; Baric, R.; Silva, R. R.; Mascuch, S. J.; Tomasi, S.; Jenkins, S.; Macherla, V.; Hoffman, T.; Agarwal, V.; Williams, P. G.; Dai, J.; Neupane, R.; Gurr, J.; C Rodríguez, A. M.; Lamsa, A.; Zhang, C.; Dorrestein, K.; Duggan, B. M.; Almaliti, J.; Allard, P.-M. M.; Phapale, P.; Nothias, L.-F. F.; Alexandrov, T.; Litaudon, M.; Wolfender, J.-L. L.; Kyle, J. E.; Metz, T. O.; Peryea, T.; Nguyen, D. D. D.-T. T.; VanLeer, D.; Shinn, P.; Jadhav, A.; Müller, R.; Waters, K. M.; Shi, W.; Liu, X.; Zhang, L.; Knight, R.; Jensen, P. R.; Ø Palsson, B.; Pogliano, K.; Linington, R. G.; Gutiérrez, M.; Lopes, N. P.; Gerwick, W. H.; Moore, B. S.; Dorrestein, P. C.; Bandeira, N. *Sharing and Community Curation of Mass Spectrometry Data with Global Natural Products Social Molecular Networking*; Nature Publishing Group, 2016; Vol. 34, pp 828–837. https://doi.org/10.1038/nbt.3597.

(124) Kumar, S.; Stecher, G.; Li, M.; Knyaz, C.; Tamura, K. MEGA X: Molecular Evolutionary Genetics Analysis across Computing Platforms. *Mol. Biol. Evol.* **2018**, *35* (6), 1547–1549. https://doi.org/10.1093/molbev/msy096.

(125) Miess, H. Genome Mining for Guanidine-Containing Antimicrobial Lipopeptides and Studies on Their Biosynthesis. **2017**, No. February.

(126) Shoji, J.; Hinoo, H.; Katayama, T.; Nakagawa, Y.; Ikenishi, Y.; Iwatani, K.; Yoshida, T. Structures of New Peptide Antibiotics, Plusbacins A1-A4 and B1-B4. *J. Antibiot. (Tokyo).* **1992**, *45* (6), 824–831. https://doi.org/10.7164/ANTIBIOTICS.45.824.

(127) Massey, L. K.; Sokatch, J. R.; Conrad, R. S. Branched-Chain Amino Acid Catabolism in Bacteria. *Bacteriol. Rev.* **1976**, *40* (1), 42.

(128) Beltrametti, F.; Jovetic, S.; Feroggio, M.; Gastaldo, L.; Selva, E.; Marinelli, F. Valine Influences Production and Complex Composition of Glycopeptide Antibiotic A40926 in Fermentations of Nonomuraea Sp. ATCC 39727. *J. Antibiot. (Tokyo).* **2004**, *57* (1), 37–44. https://doi.org/10.7164/ANTIBIOTICS.57.37.

(129) Boeck, L. D.; Wetzel, R. W. A54145, a New Lipopeptide Antibiotic Complex: Factor Control through Precursor Directed Biosynthesis. *J. Antibiot. (Tokyo).* **1990**, *43* (6), 607–615. https://doi.org/10.7164/ANTIBIOTICS.43.607.

(130) Hashizume, H.; Nosaka, C.; Hirosawa, S.; Igarashi, M.; Nishimura, Y.; Akamatsu, Y. Production of Tripropeptins in Media Supplemented with Precursors Based on the Biosynthetic Pathway. *Arkivoc* **2007**, *2007* (7), 241–253. https://doi.org/10.3998/ark.5550190.0008.720.

(131) Sugawara, K.; Numata, K.-I.; Konishi, M.; Kawaguchi, H. Empedopeptin (BMY-28117), a New Depsipeptide Antibiotic II. Structure Determination. *J. Antibiot. (Tokyo).* **1984**, *37* (9), 958–964. https://doi.org/10.7164/ANTIBIOTICS.37.958.

(132) Schmidt, Y. Investigations on the Structure , Biosynthesis and Biology of Antibacterial Cyclic Lipopeptides. **2013**.

(133) Breitmaier, E. Vom NMR-Spektrum Zur Strukturformel Organischer Verbindungen. **1992**. https://doi.org/10.1007/978-3-322-94014-8.

(134) Wingen, L. M.; Braun, C.; Rausch, M.; Gross, H.; Schneider, T.; Menche, D. Versatile Synthesis of Pathogen Specific Bacterial Cell Wall Building Blocks. *RSC Adv.* **2022**, *12* (24), 15046–15069. https://doi.org/10.1039/D2RA01915A.

(135) Ye, X.-Y.; Lo, M.-C.; Brunner, L.; Walker, D.; Kahne, D.; Walker, S. Better Substrates for Bacterial Transglycosylases. *J. Am. Chem. Soc.* **2001**, *123* (13), 3155–3156. https://doi.org/10.1021/JA010028Q.

(136) Hsu, S.-T. D.; Breukink, E.; Tischenko, E.; Lutters, M. A. G.; de Kruijff, B.; Kaptein, R.; Bonvin, A. M. J. J.; van Nuland, N. A. J. The Nisin–Lipid II Complex Reveals a Pyrophosphate Cage That Provides a Blueprint for Novel Antibiotics. *Nat. Struct. Mol. Biol.* **2004**, *11* (10), 963–967. https://doi.org/10.1038/nsmb830.

(137) Schwarzer, D.; Mootz, H. D.; Linne, U.; Marahiel, M. A. Regeneration of Misprimed Nonribosomal Peptide Synthetases by Type II Thioesterases. *Proc. Natl. Acad. Sci.* **2002**, *99* (22), 14083–14088. https://doi.org/10.1073/PNAS.212382199.

(138) Lange, A.; Sun, H.; Pilger, J.; Reinscheid, U. M.; Gross, H. Predicting the Structure of Cyclic Lipopeptides by Bioinformatics: Structure Revision of Arthrofactin. *ChemBioChem* **2012**, *13* (18), 2671–2675.

(139) Berti, A. D.; Greve, N. J.; Christensen, Q. H.; Thomas, M. G. Identification of a Biosynthetic Gene Cluster and the Six Associated Lipopeptides Involved in Swarming Motility of Pseudomonas Syringae Pv. Tomato DC3000. *J. Bacteriol.* **2007**, *189* (17), 6312. https://doi.org/10.1128/JB.00725-07.

(140) Götze, S.; Arp, J.; Lackner, G.; Zhang, S.; Kries, H.; Klapper, M.; García-Altares, M.; Willing, K.; Günther, M.; Stallforth, P. Structure Elucidation of the Syringafactin Lipopeptides Provides Insight in the Evolution of Nonribosomal Peptide Synthetases. *Chem. Sci.* **2019**, *10* (48), 10979–10990. https://doi.org/10.1039/C9SC03633D.

(141) Scherlach, K.; Lackner, G.; Graupner, K.; Pidot, S.; Bretschneider, T.; Hertweck, C. Biosynthesis and Mass Spectrometric Imaging of Tolaasin, the Virulence Factor of Brown Blotch Mushroom Disease. *ChemBioChem* **2013**, *14* (18), 2439–2443. https://doi.org/10.1002/CBIC.201300553.

(142) Rokni-Zadeh, H.; Li, W.; Sanchez-Rodriguez, A.; Sinnaeve, D.; Rozenski, J.; Martins, J. C.; Mot, R. De. Genetic and Functional Characterization of Cyclic Lipopeptide White-Line-Inducing Principle (WLIP) Production by Rice Rhizosphere Isolate Pseudomonas Putida RW10S2. *Appl. Environ. Microbiol.* **2012**, *78* (14), 4826. https://doi.org/10.1128/AEM.00335-12.

(143) Xu, F.; Wu, Y.; Zhang, C.; Davis, K. M.; Moon, K.; Bushin, L. B.; Seyedsayamdost, M. R. A Genetics-Free Method for High-Throughput Discovery of Cryptic Microbial Metabolites. *Nat. Chem. Biol.* **2019**, *15* (2), 161–168. https://doi.org/10.1038/S41589-018-0193-2.

(144) Das, M.; Manna, K. Chalcone Scaffold in Anticancer Armamentarium: A Molecular Insight. *J. Toxicol.* **2016**, *2016*. https://doi.org/10.1155/2016/7651047.

(145) Mo, Y.-Y.; Gross, D. C. Plant Signal Molecules Activate the SyrB Gene, Which Is Required for Syringomycin Production by Pseudomonas Syringae Pv. Syringae. *J. Bacteriol.* **1991**, *173* (18), 5784. https://doi.org/10.1128/JB.173.18.5784-5792.1991.

(146) Marmann, A.; Aly, A. H.; Lin, W.; Wang, B.; Proksch, P. Co-Cultivation--a Powerful Emerging Tool for Enhancing the Chemical Diversity of Microorganisms. *Mar. Drugs* **2014**, *12* (2), 1043–1065. https://doi.org/10.3390/MD12021043.

(147) Pettit, R. K. Mixed Fermentation for Natural Product Drug Discovery. *Appl. Microbiol. Biotechnol.* **2009**, *83* (1), 19–25. https://doi.org/10.1007/S00253-009-1916-9.

(148) Liu, J.-F. F.; Yang, J.; Yang, S.-Z. Z.; Ye, R.-Q. Q.; Mu, B.-Z. Z. Effects of Different Amino Acids in Culture Media on Surfactin Variants Produced by Bacillus Subtilis TD7. *Appl. Biochem. Biotechnol.* **2012**, *166* (8), 2091–2100. https://doi.org/10.1007/S12010-012-9636-5.

(149) Jakob, K.; Goss, E. M.; Araki, H.; Van, T.; Kreitman, M.; Bergelson, J. Pseudomonas Viridiflava and P. Syringae-Natural Pathogens of Arabidopsis Thaliana. *Mol. Plant-Microbe Interact.* **2002**, *15* (12), 1195–1203.

(150) Jakob, K.; Kniskern, J. M.; Bergelson, J. The Role of Pectate Lyase and the Jasmonic Acid Defense Response in Pseudomonas Viridiflava Virulence. *Mol. Plant-Microbe Interact. MPMI* **2007**, *20* (2), 146–158. https://doi.org/10.1094/MPMI.

(151) Ansari, M. Z.; Sharma, J.; Gokhale, R. S.; Mohanty, D. In Silico Analysis of Methyltransferase Domains Involved in Biosynthesis of Secondary Metabolites. *BMC Bioinformatics* **2008**, *9*, 454. https://doi.org/10.1186/1471-2105-9-454.

(152) Zachow, C.; Jahanshah, G.; De Bruijn, I.; Song, C.; Ianni, F.; Pataj, Z.; Gerhardt, H.; Pianet, I.; Lämmerhofer, M.; Berg, G.; Gross, H.; Raaijmakers, J. M. The Novel Lipopeptide Poaeamide of the Endophyte Pseudomonas Poae RE∗1-1-14 Is Involved in Pathogen Suppression and Root Colonization. *Mol. Plant-Microbe Interact.* **2015**, *28* (7), 800–810. https://doi.org/10.1094/MPMI-12-14-0406-R/ASSET/IMAGES/LARGE/MPMI-12-14-0406-R_T1.JPEG.

(153) Kodaka, H.; Iwata, M.; Yumoto, S.; Kashitani, F. Evaluation of a New Agar Medium Containing

Cetrimide, Kanamycin and Nalidixic Acid for Isolation and Enhancement of Pigment Production of Pseudomonas Aeruginosa in Clinical Samples. *J. Basic Microbiol.* **2003**, *43* (5), 407–413. https://doi.org/10.1002/JOBM.200310264.

(154) Perrin, D. D.; Dempsey, B. Buffers for PH and Metal Ion Control. *Buffers pH Met. Ion Control* **1979**. https://doi.org/10.1007/978-94-009-5874-6.

(155) Hsu, S. Te; Breukink, E.; de Kruijff, B.; Kaptein, R.; Bonvin, A. M. J. J.; van Nuland, N. A. J. Mapping the Targeted Membrane Pore Formation Mechanism by Solution NMR: The Nisin Z and Lipid II Interaction in SDS Micelles. *Biochemistry* **2002**, *41* (24), 7670–7676. https://doi.org/10.1021/BI025679T.

(156) Ho, S.-T.; Ho, Y.-N.; Lin, C.; Hsu, W.-C.; Lee, H.-J.; Peng, C.-C.; Cheng, H.-T.; Yang, Y.-L. Integrated Omics Strategy Reveals Cyclic Lipopeptides Empedopeptins from Massilia Sp. YMA4 and Their Biosynthetic Pathway. *Mar. Drugs 2021, Vol. 19, Page 209* **2021**, *19* (4), 209. https://doi.org/10.3390/MD19040209.

(157) Li, J.; Jensen, S. E. Nonribosomal Biosynthesis of Fusaricidins by Paenibacillus Polymyxa PKB1 Involves Direct Activation of a D-Amino Acid. *Chem. Biol.* **2008**, *15* (2), 118–127. https://doi.org/10.1016/J.CHEMBIOL.2007.12.014.

(158) Sørensen, D.; Nielsen, T. H.; Christophersen, C.; Sørensen, J.; Gajhede, M. Cyclic Lipoundecapeptide Amphisin from Pseudomonas Sp. Strain DSS73. *Acta Crystallogr. C.* **2001**, *57* (Pt 9), 1123–1124. https://doi.org/10.1107/S0108270101010782.

(159) Broberg, A.; Menkis, A.; Vasiliauskas, R. Kutznerides 1−4, Depsipeptides from the Actinomycete Kutzneria Sp. 744 Inhabiting Mycorrhizal Roots of Picea a Bies Seedlings. *J. Nat. Prod.* **2006**, *69* (1), 97–102.

(160) Fujie, A.; Muramatsu, H.; Yoshimura, S.; Hashimoto, M.; Shigematsu, N.; Takase, S. III. Structure Determination. *JULY2001 J. Antibiot. 54* (7), 588–594.

(161) Kim, H.; Yoo, D.; Kwon, S.; Kim, Y. G. Efficient and Stereoselective Synthesis of Threo-β-Hydroxy-l-Glutamic Acid via a Tandem (Z)-Olefination-Conjugate Addition. *Tetrahedron: Asymmetry* **2009**, *20* (23), 2715–2719. https://doi.org/10.1016/J.TETASY.2009.11.023.

(162) Struck, A. W.; Thompson, M. L.; Wong, L. S.; Micklefield, J. S-Adenosyl-Methionine-Dependent Methyltransferases: Highly Versatile Enzymes in Biocatalysis, Biosynthesis and Other Biotechnological Applications. *ChemBioChem* **2012**, *13* (18), 2642–2655. https://doi.org/10.1002/CBIC.201200556.

(163) Zolova, O. E.; Garneau-Tsodikova, S. KtzJ-Dependent Serine Activation and O-Methylation by KtzH for Kutznerides Biosynthesis. *J. Antibiot. (Tokyo).* **2014**, *67* (1), 59–64. https://doi.org/10.1038/JA.2013.98.

(164) Han, B.; Gross, H.; Goeger, D. E.; Mooberry, S. L.; Gerwick, W. H. Aurilides B and C, Cancer Cell Toxins from a Papua New Guinea Collection of the Marine Cyanobacterium Lyngbya Majuscula. *J. Nat. Prod.* **2006**, *69* (4), 572–575. https://doi.org/10.1021/NP0503911/SUPPL_FILE/NP0503911SI20051208_040758.PDF.

(165) Kralt, B.; Moreira, R.; Palmer, M.; Taylor, S. D. Total Synthesis of A54145 Factor D. *J. Org. Chem.* **2019**, *84* (18), 12021–12030. https://doi.org/10.1021/ACS.JOC.9B01938.S001.

(166) Reid, C. M.; Fanning, K. N.; Fowler, L. S.; Sutherland, A. Synthesis and Reactivity of 4-Oxo-5-Trimethylsilanyl Derived a-Amino Acids. **2014**. https://doi.org/10.1016/j.tet.2014.11.059.

(167) Katsuyama, A.; Paudel, A.; Panthee, S.; Hamamoto, H.; Kawakami, T.; Hojo, H.; Yakushiji, F.; Ichikawa, S. Total Synthesis and Antibacterial Investigation of Plusbacin A3. *Org. Lett.* **2017**, *19* (14), 3771–3774. https://doi.org/10.1021/acs.orglett.7b01629.

(168) Hirosawa, S.; Takahashi, Y.; Hashizume, H.; Miyake, T.; Akamatsu, Y. Synthesis and Antibacterial Activity of Tripropeptin C Derivatives Modified at the Carboxyl Groups. *J. Antibiot. 2014 673* **2013**, *67* (3), 265–268. https://doi.org/10.1038/ja.2013.128.

(169) Mnif, I.; Ghribi, D. Lipopeptides Biosurfactants: Mean Classes and New Insights for Industrial, Biomedical, and Environmental Applications. *Biopolymers* **2015**, *104* (3), 129–147. https://doi.org/10.1002/bip.22630.

(170) Akpa, E.; Jacques, P.; Wathelet, B.; Paquot, M.; Fuchs, R.; Budzikiewicz, H.; Thonart, P. Influence of Culture Conditions on Lipopeptide Production by Bacillus Subtilis. *Appl. Biochem. Biotechnol. 2001 911* **2001**, *91* (1), 551–561. https://doi.org/10.1385/ABAB:91-93:1-9:551.

(171) Bakhtiary, A.; Cochrane, S. A.; Mercier, P.; McKay, R. T.; Miskolzie, M.; Sit, C. S.; Vederas, J. C. Insights into the Mechanism of Action of the Two-Peptide Lantibiotic Lacticin 3147. *J. Am. Chem. Soc.* **2017**, *139* (49), 17803–17810. https://doi.org/10.1021/JACS.7B04728.

(172) Hsu, S.-T. D.; Breukink, E.; Bierbaum, G.; Sahl, H.-G.; Kruijff, B. de; Kaptein, R.; Nuland, N. A. J. van; Bonvin, A. M. J. J. NMR Study of Mersacidin and Lipid II Interaction in Dodecylphosphocholine Micelles: CONFORMATIONAL CHANGES ARE A KEY TO ANTIMICROBIAL ACTIVITY *. *J. Biol. Chem.* **2003**, *278* (15), 13110–13117. https://doi.org/10.1074/JBC.M211144200.

(173) Cochrane, S. A.; Findlay, B.; Bakhtiary, A.; Acedo, J. Z.; Rodriguez-Lopez, E. M.; Mercier, P.; Vederas, J. C. Antimicrobial Lipopeptide Tridecaptin A1selectively Binds to Gram-Negative Lipid II. *Proc. Natl. Acad. Sci. U. S. A.* **2016**, *113* (41), 11561–11566. https://doi.org/10.1073/PNAS.1608623113.

(174) Schneider, T.; Kruse, T.; Wimmer, R.; Wiedemann, I.; Sass, V.; Pag, U.; Jansen, A.; Nielsen, A. K.; Mygind, P. H.; Raventós, D. S.; Neve, S.; Ravn, B.; Bonvin, A. M. J. J.; De Maria, L.; Andersen, A. S.; Gammelgaard, L. K.; Sahl, H.-G.; Kristensen, H.-H. Plectasin, a Fungal Defensin, Targets the Bacterial Cell Wall Precursor Lipid II. *Science* **2010**, *328* (5982), 1168–1172. https://doi.org/10.1126/SCIENCE.1185723.

(175) Wiedemann, I.; Breukink, E.; Van Kraaij, C.; Kuipers, O. P.; Bierbaum, G.; De Kruijff, B.; Sahl, H. G. Specific Binding of Nisin to the Peptidoglycan Precursor Lipid II Combines Pore Formation and Inhibition of Cell Wall Biosynthesis for Potent Antibiotic Activity. *J. Biol. Chem.* **2001**, *276* (3), 1772–1779. https://doi.org/10.1074/JBC.M006770200.

(176) Müller, A.; Ulm, H.; Reder-Christ, K.; Sahl, H. G.; Schneider, T. Interaction of Type A Lantibiotics with Undecaprenol-Bound Cell Envelope Precursors. *Microb. Drug Resist.* **2012**, *18* (3), 261–270. https://doi.org/10.1089/MDR.2011.0242.

(177) Scherer, K.; Wiedemann, I.; Ciobanasu, C.; Sahl, H. G.; Kubitscheck, U. Aggregates of Nisin with Various Bactoprenol-Containing Cell Wall Precursors Differ in Size and Membrane Permeation Capacity. *Biochim. Biophys. Acta - Biomembr.* **2013**, *1828* (11), 2628–2636. https://doi.org/10.1016/J.BBAMEM.2013.07.014.

(178) Münch, D.; Roemer, T.; Lee, S. H.; Engeser, M.; Sahl, H. G.; Schneider, T. Identification and in Vitro Analysis of the GatD/MurT Enzyme-Complex Catalyzing Lipid II Amidation in Staphylococcus Aureus. *PLOS Pathog.* **2012**, *8* (1), e1002509. https://doi.org/10.1371/JOURNAL.PPAT.1002509.

(179) Zhao, M.; Wang, H.-B.; Ji, L.-N.; Mao, Z.-W. Insights into Metalloenzyme Microenvironments: Biomimetic Metal Complexes with a Functional Second Coordination Sphere. *Chem. Soc. Rev.* **2013**, *42* (21), 8360–8375. https://doi.org/10.1039/C3CS60162E.

(180) Kubik, S.; Mungalpara, D. Amino Acid-Based Receptors. *Compr. Supramol. Chem. II* **2017**, *3*, 293–310. https://doi.org/10.1016/B978-0-12-409547-2.12528-4.

(181) Takashina, K.; Katsuyama, A.; Kaguchi, R.; Yamamoto, K.; Sato, T.; Takahashi, S.; Horiuchi, M.; Yokota, S. I.; Ichikawa, S. Solid-Phase Total Synthesis of Plusbacin A3. *Org. Lett.* **2022**, *24* (11), 2253–2257. https://doi.org/10.1021/ACS.ORGLETT.2C00667/SUPPL_FILE/OL2C00667_SI_001.PDF.

(182) Katsuyama, A.; Yakushiji, F.; Ichikawa, S. Total Synthesis of Plusbacin A3 and Its Dideoxy Derivative Using a Solvent-Dependent Diastereodivergent Joullié-Ugi Three-Component Reaction. *J. Org. Chem.* **2018**, *83* (13), 7085–7101. https://doi.org/10.1021/acs.joc.8b00038.

(183) Ruinelli, M.; Blom, J.; Pothier, J. F. Complete Genome Sequence of Pseudomonas Viridiflava CFBP 1590, Isolated from Diseased Cherry in France. *Genome Announc.* **2017**, *5* (30). https://doi.org/10.1128/GENOMEA.00662-17.

(184) González, A. J.; Cleenwerck, I.; De Vos, P.; Fernández-Sanz, A. M. Pseudomonas Asturiensis Sp. Nov., Isolated from Soybean and Weeds. *Syst. Appl. Microbiol.* **2013**, *36* (5), 320–324. https://doi.org/10.1016/J.SYAPM.2013.04.004.

(185) Smirnova, A.; Li, H.; Weingart, H.; Aufhammer, S.; Burse, A.; Finis, K.; Schenk, A.; Ullrich, M. S. Thermoregulated Expression of Virulence Factors in Plant-Associated Bacteria. *Arch. Microbiol.* **2001**, *176* (6), 393–399. https://doi.org/10.1007/S002030100344.

(186) Rowley, K. B.; Clements, D. E.; Mandel, M.; Humphreys, T.; Patil, S. S. Multiple Copies of a DNA Sequence from Pseudomonas Syringae Pathovar Phaseolicola Abolish Thermoregulation of Phaseolotoxin Production. *Mol. Microbiol.* **1993**, *8* (3), 625–635. https://doi.org/10.1111/J.1365-2958.1993.TB01606.X.

(187) Budde, I. P.; Rohde, B. H.; Bender, C. L.; Ullrich, M. S. Growth Phase and Temperature Influence Promoter Activity, Transcript Abundance, and Protein Stability during Biosynthesis of the Pseudomonas Syringae Phytotoxin Coronatine. *J. Bacteriol.* **1998**, *180* (6), 1360.

(188) Girard, L.; Höfte, M.; Mot, R. De. Lipopeptide Families at the Interface between Pathogenic and Beneficial Pseudomonas-Plant Interactions. *Crit. Rev. Microbiol.* **2020**, *46* (4), 397–419. https://doi.org/10.1080/1040841X.2020.1794790.

(189) Lavermicocca, P.; Iacobellis, N. S.; Simmaco, M.; Graniti, A. Biological Properties and Spectrum of Activity of Pseudomonas Syringae Pv. Syringae Toxins. *Physiol. Mol. Plant Pathol.* **1997**, *50* (2), 129–140. https://doi.org/10.1006/PMPP.1996.0078.

(190) Gerard, J.; Lloyd, R.; Barsby, T.; Haden, P.; Kelly, M. T.; Andersen, R. J. Massetolides A−H, Antimycobacterial Cyclic Depsipeptides Produced by Two Pseudomonads Isolated from Marine Habitats. *J. Nat. Prod.* **1997**, *60* (3), 223–229. https://doi.org/10.1021/NP9606456.

(191) Scaloni, A.; Dalla Serra, M.; Amodeo, P.; Mannina, L.; Vitale, R. M.; Segre, A. L.; Cruciani, O.; Lodovichetti, F.; Greco, M. L.; Fiore, A.; Gallo, M.; D'Ambrosio, C.; Coraiola, M.; Menestrina, G.; Graniti, A.; Fogliano, V. Structure, Conformation and Biological Activity of a Novel Lipodepsipeptide from Pseudomonas Corrugata: Cormycin A. *Biochem. J.* **2004**, *384* (Pt 1), 25–36. https://doi.org/10.1042/BJ20040422.

(192) Cautain, B.; De Pedro, N.; Schulz, C.; Pascual, J.; Sousa, T. D. S.; Martin, J.; Pérez-Victoria, I.; Asensio, F.; González, I.; Bills, G. F.; Reyes, F.; Genilloud, O.; Vicente, F. Identification of the Lipodepsipeptide MDN-0066, a Novel Inhibitor of VHL/HIF Pathway Produced by a New Pseudomonas Species. *PLoS One* **2015**, *10* (5), e0125221. https://doi.org/10.1371/JOURNAL.PONE.0125221.

(193) Scholz-Schroeder, B. K.; Hutchison, M. L.; Grgurina, I.; Gross, D. C. The Contribution of Syringopeptin and Syringomycin to Virulence of Pseudomonas Syringae Pv. Syringae Strain B301D on the Basis of SypA and SyrB1 Biosynthesis Mutant Analysis. *Mol. Plant. Microbe. Interact.* **2001**, *14* (3), 336–348. https://doi.org/10.1094/MPMI.2001.14.3.336.

(194) Burch, A. Y.; Zeisler, V.; Yokota, K.; Schreiber, L.; Lindow, S. E. The Hygroscopic Biosurfactant Syringafactin Produced by Pseudomonas Syringae Enhances Fitness on Leaf Surfaces during Fluctuating Humidity. *Environ. Microbiol.* **2014**, *16* (7), 2086–2098. https://doi.org/10.1111/1462-2920.12437.

(195) Berti, A. D.; Greve, N. J.; Christensen, Q. H.; Thomas, M. G. Identification of a Biosynthetic Gene Cluster and the Six Associated Lipopeptides Involved in Swarming Motility of Pseudomonas Syringae Pv. Tomato DC3000. *J. Bacteriol.* **2007**, *189* (17), 6312–6323. https://doi.org/10.1128/JB.00725-07.

(196) Oh, D. C.; Kauffman, C. A.; Jensen, P. R.; Fenical, W. Induced Production of Emericellamides A and B from the Marine-Derived Fungus Emericella Sp. in Competing Co-Culture. *J. Nat. Prod.* **2007**, *70* (4), 515–520. https://doi.org/10.1021/NP060381F.

(197) Galli, G.; Rodriguez, F.; Cosmina, P.; Pratesi, C.; Nogarotto, R.; de Ferra; Guido Grandi, F. Characterization of the Surfactin Synthetase Multi-Enzyme Complex. *Biochim. Biophys. Acta - Protein Struct. Mol. Enzymol.* **1994**, *1205* (1), 19–28. https://doi.org/10.1016/0167-4838(94)90087-6.

(198) Ma, Z. Genome Mining and Chemical Characterization of a New Cyclic Lipopeptide Associated with MDN-0066 from Pseudomonas Moraviensis HN2 Cultured in a Valine-Rich Medium. *J. Antibiot. 2023 764* **2023**, *76* (4), 244–248. https://doi.org/10.1038/s41429-023-00597-z.

(199) Théatre, A.; Cano-Prieto, C.; Bartolini, M.; Laurin, Y.; Deleu, M.; Niehren, J.; Fida, T.; Gerbinet, S.; Alanjary, M.; Medema, M. H.; Léonard, A.; Lins, L.; Arabolaza, A.; Gramajo, H.; Gross, H.; Jacques, P. The Surfactin-Like Lipopeptides From Bacillus Spp.: Natural Biodiversity and Synthetic Biology for a Broader Application Range. *Front. Bioeng. Biotechnol.* **2021**, *9*. https://doi.org/10.3389/FBIOE.2021.623701.

VI List of Figures

VII List of Tables

VIII Appendix

Table VIII-1: MS^2 spectrum and fragment annotation of empedopeptin.

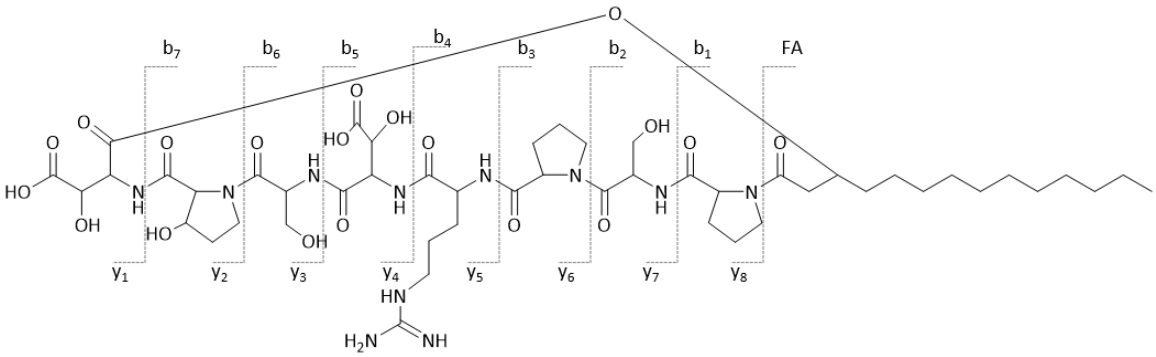

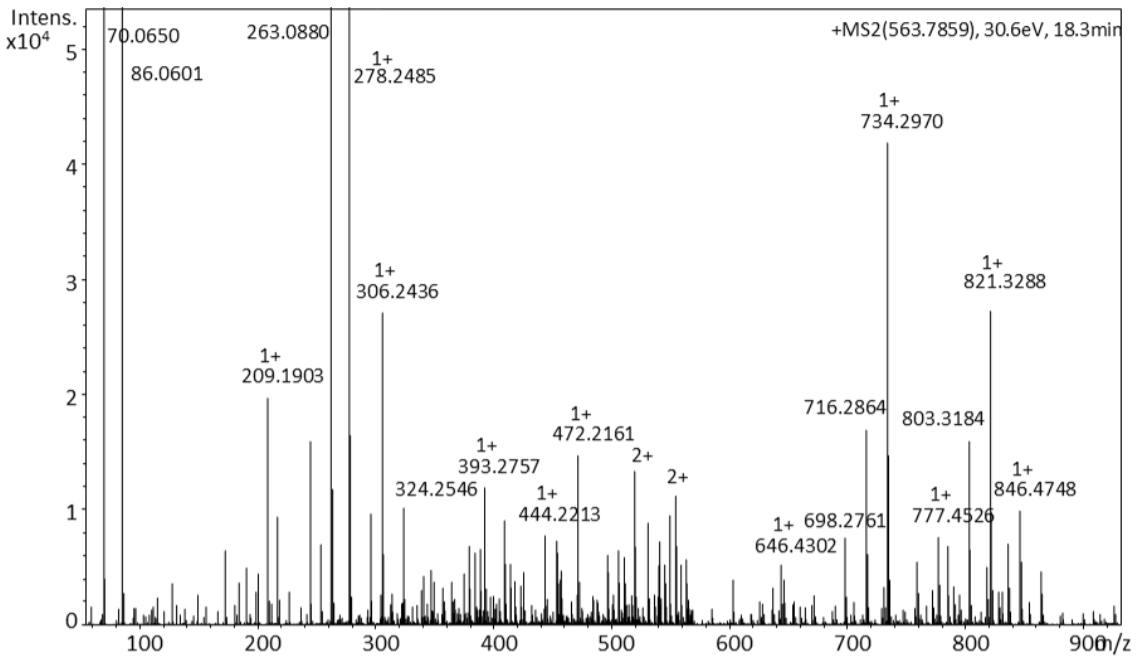

Fragment	Elemental composition	Ring and Double Bond (Rdb)	Theoretical Mass	Experimental Mass *(m/z)*	Δ_M [ppm]
$[M+2H]^{2+}$	$C_{49}H_{81}N_{11}O_{19}$	16	563.7850	563.7859	1.6
$[M+H]^{+}$	$C_{49}H_{80}N_{11}O_{19}$	16	1126.5626	1126.5636	0.8
M-H_2O	$C_{49}H_{78}N_{11}O_{18}$	17	1108.5526	1108.5574	4.3
M-Ser	$C_{46}H_{75}N_{10}O_{17}$	14	1039.5312	1039.5343	2.9
y_1	$C_4H_8NO_5$	2	150.0397	150.0400	1.9
y_2	$C_9H_{15}N_2O_7$	4	263.0874	263.0880	2.4
y_2-H_2O	$C_9H_{13}N_2O_6$	5	245.0768	245.0774	2.4
y_3	$C_{12}H_{20}N_3O_9$	5	350.1194	350.1205	3.2

y_5	$C_{22}H_{37}N_8O_{14}$	9	637.2429	637.2448	2.9
y_6	$C_{27}H_{44}N_9O_{15}$	11	734.2951	734.2970	2.5
y_6-H_2O	$C_{27}H_{42}N_9O_{14}$	12	716.2846	716.2864	2.5
y_6-$2H_2O$	$C_{27}H_{40}N_9O_{13}$	13	698.2746	698.2761	2.1
y_7	$C_{30}H_{49}N_{10}O_{17}$	12	821.3272	821.3288	2.0
y_7-H_2O	$C_{30}H_{47}N_{10}O_{16}$	13	803.3166	803.3184	2.2
FA-H_2O	$C_{14}H_{25}O$	3	209.1900	209.1903	1.6
b_1	$C_{19}H_{34}NO_3$	4	324.2533	324.2546	3.9
b_1-H_2O	$C_{19}H_{32}NO_2$	5	306.2428	306.2436	2.9
b_1-CO	$C_{18}H_{34}NO_2$	3	296.2584	296.2596	4.0
b_1-CO-H_2O	$C_{18}H_{32}NO$	4	278.2478	278.2485	2.4
b_2	$C_{22}H_{39}N_2O_5$	5	411.2853	411.2866	2.9
b_2-H_2O	$C_{22}H_{37}N_2O_4$	6	393.2748	393.2757	2.3
b_4	$C_{33}H_{58}N_7O_7$	9	664.4392	664.4402	1.4
b_4-H_2O	$C_{33}H_{56}N_7O_6$	10	646.4292	646.4302	1.8
b_5	$C_{37}H_{63}N_8O_{11}$	11	795.4616	795.4637	2.6
b_6	$C_{40}H_{68}N_9O_{13}$	12	882.4931	882.4922	-1.0
b_6-$2H_2O$	$C_{40}H_{64}N_9O_{11}$	14	846.4725	846.4748	2.7
AA_3-AA_6	$C_{18}H_{30}N_7O_8$	8	472.2150	472.2161	2.3
AA_3-CO-AA_6	$C_{17}H_{30}N_7O_7$	7	444.2201	444.2213	2.6
Pyrr	C_4H_8N	2	70.0651	70.0650	-1.5
OH-Pyrr	C_4H_8NO	2	86.0600	86.0601	0.9

Table VIII-2: MS^2 spectrum and fragment annotation of linear form of empedopeptin (b).

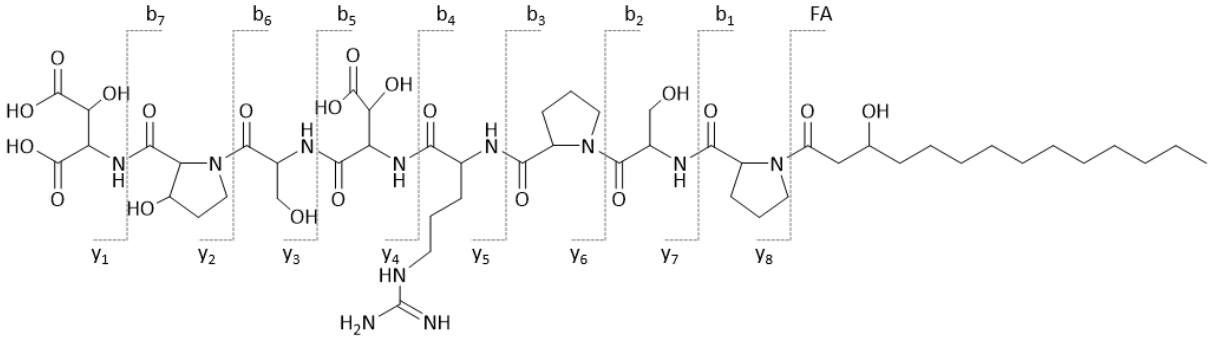

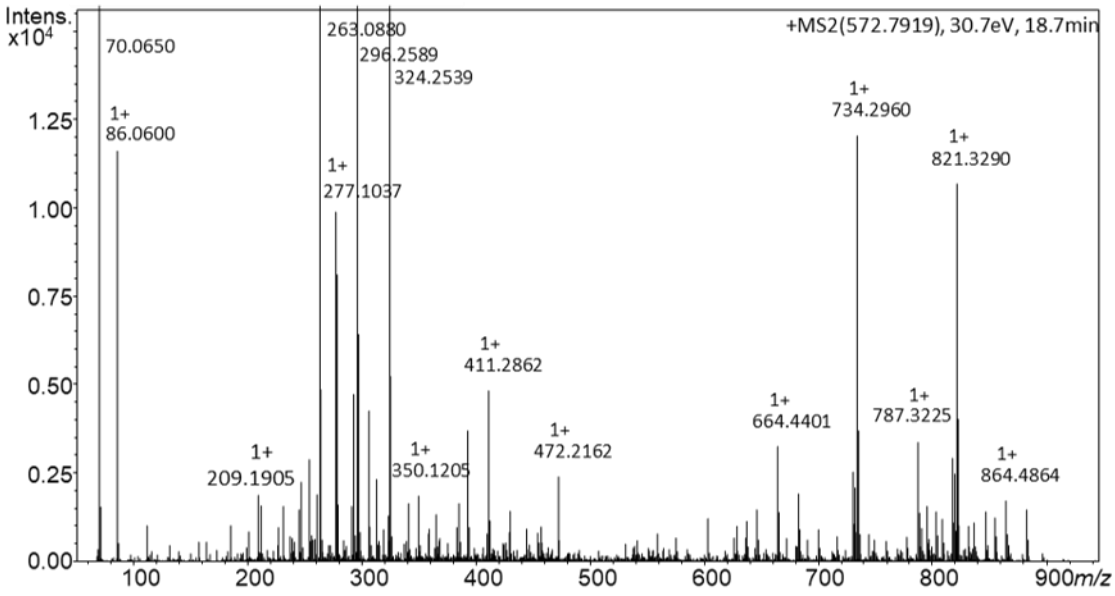

Fragment	Elemental composition	Ring and Double Bond (Rdb)	Theoretical Mass	Experimental Mass *(m/z)*	Δ_M [ppm]
$[M+2H]^{2+}$	$C_{49}H_{83}N_{11}O_{20}$	15	572.7902	572.7919	2.8
$[M+H]^{+}$	$C_{49}H_{82}N_{11}O_{20}$	15	1144.5732	1144.5746	1.2
y_1	$C_4H_8NO_5$	2	150.0397	150.0381	-10.7
y_2	$C_9H_{15}N_2O_7$	4	263.0874	263.0880	2.5
y_3	$C_{12}H_{20}N_3O_9$	5	350.1200	350.1205	1.4
y_4	$C_{16}H_{25}N_4O_{13}$	7	481.1418	481.1427	1.8
y_5	$C_{22}H_{37}N_8O_{14}$	9	637.2429	637.2429	0.0
y_6	$C_{27}H_{44}N_9O_{15}$	11	734.2951	734.2960	1.1
y_7	$C_{30}H_{49}N_{10}O_{17}$	12	821.3272	821.3290	2.2
y_7-H_2O	$C_{30}H_{47}N_{10}O_{16}$	13	803.3166	803.3177	1.4
y_7-$2H_2O$	$C_{30}H_{45}N_{10}O_{15}$	14	787.3217	787.3225	1.1
b_1	$C_{19}H_{34}NO_3$	4	324.2533	324.2539	1.9
b_1-CO	$C_{18}H_{34}NO_2$	3	296.2584	296.2589	1.8
b_1-CO-H_2O	$C_{18}H_{32}NO$	4	278.2478	278.2486	2.6
b_2	$C_{22}H_{39}N_2O_5$	5	411.2853	411.2862	2.2
b_2-H_2O	$C_{22}H_{37}N_2O_4$	6	393.2753	393.2756	2.0
b_4	$C_{33}H_{58}N_7O_7$	9	664.4392	664.4401	1.3
b_5	$C_{37}H_{63}N_8O_{11}$	11	795.4616	795.4629	2.3
b_6	$C_{40}H_{68}N_9O_{13}$	12	882.4937	882.4910	-3.1
b_6-H_2O	$C_{40}H_{66}N_9O_{12}$	13	864.4831	864.4864	3.8
AA_4-AA_7	$C_{18}H_{30}N_7O_8$	8	472.2156	472.2162	1.3
Pyrr	C_4H_8N	2	70.0657	70.0650	-1.7
OH-Pyrr	C_4H_8NO	2	86.0600	86.0600	0.0

Table VIII-3: MS^2 spectrum and fragment annotation of linear derivative 1 (c).

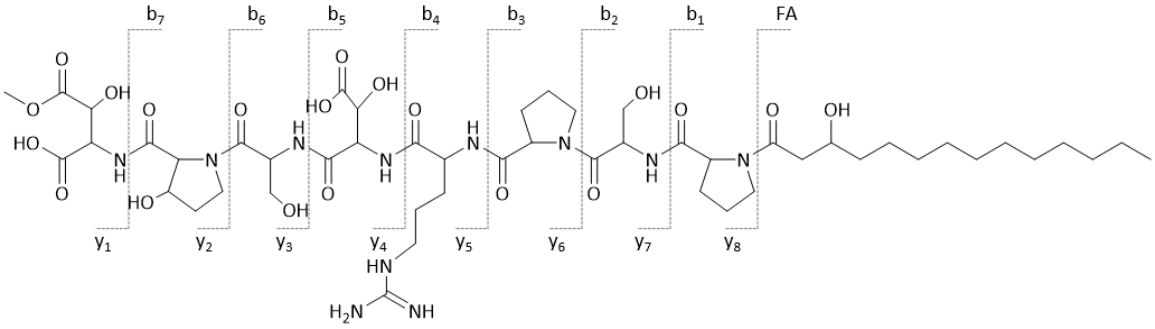

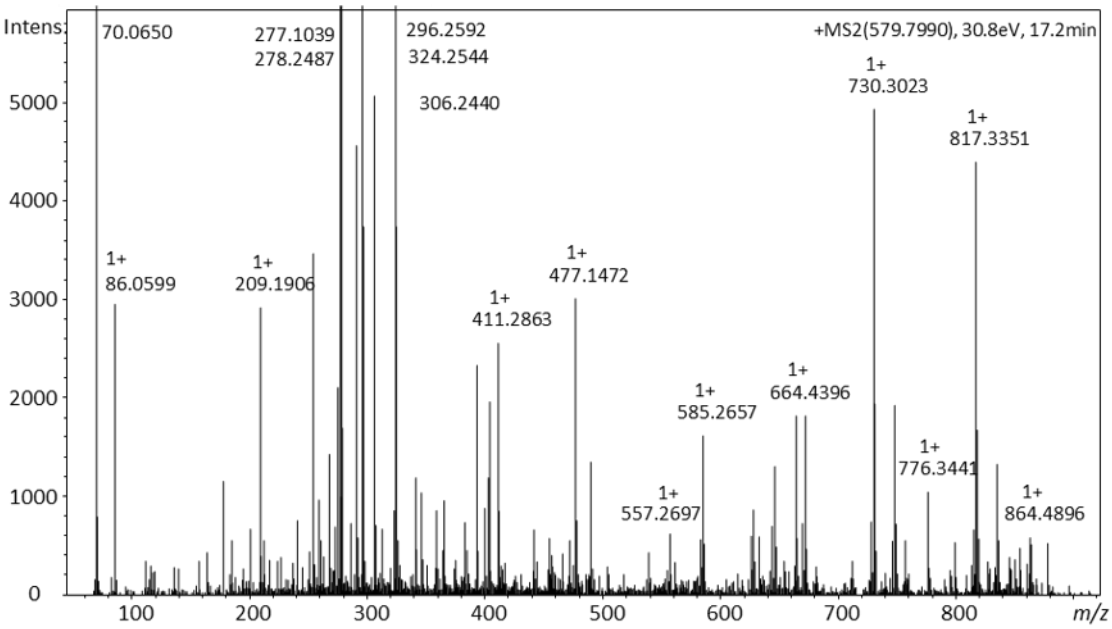

Fragment	Elemental composition	Ring and Double Bond (Rdb)	Theoretical Mass	Experimental Mass *(m/z)*	Δ_M [ppm]
$[M+2H]^{2+}$	$C_{50}H_{85}N_{11}O_{20}$	15	579.7981	579.7990	1.5
$[M+H]^{+}$	$C_{50}H_{84}N_{11}O_{20}$	15	1158.5889	1158.5882	-0.6
y_1	$C_5H_{10}NO_5$	2	164.0553	164.0551	-1.2
y_2	$C_{10}H_{17}N_2O_7$	4	277.1030	277.1039	3.3
y_3	$C_{13}H_{22}N_3O_9$	5	364.1351	364.1350	-0.1
y_4	$C_{17}H_{27}N_4O_{13}$	7	495.1569	495.1559	-2.1
y_4-H_2O	$C_{17}H_{25}N_4O_{12}$	8	477.1463	477.1472	1.7
y_5	$C_{23}H_{39}N_8O_{14}$	10	651.2586	651.2539	-7.2
y_6	$C_{28}H_{46}N_9O_{15}$	11	748.3108	748.3116	1.1
y_6-H_2O	$C_{28}H_{44}N_9O_{14}$	12	730.3002	730.3023	2.8
y_7	$C_{31}H_{51}N_{10}O_{17}$	13	835.3434	835.3468	4.1
y_7-H_2O	$C_{31}H_{49}N_{10}O_{16}$	14	817.3328	817.3351	2.8
FA-H_2O	$C_{14}H_{25}O$	3	209.1900	209.1906	1.5
b_1	$C_{19}H_{34}NO_3$	4	324.2533	324.2544	3.3
b_1-H_2O	$C_{19}H_{32}NO_2$	5	306.2428	306.2440	1.8

b_1-CO	$C_{18}H_{34}NO_2$	3	296.2584	296.2592	3.0
b_1-CO-H_2O	$C_{18}H_{32}NO$	4	278.2478	278.2487	2.9
b_2	$C_{22}H_{39}N_2O_5$	5	411.2859	411.2863	0.9
b_2-H_2O	$C_{22}H_{37}N_2O_4$	6	393.2748	393.2761	3.5
b_4	$C_{33}H_{58}N_7O_7$	9	664.4398	664.4396	-0.5
b_5	$C_{37}H_{63}N_8O_{11}$	11	795.4611	795.4621	1.3
b_6-H_2O	$C_{40}H_{66}N_9O_{12}$	13	864.4831	864.4896	7.5
y_7-CO_2-NH_2	$C_{30}H_{50}N_9O_{15}$	11	776.3426	776.3441	2.6
AA_2-AA_6	$C_{23}H_{37}N_8O_{10}$	10	585.2633	585.2657	4.1
AA_2-CO-AA_6	$C_{22}H_{37}N_8O_9$	9	557.2683	557.2697	2.5
AA_2-AA_5	$C_{18}H_{32}N_7O_9$	7	490.2256	490.2266	2.1
z_4-$C_2H_3O_3$	$C_{15}H_{22}N_3O_{10}$	7	404.1305	404.1313	3.2
Pyrr	C_4H_8N	2	70.0657	70.0650	-1.7
OH-Pyrr	C_4H_8NO	2	86.0600	86.0599	-1.5

Table VIII-4: MS^2 spectrum and fragment annotation of linear form of derivative 2 (d).

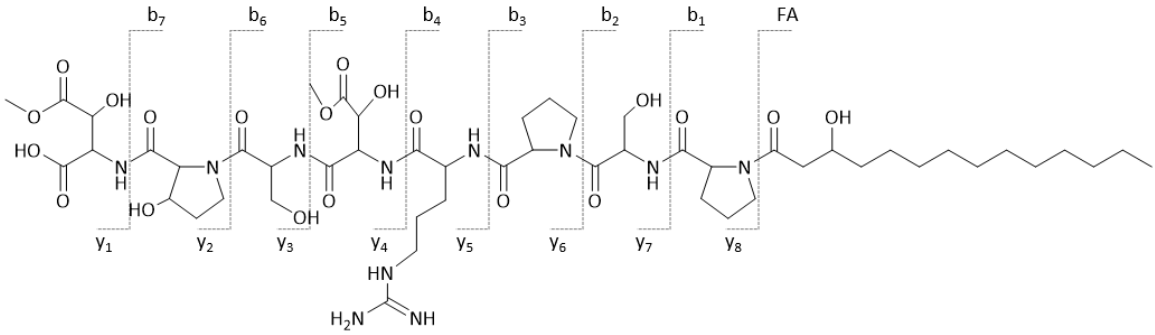

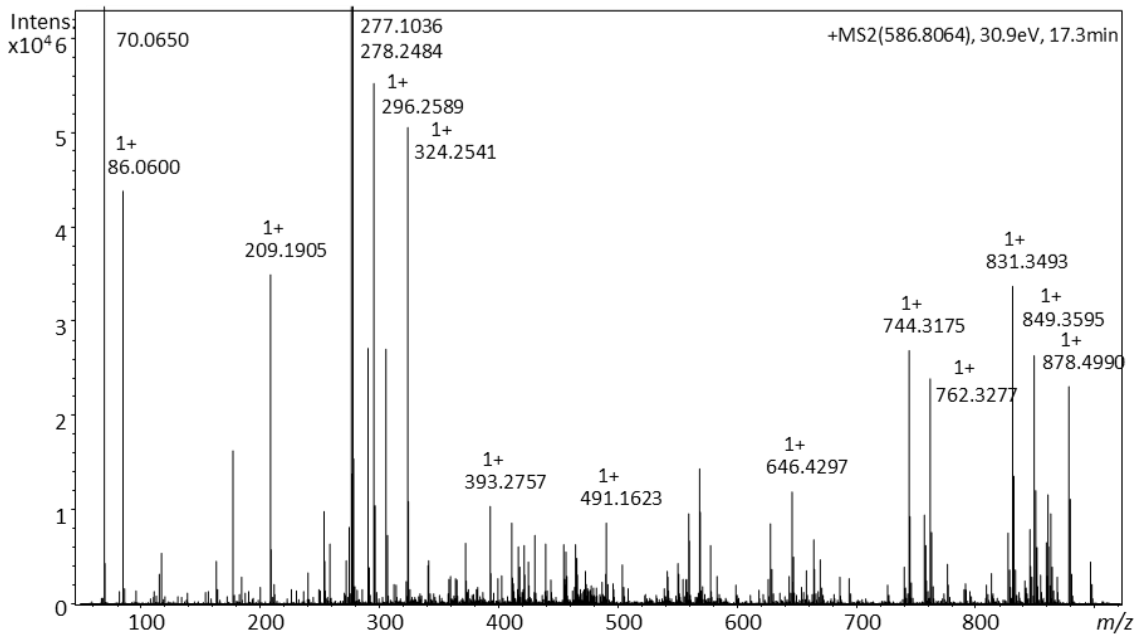

Fragment	Elemental composition	Ring and Double Bond (Rdb)	Theoretical Mass	Experimental Mass *(m/z)*	Δ_M [ppm]
$[M+2H]^{2+}$	$C_{51}H_{87}N_{11}O_{20}$	15	586.8059	586.8064	0.8
$[M+H]^{+}$	$C_{51}H_{86}N_{11}O_{20}$	15	1172.6045	1172.6051	0.5
M-H_2O	$C_{51}H_{84}N_{11}O_{19}$	16	1154.5945	1154.5981	3.1
M-2H_2O	$C_{51}H_{82}N_{11}O_{18}$	17	1136.5839	1136.5863	2.1
M-3H_2O	$C_{51}H_{80}N_{11}O_{17}$	18	1118.5734	1118.5753	1.7
M-4H_2O	$C_{51}H_{78}N_{11}O_{16}$	19	1100.5628	1100.5643	1.3
M-5H_2O	$C_{51}H_{76}N_{11}O_{15}$	20	1082.5522	1082.5553	2.8
M-6H_2O	$C_{51}H_{74}N_{11}O_{14}$	21	1064.5417	1064.5393	-2.2
M-FA-H_2O	$C_{37}H_{58}N_{11}O_{17}$	15	928.4012	928.4033	2.2
y_2	$C_{10}H_{17}N_2O_7$	4	277.1030	277.1036	2.0
y_3	$C_{13}H_{22}N_3O_9$	5	364.1351	364.1358	1.9
y_4	$C_{18}H_{29}N_4O_{13}$	7	509.1726	509.1737	2.1
y_4-H_2O	$C_{18}H_{27}N_4O_{12}$	8	491.1625	491.1623	-0.4
y_6	$C_{29}H_{48}N_9O_{15}$	11	762.3270	762.3280	1.3
y_6-H_2O	$C_{29}H_{46}N_9O_{14}$	12	744.3164	744.3175	1.5
y_7	$C_{32}H_{53}N_{10}O_{17}$	12	849.3590	849.3596	0.7
y_7-H_2O	$C_{32}H_{51}N_{10}O_{16}$	13	831.3485	831.3493	1.0
FA-H_2O	$C_{14}H_{25}O$	3	209.1900	209.1905	2.6
b_1	$C_{19}H_{34}NO_3$	4	324.2533	324.2541	2.4
b_1-H_2O	$C_{19}H_{32}NO_2$	5	306.2428	306.2433	1.8
b_1-CO	$C_{18}H_{34}NO_2$	3	296.2584	296.2589	1.6
b_1-CO-H_2O	$C_{18}H_{32}NO$	4	278.2478	278.2484	2.1
b_2	$C_{22}H_{39}N_2O_5$	5	411.2853	411.2862	2.0
b_2-H_2O	$C_{22}H_{37}N_2O_4$	6	393.2748	393.2757	2.2
b_4	$C_{33}H_{58}N_7O_7$	9	664.4392	664.4410	2.6
b_4-H_2O	$C_{33}H_{56}N_7O_6$	10	646.4287	646.4297	1.7
b_4-2H_2O	$C_{33}H_{54}N_7O_5$	11	628.4181	628.4188	1.1
b_5	$C_{38}H_{65}N_8O_{11}$	11	809.4773	809.4780	0.9
b_6	$C_{41}H_{70}N_9O_{13}$	12	896.5088	896.5099	1.3
b_6-H_2O	$C_{41}H_{68}N_9O_{12}$	13	878.4987	878.4990	0.3
b_6-2H_2O	$C_{41}H_{66}N_9O_{11}$	14	860.4882	860.4894	1.4
b_6-3H_2O	$C_{41}H_{64}N_9O_{10}$	15	842.4776	842.4781	0.6
b_7-CO-H_2O	$C_{45}H_{73}N_{10}O_{12}$	14	945.5409	945.5421	1.3
AA_2-AA_6	$C_{24}H_{39}N_8O_{10}$	10	599.2789	599.2796	1.1
AA_2-CO-AA_6	$C_{23}H_{39}N_8O_9$	9	571.2840	571.2852	2.1
AA_2-AA_5	$C_{19}H_{34}N_7O_9$	7	504.2418	504.2422	0.8
Pyrr	C_4H_8N	2	70.0651	70.0650	-1.4
OH-Pyrr	C_4H_8NO	2	86.0600	86.0600	0.0

Table VIII-5: MS^2 spectrum and fragment annotation of derivative 3 (e).

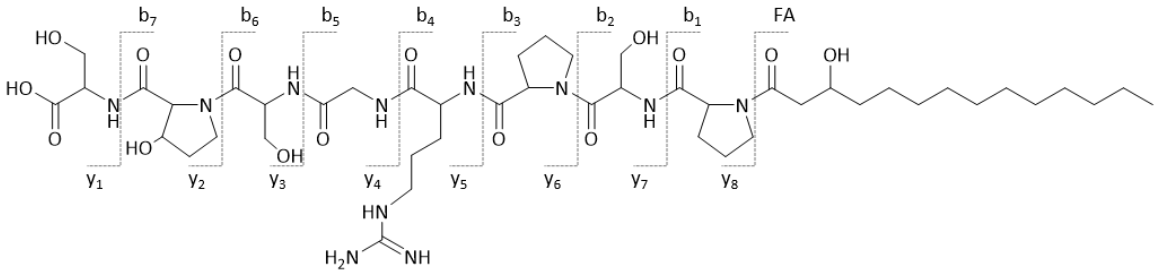

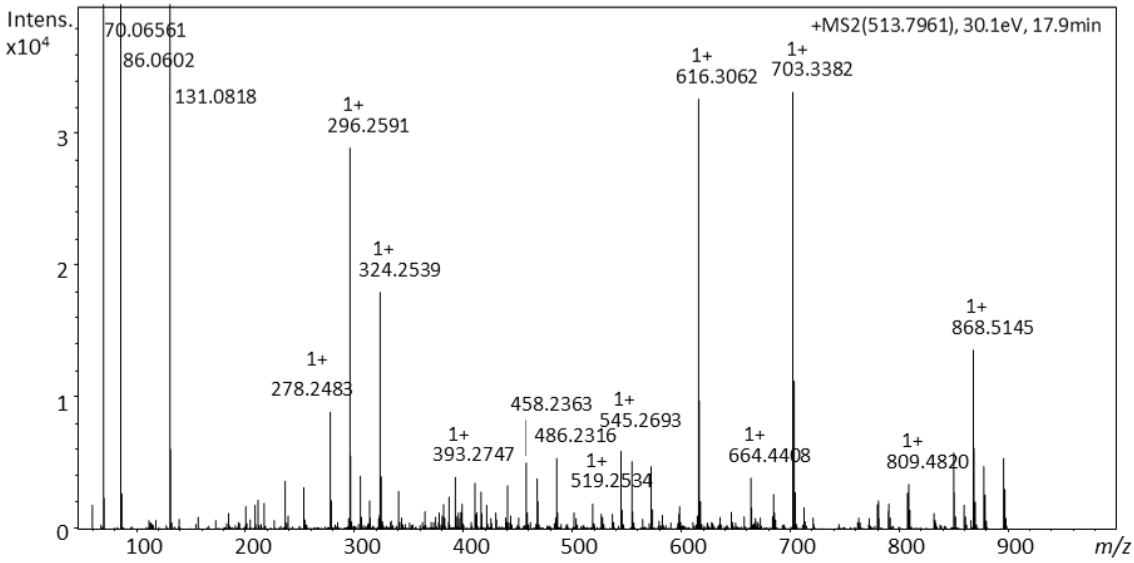

Fragment	Elemental composition	Ring and Double Bond (Rdb)	Theoretical Mass	Experimental Mass *(m/z)*	Δ_M [ppm]
$[M+2H]^{2+}$	$C_{46}H_{81}N_{11}O_{15}$	13	513.7951	513.7961	1.8
$[M+H]^{+}$	$C_{46}H_{80}N_{11}O_{15}$	13	1026.5830	1026.5836	0.6
y_1	$C_3H_8NO_3$	1	106.0504	106.0498	-0.5
y_2	$C_8H_{15}N_2O_5$	3	219.0981	219.0995	8.9
y_4	$C_{13}H_{23}N_4O_8$	5	363.1516	363.1521	3.0
y_5	$C_{19}H_{35}N_8O_9$	7	519.2522	519.2534	2.4
y_6	$C_{24}H_{42}N_9O_{10}$	9	616.3055	616.3062	2.1
y_7	$C_{27}H_{47}N_{10}O_{12}$	10	703.3369	703.3382	1.8
FA-H_2O	$C_{14}H_{25}O$	3	209.1900	209.1902	0.9
b_1	$C_{19}H_{34}NO_3$	4	324.2533	324.2539	1.6
b_1-H_2O	$C_{19}H_{32}NO_2$	5	306.2428	306.2437	3.0
b_1-CO	$C_{18}H_{34}NO_2$	3	296.2584	296.2591	2.5
b_1-CO-H_2O	$C_{18}H_{32}NO$	4	278.2478	278.2483	1.5
b_2	$C_{22}H_{39}N_2O_5$	5	411.2853	411.2856	0.6
b_2-H_2O	$C_{22}H_{37}N_2O_4$	6	393.2748	393.2747	-0.2
b_4	$C_{33}H_{58}N_7O_7$	9	664.4392	664.4408	2.4
b_5	$C_{35}H_{61}N_8O_8$	10	721.4607	721.4619	1.7
b_6	$C_{38}H_{66}N_9O_{10}$	11	808.4927	808.4936	1.1

b_6-CO	$C_{40}H_{62}N_9O_{10}$	10	780.4983	780.4975	-1.0
b_7-3H_2O	$C_{43}H_{68}N_{10}O_9$	16	868.5171	868.5145	-3.0
b_7-4H_2O	$C_{43}H_{66}N_{10}O_8$	17	850.5065	850.5050	-1.7
b_8-4H_2O-CH_5N_3	$C_{45}H_{68}N_8O_{11}$	15	896.5008	896.5096	9.8
AA_1-OH-AA_5-NH	$C_{19}H_{32}N_7O_8$	8	486.2307	486.2316	1.9
AA_1-CO_2-AA_5-NH	$C_{18}H_{32}N_7O_7$	7	458.2358	458.2363	1.1
AA_1-AA_6-NH-CH_4N_3	$C_{23}H_{39}N_5O_{10}$	6	545.2697	545.2693	-0.7
AA_1-AA_6-C_2H_5N	$C_{22}H_{37}N_8O_{10}$	9	573.2627	573.2633	1.1
AA_1-AA_6-C_2H_5N-H_2O	$C_{22}H_{35}N_8O_9$	10	555.2522	555.2535	2.3
OH-Pro+NH	$C_5H_{11}N_2O_2$	2	131.0815	131.0818	2.6
Pyrr	C_4H_8N	2	70.0651	70.0651	0.0
OH-Pyrr	C_4H_8NO	2	86.0600	86.0602	1.4

Table VIII-6: MS^2 spectrum and fragment annotation of derivative 4.

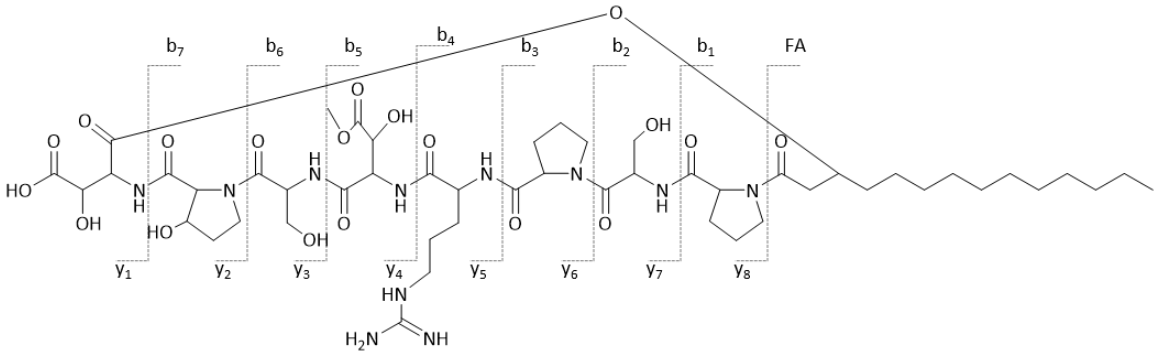

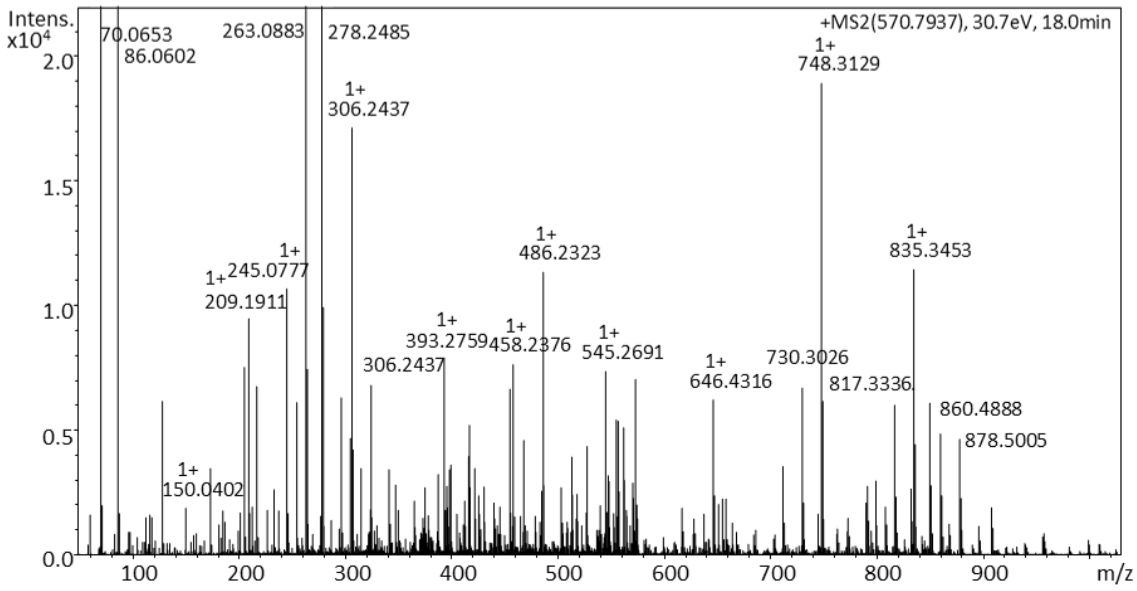

Fragment	Elemental composition	Ring and Double Bond (Rdb)	Theoretical Mass	Experimental Mass *(m/z)*	Δ_M [ppm]
$[M+2H]^{2+}$	$C_{50}H_{83}N_{11}O_{19}$	16	570.7928	570.7937	1.5
$[M+H]^+$	$C_{50}H_{82}N_{11}O_{19}$	16	1140.5783	1140.5789	0.5

y_1	$C_4H_8NO_5$	2	150.0397	150.0402	3.4
y_2	$C_9H_{15}N_2O_7$	4	263.0874	263.0883	3.6
y_2-H_2O	$C_9H_{13}N_2O_6$	5	245.0768	245.0777	3.6
y_3	$C_{12}H_{20}N_3O_9$	5	350.1194	350.1206	3.4
y_5	$C_{23}H_{39}N_8O_{14}$	9	651.2580	651.2596	2.4
y_6	$C_{28}H_{46}N_9O_{15}$	11	748.3113	748.3129	2.1
y_6-H_2O	$C_{28}H_{44}N_9O_{14}$	12	730.3008	730.3026	2.5
y_6-$2H_2O$	$C_{28}H_{42}N_9O_{13}$	13	712.2902	712.2923	2.9
y_7	$C_{31}H_{51}N_{10}O_{17}$	12	835.3434	835.3453	2.3
y_7-H_2O	$C_{31}H_{49}N_{10}O_{16}$	13	817.3323	817.3336	1.6
y_8	$C_{36}H_{58}N_{11}O_{18}$	14	932.3956	932.3962	0.6
FA-H_2O	$C_{14}H_{25}O$	3	209.1900	209.1911	5.4
b_1	$C_{19}H_{34}NO_3$	4	324.2533	324.2544	3.4
b_1-H_2O	$C_{19}H_{32}NO_2$	5	306.2428	306.2437	3.2
b_1-CO	$C_{18}H_{34}NO_2$	3	296.2584	296.2589	4.8
b_1-CO-H_2O	$C_{18}H_{32}NO$	4	278.2478	278.2488	3.5
b_2	$C_{22}H_{39}N_2O_5$	5	411.2859	411.2854	-0.2
b_2-H_2O	$C_{22}H_{37}N_2O_4$	6	393.2748	393.2759	3.0
b_4	$C_{33}H_{58}N_7O_7$	9	664.4398	664.4390	-0.4
b_4-H_2O	$C_{33}H_{56}N_7O_6$	10	646.4292	646.4316	3.7
b_6	$C_{41}H_{70}N_9O_{13}$	12	896.5093	896.5118	2.8
b_6-H_2O	$C_{41}H_{68}N_9O_{12}$	13	878.4987	878.5005	2.0
b_6-$2H_2O$	$C_{41}H_{66}N_9O_{11}$	14	860.4876	860.4888	1.4
AA_3-AA_6	$C_{19}H_{32}N_7O_8$	8	486.2307	486.2323	3.3
AA_3-CO-AA_6	$C_{18}H_{32}N_7O_7$	7	458.2358	458.2376	4.0
AA_3-CO-AA_7	$C_{21}H_{37}N_8O_9$	8	545.2683	545.2691	2.3
Pro	C_4H_8N	2	70.0651	70.0653	2.2
OH-Pyrr	C_4H_8NO	2	86.0600	86.0602	2.4

Table VIII-7: MS^2 spectrum and fragment annotation of derivative 5.

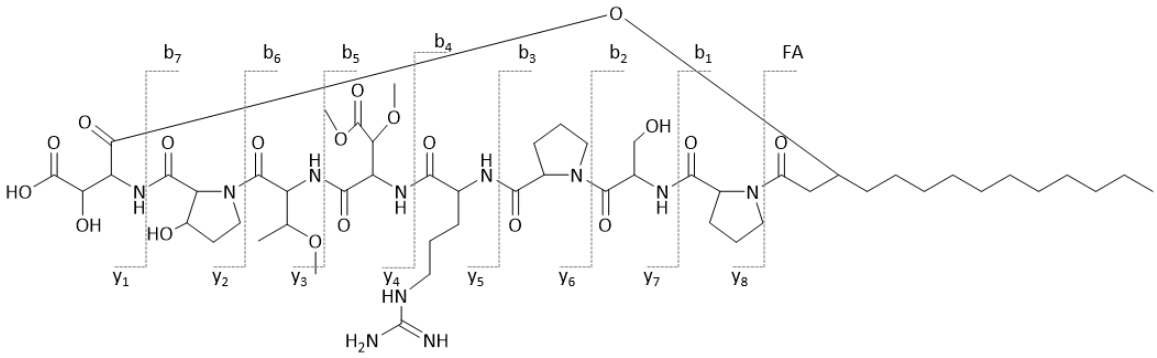

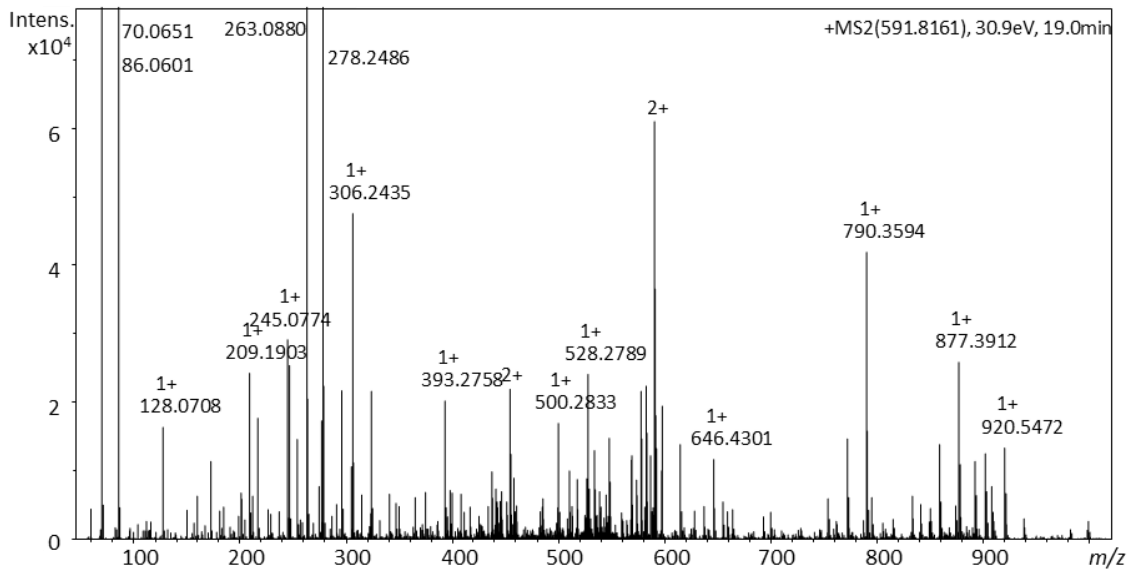

Fragment	Elemental composition	Ring and Double Bond (Rdb)	Theoretical Mass	Experimental Mass *(m/z)*	Δ_M [ppm]
$[M+2H]^{2+}$	$C_{53}H_{89}N_{11}O_{19}$	16	591.8163	591.8161	-0.3
$[M+H]^{+}$	$C_{53}H_{88}N_{11}O_{19}$	16	1182.6252	1182.6234	-1.6
M-H_2O	$C_{53}H_{86}N_{11}O_{18}$	17	1164.6152	1164.6177	2.1
M-2H_2O	$C_{53}H_{84}N_{11}O_{17}$	18	1146.6047	1146.6069	1.9
M-CO	$C_{52}H_{88}N_{11}O_{18}$	15	1154.6309	1154.6335	2.2
M-CO-H_2O	$C_{52}H_{86}N_{11}O_{17}$	16	1136.6203	1136.6227	2.1
M-Ser	$C_{50}H_{83}N_{10}O_{17}$	15	1095.5938	1095.5965	2.5
M-Ser-H_2O	$C_{50}H_{81}N_{10}O_{16}$	16	1077.5832	1077.5861	2.7
M-Ser-CO	$C_{49}H_{83}N_{10}O_{16}$	14	1067.5989	1067.6005	1.5
y_2	$C_9H_{15}N_2O_7$	4	263.0874	263.0880	2.5
y_2-H_2O	$C_9H_{13}N_2O_6$	5	245.0768	245.0774	2.3
y_6	$C_{31}H_{52}N_9O_{15}$	11	790.3577	790.3590	2.1
y_6-H_2O	$C_{31}H_{50}N_9O_{14}$	12	772.3472	772.3481	1.6
y_6-2H_2O	$C_{31}H_{48}N_9O_{13}$	13	754.3366	754.3374	2.8
y_7	$C_{34}H_{57}N_{10}O_{17}$	12	877.3898	877.3912	1.6
y_7-H_2O	$C_{34}H_{55}N_{10}O_{16}$	13	859.3792	859.3808	2.2
y_8	$C_{39}H_{64}N_{11}O_{18}$	14	974.4425	974.4436	1.1
FA-H_2O	$C_{14}H_{25}O$	3	209.1900	209.1903	1.7
b_1	$C_{19}H_{34}NO_3$	4	324.2533	324.2544	3.4
b_1-H_2O	$C_{19}H_{32}NO_2$	5	306.2428	306.2435	2.4
b_1-CO	$C_{18}H_{34}NO_2$	3	296.2584	296.2593	3.1
b_1-CO-H_2O	$C_{18}H_{32}NO$	4	278.2484	278.2486	2.6
b_2	$C_{22}H_{39}N_2O_5$	5	411.2859	411.2866	2.6
b_2-H_2O	$C_{22}H_{37}N_2O_4$	6	393.2748	393.2758	2.6
b_4	$C_{33}H_{58}N_7O_7$	9	664.4392	664.4402	1.5

b_4-H_2O	$C_{33}H_{56}N_7O_6$	10	646.4287	646.4301	2.2
b_4-$2H_2O$	$C_{33}H_{54}N_7O_5$	11	628.4181	628.4198	2.8
b_6	$C_{44}H_{76}N_9O_{13}$	12	938.5557	938.5555	-0.2
b_6-H_2O	$C_{44}H_{74}N_9O_{12}$	13	920.5451	920.5472	2.2
b_6-$2H_2O$	$C_{44}H_{72}N_9O_{11}$	14	902.5351	902.5368	1.8
b_6-CO-H_2O	$C_{43}H_{74}N_9O_{11}$	12	892.5502	892.5521	2.1
AA_3-AA_7	$C_{25}H_{43}N_8O_{10}$	9	615.3097	615.3112	2.5
AA_3-CO-AA_7	$C_{24}H_{43}N_8O_9$	8	587.3148	587.3157	1.6
AA_3-AA_6	$C_{22}H_{38}N_7O_8$	8	528.2776	528.2789	2.4
AA_3-CO-AA_6	$C_{21}H_{38}N_7O_7$	7	500.2827	500.2833	1.2
AA_4-AA_8	$C_{25}H_{41}N_8O_9$	10	597.2991	597.3001	1.6
Thr-Me	$C_6H_{10}NO_2$	3	128.0706	128.0708	1.7
Pyrr	C_4H_8N	2	70.0651	70.0651	0.0
OH-Pyrr	C_4H_8NO	2	86.0606	86.0601	-1.2

Table VIII-8: MS^2 spectrum and fragment annotation of derivative 6.

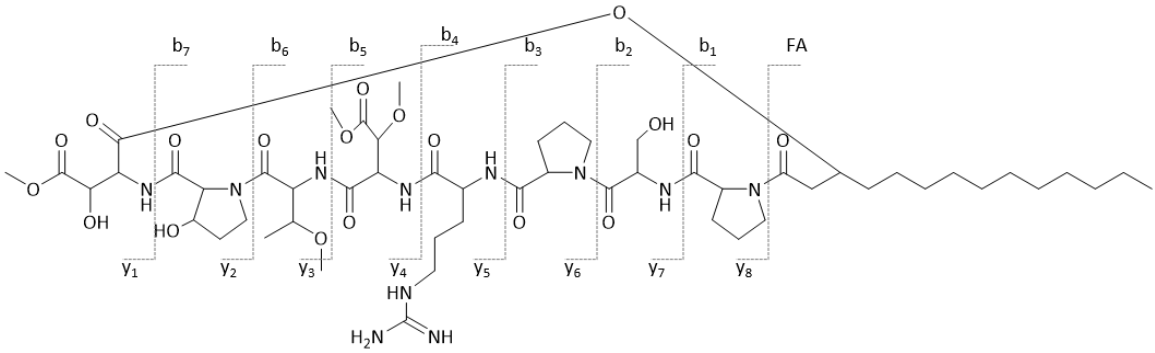

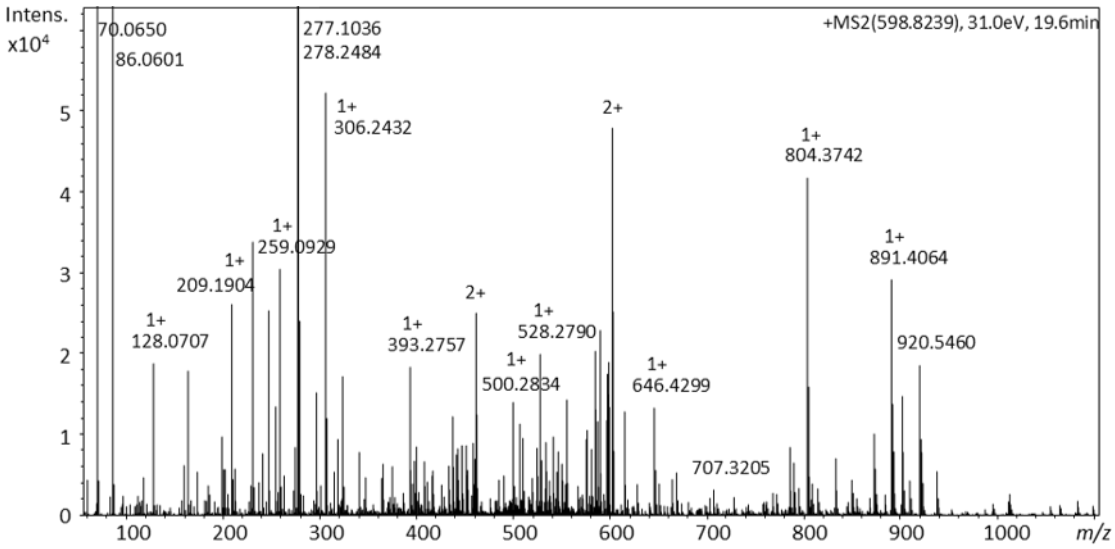

Fragment	Elemental composition	Ring and Double Bond (Rdb)	Theoretical Mass	Experimental Mass *(m/z)*	Δ_M [ppm]
$[M+2H]^{2+}$	$C_{54}H_{91}N_{11}O_{19}$	16	598.8241	598.8239	-0.3

$[M+H]^+$	$C_{54}H_{90}N_{11}O_{19}$	16	1196.6409	1196.6391	-1.5
M-H_2O	$C_{54}H_{88}N_{11}O_{18}$	17	1178.6309	1178.6339	2.5
M-CO	$C_{53}H_{90}N_{11}O_{18}$	15	1168.6465	1168.6489	2.0
M-Ser	$C_{51}H_{85}N_{10}O_{17}$	15	1109.6094	1109.6123	2.6
M-Ser-H_2O	$C_{51}H_{83}N_{10}O_{16}$	16	1091.5989	1091.6023	3.1
M-Ser-CO	$C_{50}H_{85}N_{10}O_{16}$	14	1081.6145	1081.6149	0.4
M-Ser-Pro	$C_{46}H_{78}N_9O_{16}$	13	1012.5567	1012.5587	1.9
y_1	$C_5H_{10}NO_5$	2	164.0553	164.0556	1.6
y_2	$C_{10}H_{17}N_2O_7$	4	277.1030	277.1036	2.0
y_2-H_2O	$C_{10}H_{15}N_2O_6$	5	259.0925	259.0929	1.7
y_5	$C_{27}H_{47}N_8O_{14}$	9	707.3206	707.3205	-0.2
y_6	$C_{32}H_{54}N_9O_{15}$	11	804.3734	804.3742	1.0
y_6-H_2O	$C_{32}H_{52}N_9O_{14}$	12	786.3628	786.3648	2.6
y_7	$C_{35}H_{59}N_{10}O_{17}$	12	891.4054	891.4064	1.1
y_7-H_2O	$C_{31}H_{49}N_{10}O_{16}$	13	873.3949	873.3954	0.7
FA-H_2O	$C_{14}H_{25}O$	3	209.1900	209.1904	2.1
b_1	$C_{19}H_{34}NO_3$	4	324.2533	324.2541	2.3
b_1-H_2O	$C_{19}H_{32}NO_2$	5	306.2428	306.2432	1.5
b_1-CO	$C_{18}H_{34}NO_2$	3	296.2584	296.2593	2.8
b_1-CO-H_2O	$C_{18}H_{32}NO$	4	278.2478	278.2484	2.0
b_2	$C_{22}H_{39}N_2O_5$	5	411.2853	411.2857	0.8
b_2-H_2O	$C_{22}H_{37}N_2O_4$	6	393.2748	393.2757	2.2
b_4	$C_{33}H_{58}N_7O_7$	9	664.4392	664.4396	0.6
b_4-H_2O	$C_{33}H_{56}N_7O_6$	10	646.4287	646.4299	1.9
b_4-$2H_2O$	$C_{33}H_{54}N_7O_5$	11	628.4181	628.4190	1.4
b_6	$C_{44}H_{76}N_9O_{13}$	12	938.5557	938.5571	1.5
b_6-H_2O	$C_{44}H_{74}N_9O_{12}$	13	920.5451	920.5460	1.0
b_6-$2H_2O$	$C_{44}H_{72}N_9O_{11}$	14	902.5346	902.5361	1.6
b_6-$3H_2O$	$C_{44}H_{70}N_9O_{10}$	15	884.5246	884.5239	-0.2
b_6-CO-H_2O	$C_{43}H_{74}N_9O_{11}$	12	892.5502	892.5512	1.1
b_6-CO-$2H_2O$	$C_{43}H_{72}N_9O_{10}$	13	874.5397	874.5402	0.6
b_7-H_2O	$C_{49}H_{81}N_{10}O_{14}$	15	1033.5934	1033.5964	2.9
AA_3-AA_7	$C_{25}H_{43}N_8O_{10}$	9	615.3097	615.3106	1.5
AA_3-CO-AA_7	$C_{24}H_{43}N_8O_9$	8	587.3148	587.3158	1.9
AA_3-AA_6	$C_{22}H_{38}N_7O_8$	8	528.2782	528.2790	1.5
AA_3-CO-AA_6	$C_{21}H_{38}N_7O_7$	7	500.2827	500.2834	1.4
Thr-Me	$C_6H_{10}NO_2$	3	128.0706	128.0707	0.7
Pro	C_4H_8N	2	70.0651	70.0650	-1.2
OH-Pro	C_4H_8NO	2	86.0600	86.0601	0.7

Table VIII-9: MS^2 spectrum and fragment annotation of derivative 7.

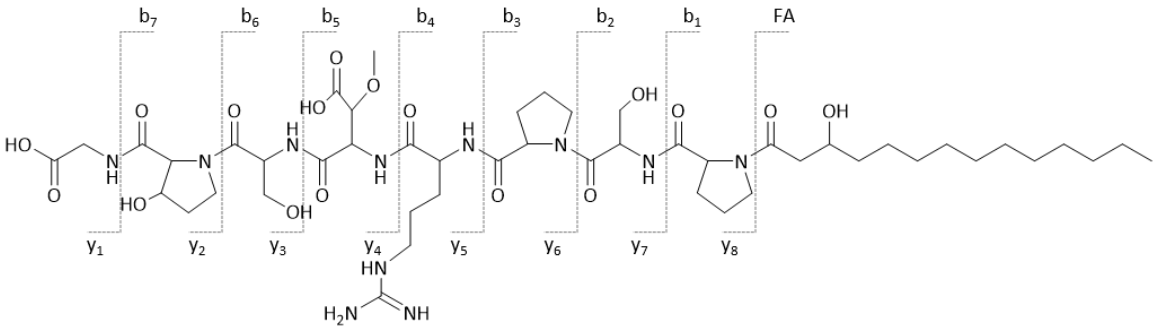

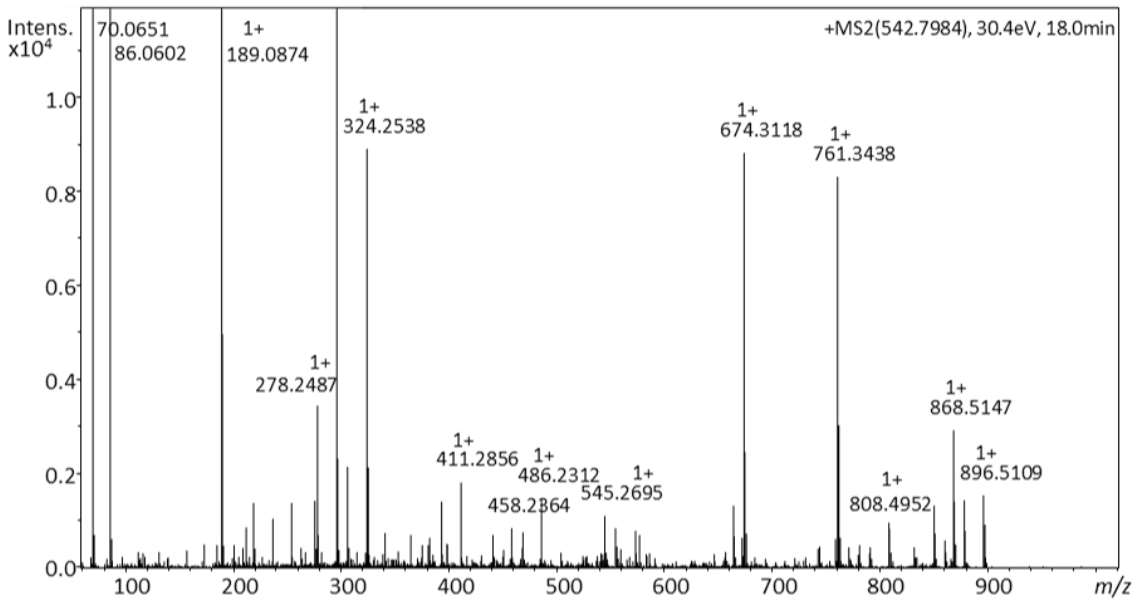

Fragment	Elemental composition	Ring and Double Bond (Rdb)	Theoretical Mass	Experimental Mass *(m/z)*	Δ_M [ppm]
$[M+2H]^{2+}$	$C_{48}H_{83}N_{11}O_{17}$	14	542.7979	542.7984	0.2
$[M+H]^{+}$	$C_{48}H_{82}N_{11}O_{17}$	14	1084.5885	1084.5881	-0.3
Y_2	$C_7H_{13}N_2O_4$	3	189.0870	189.0874	2.1
Y_3	$C_{10}H_{18}N_3O_6$	4	276.1190	276.1196	2.0
Y_5	$C_{21}H_{37}N_8O_{11}$	8	577.2582	577.2604	3.8
Y_6	$C_{26}H_{44}N_9O_{12}$	10	674.3104	674.3118	2.1
Y_7	$C_{29}H_{49}N_{10}O_{14}$	11	761.3424	761.3438	1.8
FA-H_2O	$C_{14}H_{25}O$	3	209.1900	209.1904	2.0
B_1	$C_{19}H_{34}NO_3$	4	324.2533	324.2538	1.5
B_1-H_2O	$C_{19}H_{32}NO_2$	5	306.2428	306.2435	2.5
B_1-CO	$C_{18}H_{34}NO_2$	3	296.2584	296.2591	2.5
B_1-CO-H_2O	$C_{18}H_{32}NO$	4	278.2487	278.2487	0.0
B_2	$C_{22}H_{39}N_2O_5$	5	411.2853	411.2856	0.7
B_2-H_2O	$C_{22}H_{37}N_2O_4$	6	393.2748	393.2756	2.0
B_4	$C_{33}H_{58}N_7O_7$	9	664.4398	664.4409	1.6
B_5	$C_{38}H_{65}N_8O_{11}$	11	809.4773	809.4801	3.5

B_5-CO	$C_{37}H_{65}N_8O_{10}$	10	781.4818	781.4827	1.1
B_6	$C_{41}H_{70}N_9O_{13}$	12	896.5093	896.5109	1.8
B_6-H_2O	$C_{41}H_{68}N_9O_{12}$	13	878.4982	878.4994	1.4
B_6-CO	$C_{40}H_{70}N_9O_{12}$	11	868.5138	868.5147	1.0
B_6-CO-H_2O	$C_{40}H_{68}N_9O_{11}$	12	850.5038	850.5037	-0.1
AA_4-AA_7	$C_{19}H_{32}N_7O_8$	8	486.2307	486.2312	3.8
AA_4-CO-AA_7	$C_{18}H_{32}N_7O_7$	7	458.2358	458.2364	1.4
AA_3-CO-AA_7	$C_{21}H_{37}N_8O_9$	8	545.2678	545.2695	3.2
Pyrr	C_4H_8N	2	70.0651	70.0651	0.0
OH-Pyrr	C_4H_8NO	2	86.0600	86.0602	2.0

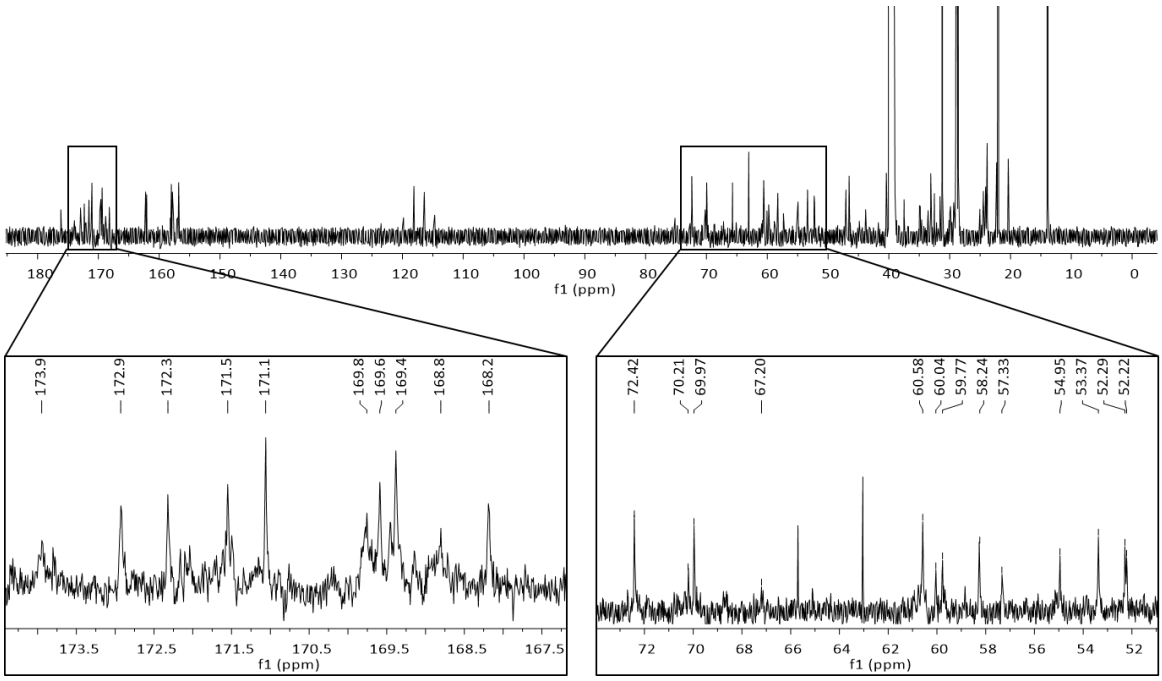

Figure VIII-1: ^{13}C NMR spectrum of empedopeptin in d_6-DMSO (101 MHz, 308 K).

Overview about the ^{13}C NMR spectrum of empedopeptin (top) and detail region of the carbonyl region (167 – 174 ppm) and the α-proton region (52 – 72 ppm) (bottom).

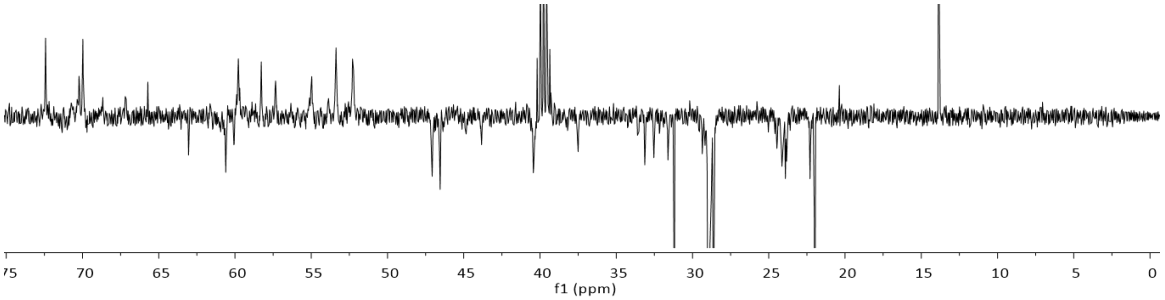

Figure VIII-2: DEPT135 NMR spectrum of empedopeptin in d_6-DMSO (101 MHz, 308 K).

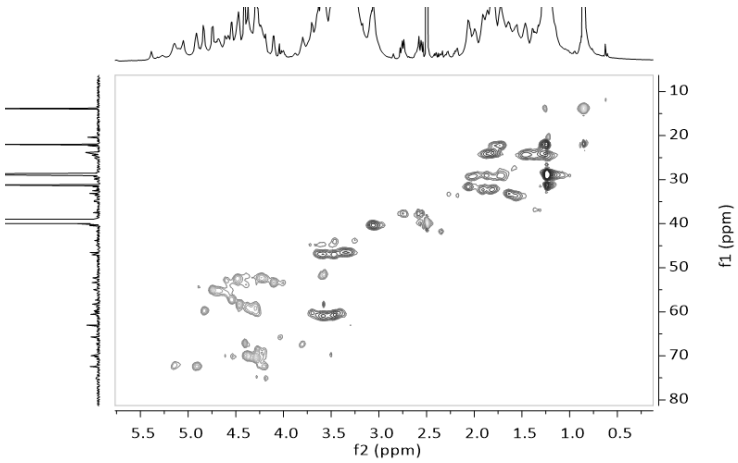

Figure VIII-3: ^{1}H-^{13}C HSQC spectrum of empedopeptin in d_6-DMSO (700 MHz, 308 K).

The edited version showed CH and CH_3 peaks in light grey and CH_2 peaks in dark grey.

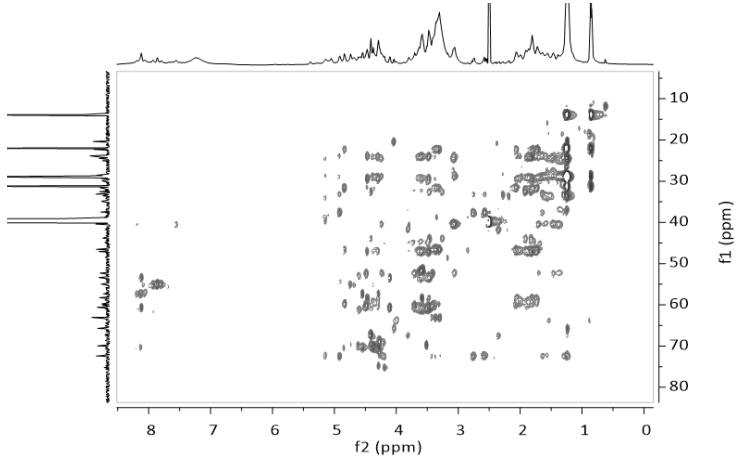

Figure VIII-4: ^{1}H-^{13}C HSQC-TOCSY spectrum of empedopeptin in d_6-DMSO (700 MHz, 308 K).

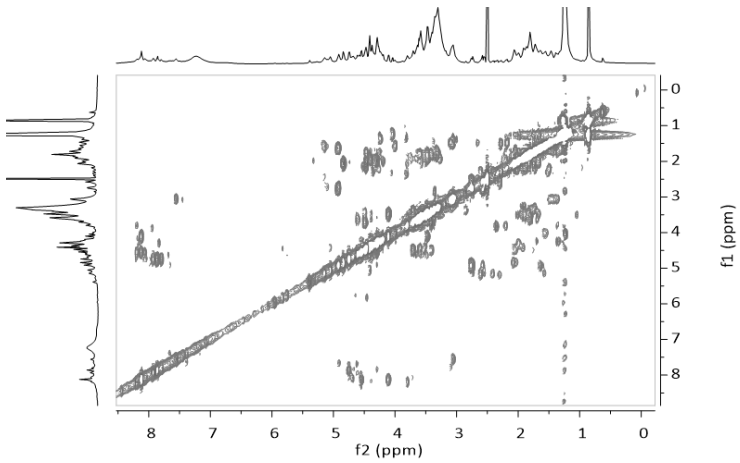

Figure VIII-5: ^{1}H-^{1}H COSY spectrum of empedopeptin in d_6-DMSO (700 MHz, 308 K).

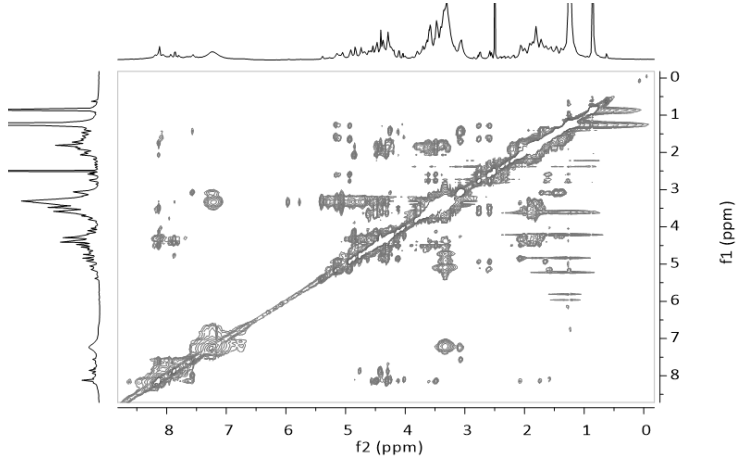

Figure VIII-6: ^{1}H-^{1}H NOESY spectrum of empedopeptin in d_6-DMSO (700 MHz, 308 K).

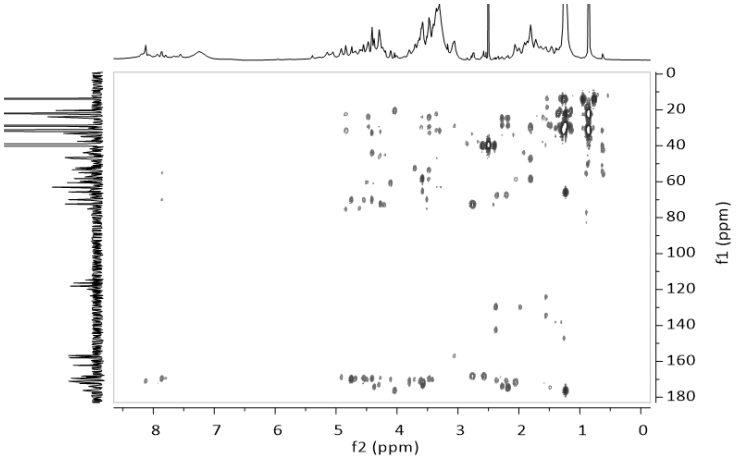

Figure VIII-7: ^{1}H-^{13}C HMBC spectrum of empedopeptin in d_6-DMSO (700 MHz, 308 K).

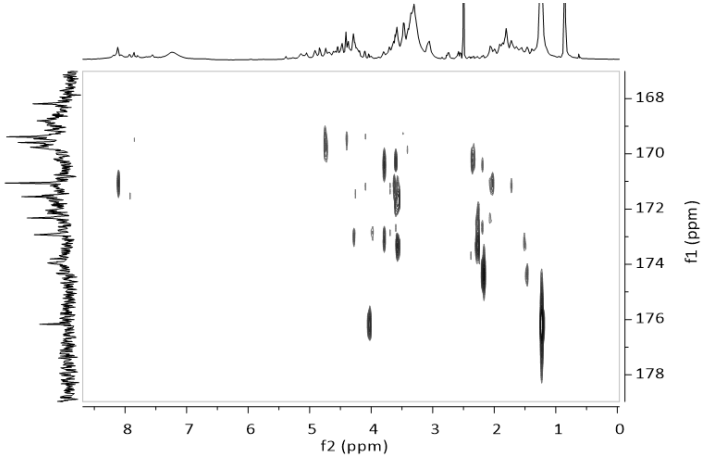

Figure VIII-8: ^{1}H-^{13}C band selective HMBC spectrum of empedopeptin in d_6-DMSO (700 MHz, 308 K).

The band selective HMBC spectrum was performed in the region of 160 – 190 ppm.

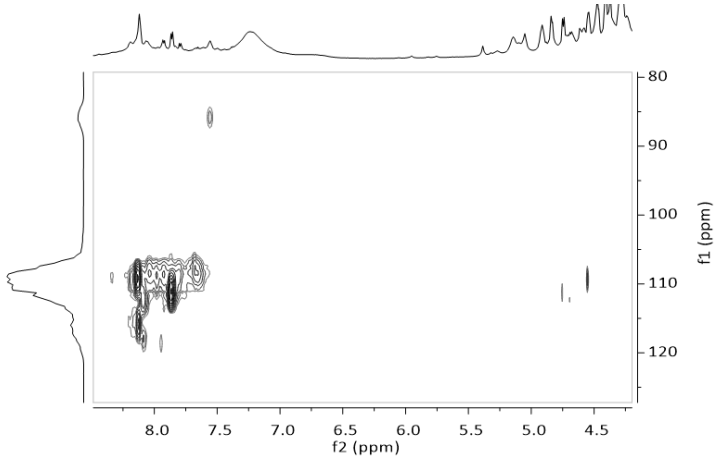

Figure VIII-9: ^{1}H-^{15}N HSQC spectrum of empedopeptin in d_6-DMSO (700 MHz, 308 K).

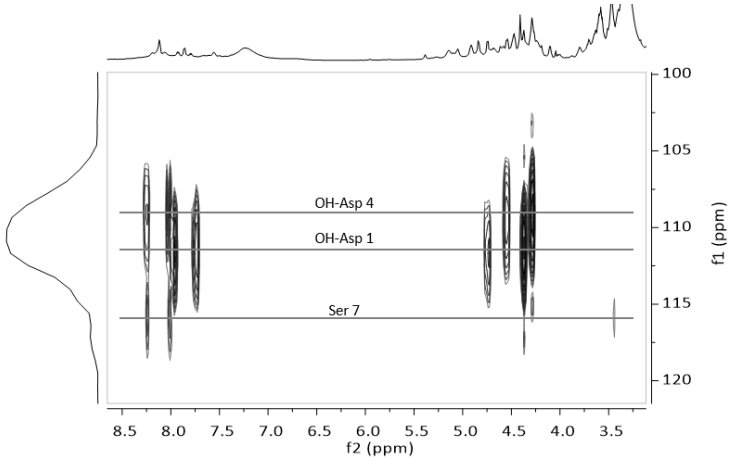

Figure VIII-10: ^{1}H-^{15}N HMBC spectrum of empedopeptin in d_6-DMSO (700 MHz, 308 K).

Horizontal lines indicate spin systems of amino acids.

Table VIII-10: TE proteins used for the phylogenetic analysis.

Abbreviation	Cluster	Strain
Acn	Actinomycin	*Streptomyces chrysomallus* ATCC 11523
Arf	Arthrofactin	*Pseudomonas* sp. MIS38
Ban	Bananamide	*Pseudomonas fluorescens* BW11P2
Bmy	Bacillomycin	*Bacillus velezensis* FZB42
CDA	Calcium Dependent Antibiotic	*Streptomyces coelicolor* A3
Dapto	Daptomycin	*Strepotmyces roseosporus* NRRL 11379
DhbF	Bacillibactin	*Bacillus velezensis* FZB42
Emp	Empedopeptin	*Massilia* sp. ATCC 31962
End	Enduracidin	*Streptomyces fungicidicus* ATCC 21013
Etl	Entolysin	*Pseudomonas entomophila* L48
Fgy	Fengycin	*Bacillus velezensis* FZB42
Fri	Friulimycin	*Actinoplanes friuliensis* HAG010964
Grs	Gramicidin S	*Brevibacillus brevis* NBRC 100599
Hrm	Hormaomycin	*Streptomyces griseoflavus* W-384
Itu	Iturin	*Bacillus subtilis* RB14
Lic	Lichenysin	*Bacillus licheniformis* DSM13
Les	Lysocin	*Lysobacter* sp. RH2180-5
Lyb	Lysobactin	*Lysobacter* sp. ATCC 53042
Mass	Massetolide	*Pseudomonas fluorescens* SS101
Mch	Myxochromide	*Stigmantella aurantiaca* DW4/3-1
Myc	Mycosubtilin	*Bacillus subtilis* subspec. s*pizizenii* ATCC 6633
Orf	Orfamide	*Pseudomonas* sp. CMR5c
Plus	Plusbacin	*Lysobacter firmicutimachus* PB-6250
Pmx	Polymyxin	*Paenibacillus polymyxa* PKB1
Pso	Putisolvin	*Pseudomonas putida* PCL 1445
Srf	Surfactin	*Bacillus velezensis* FZB42
Syr	Syringamycin	*Pseudomonas syringae* pv. *syringae* B301D
Syp	Syringapeptin	*Pseudomonas syringae* pv. *syringae* B301D
Tha	Thanamycin	*Pseudomonas* sp. SHC52
Tpp	Tripropeptin	*Lysobacter* sp. BMK333-48F3
WAP	WAP-8294A2	*Lysobacter enzymogenes* OH11
WLIP	White line-inducing principle	*Pseudomonas putida* RW10S2

NMR Analysis of Tripropeptin C

Table VIII-11: NMR spectroscopic data of tripropeptin C in d_6-DMSO (700 MHz, 298 K).

residue	position	$\delta_{C/N}$[a]	δ_H (J in Hz)[b]	residue	position	$\delta_{C/N}$[a]	δ_H (J in Hz)[b]
3-HMTDA	CO	169.7		**OH-Asp 4**	α	58.1	4.37, m
	2	39.0	2.34 (d, 13.2)		β	71.2	3.89, m
			2.81 (t, 13.2)		α-CO	170.6	
	3	72.9	4.94 (brs)		α-NH	111.1	7.96
	4	32.9	1.59, m		β-CO	173.2	
			1.67, m		β-OH		n.d.
	5-11	28.97	1.24 – 1.29		OH		n.d.
		29.04		**Arg 5**	α	52.1	4.26
		29.1			β	29.0	1.67
		29.4			γ	24.6	1.33
	12	38.5	1.13, m				1.37
	13	27.4	1.49, m		δ	40.3	3.06
	14	22.6	0.84, d, 6.6		ε	156.9	
	15	22.6	0.84, d, 6.6		α-CO	171.1	
OH-Asp 1	α	54.9	4.56,d		α-NH	n.d.	n.d.
	β	70.6	4.22, brs		δ-NH	85.3	7.89, brs
	α-CO	170.1			ε-NH	74.0	6.92 – 7.46
	α-NH	111.5	7.78, d, 8.8	**Pro 6**	α	59.9	4.83, t, 5.3
	β-CO	174.0			β	31.6	2.09, m
	β-OH		n.d.		γ	22.7	1.72
	OH		n.d.				1.83
OH-Pro 2	α	67.0	4.40		δ	46.9	3.33, m
	β	69.4	4.39		α-CO	172.4	
	γ	32.6	1.81		α-N	n.d.	
			1.86	**Pro 7**	α	57.7	4.26
	δ	43.9	3.23		β	28.8	1.77
			3.45		γ	25.1	1.69
	β-OH		5.08				2.00
	α-CO	169.5			δ	47.3	3.56
	α-N	n.d.					3.69
Ser 3	α	52.18	4.52		α-CO	171.3	
	β	61.0	3.48		α-N	n.d.	
			3.63	**Thr 8**	α	55.8	4.70
	β-OH		n.d.		β	65.8	3.86,m
	α-CO	170.6			γ	18.6	0.96,d, 6.2
	α-NH	112.6	8.25, brs		β -OH		4.63
					α-CO	168.3	
					α-NH	120.5	8.18, d, 8.9

3-HMTDA: 3-hydroxy-13-methyltetradecanoic acid. [a] Recorded at 176/101 MHz for ^{13}C and ^{15}N values were extracted from the corresponding ^{1}H-^{15}N HSQC NMR spectrum. Multiplicity determined by an edited ^{1}H-^{13}C HSQC NMR experiment. [b] Recorded at 700/400 MHz.

Table VIII-12: A and C domains used for the phylogenetic analyses.

Abbreviation	Cluster	Amino acid sequence	Strain
Arf	Arthrofactin	Leu-Asp-Thr-Leu-Leu-Ser-Leu-Ser-Ile-Ile-Asp (11 AA)	*Pseudomonas* sp. MIS38
Ban	Bananamide	Leu-Asp-Thr-Leu-Leu-Gln-Leu-Leu-Ile (8 AA)	*Pseudomonas fluorescens* BW11P2
Cif	Cichofactin	Leu-Leu-Gln-Leu-Gln-Val-Leu-Leu (8 AA)	*Pseudomonas cichorii* SF1-54
Etl	Entolysin	Xle-Glu-Gln-Val-Xle-Gln-Val-Xle-Gln-Ser-Val-Xle-Ser-Xle (14 AA)	*Pseudomonas entomophila* L48
Gam	Gacamide	Leu-Asp-Gln-Ile-Leu-Gln-Ser-Leu-Leu-Ser-Ile (11 AA)	*Pseudomonas fluorescens* Pf0-1
Mass	Massetolide	Leu-Glu-aThr-aIle-Leu-Ser-Leu-Ser-Ile (9 AA)	*Pseudomonas fluorescens* SS101
Ofa	Orfamide	Leu-Asp-Thr-Ile-Leu-Ser-Leu-Leu-Ser-Ile (10 AA)	*Pseudomonas* sp. CMR12a *Pseudomonas* protegens Pf-5
P1.A2	Cichofactin	Leu-Leu-Gln-Leu-X-Val-Leu-Leu (8 AA)	*Pseudomonas viridiflava* P1.A2
P13.F2	Cichofactin	Leu-Leu-Gln-Leu-X-Ile-Leu-Leu (8 AA)	*Pseudomonas viridiflava* P13.F2
P22.F1	Cichofactin	Leu-Leu-Gln-Leu-X-Ile-Leu-Leu (8 AA)	*Pseudomonas viridiflava* P22.F1
P25.C2	Cichofactin	Leu-Leu-Gln-Leu-X-Val-Leu-Leu (8 AA)	*Pseudomonas viridiflava* P25.C2
P8.B2	Cichofactin	Leu-Leu-Gln-Leu-X-Val-Leu-Leu (8 AA)	*Pseudomonas viridiflava* P8.B2
P8.B3	Cichofactin	Leu-Leu-Gln-Leu-X-Val-Leu-Leu (8 AA)	*Pseudomonas viridiflava* P8.B3
P8.B9	Cichofactin	Leu-Leu-Gln-Leu-X-Ile-Leu-Leu (8 AA)	*Pseudomonas viridiflava* P8.B9
Poa	Poaeamide	Leu-Glu-aThr-Leu-Leu-Ser-Leu-Leu-Ser-Ile (10 AA)	*Pseudomonas poae* RE*1-1-14
Pso	Putisolvin	Leu-Glu-Leu-Ile-Gln-Ser-Val-Ile-Ser-Leu-Val-Ser (12 AA)	*Pseudomonas putida* PCL1445
Ses	Sessilin	dhAbu-Pro-Ser-Leu-Val-Gln-Leu-Val-Val-Gln-Leu-Val-dhAbu-Thr-Ile-Hse-Dab-Lys (18 AA)	*Pseudomonas* sp. CMR12a
Syf	Syringafactin	Leu-Leu-Gln-Leu-Thr-Val-Leu-Leu (8 AA)	*Pseudomonas syringae* DC3000
Syr	Syringamycin	Ser-Ser-Dab-Dab-Arg-Phe-Dhb-3-OH-Asp-Cl-Thr (9 AA)	*Pseudomonas syringae* pv. *syringae* B301D
Syp	Syringopeptin	Dhb-Pro-Val-Val-Ala-Ala-Val-Val-Dhb-Ala-Val-Ala-Ala-Dhb-Thr-Ser-Ala-Dhb-Ala-Dab-Dab-Tyr (22 AA)	*Pseudomonas syringae* pv. *syringae* B301D
Tha	Thanamycin	Ser-Orn-Asn-Lys-His-Thr-Dhb-Asp-Thr (9 AA)	*Pseudomonas* sp. SHC52
Vif	Virginiafactin	Leu-Leu-Gln-Leu-Ser-Ile-Leu-Leu (8 AA)	*Pseudomonas* sp. QS1027

Vis	Viscosin	Leu-Glu-aThr-Val-Leu-Ser-Leu-Ser-Ile (9 AA)	*Pseudomonas fluorescens* SBW25
Wlp	WLIP	Leu-Asp-aThr-Val-Val-Ser-Leu-Ser-Ile (9 AA)	*Pseudomonas putida* RW 10S2
Xtl	Xantholysin	Leu-Glu-Gln-Val-Leu-Gln-Ser-Val-Leu-Gln-Leu-Leu-Gln-Ile/Val (14 AA)	*Pseudomonas putida* BW 11M1

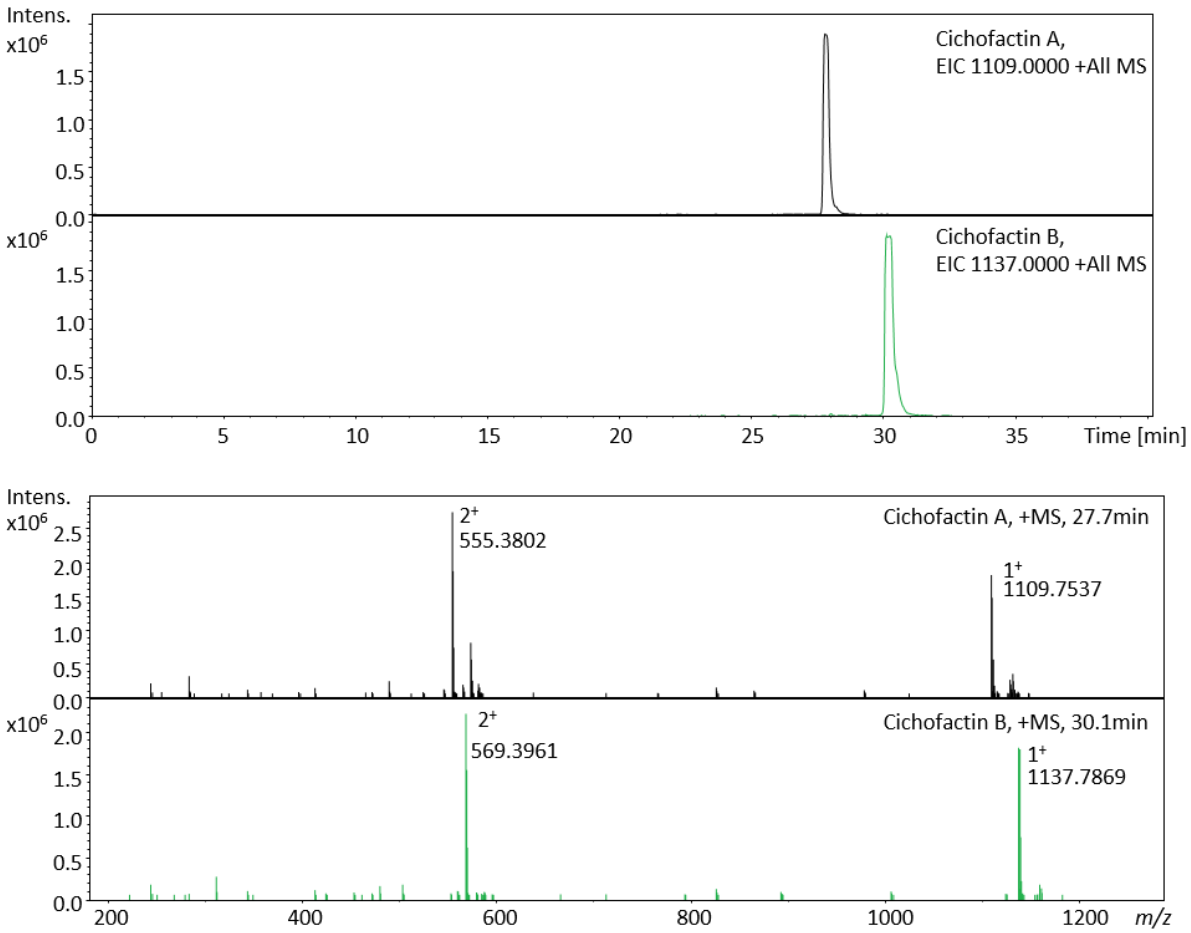

Figure VIII-11: Extracted ion chromatogram (EICs) and MS^1 of cichofactin A (*m/z* 1109 $[M+H]^+$) and B (*m/z* 1137 $[M+H]^+$).

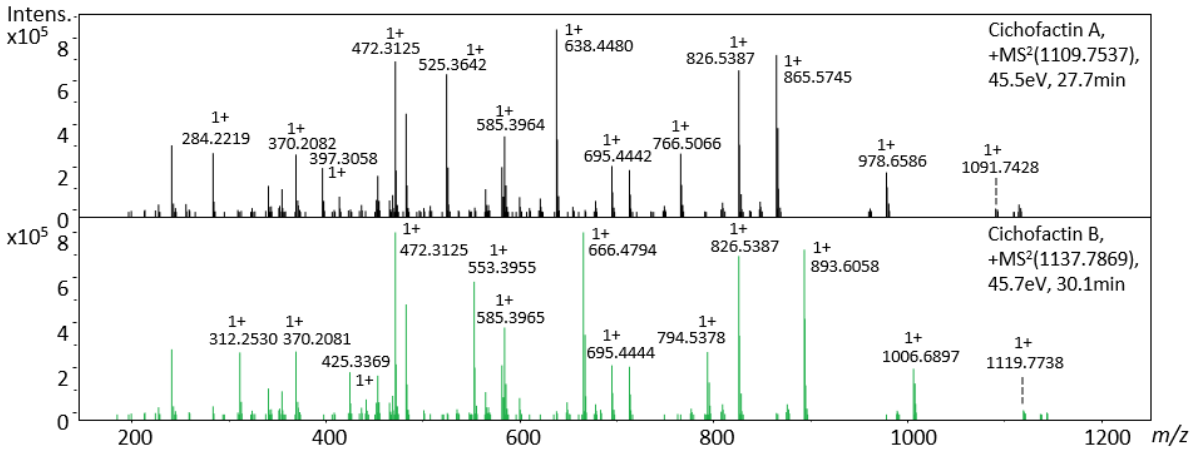

Figure VIII-12: Comparative MS^2 of cichofactin A and B (1109 and 1137 Da).

Table VIII-13: Listing of b and y ions obtained from the $[M+H]^+$ form of the compounds cichofactin A and B. The values in brackets were not oberserved in the spectra.

	Cichofactin A		Cichofactin B	
Peptide	**b ions**	**y ions**	**b ions**	**y ions**
FA	(171)		(199)	
Leu	284.2219	939.6207	312.2530	939.6233
Leu	397.3058	826.5387	425.3369	826.5387
Gln	525.3642	713.4548	553.3955	713.4548
Leu	638.4480	585.3964	666.4794	585.3965
Gln	766.5066	472.3125	794.5378	472.3125
Val	865.5745	344.2542	893.6058	344.2540
Leu	978.6586	245.1860	1006.6897	245.2540
Leu	1091.7428	(132)	1119.7757	(132)
$[M+H]^+$	1109.7537		1137.7869	

NMR Analysis of Cichofactin A

Table VIII-14: NMR spectroscopic data of cichofactin A in d_3-MeOH/ d_4-MeOH (δ in ppm).

residue	pos.	$\delta_{C/N}$ [a]	δ_H, mult (J in Hz) [b]	residue	pos.	$\delta_{C/N}$ [a]	δ_H, mult (J in Hz) [b]
3-HDA	CO	174.9 C_q		**Leu 4**	α	53.8 CH	4.35
	2	44.6 CH_2	2.37		β	41.3 CH_2	1.69
			2.47		γ [c]	26.1 CH	1.58 – 1.76
	3	70.0 CH	3.99		δ_1 [d]	23.7 CH_3	0.89 – 0.94
	4	38.4 CH_2	1.49		δ_2 [e]	21.9 CH_3	0.93 – 0.98
	5 - 8	33.1 CH_2	1.31		α-CO	175.0 C_q	
		30.7 CH_2	1.32		α-NH	125.0 NH	8.26
		30.5 CH_2	1.32	**Gln 5**	α	54.9 CH	4.36
		26.8 CH_2	1.33		β	28.4 CH_2	2.02
			1.47				2.16
	9	23.8 CH_2	1.33		γ [f]	32.7 CH_2	2.28
	10	14.5 CH_3	0.90		α-CO	173.8 C_q	
Leu 1	α	53.3 CH	4.39		α-NH	117.5 NH	8.28
	β	41.7 CH_2	1.61		γ-CO	177.8 C_q	
	γ [c]	25.9 CH	1.58 – 1.76		γ-NH_2	107.5 NH_2	6.86 + 7.61
	δ_1 [d]	23.7 CH_3	0.89 – 0.94	**Val 6**	α	60.7 CH	4.17, d (7.1 Hz)
	δ_2 [e]	21.9 CH_3	0.93 – 0.98		β	31.4 CH	2.15
	α-CO	175.6 C_q			γ	19.8 CH_3	0.96
	α-NH	125.0 NH	8.19 (d, 6.9 Hz)			18.9 CH_3	0.95
Leu 2	α	54.0 CH	4.31		α-CO	173.5 C_q	
	β	41.0 CH_2	1.65		α-NH	116.5 NH	7.90 (d, 7.5 Hz)
	γ [c]	26.0 CH	1.58 – 1.76	**Leu 7**	α	53.1 CH	4.50
	δ_1 [d]	23.4 CH_3	0.89 – 0.94		β	42.0 CH_2	1.63
	δ_2 [e]	22.1 CH_3	0.93 – 0.98		γ [c]	26.0 CH	1.58 – 1.76
	α-CO	175.4 C_q			δ_1 [d]	23.6 CH_3	0.89 – 0.94
	α-NH	119.1 NH	8.28		δ_2 [e]	21.9 CH_3	0.93 – 0.98
Gln 3	α	54.8 CH	4.30		α-CO	174.6 C_q	
	β	28.2 CH_2	2.05		α-NH	122.7 NH	8.24
			2.20	**Leu 8**	α	52.1 CH	4.43
	γ [f]	32.8 CH_2	2.32		β	41.6 CH_2	1.65
	α-CO	174.1 C_q			γ [c]	26.1 CH	1.58 – 1.76
	α-NH	118.9 NH	8.31		δ_1 [d]	23.8 CH_3	0.89 – 0.94
	γ-CO	177.8 C_q			δ_2 [e]	21.9 CH_3	0.93 – 0.98
	γ-NH_2	108.3 NH_2	6.86 + 7.61		α-CO	175.9 C_q	
					α-NH	120.3 NH	8.13 (d, 8.0 Hz)

[a] Recorded at 176/ 101 MHz for ^{13}C and ^{15}N values were extracted from the corresponding ^{1}H-^{15}N HSQC NMR spectrum. Multiplicity determined by an edited ^{1}H-^{13}C HSQC and a DEPT135 NMR experiment. [b] Recorded at 700/ 400 MHz. [c] The γ-Leu values are interchangeable. [d] The δ_1-Leu values are interchangeable. [e] The δ_2-Leu values are interchangeable. [f] The γ-Gln values are interchangeable.

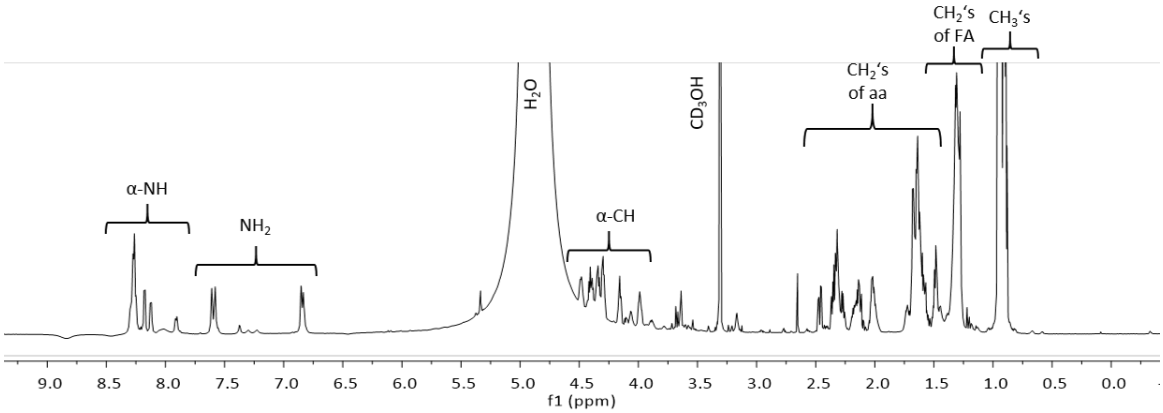

Figure VIII-13: ^{1}H NMR spectrum of cichofactin A in d_3-MeOH (700 MHz).

This spectrum indicates the different type of protons.

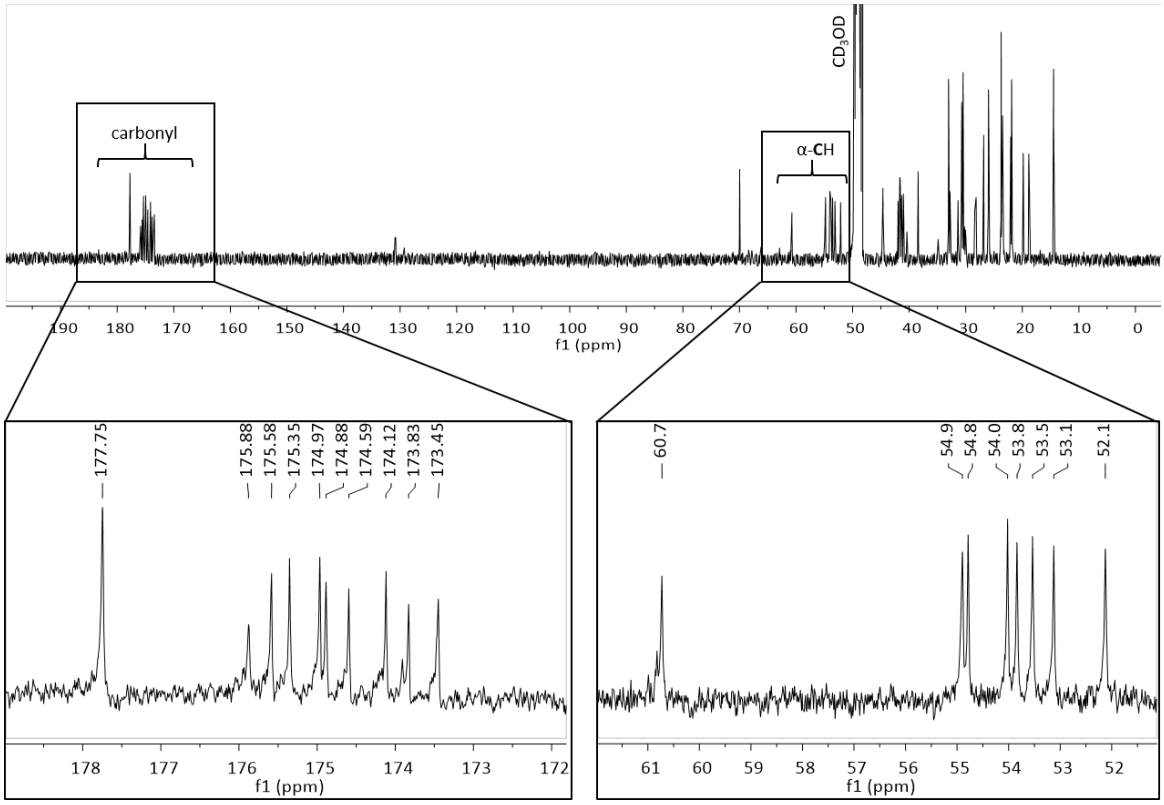

Figure VIII-14: ^{13}C NMR spectrum of cichofactin A in d_4-MeOH (101 MHz).

Overview about the ^{13}C NMR spectrum of cichofactin A (top) and detail region of the carbonyl region (173 – 178 ppm) and the α-proton region (52 – 61 ppm) (bottom).

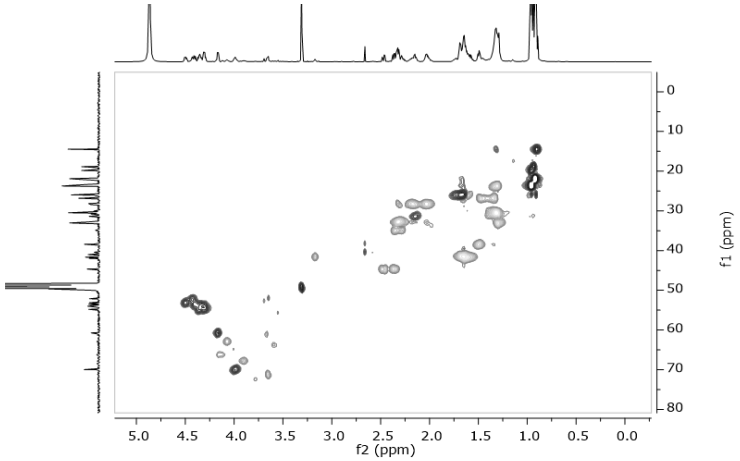

Figure VIII-15: ^{1}H-^{13}C HSQC spectrum of cichofactin A in d_4-MeOH (400 MHz).

The edited version showed CH and CH_3 peaks in dark grey and CH_2 peaks in light grey.

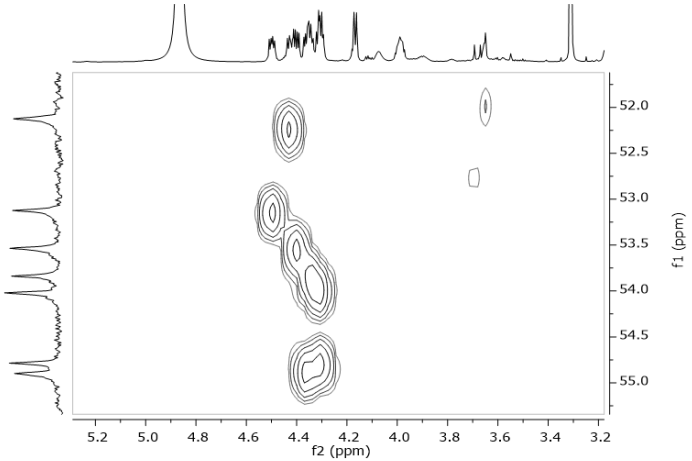

Figure VIII-16: ^{1}H-^{13}C band selective HSQC of cichofactin A in d_4-MeOH (400 MHz).

Detail region of 51 – 56 ppm (α-proton resonances).

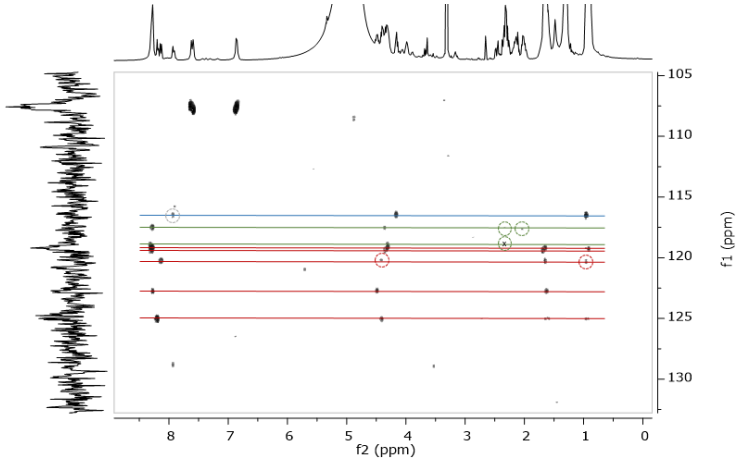

Figure VIII-17: ^{1}H-^{15}N HSQC-TOCSY of cichofactin A in d_3-MeOH (400 MHz).

Detail region of 90 – 140 ppm. Horizontal lines indicate the different amino acids. Circles indicate cross peaks which are slightly visible.

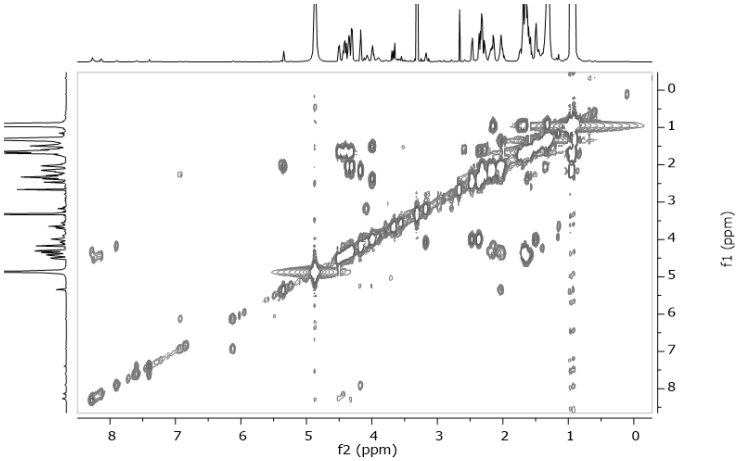

Figure VIII-18: ^{1}H-^{1}H COSY spectrum of cichofactin A in d_4-MeOH (700 MHz).

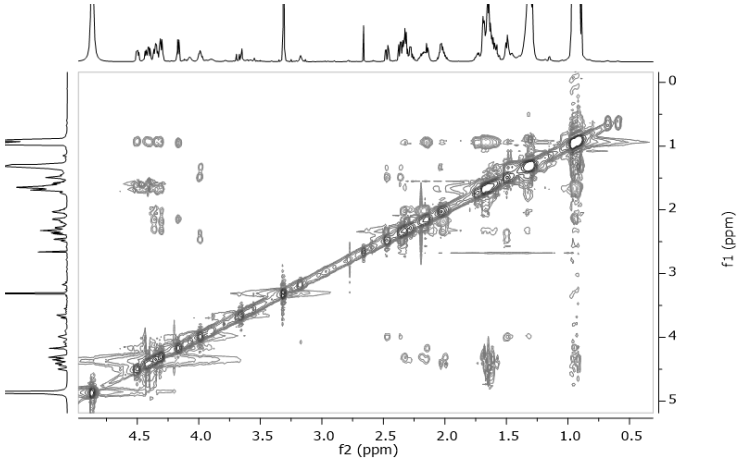

Figure VIII-19: ^{1}H-^{1}H ROESY spectrum of cichofactin A in d_4-MeOH (700 MHz).

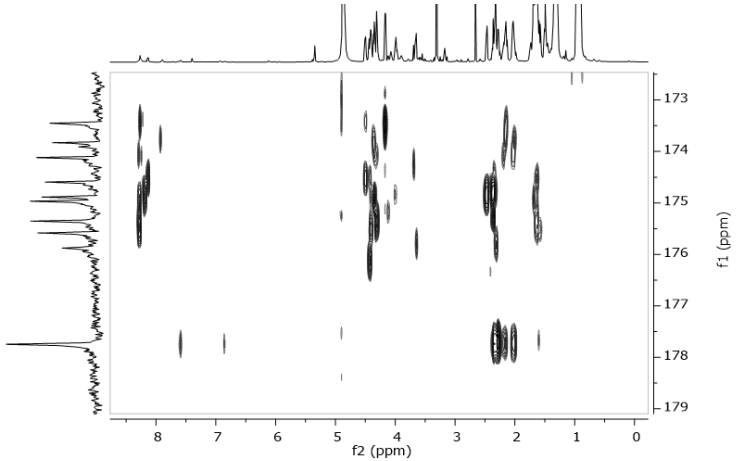

Figure VIII-20: ^{1}H-^{13}C band selective HMBC spectrum of cichofactin A in d_3-MeOH (700 MHz).

The band selective HMBC spectrum was performed in the carbonyl region (160 – 190 ppm).

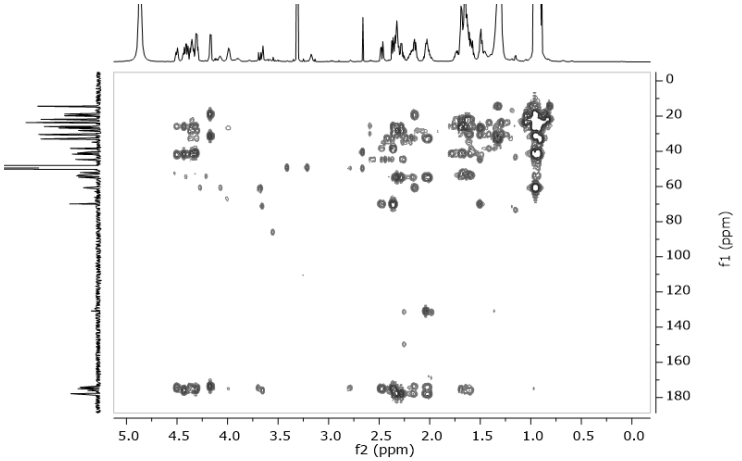

Figure VIII-21: ^{1}H-^{13}C HMBC spectrum of cichofactin A in d_4-MeOH (700 MHz).

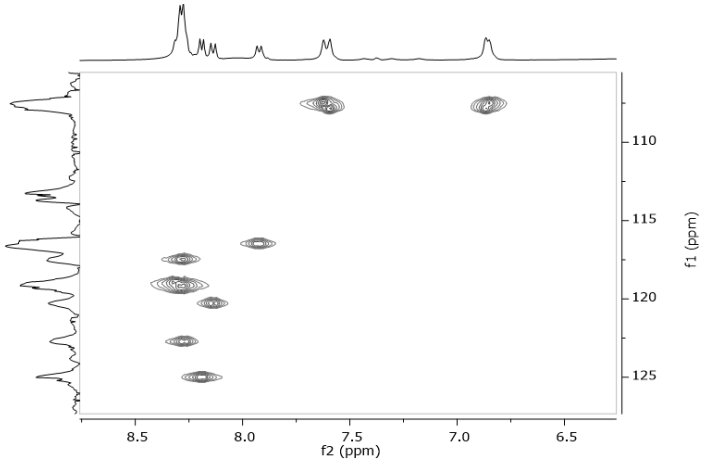

Figure VIII-22: ^{1}H-^{15}N HSQC spectrum of cichofactin A in d_3-MeOH (400 MHz).

Detail region of 90 – 140 ppm.

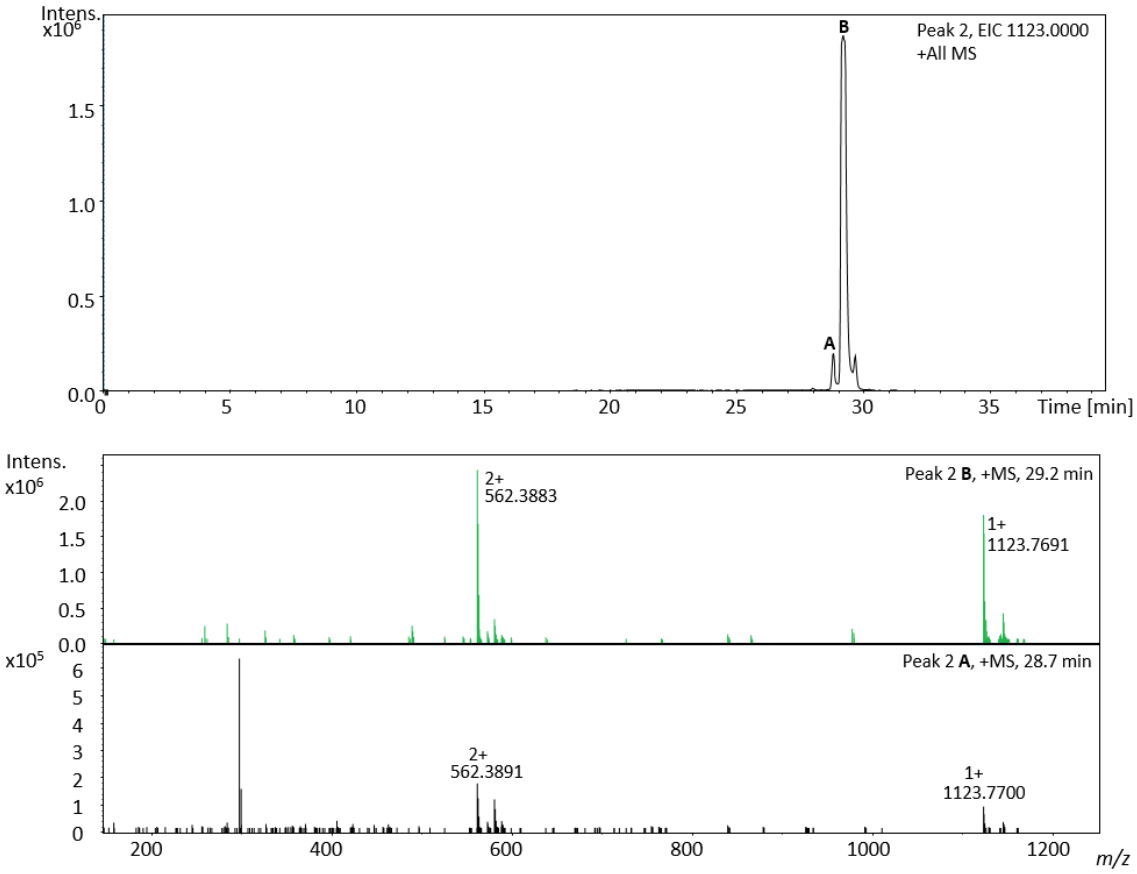

Figure VIII-23: Extracted ion chromatogram (EIC) for 1123 Da $[M+H]^+$ and MS^1 of peak 2 **A** (cichofactin C2) and **B** (cichofactin C).

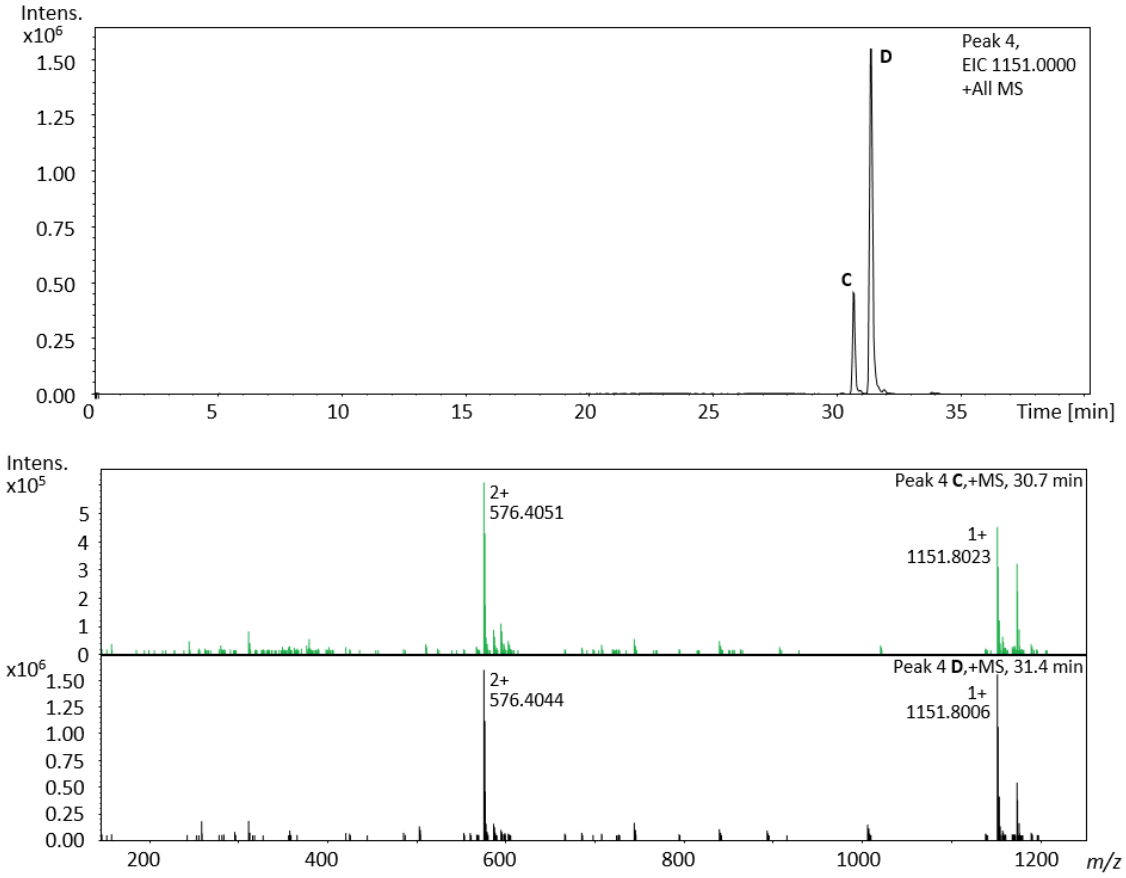

Figure VIII-24: Extracted ion chromatogram (EIC) for 1151 Da $[M+H]^+$ and MS^1 of peak 4 **C** (cichofactin D2) and **D** (cichofactin D).

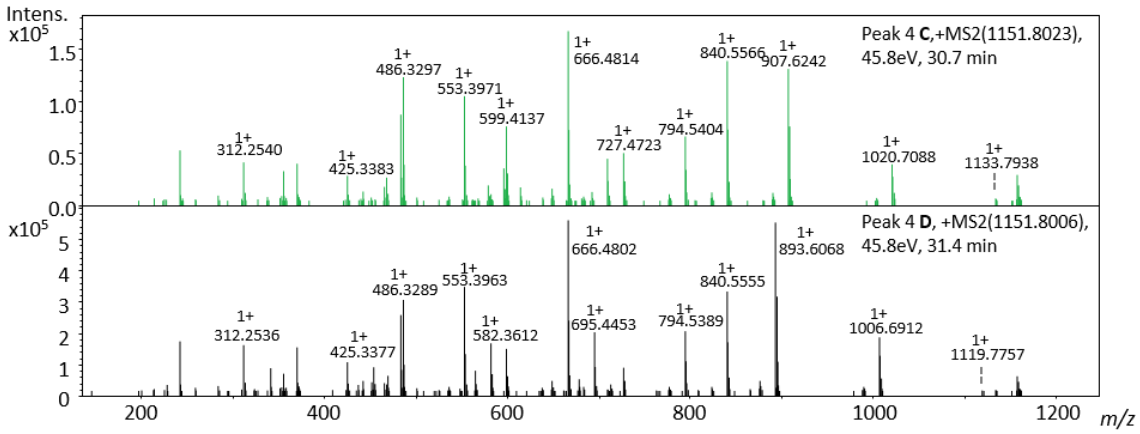

Figure VIII-25: Comparative MS^2 of peak 4 **C** at 30.7 min (cichofactin D2) and of peak 4 **D** at 31.4 min (cichofactin D) (1151 Da $[M+H]^+$).

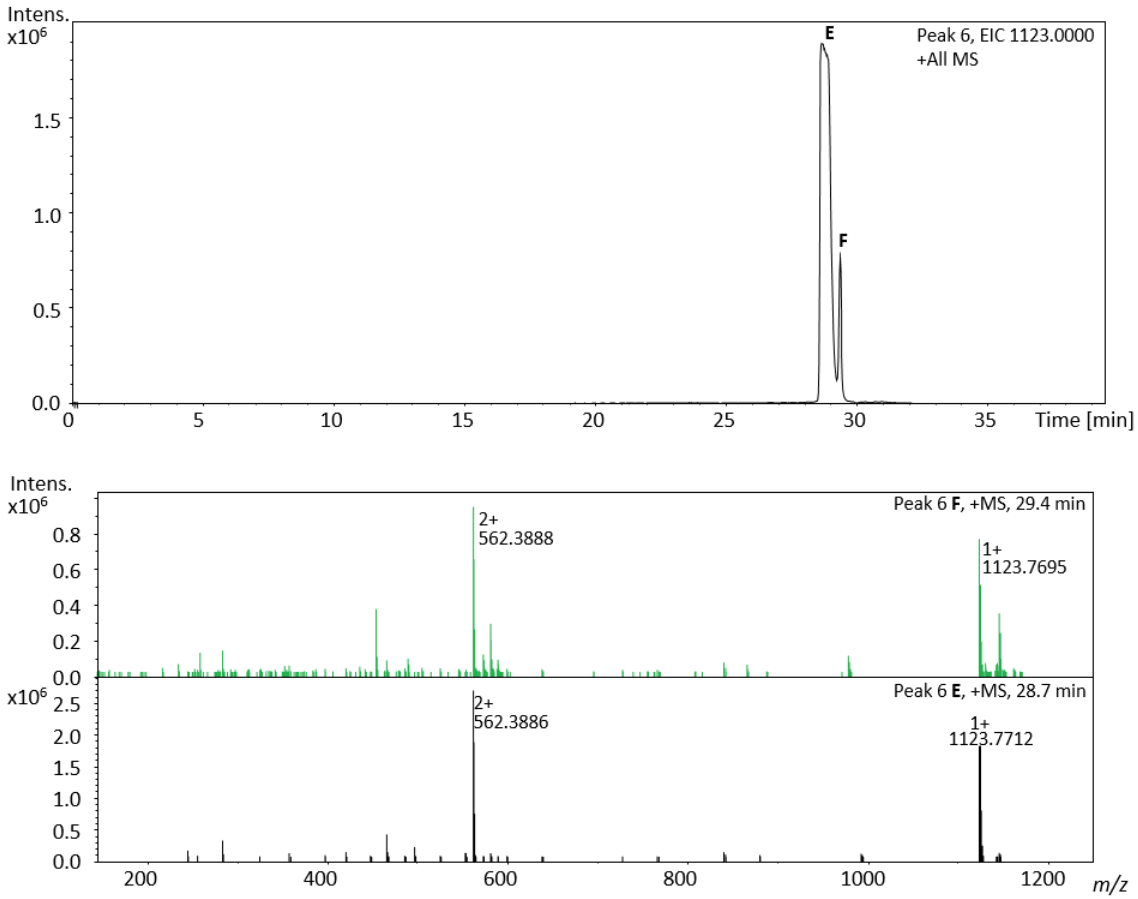

Figure VIII-26: Extracted ion chromatogram (EIC) for 1123 Da $[M+H]^+$ and MS^1 of peak 6 **E** (cichofactin E) and **F** (cichofactin E2).

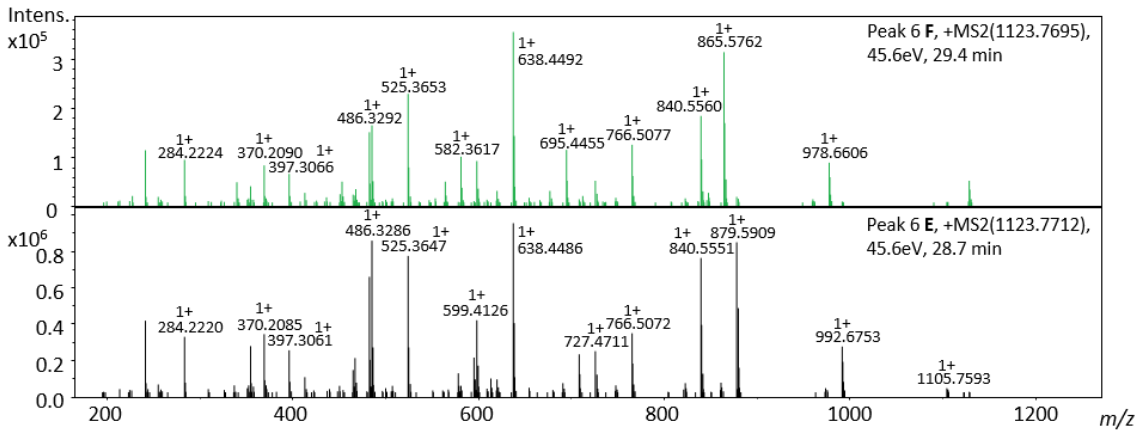

Figure VIII-27: Comparative MS^2 of peak 6 **E** at 28.7 min (cichofactin E) and of peak 6 **F** at 29.4 min (cichofactin E2) (1123 Da $[M+H]^+$).

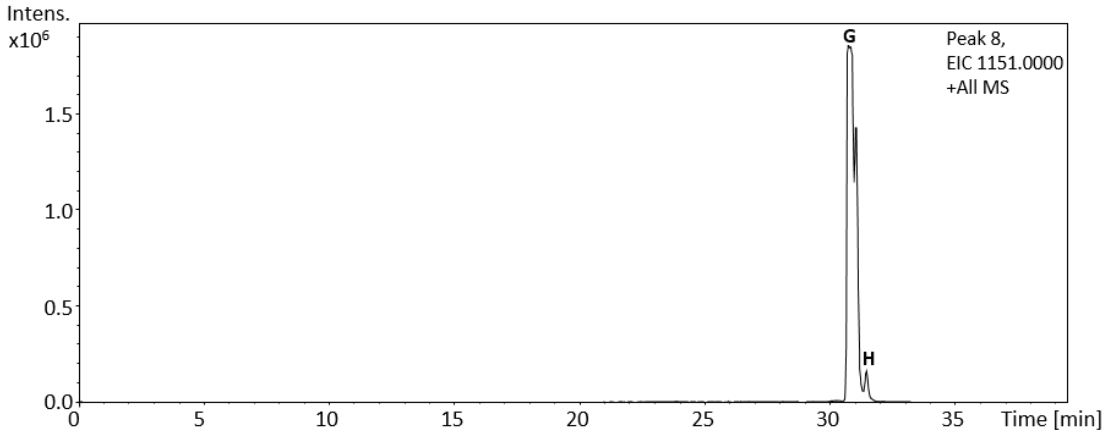

Figure VIII-28: Extracted ion chromatogram (EIC) for 1151 Da $[M+H]^+$.

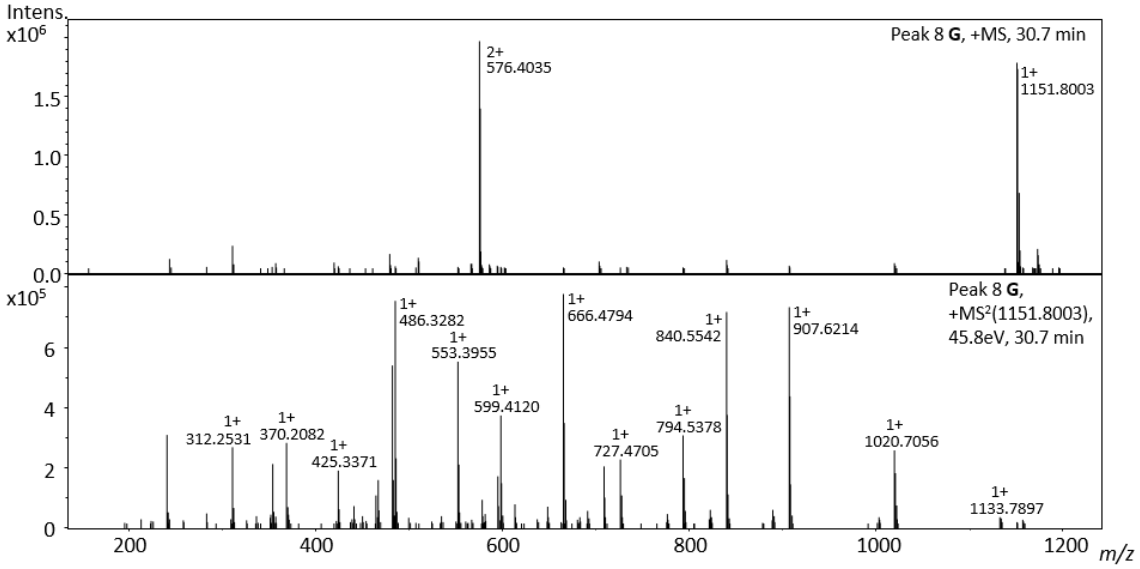

Figure VIII-29: MS^1 and MS^2 spectrum of peak 8 **G** at 30.7 min (cichofactin F) (1151 Da $[M+H]^+$).

Table VIII-15: Listing of b and y ions obtained from the $[M+H]^+$ form of the compounds cichofactin C and E.
The values in brackets were not observed in the spectra.

	Cichofactin C		Cichofactin E	
Peptide	**b ions**	**y ions**	**b ions**	**y ions**
FA	(171)		(171)	
Leu	284.2220	(953)	284.2220	953.6387
Leu	397.3061	840.5548	397.3061	840.5551
Gln	525.3644	727.4708	525.3647	727.4711
Leu	638.4484	599.4125	638.4486	599.4126
Gln	766.5071	486.3284	766.5072	486.3284
Val/Xle	865.5748	358.2701	879.5909	358.2702
Leu	978.6591	259.2014	992.6753	245.1858
Leu	1091.7439	146.1177	1105.7583	132.1025
$[M+H]^+$	1123.7691		1123.7715	

Table VIII-16: Listing of b and y ions obtained from the $[M+H]^+$ form of the compounds cichofactin D and F.
The values in brackets were not observed in the spectra.

	Cichofactin D		Cichofactin F	
Peptide	**b ions**	**y ions**	**b ions**	**y ions**
FA	(199)		(199)	
Leu	312.2536	953.6412	312.2531	953.6393
Leu	425.3377	840.5555	425.3371	840.5542
Gln	553.3963	727.4714	553.3955	727.4705
Leu	666.4802	599.4130	666.4794	599.4120
Gln	794.5389	486.3298	794.5378	486.3282
Val/Xle	893.6068	358.2703	907.6242	358.2071
Leu	1006.6912	259.2019	1020.7056	245.1862
Leu	1119.7757	146.1178	1133.7897	132.1010
$[M+H]^+$	1151.8006		1151.8003	

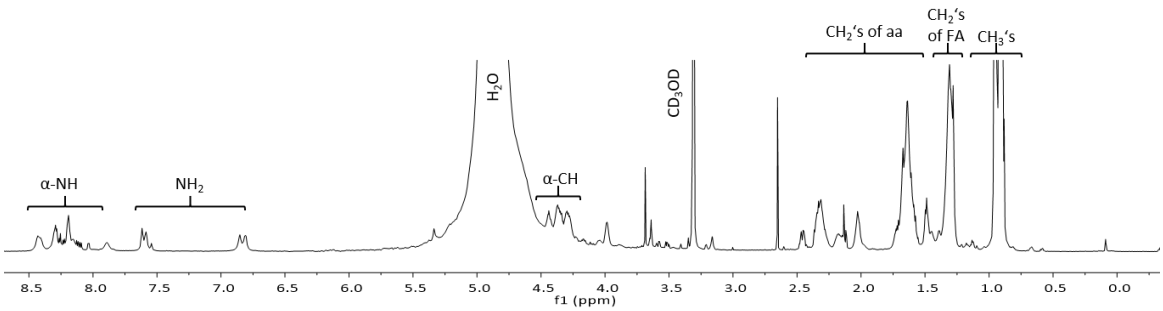

Figure VIII-30: ^{1}H NMR spectrum of cichofactin E in d_3-MeOH (700 MHz).

This spectrum indicates the different type of protons.

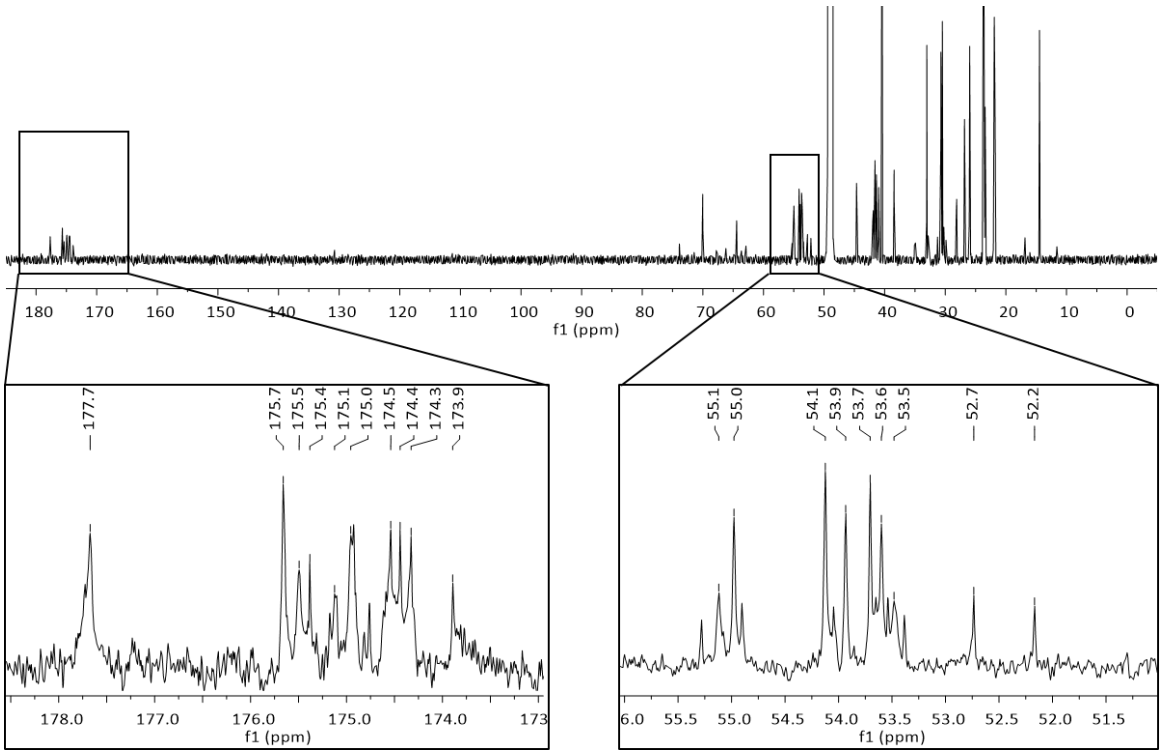

Figure VIII-31: ^{13}C NMR spectrum of cichofactin E in d_3-MeOH (700 MHz).

Overview about the ^{13}C NMR spectrum of cichofactin E (top) and detailed region of the carbonyls (173 – 178 ppm) and the α-proton region (51 – 56 ppm) (bottom).

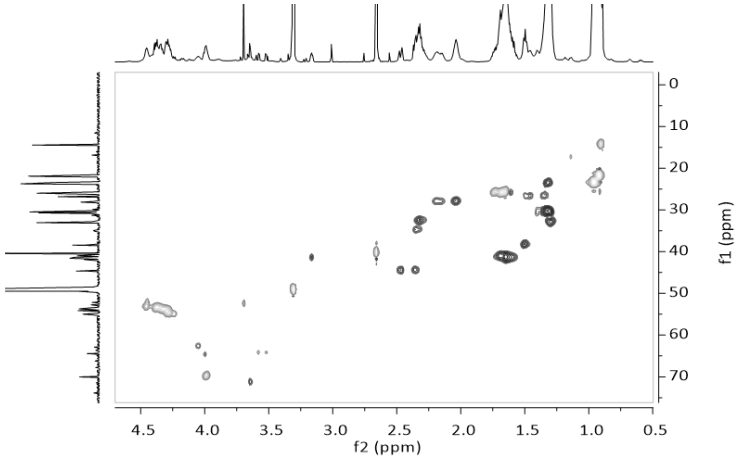

Figure VIII-32: ^{1}H-^{13}C HSQC spectrum of cichofactin E in d_4-MeOH (700 MHz).

The edited version showed the CH_2 peaks in dark grey and CH and CH_3 peaks in light grey.

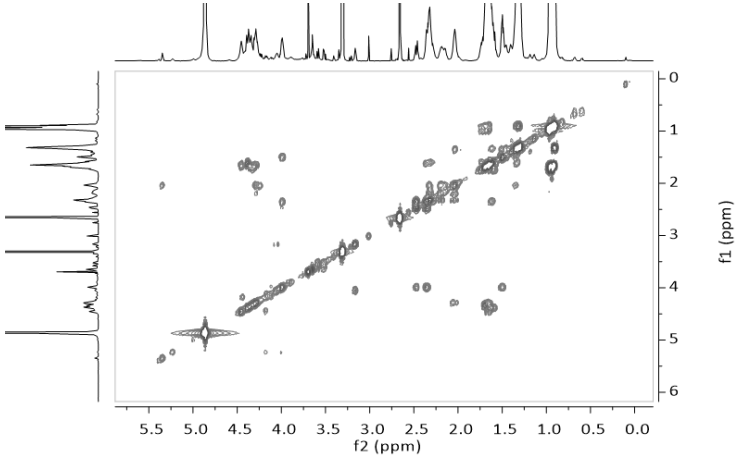

Figure VIII-33: ^{1}H-^{1}H COSY spectrum of cichofactin E in d_4-MeOH (700 MHz).

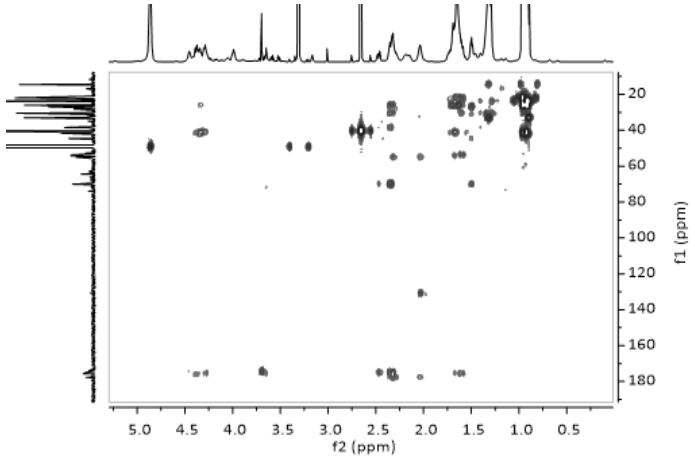

Figure VIII-34: ^{1}H-^{13}C HMBC spectrum of cichofactin E in d_4-MeOH (700 MHz).

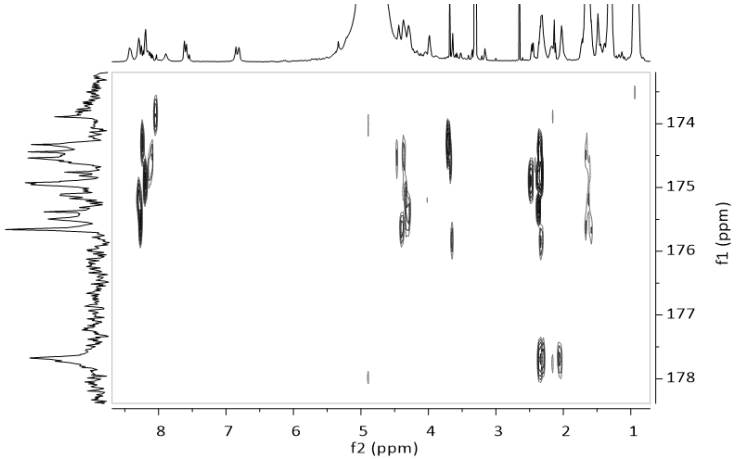

Figure VIII-35: ^{1}H-^{13}C band selective HMBC spectrum of cichofactin E in d_4-MeOH (700 MHz).

The band selective HMBC spectrum was performed in the carbonyl region (160 - 190 ppm).

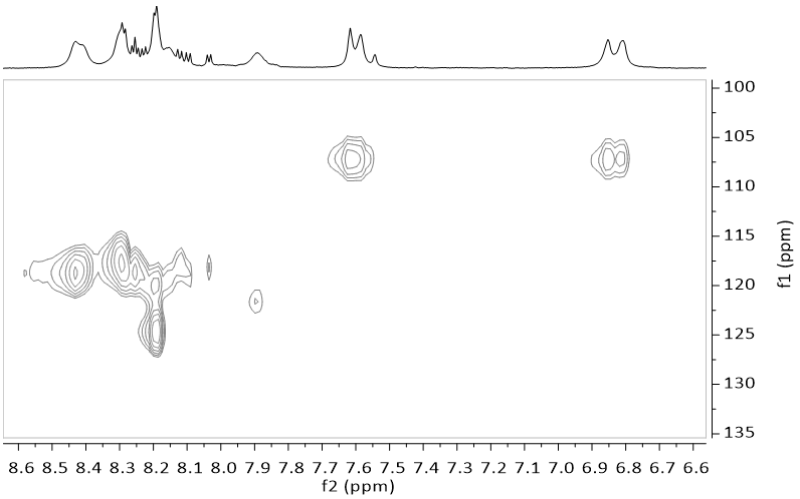

Figure VIII-36: ^{1}H-^{15}N HSQC spectrum of cichofactin E in d_4-MeOH (700 MHz).

Acknowledgements

First of all, I want to thank my supervisor Prof. Dr. Harald Groß for giving me the opportunity to work in his research group. I sincerely appreciate all the advice and broad experience you have shared with me. I would like to express my thanks for the many constructive and helpful discussions and the always open door.

Secondly, I would like to thank PD Dr. Bertolt Gust for his work as a second reviewer and for the advice and suggestions he gave me during my dissertation.

I thank Prof. Dr. Leonard Kaysser and JProf. Dr. Silja Mordhorst for acting as examiners.

I wish to thank Dr. Dorothee Wistuba for her reliable and competent help with the (HR-) LCMS measurements and analysis.

Furthermore, I would like to thank all members of the Collaborative Research Center Transregional (CRC-TR) 261 for fruitful meetings and discussions and for the good cooperation.

I would also like to thank Marlene Vogt for her good work on her master thesis.

Special thanks go to Corinna Fischer for her help concerning bureaucratic matters and to Manuela Haußmann and Wolfgang Kornberger for the excellent organisation of the lab and their constant help with problems with orders.

I wish to thank my lab mates Patricia Arlt, Thomas Majer, Anina Buchmann and Hamada Saad for the helpful discussions, their experience in analytical as well as practical issues and for the pleasant working atmosphere in the lab and office.

A big thanks also goes to all my colleagues for the excellent atmosphere in the lab and for the great time we had together at the countless movie nights, dinners, barbecues, parties and other events: Alexandra, Alicia, Aziz, Caro, Cathrin, Daniel, Felix, Fred, Franzi, Hannah, Lina, Marius, Niraj, Nhomsai, Patricia, Patrick, Philipp, Richard, Sarah, Simon, Tomke and all already mentioned above. Special thanks go to the girls for our joint activities.

Finally, I would like to express my deepest gratitude to my family and friends for always supporting me! Without their love and help, this work would not have been accomplished.